STUDY OF THE AMMONIA ABSORPTION PROCESS INTO AMMONIA/WATER SOLUTIONS USING POLYMERIC MEMBRANES FOR ABSORPTION-RESORPTION REFRIGERATION SYSTEMS

Miguel Ángel Berdasco Ruiz

Miguel Ángel Berdasco Ruiz

STUDY OF THE AMMONIA ABSORPTION PROCESS INTO AMMONIA/WATER SOLUTIONS USING POLYMERIC MEMBRANES FOR ABSORPTION-RESORPTION REFRIGERATION SYSTEMS

DOCTORAL THESIS

UNIVERSITAT ROVIRA i VIRGILI

Tarragona, 2018

UNIVERSITAT ROVIRA I VIRGILI
STUDY OF THE AMMONIA ABSORPTION PROCESS INTO AMMONIA/WATER SOLUTIONS USING POLYMERIC MEMBRANES FOR ABSORPTION-RESORPTION REFRIGERATION SYSTEMS
Miguel Ángel Berdasco Ruiz

Miguel Ángel Berdasco Ruiz

STUDY OF THE AMMONIA ABSORPTION PROCESS INTO AMMONIA/WATER SOLUTIONS USING POLYMERIC MEMBRANES FOR ABSORPTION-RESORPTION REFRIGERATION SYSTEMS

DOCTORAL THESIS

Supervised by

Prof. Alberto Coronas

Dr. Manel Vallès

Department of Mechanical Engineering

UNIVERSITAT ROVIRA i VIRGILI

Tarragona, 2018

UNIVERSITAT ROVIRA I VIRGILI
STUDY OF THE AMMONIA ABSORPTION PROCESS INTO AMMONIA/WATER SOLUTIONS USING POLYMERIC MEMBRANES FOR ABSORPTION-RESORPTION REFRIGERATION SYSTEMS
Miguel Ángel Berdasco Ruiz

UNIVERSITAT
ROVIRA I VIRGILI
DEPARTAMENT D'ENGINYERIA MECÀNICA
Escola Tècnica Superior d'Enginyeria Química (ETSEQ).
Av. Països Catalans 26. 43007 Tarragona (Spain)

Declaration

We STATE that the present thesis, entitled "Study of the ammonia absorption process into ammonia/water solutions using polymeric membranes for absorption-resorption refrigeration systems", presented by Miguel Angel Berdasco Ruiz for the award of the degree of Doctor, has been carried out under our supervision at the CREVER research group in the Department of Mechanical Engineering of this university, and that it fulfills all the requirements to be eligible for the International Doctorate Award.

Tarragona, May 11th, 2018

Dr. Manel Valles

Prof. Alberto Coronas

UNIVERSITAT ROVIRA I VIRGILI
STUDY OF THE AMMONIA ABSORPTION PROCESS INTO AMMONIA/WATER SOLUTIONS USING POLYMERIC MEMBRANES FOR ABSORPTION-RESORPTION REFRIGERATION SYSTEMS
Miguel Ángel Berdasco Ruiz

AGRADECIMIENTOS

La realización de esta tesis doctoral ha sido un largo camino que queda culminado con la redacción de este documento. Muchas personas me han ayudado a poder realizarlo y desde estas líneas quisiera tener un recuerdo para todas ellas. Ante todo, quisiera agradecer a mis directores Alberto Coronas y Manel Vallès por tener siempre su puerta abierta para atenderme y ayudarme. A ti, Alberto, por confiar en mi para realizar esta tesis, por todo lo que me has enseñado y por tu infinita paciencia incluso en mis momentos más bajos. A ti, Manel, por ayudarme tanto en el trabajo diario de la tesis, bajando a echarme una mano a la planta piloto si era necesario o dedicando muchísimas horas durante la elaboración de los modelos. Muchísimas gracias a los dos.

Gracias también al Ministerio de Economía y Competitividad (MINECO) del Gobierno de España por otorgarme una de sus "Ayudas para contratos predoctorales para la formación de doctores" (BES-2013-066917) que me ha permitido dedicarme al 100% a la elaboración de esta tesis gracias a su sustento económico. Gracias también al MINECO por los proyectos del Plan Nacional I+D+I (DPI2012-38841-C02-01, DPI2015-71306-R y ENE2015-64117-C5-3-R) que han permitido financiar esta investigación, así como a la Universitat Rovira i Virgili por poner a mi disposición sus recursos.

Gracias al Prof. Dr.-Ing. Ullrich Hesse del Institut für Energietechnik de la Technische Universität Dresden (Alemania) por permitirme realizar allí mi estancia investigadora y gracias también a todos los compañeros del grupo de investigación de Kälte-, Kryo- und Kompressorentechnik (Martin, Christiane, Thobias, Marcel, Felix, etc) por la ayuda y amabilidad mostrada durante toda mi estancia. Quisiera agradecer una vez más al MINECO por su programa de "Ayudas a la movilidad predoctoral para la realización de estancias breves en centros de I+D españoles y extranjeros 2014" (EEBB-I-15-10494), que permitió financiar mi estancia investigadora en Alemania.

A la Dra. M. Soledad Larrechi del Departamento de Química Analítica y Química Orgánica por su inestimable ayuda durante el trabajo realizado con el NIR. Fue un placer colaborar contigo en ese proyecto. A todos mis compañeros del Grup d'Innovació Tecnològica en Revalorització Energètica i Refrigeració (CREVER), especialmente a Adriana, Isabel, Andry, Maycon, Rubén y Jaume, con quienes he tenido la suerte de poder compartir muchas horas de oficina o de planta piloto pero también muy buenos ratos fuera del trabajo. Muchas gracias también al Dr. Daniel Salavera por su ayuda y predisposición siempre que necesité utilizar cualquier instrumento del laboratorio, y a Samuel García y Maria José Durán por facilitarnos tanto las cosas con todo lo relativo a trámites y papeleos. Finalmente, me gustaría tener un recuerdo especial para el profesor Hugo Segura de la Universidad de Concepción (Chile) y para el Dr. James Muye, compañero del CREVER, a quienes el destino quiso que nos dejaran demasiado pronto. A ti, Hugo, por haber sido tan buen anfitrión durante nuestra estancia en Chile. A ti, James, por tu amistad y ayuda en las interminables horas que pasamos juntos en la planta piloto. Te mando un fuerte abrazo allá donde estés.

Pero no todo ha sido trabajo durante estos cuatro años. He tenido la inmensa suerte de conocer gente maravillosa fuera de la URV. Empezando por los Néstor, Olga, Ricardo, Jenny, Elena y compañía, que me acogieron en su grupo con los brazos abiertos nada más llegar a Tarragona y que tan buenos ratos pasamos juntos. Muchas gracias a todo el clan villacucarachero por vuestra amistad: Rafa, Ana, Laura, Simo, Jose, Jesús y muy especialmente María y Neus, con quienes

tantas risas y buenos momentos he compartido. Por suerte, aun nos quedan mucho más buenos ratos que pasar juntos, ya sea alrededor de un buen juego de mesa, con unas cañas en las manos o de viaje. Pero si algo realmente importante me tenía reservado el destino cuando me vine a vivir a Tarragona fue poder encontrarme con la persona más especial que he conocido nunca. Aquella que me complementa y con quien deseo pasar el resto de mi vida a su lado. Esa persona eres tú, Maria. T´estimo molt.

Por último, y no por ello menos importante, quiero dar las gracias a mi maravillosa familia, de la que cada día me siento más orgulloso. Gracias por vuestro cariño, apoyo y respeto. Especialmente quiero dedicar esta tesis a mis padres, por sus sacrificios para sacar adelante nuestra familia. A mi madre, que es quien más ha sufrido por los 700 km de distancia que nos separan y a quien admiro más que a nadie en este mundo por su manera de cuidar y amar a todos sus seres queridos. A mi padre, por todo lo que me has enseñado a lo largo de mi vida y con quien comparto tantos gustos y aficiones. Gracias por transmitirme tu interés por la ciencia, sin duda eso ha sido clave para llegar a donde he llegado. Pero sobre todo gracias por enseñarme a ver el mundo con una mirada crítica, a no creerme todo lo que nos cuentan sino a buscar la verdad oculta detrás de las apariencias.

RESUMEN

Los sistemas de refrigeración por absorción son una excelente alternativa a los sistemas de refrigeración de compresión convencionales cuando hay disponible una fuente de calor de baja temperatura que puede ser aprovechada. Sin embargo, este tipo de sistemas no han conseguido ampliar su nicho de mercado principalmente por su elevado coste y tamaño, lo cual ha limitado mucho su utilización en ciertas aplicaciones en las que hay gran cantidad de calor residual disponible, como por ejemplo el sector del transporte.

En los últimos años se han llevado a cabo varias investigaciones sobre el uso de materiales poliméricos en los sistemas de refrigeración por absorción con la idea de reducir el tamaño, peso y coste de estos equipos. Entre estos estudios destacan especialmente aquellos referidos al uso de membranas poliméricas porosas absorbedores y desorbedores, ya que gracias a su elevada relación superficie/volumen permiten reducir el tamaño y peso de estos componentes de forma muy importante. La gran mayoría de estos estudios se han llevado a cabo para la mezcla agua/bromuro de litio ya que las típicamente elevadas presiones de trabajo de la mezcla amoniaco/agua limita la utilización de materiales poliméricos. Ante esta situación, en esta tesis se propone la utilización de la tecnología de absorción-resorción como solución a esta problemática. Estos ciclos proporcionan una gran flexibilidad de operación que permite reducir la alta presión de trabajo de forma muy importante al utilizar disoluciones de amoniaco/agua en lugar de amoniaco puro en el circuito de refrigeración. El objetivo principal de esta tesis es estudiar el proceso de absorción de amoniaco en disoluciones de amoniaco/agua usando membranas porosas como contactores para ser utilizadas en los sistemas de refrigeración por absorción-resorción. De esta forma se podrían diseñar equipos más compactos, ligeros y baratos con los que poder ampliar la utilización de los sistemas de refrigeración por absorción.

En primer lugar, se realizó un estudio del ciclo de refrigeración por absorción-resorción de amoniaco/agua para determinar el rango de presiones de operación cuando las temperaturas de trabajo han sido fijadas. El hecho de poder variar la alta presión en un amplio intervalo dota a estos ciclos de una gran flexibilidad, teniendo siempre en cuenta que una reducción de la alta presión del ciclo implica una disminución en el COP. Mediante el desarrollo de un modelo termodinámico se determinó que la mejor configuración del ciclo es aquella que no utiliza rectificador después del generador ya que la mejora en términos de COP es pequeña (menor del 8%) y sin embargo la complejidad y coste del equipo será mucho mayor si se incluye el rectificador. Este hecho supone una gran ventaja de los ciclos de absorción-resorción en comparación con los ciclos de absorción convencionales. A su vez, se puso de manifiesto la gran importancia del parámetro de la eficacia del intercambiador de calor del circuito de resorción ya que si esta eficacia es menor de un cierto valor límite no solo se ve afectado el COP del ciclo, sino que el sistema sería incapaz de funcionar a las condiciones de temperatura previamente fijadas. El modelo termodinámico fue también utilizado para el estudio de sensibilidad del ciclo y para establecer unas condiciones de operación que permitan un buen compromiso entre reducción de la presión de trabajo, COP y potencia de refrigeración.

Se desarrolló un segundo modelo termodinámico en el que se tuvo en cuenta la transferencia de calor a los fluidos externos. Dicho modelo se utilizó para determinar la influencia de la temperatura de las corrientes externas así como del tamaño de los intercambiados de calor (UA) en el funcionamiento del ciclo. A su vez, el modelo fue empleado para analizar el funcionamiento de una planta de absorción-resorción de 25kW de potencia de refrigeración nominal situada en la Technische Universität Dresden (Alemania). De dicho análisis se concluyó que el proceso de

absorción en el resorbedor debe ser mejorado. Del trabajo experimental llevado a cabo con el equipo de 25kW cabe destacar la dificultad de mantenerlo operando en condiciones estables, lo cual ya había sido señalado anteriormente por varios autores. Como propuesta de mejora del funcionamiento de la planta se propuso un sistema de control basado en las medidas de concentración de las disoluciones de amoniaco/agua usando espectroscopía de infrarrojo cercano (NIR).

Por otra parte, se realizó un estudio teórico-experimental del proceso de absorción adiabático de amoniaco en disoluciones de amoniaco/agua utilizando un módulo de membrana plana como contactor. Para ello se diseñó y construyó un banco de ensayos donde realizar los experimentos y se desarrolló un modelo teórico que fue validado con los resultados experimentales. Este modelo fue empleado para determinar las características requeridas por una membrana polimérica porosa para ser utilizada en el proceso de absorción de amoniaco, lo cual supone una novedad ya que no había sido determinado con anterioridad para la mezcla de amoniaco/agua. Dichas características son: hidrofobicidad del material, tamaño de poro entre 0.03µm y 0.1µm, porosidad mayor del 40% y un grosor menor de 400µm siempre y cuando le permita mantener su resistencia mecánica. Teniendo en cuenta estas características, se seleccionó un módulo comercial de membranas de fibra hueca con flujo cruzado que cumpliera con estos requisitos ya que dicha configuración proporciona mayor relación superficie/volumen y un mejor coeficiente transferencia de materia que el módulo de membrana plana previamente utilizado. Se realizó un estudio experimental del proceso de absorción adiabático de amoniaco en las condiciones de trabajo previamente determinadas durante el estudio del ciclo de absorción-resorcion. Se obtuvieron flujos de absorción entre $5.4 \cdot 10^{-5}$ y $3.1 \cdot 10^{-4}$ kg/(m^2·s) en los experimentos realizados en las condiciones de presión (1.3-1.5 bar) y fracción másica de amoniaco (0.29-0.32) del absorbedor y flujos de absorción entre $6.3 \cdot 10^{-5}$ y $9.7 \cdot 10^{-4}$ kg/(m^2·s) en los experimentos realizados en las condiciones de presión (5.0-5.5 bar) y fracción másica de amoniaco (0.56-0.60) del resorbedor. Se desarrolló a su vez un modelo bidimensional que fue validado con los resultados experimentales y que permite analizar la evolución de las temperaturas, concentración de la disolución y flujo de absorción en la dirección axial y radial del módulo de membranas. Este modelo fue utilizado como base para el desarrollo de un nuevo modelo bidimensional de un módulo de membranas de fibra hueca con intercambiador de calor integrado (HEXHFMA), el cual permitirá diseñar absorbedores y resorbedores más compactos y ligeros para los sistemas de refrigeración por absorción-resorción de amoniaco/agua.

Con el modelo previamente desarrollado se diseñaron dos módulos de membranas de fibra hueca con intercambiador de calor integrado para ser empleados en el absorbedor y en el resorbedor de un equipo de absorción-resorción de amoniaco/agua de 25kW de potencia refrigeradora. Como principales conclusiones destacar que la integración de módulos de membranas en el resorbedor requiere de una modificación del propio ciclo de refrigeración, ya que la corriente de vapor procedente del generador debe ser enfriada antes de entrar en el módulo de membranas para así evitar su condensación dentro de la membrana y con ello impedir el bloqueo de los poros de la membrana. Además, el diseño del módulo de membranas para el resorbedor requiere un 22% más de área de membrana que para el caso del absorbedor debido a que la menor temperatura del vapor a la entrada del absorbedor (-5^{o}C) favorece el proceso de absorción. Finalmente se pudo confirmar que los módulos de membranas permiten reducir el peso y el tamaño de los equipos de absorción de forma muy significativa ya que proporcionan relaciones de carga térmica/volumen de hasta 10000 kW/m^3, significativamente mayores que las proporcionadas por los absorbedores de placas (2000 kW/m^3) o los de carcasa y tubos (300 kW/m^3).

ABSTRACT

Absorption refrigeration systems are a great alternative to the conventional compression refrigeration systems when a low-grade waste heat is available to drive the cycle. However, these systems have not been fully implemented in the market mainly due to their large size and cost, which is an important concern for the integration of the absorption systems in some applications where a great amount of low-grade waste heat is available, such as the transport sector.

In recent years, several research works have been done related to the use of polymeric materials in absorption cycles with the aim of reducing the size, weight and cost of these systems. Particularly interesting are those referred to the use of polymeric porous membranes in the absorber and desorber of the absorption systems due to the high surface/volume ratio provided by the membranes that enable to reduce the size and weight of the components in a very significant way. The vast majority of studies have been carried out for the water/lithium bromide mixture since the typically high working pressures of the ammonia/water mixture limits the use of polymeric materials. To face this problem, the use of the ammonia/water absorption-resorption technology could be a good solution thanks to the operation flexibility provided by these systems that enable to greatly decrease the working pressure by reducing the concentration of the ammonia/water solutions circulating in the absorption and resorption circuits. For this reason, the main objective of this thesis is to study the ammonia absorption process into ammonia/water solutions using polymeric porous membranes as contactors in order to be used in absorption-resorption refrigeration systems. In this way, more compact, lighter and cheaper thermally driven systems could be designed to expand the niche market of absorption refrigeration systems.

First, a study of the ammonia/water absorption-resorption refrigeration cycle was carried out and the determination of the operational pressure ranges was showed. Resorption systems provides a great flexibility but considering that a reduction in the high-pressure implies a decrease in the COP. A thermodynamic model was developed and used for a sensitivity analysis of the cycle. It was concluded that removing the rectifier after the generator lead into a lower complexity and cost of the system with low COP losses (less than 8%). This fact is a great advantage of absorption-resorption cycles compared to conventional absorption cycles. At the same time, the importance of the effectiveness of the solution heat exchanger in the resorption circuit was highlighted because if this effectiveness is lower than a certain limit value, not only the COP of the cycle is affected, but also the system cannot work at the previously set temperature conditions. Finally, adequate working conditions were suggested for the base case in order to obtain a good compromise between the reduction of high-pressure, COP and cooling capacity. Such operating conditions were used for the subsequent study of the ammonia absorption process using membrane modules as contactors.

Another thermodynamic model with external heat transfer was developed and used for studying the influence of the inlet temperatures of the external streams and the size of the heat exchangers (UA) on the cycle performance. Moreover, this model was also used for the analysis of the performance of a 25-kW ammonia/water absorption-resorption refrigeration plant set at Technische Universität Dresden (Germany) and it was determined that the absorption process in the resorber should be improved. From the experimental work carried out with the experimental plant, it is worth highlighting the difficulty of keeping the system operating under stable conditions. This problem was pointed out by several authors in previous studies. A

method based on the measurements of the ammonia concentration in the solution circuits using Near-infrared (NIR) spectroscopy was proposed to improve the performance of the plant.

Furthermore, a theoretical and experimental study of the adiabatic ammonia absorption process using a flat sheet membrane module as contactor was done. For this purpose, a test bench was designed and built, and a theoretical model was developed and validated with the experimental results. This model was used for a sensitivity analysis of the absorption process and for the determination of the main characteristics required of a polymeric membrane to be used as contactor in the ammonia absorption process. These characteristics are: hydrophobicity of the material, pore size between 0.03µm and 0.1µm, porosity higher than 40% and a membrane thickness lower than 400µm in order to obtain a low transport resistance across the pores of the membrane but at the same time keeping the mechanical robustness. This study constituted a novelty because these membrane characteristics were reported in the literature for the water/lithium bromide mixture but not for the ammonia/water working pair. The membrane characteristics previously determined were considered for the selection of a commercial cross-flow hollow fibre membrane module, which provides much higher surface-to-volume ratio and better mass transfer coefficient than the flat sheet membrane module. An experimental study of the adiabatic ammonia absorption process was carried out using the hollow fibre membrane module as contactor and the working conditions during the experiments were previously determined in the study of the ammonia/water absorption-resorption refrigeration cycle. The ammonia absorption rates obtained range between $5.4 \cdot 10^{-5}$ and $3.1 \cdot 10^{-4}$ kg/(m^2·s) for the experiments carried out at absorber working conditions (pressure between 1.3-1.5 bar and ammonia mass fraction between 0.29-0.32). In the case of the experiments done at resorber working conditions (pressure between 5.0-5.5 bar and ammonia mass fraction between 0.56-0.60) the absorption rate obtained range between $6.3 \cdot 10^{-5}$ and $9.7 \cdot 10^{-4}$ kg/(m^2·s). Furthermore, a two-dimensional model was developed and validated with the experimental results. This model was used to study the evolution of the temperatures, ammonia solution concentration and absorption rate in the axial and radial directions in the membrane module. This validated model was used as basis for a new two-dimensional model of a hollow fibre membrane absorber with heat exchanger integrated (HEXHFMA), which enable to design more compact and lighter absorbers and resorbers for the ammonia/water absorption-resorption refrigeration systems.

By means of the previously developed model, two HEXHFMA were designed to be used in the absorber and in the resorber of a 25-kW ammonia/water absorption-resorption refrigeration system. It is important to note that the integration of membrane modules in the resorber requires a modification of the configuration of the cycle, since the hot vapour stream from the generator must be cooled down before entering the membrane module of the resorber to avoid condensation of the water and pore blocking. In addition, the design of the HEXHFMA for the resorber requires 22% more membrane area than in the case of the absorber because of the much lower temperature of the vapour at the inlet of the absorber (-5ºC) enhance the absorption process in a very significant way. Finally, it was confirmed that using membrane modules allow to reduce the weight and size of the absorption systems since they provide heat duties per absorber volume up to 10000 kW/m^3, significantly higher than those provided by the plate absorbers (2000 kW/m^3) or shell and tube absorbers (300 kW/m^3).

CONTRIBUTIONS BY THE AUTHOR

Articles in scientific journals

- M.I. Barba, M. Berdasco, D. Salavera, M.S. Larrechi, A. Coronas, Implementing a method based on near infrared spectroscopy for the 'in-situ' determination of ammonia/water composition in an absorber test bench. *Journal of Physics: Conference Series (745), 2016, 032106.* doi:10.1088/1742-6596/745/3/032106.

- M. Berdasco, A. Coronas, M. Vallès, Theoretical and experimental study of the ammonia/water absorption process using a flat sheet membrane module, *Applied Thermal Engineering* 124 (2017) 477–485. doi:10.1016/j.applthermaleng.2017.06.027.

- M.I. Barba, M. Berdasco, D. Salavera, M.S. Larrechi, A. Coronas, A method based on near-infrared spectroscopy for the in-situ determination of the ammonia concentration in ammonia/water mixtures in an absorber test bench, *Talanta*. 175 (2017) 528–534. doi:10.1016/j.talanta.2017.07.083.

- M. Berdasco, A. Coronas, M. Vallès, Study of the adiabatic absorption process in polymeric hollow fiber membranes for ammonia/water absorption refrigeration systems, *Applied Thermal Engineering* 137 (2018) 594–607. doi:10.1016/j.applthermaleng.2018.04.004.

- M. Berdasco, M. Vallès, A. Coronas, Ammonia/water resorption heat pumps: theoretical study and determination of the optimal working conditions, *Energy* (in progress).

- M. Berdasco, A. Coronas, M. Vallès, Design of a hybrid heat exchanger-hollow fibre membrane absorber for the ammonia/water absorption-resorption refrigeration cycle, *Applied Thermal Engineering* (in progress).

- M. Berdasco, A. Coronas, M. Vallès, Study of the effect of the water content on the ammonia/water absorption process using polymeric membranes as contactors, *Applied Thermal Engineering* (in progress).

Communications in Congresses, Conferences, Seminars, Workshops and Symposia

- M. Berdasco, A. Coronas, M. Vallès, Estudio teórico-experimental del proceso de absorción de amoniaco en disoluciones de amoniaco-agua utilizando membranas porosas poliméricas: resultados preliminares. *Libro de Actas del IX Congreso Nacional de Ingeniería Termodinámica (9CNIT).* Cartagena, Spain, 3-5 June, 2015, (Oral presentation). ISBN: 978-84-606-8931-7.

- M. Berdasco, A. Coronas, M. Vallès, U. Hesse, C. Thomas, M. Grund, T. Weimer, Estudio del funcionamiento de sistemas de refrigeración por absorción-resorción con amoniaco-agua*. Libro de Actas del IX Congreso Nacional de Ingeniería Termodinámica (9CNIT).* Cartagena, Spain, 3-5 June, 2015, (Oral presentation). ISBN: 978-84-606-8931-7.

- M.I. Barba, M. Berdasco, D. Salavera, M.S. Larrechi, A. Coronas, Implementing a method based on near infrared spectroscopy for the 'in-situ' determination of ammonia/water composition in an absorber test bench. *7th European Thermal-Sciences Conference (EUROTHERM),* 19-23 June, Krakow, Poland, 2016, (Poster presentation).

- M. Berdasco, A. Coronas, M. Vallès, Theoretical and experimental study of NH3 absorption into ammonia/water solution using polymeric porous membranes. *Proceedings of the 12th International Conference on Heat Transfer, Fluid Mechanics and Thermodynamics (HEFAT).* Malaga, Spain, 11-13 July, 2016.

- M. Berdasco, A. Coronas, M. Vallès, Membrane absorber integration in absorption-resorption refrigeration systems. *6th International Seminar on Thermodynamic Engineering of Fluids.* Universitat Rovira i Virgili, 25th-26th July 2016, Tarragona, Spain, (Oral presentation).

- L.C. Mendoza, M. Berdasco, A. Coronas, J. Schiffmann, Theoretical study of a novel oil-free co-rotating scroll compressor integrated into a hybrid absorption heat pumps. *Proceedings of the 12th IIR Gustav Lorentzen Conference on Natural Refrigerants (GL2016),* Edinburgh, United Kingdom, August 21st-24th, 2016. ISBN: 9782362150180.

- M. Berdasco, A. Coronas, M. Vallès, U. Hesse, C. Thomas, M. Grund, T. Weimer, Theoretical study of the performance of an ammonia/water absorption-resorption refrigeration system. *Proceedings of the 12th IIR Gustav Lorentzen Conference on Natural Refrigerants (GL2016),* Edinburgh, United Kingdom, August 21st-24th, 2016 (Oral presentation). ISBN: 9782362150180.

- M. Berdasco, A. Coronas, M. Vallès, Study of the performance of three different polymeric porous membrane modules for NH3 absorption into NH3/H2O solution. *Proceedings of the Innovative Materials for Processes in Energy Systems 2016 (IMPRES 2016)*, Taormina, Italy, (Oral presentation). ISBN: 978-4-944005-21-5.

- M. Berdasco, A. Coronas, M. Vallès, Study of the adiabatic absorption process in polymeric hollow fiber membranes for ammonia/water absorption-resorption refrigeration systems. *Proceedings of the 9th World Conference on Experimental Heat Transfer, Fluid Mechanics and Thermodynamics (ExHFT-9),* Foz do Iguaçu, Brazil, 11-15 June 2017, (Oral presentation).

- M. Berdasco, A. Coronas, M. Vallès, Theoretical study of a hybrid membrane absorber–heat exchanger for the ammonia/water absorption-resorption cycle. *7th International Workshop on Thermodynamic Engineering of Fluids (7IWTEF)*, Universitat Rovira i Virgili, Tarragona, 24-25 July 2017, Spain (Oral presentation).

- M. Berdasco, A. Coronas, Absorption/resorption refrigeration systems working with ammonia/water mixtures: modelling and performance. *9ème édition du colloque francophone en énergie, environnement, économie et thermodynamique (COFRET2018), Strasbourg, 28-29 June 2018, France.* (Accepted).

Participation in projects

- Desarrollo de Nuevos Fluidos de Trabajo, Componentes y Configuraciones para Bombas de Calor de Absorción de Altas Prestaciones. Ministerio de Economía y Competitividad. Plan Nacional I+D+I (DPI2012-38841-C02-01). CREVER - Research Group of Applied Thermal Engineering. Tarragona (Spain), 01/01/2013 - 01/01/2016.

Internships

- **Technische Universität Dresden, Department of Refrigeration, Cryogenics and Compressor Technology, Faculty of Mechanical Engineering (Germany).**
  Advisor: Prof. Ullrich Hesse.
  Period: 1st April – 29th July 2015.
  Topic: Study of the ammonia/water absorption-resorption refrigeration systems.
  Grant: Ministerio de Economía y Competitividad. Ayudas a la movilidad predoctoral para la realización de estancias breves en centros de I+D españoles y extranjeros 2014. Ref: EEBB-I-15-10494.

LIST OF CONTENTS

LIST OF FIGURES

LIST OF TABLES

Chapter 1

Introduction, Objectives, Methodology and Structure of the Thesis

1.1 Introduction

Every part of our society depends on energy. The spread of the access to energy has improved the living conditions of people all around the world and this continuous increase in energy consumption, which is mainly based on fossil fuels, has caused that our society faces three fundamental problems: the global warming, the pollution and the strong dependency on a finite supply of fossil fuels. The European Union has taken very seriously the fight against these problems by the adoption of several directives focused on the need to use renewable energy sources and on the maximum harnessing of energy that reduces as much as possible the waste of resources.

Energy consumer sectors include the buildings, industry, and transport. Many large factories have optimized their energy consumption by the implementation of cogeneration and trigeneration systems. However, these systems have not been fully implemented in small and medium-sized enterprises (SMEs) due to their high cost. The high initial cost is also the main obstacle that has impeded a wide diffusion of systems that reduce the primary energy consumption in buildings. Recent Commission Recommendation (EU) 2016/1318 of 29 July 2016 [1] set that all new buildings in the European Union should be nearly zero energy buildings (NZEB) by the end of 2020, so the development of cost-effective systems that meet the cooling, heating and electricity demands of buildings becomes a very important issue.

Refrigeration industry plays a major role in today´s global economy. According to a recent report from the International Institute of Refrigeration (IIR), this sector consumes about 17% of the overall electricity used worldwide and is expected to grow further in the coming years because of increasing cooling needs in numerous fields and global warming [2]. Refrigeration is required in the vast majority of sectors, but it becomes crucial in food industry because refrigeration ensures optimal preservation of perishable foodstuffs and provides consumers with safe and healthy products. However, the food cold chain needs to be improved in order to reduce food waste and economic losses. According to IIR [2], food losses from the absence of refrigeration account for nearly 9% of the total food production in developed countries, and 23% on average in developing countries. The transport sector plays a very important role in maintaining the cold chain. This fact, together with the need to reduce the fossil fuels consumption, have produced a growing interest over the last years in developing compact and lightweight refrigeration systems that enable to reduce the fuel consumption by means of the harnessing of the waste heat generated in the engines.

Vapour-compression refrigeration systems, which are based on the reverse Rankine cycle, are the most commonly used systems for refrigeration purposes in the vast majority of sectors. Nowadays, the refrigerants typically used in the vapour-compression cycles are hydrofluorocarbons (HFCs) with no ozone depletion, but they are potent greenhouse gases (GHG). Although the vapour compression cycle is a well-known technology and provides very good performance, the rising cost of electricity and the need to reduce environmental impacts has renewed interest in thermally driven technologies, such as absorption refrigeration. Difference between both systems lies in the way how refrigerant vapour is compressed from the low-pressure to the high-pressure level. The absorption refrigeration systems do not use a mechanical compressor because the compression process is done by a “thermal compressor” (solution circuit) which consists mainly of an absorber, a solution pump, a generator and an expansion device. It is a well-known fact that the energy required for compressing a vapour is much higher than the energy required for pumping a liquid, so the mechanical/electrical energy consumption in the absorption cycle is almost negligible compared to the vapour-compression

cycle. The rest of the energy required for driving the absorption cycle is provided by a source of heat. Although the energy efficiency of the absorption systems is much lower than the vapour compression, when a low-grade waste heat is available for driving the absorption cycle these systems become a very interesting alternative. Moreover, absorption systems typically use natural refrigerants (such us ammonia/water) which means zero ozone depletion as well as zero-global warming potential.

Despite the advantages of using absorption refrigeration systems driven by low-grade energy sources, these systems have not been fully implemented in the industry, transport and tertiary sector compared to the vapour-compression systems. The main problem lies in the higher cost and size of the absorption systems, so developing more compact and cheaper absorption systems is a key factor to make the absorption technology cost competitive in the market. The size can be reduced by more compact designs of the main components. The cost is a function of the size and the assembly materials. The materials must be chemically resistant to the working fluid used and, at the same time, they must be mechanically resistant to the working pressure level of the system.

Two possible solutions are proposed in this thesis to face the problems of size and cost of the absorption refrigeration systems: First, the use of polymeric membranes as contactors between the vapour and the solution in the absorbers to solve the problem of the large size of the components in the cycle due to the high surface/volume ratio provided by the membrane modules. Using polymeric materials would also reduce the price of the absorption systems but these materials do not withstand the typically high working pressure of the absorption cycles. For this reason, the second solution proposed in this thesis consists in using the resorption technology to reduce the operating high-pressure of the conventional absorption refrigeration systems.

1.2 Resorption refrigeration systems: fundamentals

The concept of resorption is based on the following principles [3]:

- The working fluid is a zeotropic mixture (refrigerant/absorbent) with a large boiling temperature difference (typical of working fluids for absorption heat pumps).

- The conventional evaporating and condensing processes taking place at the evaporator and condenser are replaced by desorption and absorption processes at non-isothermal conditions (Lorentz Cycle) that take place in the desorber and in the resorber, respectively.

As the evaporation in the desorber of the zeotropic mixture is not complete, along with the vapor stream a residual solution stream is generated and returns to the resorber by means of a solution circuit called “resorption circuit”. The two pressure levels in the conventional reverse Rankine cycle are fixed by the condensing and evaporating temperatures, however in the resorption cycle there is an additional degree of freedom so the pressure levels can be varied, within certain limits, by changing the concentration of the working fluid mixture at fixed temperature values in the resorber and the desorber [4]. A very significant reduction of the high-pressure level in the system can be achieved just by decreasing the concentration of the refrigerant in the mixture, so that it opens up new possibilities for using cheaper assembly materials. In the same way, it is also possible to operate at the same pressure level of that of the conventional absorption cycle but at much higher working temperatures. All these advantages

make the resorption refrigeration systems a very interesting technological alternative that provide more flexible design options compared to vapour-compression or absorption systems.

1.2.1 Working fluids

The typical working pairs (refrigerant/absorbent) in resorption systems are water/lithium bromide and ammonia/water, both natural refrigerants with excellent thermophysical properties. Apart from the conventional working pairs, the mixture carbon dioxide/organic solvent has showed a very good potential to be used as working fluid in resorption systems.

Water/lithium bromide mixtures are typically used for air-conditioning applications (evaporation temperature above 5ºC). In this working pair, water is the refrigerant while the salt (LiBr) is the absorbent. The use of water/lithium bromide offers outstanding features such as the high enthalpy of vaporization of water and the non-volatility of the absorbent. The main drawbacks of this working pair are the corrosion, the crystallization problems at high temperature and high LiBr concentration and finally the complications associated to work under high vacuum conditions in the system. The addition of other salts to the conventional working fluid pair, such as LiI, $LiNO_3$, and LiCl, have been reported in the literature [5–7]. Some of these mixtures reduce in a very significant way the corrosion and crystallization problems.

Carbon dioxide meets all environmental requirements. It is non-toxic, non-flammable, abundantly available and inexpensive. However, conventional transcritical carbon dioxide-based refrigeration systems operate at ultra-high pressures (above 70 bar). In order to overcome this issue, the use of resorption technology with carbon dioxide/organic solvent as working pair enables to reduce the working pressure below 35 bar, thus becoming a very attractive alternative to the conventional working fluids due to the better technical performance [8].

Ammonia/water mixtures are typically used when deep low temperatures are needed and provide a wider operating range compared to the water/lithium bromide because it does not present crystallization problems under typical working conditions. In this working pair, ammonia is the refrigerant and water is the absorbent. There are some drawbacks that are important to mention: toxicity of the ammonia, high vapour pressure of the ammonia and problems related to the fact that both ammonia and water are volatile. In the case of the resorption cycles, problems related to the high ammonia vapour pressure and the volatility of the ammonia and water can be easily avoided (Chapter 2). For this reason, the ammonia/water mixture is the most widely used working pair in resorption cycles.

1.2.2 Types of resorption cycles

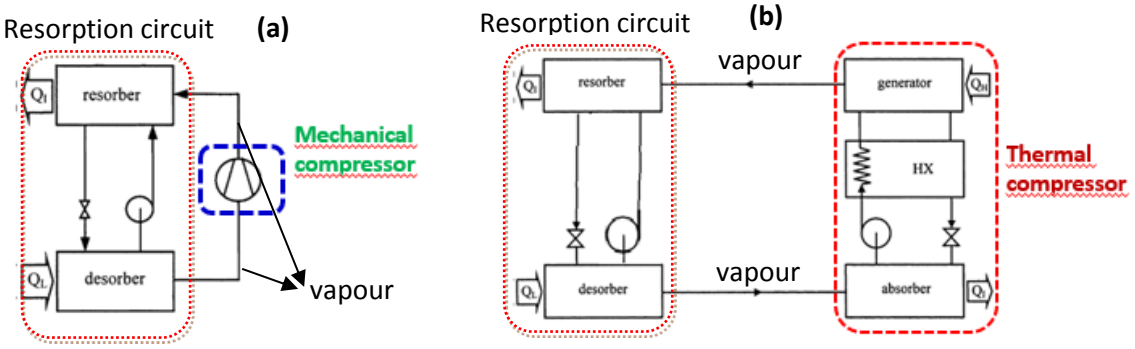

Figure 1.1 ***(a)*** *Compression-resorption system.* ***(b)*** *Absorption-resorption system.*

Resorption refrigeration systems can be classified as compression-resorption or absorption-resorption depending on how the compression process takes place: with a "mechanical compressor" or with a "thermal compressor", respectively. Figures 1.1a and 1.1b show a scheme of both configurations [3]. In order to improve the COP of such cycles, a solution heat exchanger is used for internal heat recovery. Figure 1.2 shows a scheme of the main components of the resorption circuit.

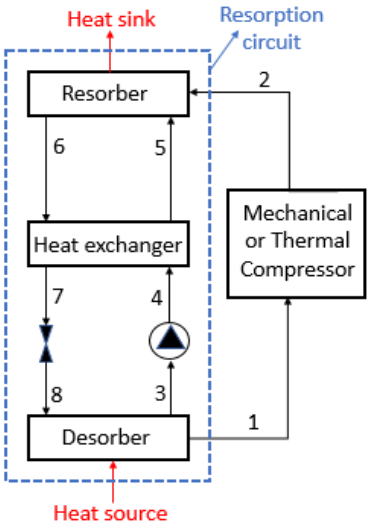

Figure 1.2 Scheme of the resorption circuit.

As mentioned before, ammonia/water is the most commonly used working pair in resorption cycles because many of the drawbacks associated to this mixture (high pressure and low relative volatility of ammonia and water) can be avoided thanks to the use of the resorption technology. Therefore, ammonia/water resorption systems are a very interesting option for heating at high temperatures, refrigeration at deep low temperatures, or heating and cooling simultaneously at high-temperature lift conditions. Some of the advantages of the resorption systems compared to the conventional absorption systems are summarized below:

- Can operate delivering heat at higher temperatures (resorber) or with higher temperature lift conditions.
- Can operate at lower high-pressures and lower pressure ratios.
- Better efficiencies due to the lower irreversibilities by the non-isothermal behaviour of the desorption and absorption processes when sensible heat sources and sinks are used [9].

In order to better understand all these advantages, the resorption circuit has been represented on the Dühring diagram (PTX) of the mixture ammonia/water (Figure 1.3). The state-points showed in Figure 1.3 correspond to those represented in the scheme of the resorption circuit of Figure 1.2. Figure 1.3a shows how a change in the concentration of the solution at constant high and low pressures can be used to achieve higher heat sink temperatures. In the case study showed in Figure 1.3a, the high-pressure is set at 20bar, the low-pressure at 2bar, the outlet temperature in the resorber (state-point 6) is 80^{o}C and the ammonia mass fraction of the solution leaving the desorber is 0.40 (state-point 3). By way of example, for the same high-

pressure value (20bar) the temperature in the resorber can be increased to 140ºC (state-point 6') just decreasing the ammonia mass fraction of the solution leaving the desorber to 0.10 (state-point 3').

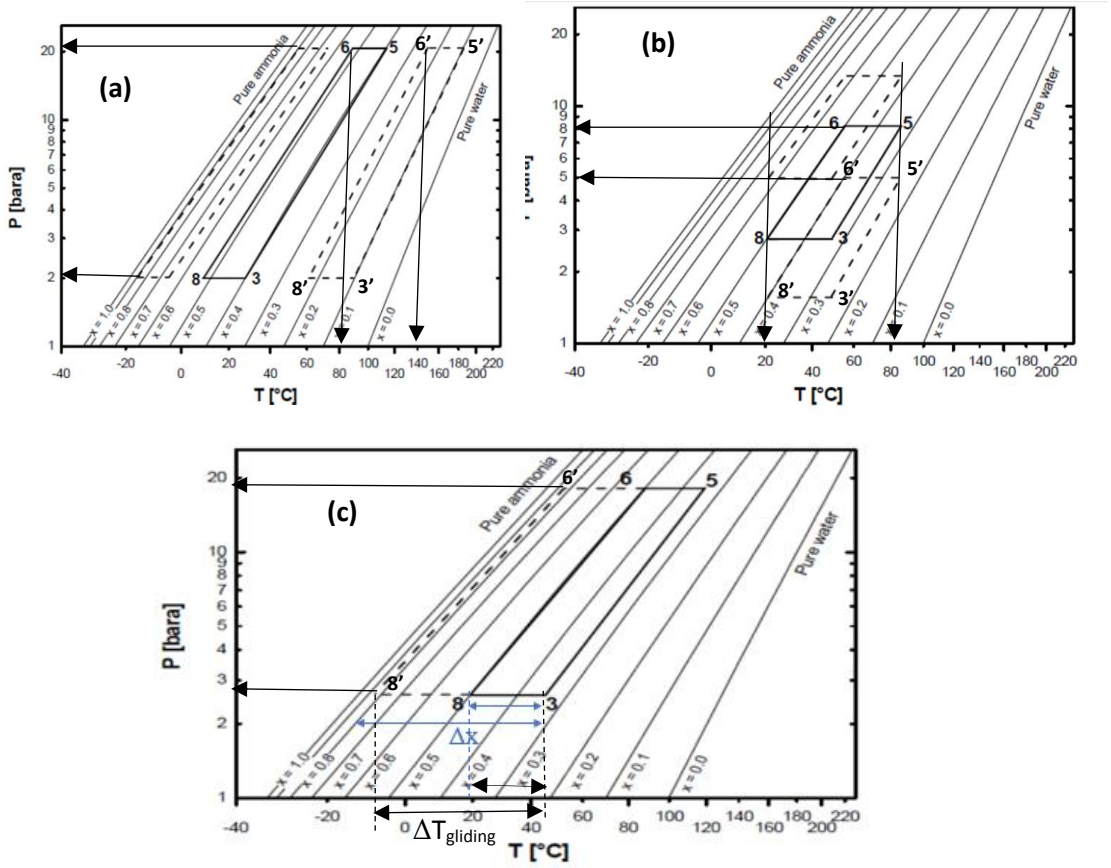

*Figure 1.3 Resorption circuit of Figure 1.2 represented on the PTX diagram of the ammonia/water mixture. Influence of the ammonia solution concentration on **(a)** Working temperatures; **(b)** Operating pressures; **(c)** Temperature glide in the desorber.*

On the other hand, Figure 1.3b shows how the operating pressures can be modified just changing the composition of the solution circulating between the resorber and the desorber at constant temperatures. In the example showed in Figure 1.3b can be observed how the high-pressure value is reduced from 8bar to 5bar just decreasing the ammonia mass fraction in the resorption circuit from 0.33 to 0.25. In the case of the compression-resorption systems, the compressor can be feed with lower or higher density vapour just decreasing or increasing the ammonia concentration of the solution, resulting in a capacity control of the system but keeping constant the compressor rotary speed. Moreover, reducing the pressure ratio in the compressor not only provides lower power consumption, but also reduces the compressor discharge temperature in a very significant way [3].

Finally, Figure 1.3c shows how the temperature glide in the desorber and resorber can be modified by changing the solution concentration difference (Δx) in the resorption circuit at constant high and low working pressures. The resulting temperature glides can be matched to the temperature glides of the heat source and heat sink streams, thereby reducing the exergetic losses by heat exchange. This may lead to improvements of the COP of the cycle. In the example showed in Figure 1.3c, the ammonia mass fraction of the solution in the desorber decreases

from 0.50 (state-point 8) to 0.35 (state-point 3), which corresponds to a temperature glide ($\Delta T_{gliding}$) of 25°C because the temperature of the solution increases from 20°C at the inlet to 45°C at the outlet of the desorber. However, this temperature glide can be doubled (from -5°C at the inlet to 45°C at the outlet of the desorber) just increasing the solution concentration difference (Δx) in the resorption circuit from state point 8' (ammonia mass fraction 0.80) to state-point 3 (ammonia mass fraction 0.35).

As a conclusion, the wide operation flexibility is one of the main strengths of the resorption systems because it allows to adjust the working temperatures and pressures to the application requirements.

1.2.3 Compression-resorption cycles

Compression-resorption cycles are also known in the literature with different names such as "Vapor compression cycles with solution circuit" [10], "compression/absorption hybrid cycles" [11] or "Osenbrück Cycle", because it was patented in 1895 by August Osenbrück [12]. As shown in Figure 1.2, vapour and liquid leaving the desorber are separated in two different streams; the vapour (stream 1) proceeds to the compressor and the liquid (stream 3) is re-circulated to the resorber by means of a solution pump. The compressed vapour (stream 2) is absorbed by the solution (stream 5) in the resorber. Finally, the enriched solution leaving the resorber (stream 6) returns to the desorber (stream 8), closing then the cycle.

In 1950 Altenkirch [13] carried out a theoretical study showing its large energy-saving potential. Since 1980, research activities in this technology have increased rapidly and several pilot plants have been built due to this potential and the additional need to replace the halogenated refrigerants in vapour-compression refrigeration systems. Despite the potential of efficiency improvement that the compression-resorption cycles offered compared to single fluid Rankine cycles, Altenkirch [14] pointed out that the superiority of the compression-resorption systems depends greatly on being able to make the driving temperature difference (pinch) in the resorber and desorber very small ($\Delta T << 10$°C) and on the use of countercurrent flow. An ammonia/water compression-resorption heat pump was designed and built by Stokar and Trepp [15] in order to study the performance of the cycle. The test plant was equipped with an oil-free compressor and it was able to heat water from 40 to 70°C and cool water from 40 to 15°C simultaneously. In that study, Stokar and Trepp showed the wide range of capacity control of the system by simply adjusting the composition of the solution in the resorption circuit. Finally, they also highlighted the improvement on the COP compared to the conventional Rankine cycles due to gliding temperatures in resorber and desorber.

Since 1995, the Institute for Energy Technology (Norway) has been doing research on industrial energy recovery and as a result, it was developed a 60-kW compression-resorption heat pump using ammonia/water as working fluid and standard components for the compressor and heat exchangers. It was designed and built to evaluate the performance and long-term operation consequences. The heat pump system was designed to simultaneously deliver heat at 95 °C and cooling at 5°C using waste heat of 50°C as a heat source, with a COP of 3.4 [16]. As a result of this research work, a pilot plant hybrid heat pump was installed in a Norwegian dairy factory and in the year 2004 the company Hybrid Energy AS was formed, providing commercial compression-resorption heat pumps to several companies mainly located in Denmark and Norway.

An experimental ammonia/water compression-resorption test facility was constructed and tested by Hewitt et al. [17]. They provided a detailed description of the start-up process and it

was highlighted the considerable scope for composition modulation of the working fluid and thus the capability to operate over a wide range of source and sink conditions. In 2013, Kim et al. [11] carried out an experimental study of the NH_3/H_2O compression-resorption heat pump. The aim of the study was to observe the characteristics of the heat pump system with respect to the ammonia concentration of the solution. They found an optimum composition of ammonia/water mixture (0.421) for the desired operating conditions (hot water production at temperatures over 90°C using heat source and sink at 50°C) and the system showed approximately 10 kW of heating capacity. They concluded that the composition of ammonia/water mixture for an initial charge of the system should be determined carefully considering a target temperature and capacity.

It is particularly interesting the case where the resorption system incorporates a "wet" compressor, which is able to perform a compression of the two-phase stream leaving the desorber, because in this way the resulting device has the same number of components as a conventional vapour-compression system, that is, two heat exchangers (desorber and resorber), a "wet" compressor and an expansion device. Another important advantage of the "wet" compression is the lubrication effect provided by the liquid inside the compressor, leading in a reduction of the discharge temperature. Following this concept, a carbon dioxide/organic solvent compression-resorption refrigeration system was patented by Spauschus and Hesse in the year 2000 [8]. The performance of this system showed a significant reduction of the working pressure (below 35 bar) and improved cooling capacities thanks to the resorption technology and the use of a scroll-compressor. Regarding the ammonia/water mixture there is still a lot of research work to do in order to design a "wet" compressor that can work under the cycle requirements [18].

1.2.4 Absorption-resorption cycles

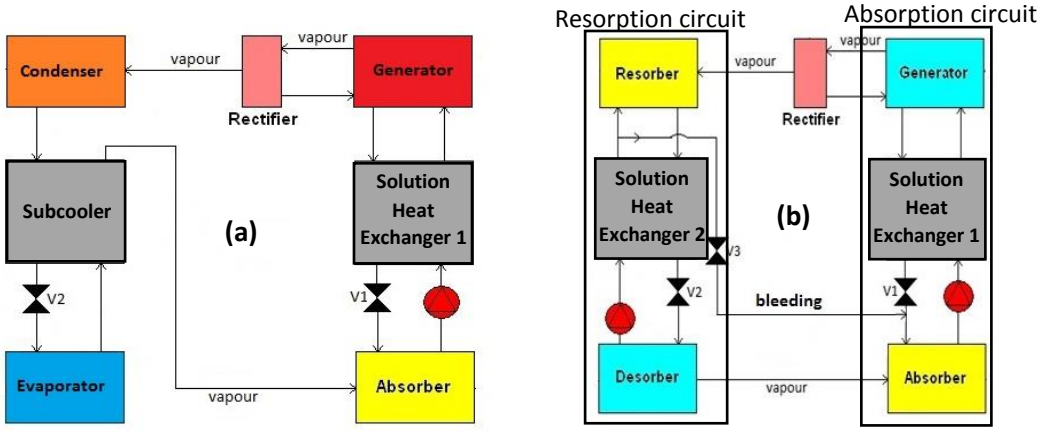

Figure 1.4 Comparison between the conventional NH_3/H_2O absorption cycle and the NH_3/H_2O absorption-resorption cycle. ***(a)*** *Absorption cycle.* ***(b)*** *Absorption-resorption cycle with rectifier and bleeding line.*

The absorption-resorption cycle was first proposed by Altenkirch in 1913 [19] and it can be considered as a modification of the conventional absorption cycle, where the condenser and the evaporator have been replaced by a second absorber called resorber and a second generator called desorber, respectively. Figure 1.4 compares both cycles: Figure 1.4a shows a scheme of the absorption cycle and Figure 1.4b a scheme of the absorption-resorption cycle, both working

with ammonia/water. Figure 1.4b shows that the absorption-resorption cycle consists of two solution circuits (absorption and resorption circuits), coupled to each other through two vapour streams.

As mentioned before, the main advantage of the absorption-resorption systems compared to the compression-resorption ones is the fact that they can be driven by low-grade heat with very small electrical consumption. Nevertheless, only if the heat required for driving the cycle is available at very low cost the absorption-resorption systems are cost competitive for refrigeration applications compared to the compression technology. This is because, at the same cooling capacity, the absorption-resorption systems consume seven times more heat compared to the electricity consumption of the compression refrigeration systems [20].

1.2.4.1 Theoretical studies of the absorption-resorption cycle

Most of the available references in the literature related to absorption-resorption systems correspond to theoretical studies and very few experimental works can be found. Baehr [21] studied the performance of the ammonia/water absorption and the ammonia/water absorption-resorption heat pumps for the heating of buildings. In that work, absorption-resorption was proposed in order to reduce the relatively high working pressures of the conventional ammonia/water absorption heat pumps. It was concluded that the advantage of having lower working pressure must be paid for by a reduction in the COP. Pande and Herold [22] described and modelled an ammonia/water absorption-resorption heat pump for high-temperature applications. They studied the effect of changes in solution mass flow rate, external streams inlet temperatures and heat exchangers size on the COP and heat capacity. Pande and Herold pointed out that the resorption cycle is unstable because any mismatch in the mass balance between both solution circuits tends to cause more mismatches, so it would be required an active control to maintain operation of the system under steady-state conditions. In practice, this problem could be solved by control devices such as liquid level, temperature or concentration measurements. Costiuc and Costiuc [23] presented a theoretical study of a solar-powered ammonia/water absorption-resorption refrigeration system. They analysed the performance of the cycle at different heat sources temperatures provided by the solar collector.

In their book, Herold et al. [24] studied the water/lithium bromide absorption-resorption refrigeration cycle and a UA-type thermodynamic model was developed. They pointed out the need of active controls to make the cycle operate stably. It was also suggested the possibility of using this kind of system as a component of more complex multi-stage cycles. A theoretical comparison between water/lithium bromide absorption and absorption-resorption cycles was done by Sabir and Eames [25]. They concluded that absorption-resorption cycle produces higher COPs than the conventional absorption cycle. This improvement can be explained because a better temperature matching of the internal and external streams results in a better system performance. This relative improvement was higher at lower chilled water temperature, so the use of absorption-resorption systems would be more interesting for refrigeration applications. Finally, in spite of the fact that in an absorption-resorption cycle there are two solution pumps, the pumping requirements are not doubled compared to the absorption cycle due to the smaller pressure difference between the low and high-pressure sides.

1.2.4.2 Absorption-resorption experimental plants

In the year 1994, a European Project entitle “Ammonia resorption refrigeration plant for chilled water production with district heating” was coordinated by the German company DEUTSCHE BABCOCK-BORSIG AG [26]. A 500-kW ammonia/water absorption-resorption refrigeration system was designed and tested to produce chilled water using district heating at very low

supply temperatures (80°C). The resorption system was planned to be installed in Berlin but the detail planning for the integration into the existing supply and consumer system showed that for a yearly operating time of less than 1000 h/a such an investment could not be justified from an economical point of view. Furthermore, a modified design for a refrigeration demand of 250-kW (at temperature below 0°C) was completed in order to be used in a food processing plant, where a yearly operating time of more than 5000 h/a seems to be possible and a cogeneration system with combustion motors should be installed. However, one more time the installation of the refrigeration unit was cancelled due to the high investment cost.

More recently, the German company Makatec GmbH, in collaboration with various research centres, designed and tested several ammonia/water absorption-resorption machines over the last years. One of them was a 1-2 kW experimental prototype presented by Helle et al. [27]. In that system, a cyclone and a packed column were used for phase separation after the generator and the desorber, respectively. In order to assure the continuous supply of fluid to the pumps, two reservoirs were installed downstream of the absorber and the resorber. The preliminary results of the performance of the system were presented and a maximum COP of 0.5 was obtained. The problems related to the process stability were pointed out, however they showed that a stable and reliable process is possible. They highlighted that further investigation must be done in order to develop an automatic control of the pumps and the bleeding.

Figure 1.5 80-kW ammonia/water absorption-resorption refrigeration plant delivered by Makatec GmbH to a chicken farm, Geflügelhof Zapf, in Gengenbach (Germany).

An 80-kW ammonia/water absorption-resorption plant was delivered by Makatec GmbH to a chicken farm, Geflügelhof Zapf, in Gengenbach (Germany). The resorption system is used for the cold production in a trigeneration plant, which provides all the energy requirements (heat, electricity and cold) of the farm. The trigeneration plant is fed with the gas generated in a wood gasification plant. A picture of the 80-kW absorption-resorption plant is showed in Figure 1.5 [20].

A 60-kW ammonia/water absorption-resorption refrigeration system was set up at the Institute of Combustion and Power Plant Technology of the University of Stuttgart (Germany). The refrigeration system is coupled to a flameless (flox-)burner system for combustion of various liquid fuels (mainly biogenic and low calorific fuels). The exhaust gases of the boiler drive the absorption-resorption refrigeration system, leading to a heat and cooling energy generation with low CO and NO emissions. A scheme of the test rig is shown in Figure 1.6.

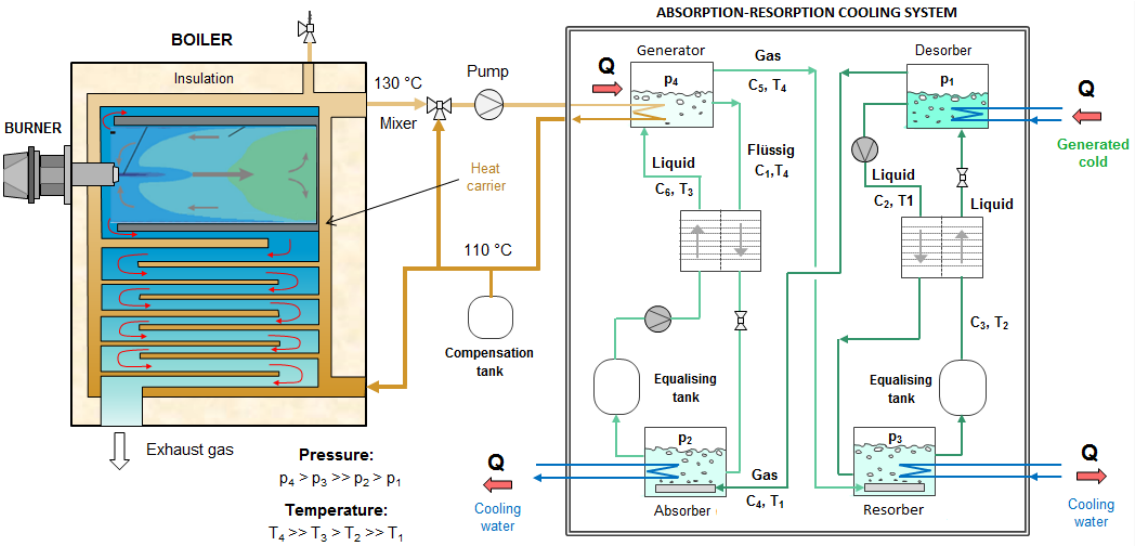

Figure 1.6 Scheme of the combined boiler/absorption-resorption cooling system. Source: Institute of Combustion and Power Plant Technology of the University of Stuttgart [28].

Grund et al. [29], in collaboration with Makatec GmbH, designed, built and tested a 25-kW absorption-resorption refrigeration plant with an attached ice storage system. All the start-up process is fully explained and ice production in the storage tanks was observed during the initial tests. The plant is located in the Zentrum für Energietechnik (ZET) of Technische Universität Dresden (Germany) and the experimental work is currently being carried out. A detailed description of the 25-kW absorption-resorption system is shown in Chapter 2 (section 2.3) because a research stay was done at TU Dresden in the frame of this thesis. There is also another ammonia/water absorption-resorption machine at TU Dresden with a smaller cooling capacity (1 kW). All the main components of the 1-kW absorption-resorption refrigeration plant (generator, absorber, desorber, and resorber) consist of a stainless-steel plate heat exchanger and a reservoir installed downstream of the heat exchanger to ensure the phase separation and a continuous supply of fluid to the pumps. In order to reduce the cost of the system some of the components of the test bench are made of plastic. A peristaltic pump was used for bleeding the solution from the resorption circuit to the absorption circuit. The system was designed to withstand a maximum working pressure of 3 bar and a picture of the test bench can be observed in Figure 1.7.

Figure 1.7 1-kW ammonia-water absorption-resorption plant set at TU Dresden [20].

Ammonia/water absorption-resorption refrigeration systems have been much less studied and developed than the compression-resorption systems, probably due to the difficulty of keeping the system working under steady-state conditions that was pointed out by several authors. Another disadvantage is the bigger size of the absorption-resorption systems due to the higher number of components in the cycle. This fact makes the study of more compact designs for the absorber/desorber a very important task.

1.3 Polymeric materials in absorption cycles

In recent years, several research works have been done related to the use of polymeric materials in absorption cycles, particularly for the use of polymeric membranes as contactors in the absorber and desorber of water/lithium bromide absorption refrigeration systems. The use of polymeric membranes in this field has a very high potential for reducing the size and weight of the modules but keeping a large surface area. These advantages make polymeric membrane modules as great candidates for being used in absorption refrigeration systems in order to design more compact, lighter and cheaper systems. There is a wide variety of polymeric membrane contactors typically used in the industry. However, hollow fibre membrane and plate-and-frame/flat sheet membrane modules are the types mostly investigated as membrane-based components in the absorption refrigeration systems [30]. According to the literature, the hollow fibre membrane module allows more efficient mass transfer due to the external transverse flow but it also provides higher pressure drops compared to the plate-and-frame/flat sheet membrane module [30]. That is why hollow fibre membrane modules have been mainly selected as contactor for the ammonia/water absorption systems and the plate-and-frame/flat

sheet membrane contactor for the water/lithium bromide absorption systems. Figure 1.8 shows three schemes of commercially available microporous membrane modules typically used for filtration applications. Figure 1.8(a) shows a scheme of a plate and frame membrane module provided by Alfa Laval. It consists of several flat sheet membranes individually stacked between plates. Figure 1.8(b) shows a picture of a hollow fibre membrane module provided by Daicen Membrane Systems. It consists of a hollow fibre bundle inside of a housing. Fluids can flow both inside and over the outside the hollow fibres. Finally, Figure 1.8(c) depicts a scheme of a spiral wound membrane module provided by Fujifilm.

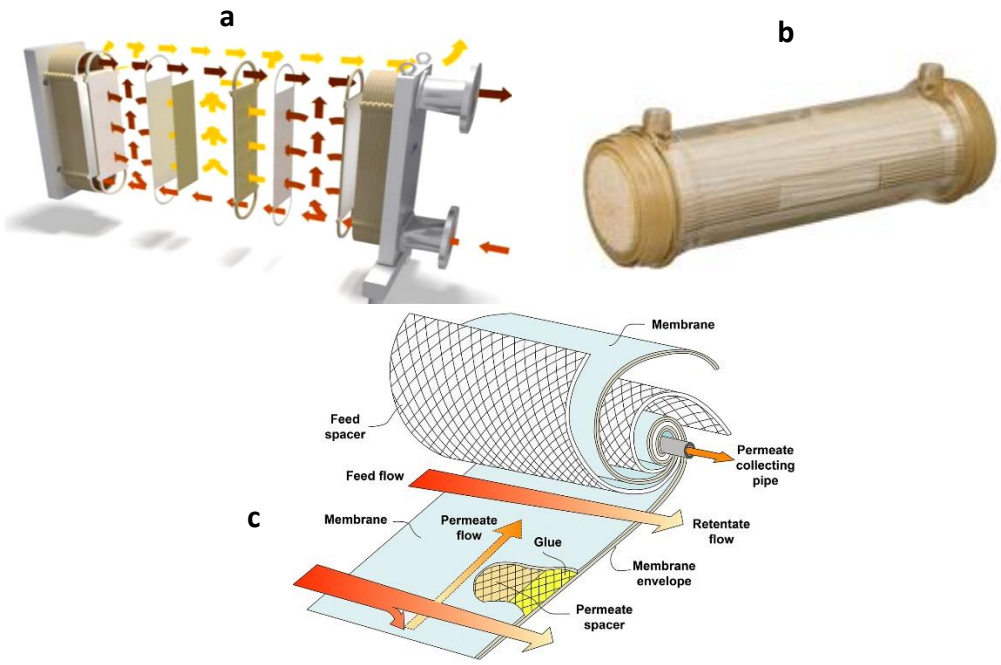

Figure 1.8 Pictures/schemes of commercially available membrane modules typically used for filtration applications. ***(a)*** *Alfa Laval M39 Plate-and-frame membrane module.* ***(b)*** *Daicen Membrane Systems FS03 Hollow Fibre membrane module.* ***(c)*** *Fujifilm Spiral wound membrane module.*

1.3.1 Polymeric membrane contactors used in water/lithium bromide absorption systems. Literature review

Several authors have studied the absorption and desorption processes of the water/lithium bromide working mixture using membrane contactors. Ali and Schwerdt [31] experimentally and theoretically determined the desired membrane characteristics for absorption chiller applications of the water/lithium bromide mixture: high permeability to the refrigerant (water vapour), hydrophobic to the aqueous solution with a high liquid entry pressure to avoid wettability of the membrane pores and no capillary condensation of water vapour to prevent the pores from blocking. For practical use, the membrane should have a thin hydrophobic microporous active layer up to 60µm thick, mean pore sizes around 0.45µm and a porosity of up to 80%. In a subsequent study, Ali [32] designed a compact plate-and-frame absorber with a hydrophobic microporous membrane contactor. The results clearly indicate that the aqueous solution channel thickness is the most significant design parameter affecting the compactness of the absorber. Furthermore, the study showed that the countercurrent cooling water flow with the aqueous solution has a positive effect on the absorber compactness. Yu et al. [33] developed

a theoretical model and studied the performance of a membrane-based absorber for potential use in water/lithium bromide absorption refrigeration systems. They concluded that the solution film thickness is the critical parameter affecting the absorption rate, consequently a constrained thin film absorber design was proposed. They also pointed out that increasing the solution velocity enhances the absorption rate by bringing fresher layers of the solution to the vapour for absorption. Wang et al. [34] studied at lab-scale the application of vacuum membrane distillation to a lithium bromide absorption refrigeration system using a hollow fiber membrane module made of polyvinylidene fluoride (PVDF) as a desorption device. They concluded that feed temperature has the greatest effect on the water vapour permeation flux, followed by vacuum pressure in the permeation side and, finally, the feed flux. Finally, they proposed that PVDF hollow fibre membrane modules could be used as a traditional generator or as a secondary generator to enhance the COP of the whole system.

Isfahani et al. [35] went one step further and studied the efficacy of highly porous nanofibrous membranes in membrane-based absorbers and generators. An experimental plant with all the main components present in the absorption refrigeration systems (evaporator, absorber, generator, and condenser) was set up. Absorption and desorption rates were significantly higher than those of conventional falling film absorbers and generators. More recently, Asfand et al. [36] carried out a CFD simulation to investigate heat and mass transfer processes in a membrane-based absorber for water/lithium bromide absorption cooling systems. The absorber consists of a plate-and-frame absorber module incorporating membrane contactor at the solution-vapour interface. They found an optimum value of 0.5 mm for the solution channel thickness and a solution inlet velocity of about 0.005 m/s was recommended to achieve high absorption rates with acceptable pressure drop along the solution channel. In a subsequent study, Asfand et al. [37] showed that the membrane characteristics have a less prominent effect on the absorption rate and the solution resistance is dominant in refrigerant mass transfer in the case of thicker solution channels, so that the selection of appropriate membrane characteristics should be made taking into account the solution channel thickness. In accordance with the results obtained in their previous study, a solution channel thickness of about 0.5 mm was considered appropriate to avoid a higher pressure drop in the solution channel and because the effect of membrane characteristics is low when the solution channel thickness is in the range of 0.5 mm. Finally, Asfand et al. [38] studied (by CFD simulations) the heat and mass transfer processes in the membrane-based absorber with no conventional working pairs in order to cope with the limitations of the conventional water/lithium bromide working pair (thermal instability, crystallization and corrosion problems). The working pairs and applications selected were H_2O/(LiBr + LiI + $LiNO_3$ + LiCl) for air-cooled systems and H_2O/($LiNO_3$ + KNO_3 + $NaNO_3$) for multi-stage high-temperature heat source absorption cooling systems. Very promising results were obtained in terms of absorption rate for H_2O/(LiBr + LiI + $LiNO_3$ + LiCl) and lower pressure drops in the case of H_2O/($LiNO_3$ + KNO_3 + $NaNO_3$) because of the higher operating pressure.

Venegas et al. [39] presented a model for optimizing the geometry and operating conditions of the lithium bromide/water membrane absorber under typical operating conditions of absorption cooling chillers. A microporous membrane was proposed in combination with rectangular microchannels in the absorber of an absorption chiller with the aim of reducing the size of this cooling technology. These authors pointed out the importance of reducing the solution film thickness in order to improve the absorber performance and reduce their size. For maximizing the ratio between the cooling capacity of the chiller and the absorber volume, it was not recommended using very long channels because the increase of the absorber size is higher than the increment obtained in the cooling power. Finally, they reported a maximum value of

the ratio between the cooling capacity of the chiller and absorber volume of 1090 kW/m^3, more than twice the one obtained using falling film absorbers of conventional diameter tubes. In a subsequent study, Venegas et al. [40] determined the most important parameters (in decreasing order of importance) in the design stage of the membrane absorber: porosity and pore diameter of the membrane, solution channel depth, thicknesses of the membrane and the interface wall between the solution and the cooling water, solution channel width and cooling water channel depth. Their conclusions were in good agreement with those presented by Ali and Schwerdt [31]. Finally, Venegas et al. [41] compared the performance of adiabatic and non-adiabatic membrane-based rectangular micro-absorbers for water/lithium bromide absorption chillers. As expected, the results provided by the models showed that the non-adiabatic absorber performs better in terms of pressure potential (subcooling), absorption rate, and cooling power along the membrane module because the absorption heat is extracted by the cooling water and the solution is continuously cooled. However, they also pointed out that adiabatic configuration combined with pre-cooling using ambient air has significant advantages respect to the non-adiabatic one in terms of a higher ratio between cooling capacity and absorber volume (kW/m^3) and fabrication simplicity.

1.3.2 Polymeric membrane contactors used in ammonia/water absorption systems. Literature review

The use of membrane contactors in absorption and desorption processes for the ammonia/water absorption cycle has been much less studied than in the case of water/lithium bromide, probably due to the fact that the pressure conditions of the ammonia/water absorption cycle is not favourable for the use of polymeric materials. As far as the author concerns, there are no available studies in the literature concerning the use of membrane contactors for the desorption process of the ammonia/water mixture, whereas with regard to the absorption process only two references were found. One of these studies was carried out by Chen et al. [42], that developed a unidimensional model to study the performance of a hybrid absorber-heat exchanger device using hollow fibre membranes (HFMAE) for application to the ammonia/water absorption heat pump. The HFMAE absorber proposed utilized porous fibres for the heat and mass transfer between the solution and the vapour phase, while nonporous fibres were used for the heat transfer between the solution and the cooling fluid. The performance of the HFMAE absorber in a typical ammonia/water absorption refrigeration cycle was compared to the performance provided by a plate heat exchanger falling film type absorber (PHEFFA). They concluded that the HFMAE absorber provided higher absorption performance than PHEFFA absorber due to its vast interfacial area. The study also highlighted that the only significant factor affecting the performance of the HFMAE absorber was the solution mass transfer. Finally, it was also concluded that applying the HFMAE absorber increases by 14.8% the COP of the refrigeration cycle and reduces the overall exergy loss by 26.7%.

In his doctoral thesis, Schaal [43] carried out several lab-scale experiments in order to study the absorption process of the ammonia vapour into ammonia/water solutions using microporous membranes as contactors. Three different prototypes of hollow fibre membrane absorbers were tested under typical absorber conditions of an ammonia/water absorption refrigeration plant. The hollow fibre membranes were made of polypropylene in all cases, but the pore diameter, number of fibres, packing density, housing material, length of the module and thickness of the fibres were different for each module. The hollow fibre membrane modules designed and built for the study were tested under adiabatic conditions because no cooling channels were

integrated inside the membrane module. Two parallel flow configurations were tested during the experiments:

- Gas flowing inside the hollow fibres and solution supplied to the shell side. This configuration could lead to lower absorption rates if there is a wide gap between the hollow fibre bundle and the housing. Then, this flow configuration requires an optimal design and construction in order to avoid this issue.

- Solution flowing inside the hollow fibres and ammonia gas through the shell side. This configuration provided higher pressure drops than the previous one.

Schaal pointed out that the pressure control in the gas and liquid sides is a key parameter during the absorption process in order to avoid liquid breakthroughs when the pressure in the liquid side exceeds the gas pressure by the so-called *breakthrough pressure*. The breakthrough pressure depends on the surface tension and the pore size of the membrane. Small pore sizes increase the breakthrough pressure. When liquid breakthroughs occur, the liquid blocks the pores and the absorption rate drops or even stops.

The main advantage of the membrane absorbers over other technologies such as plate or shell and tube absorbers is that they are smaller and lighter because the membranes have higher surface areas per volume unit. This advantage was pointed out and quantified by Schaal [43] by achieving stable operation in an ammonia/water absorption refrigeration plant with a membrane-based absorber integrated in the system. The membrane absorber was placed in parallel with a plate absorber in order to compare the performance of both configurations. It was showed that membranes can reduce the absorber size up to 10 times more than plate absorbers and 100 times more than shell and tube absorbers. The operating capability of membrane absorbers was then demonstrated but the need of designing a membrane absorber with heat exchanger integrated was also pointed out in order to obtain a more compact designs.

Unlike in the case of the water/lithium bromide, neither of the two mentioned studies determined the characteristics required for a membrane in order to be used as contactor in the ammonia/water absorption process. Such important membrane characteristics as porosity, pore diameter or thickness are required to be studied to select the adequate membrane contactor available in the market before starting the experimental work.

As mentioned before, the major drawback for using polymeric materials in ammonia/water absorption refrigeration systems is the typically high working pressure that impedes its use in the components of the high-pressure side of the cycle (the generator and the solution heat exchanger). That is why the studies carried out in this field were only focused in the absorber, because the pressure in this component is the lowest one in all the absorption refrigeration system. For this reason, the use of resorption technology becomes particularly interesting because the reduction of the pressure enables the integration of polymeric materials in all the components of the cycle. By way of example, the German company Makatec GmbH developed a polymer-based heat exchanger for substitution of the solution stainless steel HEX in the ammonia/water absorption-resorption cycle. The spiral winding in combination with spacers creates flow channels in a pressure resistant design (up to six bar) and provides a heat exchanger thermal capacity of 3 kW/K. Figure 1.9 shows a picture of the device [20].

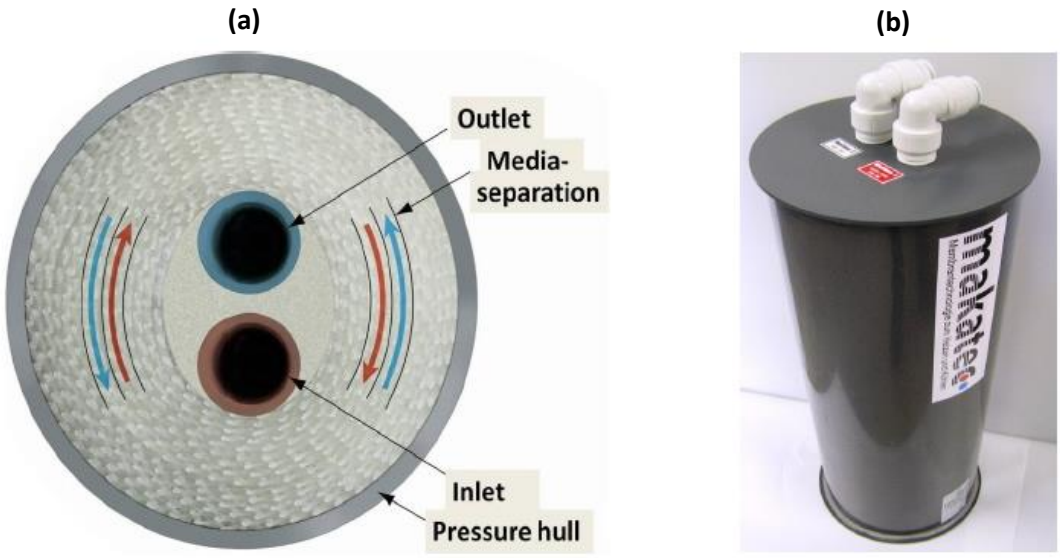

Figure 1.9 Polymer-based heat exchanger developed by Makatec GmbH. ***(a)*** *Inside view (from the top).* ***(b)*** *External view.*

1.4 Objectives, thesis structure, and methodological approach

As have been reported in previous sections, ammonia/water absorption-resorption refrigeration systems are a very interesting technological option that make possible to achieve a very significant reduction of the high-pressure level compared to the conventional absorption systems, so that it opens up new possibilities for using cheaper assembly materials (such as polymers) in the main components. Furthermore, the absorption-resorption systems can be driven by low-grade energy sources, so the electrical consumption would be much lower compared to the vapour-compression technology. However, the large size and cost of the absorption-resorption systems are their main handicaps.

In turn, membrane absorbers have been studied in recent years in order to be used as an alternative to the conventional plate or shell and tube absorbers typically used in absorption refrigeration systems. The use of polymeric membrane modules in this field has a very high potential for reducing the size and weight of the modules but keeping a large surface area. These advantages make possible to design more compact, lighter and cheaper absorbers. Therefore, the aim of this research work is to study the ammonia absorption process using polymeric membranes as contactors in order to be used in ammonia/water absorption-resorption refrigeration systems.

1.4.1 Specific objectives

To reach the above-mentioned objective, the more specific objectives were raised as follows:

- Study of the ammonia/water absorption-resorption refrigeration cycle and suggest an adequate operating condition for the base case selected that take advantage of the strengths of the absorption-resorption cycles.

- Determination of the main characteristics required for the membrane in order to be used as contactor for the ammonia/water absorption process.

- Experimental and theoretical study of the adiabatic ammonia/water absorption process using a commercial membrane module as contactor. Validation of the model with the experimental results.

- Use the theoretical model previously validated as a basis for developing a theoretical model of a hybrid membrane absorber-heat exchanger.

- Design two hybrid membrane absorber-heat exchanger: One for the absorption circuit and the other one for the resorption circuit of the ammonia/water absorption-resorption refrigeration cycle.

1.4.2 Thesis structure and methodological approach

The thesis was composed of the following chapters:

CHAPTER 1 is dedicated to explaining the background and justifications of this research that raise the motivation and objectives of this thesis. The fundamentals of the resorption technology, a literature review and a compilation of the ammonia/water absorption-resorption experimental plants available in several research centres/companies were presented. Finally, literature review related to the use of membrane contactors in absorption refrigeration systems was showed.

CHAPTER 2 is dedicated to study the ammonia/water absorption-resorption refrigeration system. The different configurations of the cycle (with or without rectifier) are described and it is showed how the operating pressure range can be determined when the working temperatures are previously fixed. A thermodynamic model of the cycle is described and used for determining the influence of the pressure, the effectiveness of the heat exchangers and the presence/absence of the rectifier on the performance of the cycle. This theoretical study is also used for suggesting an adequate operating condition for the base case previously set. Furthermore, another thermodynamic model with external heat transfer (A-type model) is described for studying the influence of the temperatures of the external streams and the UA values of the heat exchangers on the performance of the cycle, low-pressure level, cooling capacity and gliding temperature in the desorber. Furthermore, a description of a 25-kW ammonia/water absorption-resorption experimental plant set at TU Dresden is included and its performance is analysed by means of the thermodynamic model. Finally, a new method based on near-infrared spectroscopy for the “in-situ” determination of the ammonia concentration in ammonia/water mixtures is described and proposed to be used as an alternative to improve the performance of the absorption-resorption plants.

CHAPTER 3 is dedicated to study the ammonia/water absorption process using a flat sheet membrane module. The heat and mass transfer process in the adiabatic flat sheet membrane module is investigated experimentally and analytically. Moreover, a detailed description of the experimental test bench used is shown in this chapter. On the other hand, a unidimensional model was validated with the experimental results and used to evaluate the influence of the temperature, concentration, flow rate and membrane characteristics on the absorption process. The conclusions obtained about the characteristics required for the membrane to be used as contactor for the ammonia absorption process will be taken into account for the selection of the commercial hollow fibre membrane module used in Chapter 4.

CHAPTER 4 is dedicated to study the ammonia/water absorption process using a hollow fibre membrane module. The experimental work was carried out in the test bench described in

Chapter 3. A novel two-dimensional model was developed and validated with the experimental results. This model was used as a basis for the model developed in Chapter 5.

CHAPTER 5 is dedicated to study the integration of the heat exchanger in the hollow fibre membrane module (hybrid membrane absorber-heat exchanger). A new two-dimensional model of a hybrid membrane absorber-heat exchanger was developed and used for the specific design of an absorber and a resorber for the ammonia/water absorption-resorption refrigeration system.

CHAPTER 6 gives the general conclusions and future outlooks regarding the study reported in this thesis. The future outlooks provide suggestion for future research directions.

In order to better understand the thesis structure, Figure 1.10 illustrates the methodological approach followed for the development of the thesis. This figure shows how results from previous chapters are used as inputs of following chapters.

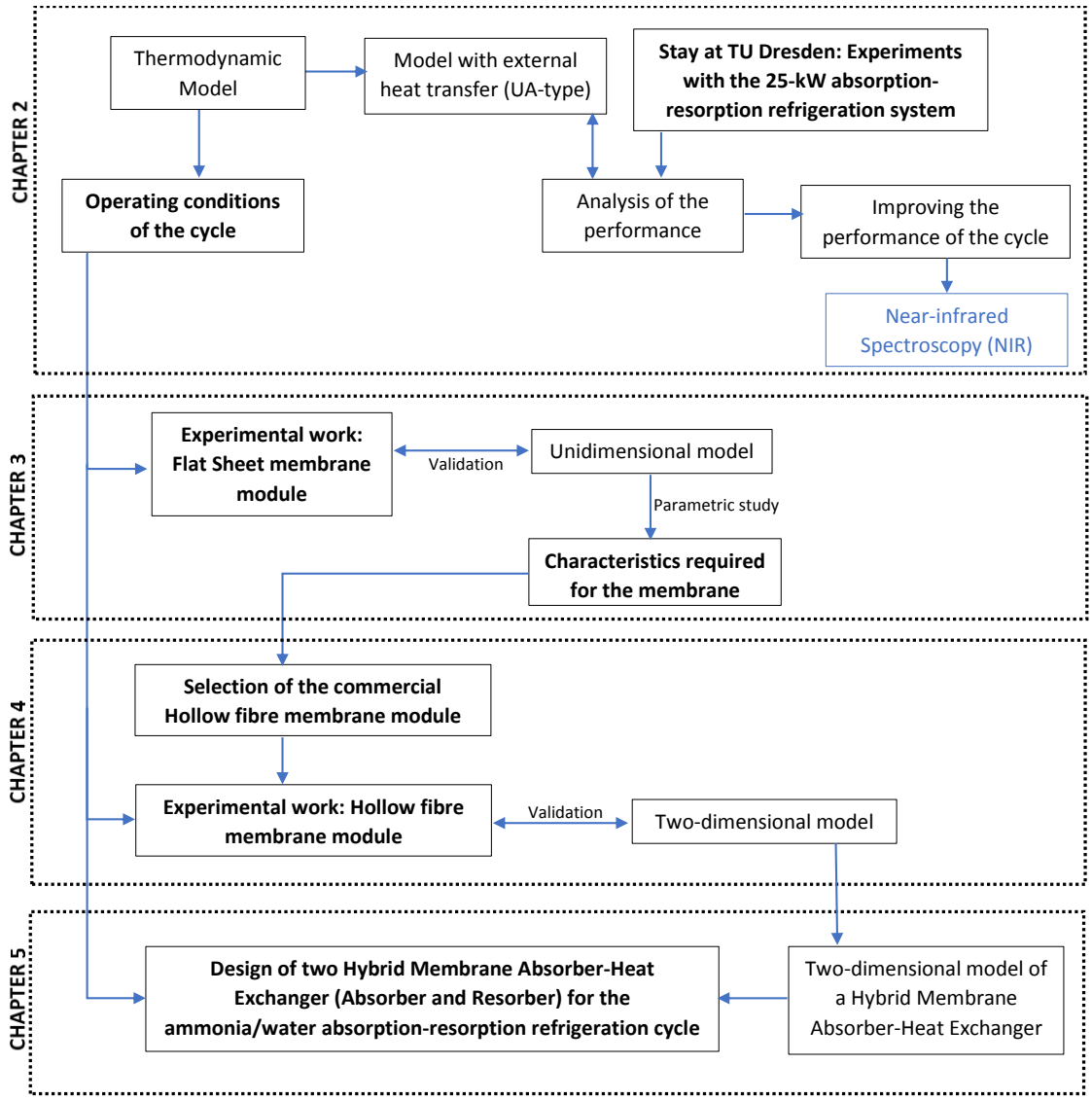

Figure 1.10 Methodological approach

Chapter 2

Study of the Ammonia/Water Absorption-Resorption Refrigeration Cycle

The aim of this chapter is to study the ammonia/water absorption-resorption refrigeration cycle. For that purpose, the first step is to describe the cycle emphasizing specially the wide operation flexibility provided by the resorption technology in terms of reduction of the high-pressure. The determination of the operational high and low-pressure ranges at fixed working temperatures is explained in detail and the influence of such temperatures on the operational pressure ranges was also studied. Two thermodynamic models of the ammonia/water absorption-resorption refrigeration cycle were developed. The first model considers only the internal variables of the cycle and it was used for studying the influence of the effectiveness of the solution heat exchangers, the presence/absence of the rectifier and the operational pressure ratio on the performance of the cycle. The base case for the theoretical study was selected from the typical working conditions of the ammonia/water absorption-resorption refrigeration systems. Finally, adequate operating conditions are suggested for the base case that enables to harness the strengths of the absorption-resorption refrigeration cycle.

The second thermodynamic model considers the external heat transfer (UA-type) on the main thermal components, so a study of the effect of the temperature of the external streams and the size of the heat exchangers on the performance of the cycle was done. This model was also used to analyse the experimental performance of a 25-kW absorption-resorption refrigeration plant operating in a test bench at Technische Universität Dresden (Germany). Finally, some modifications in the plant were suggested for improving the performance and control.

2.1 Configuration of the ammonia/water absorption-resorption refrigeration cycle

Figure 2.1a shows the scheme of an absorption-resorption refrigeration cycle while Figure 2.1b represents the main state points of the cycle on the PTX diagram of the ammonia/water mixture. As mentioned in the previous chapter, the cycle consists of two solution loops (the absorption circuit and the resorption circuit) coupled to each other through two vapour streams. Regarding the absorption circuit, the ammonia vapour stream (vapour 2) coming from the desorber (DES) is absorbed by the inlet ammonia/water solution (state-point 4) in the absorber (ABS). This absorption process is exothermic and in order to maintain the absorption potential, the heat generated during the absorption process is transferred to an external fluid (usually water or air). The solution rich in ammonia leaving the absorber (state-point 1) is then pumped to the high-pressure side by means of a solution pump (P1). This rich solution is pre-heated in the solution heat exchanger 1 (SHX1) before entering to the generator (GEN), where heat is supplied by an external heat source to desorb the ammonia. The ammonia vapour produced (vapour 1) is sent to the resorber (RES) and the remaining solution (poor in ammonia) leaves the generator (state-point 3) and is sent back to the absorber. Before entering the absorber, the poor solution 1 is cooled down in the SHX1 by the rich solution 1 and then passes through the expansion valve (V1) where it undergoes an abrupt reduction in pressure to the state-point 4. The aim of including an internal heat recovery by means of a solution heat exchanger is to increase the COP of the cycle.

Regarding the resorption circuit, the vapour coming from the generator (vapour 1) is absorbed by the poor solution (state-point 6) in the resorber, releasing heat to an external cooling fluid. The rich solution leaving the resorber (state-point 7) is cooled down by the poor solution in the solution heat exchanger 2 (SHX2) and throttled in the expansion valve (V2). This rich and cold solution (state-point 8) enters to the low-pressure desorber, where heat is supplied by an external load in order to desorb the ammonia. The ammonia vapour released in the desorber

(vapour 2) is then absorbed in the absorber by the poor solution of the absorption circuit (state-point 4), closing the cycle.

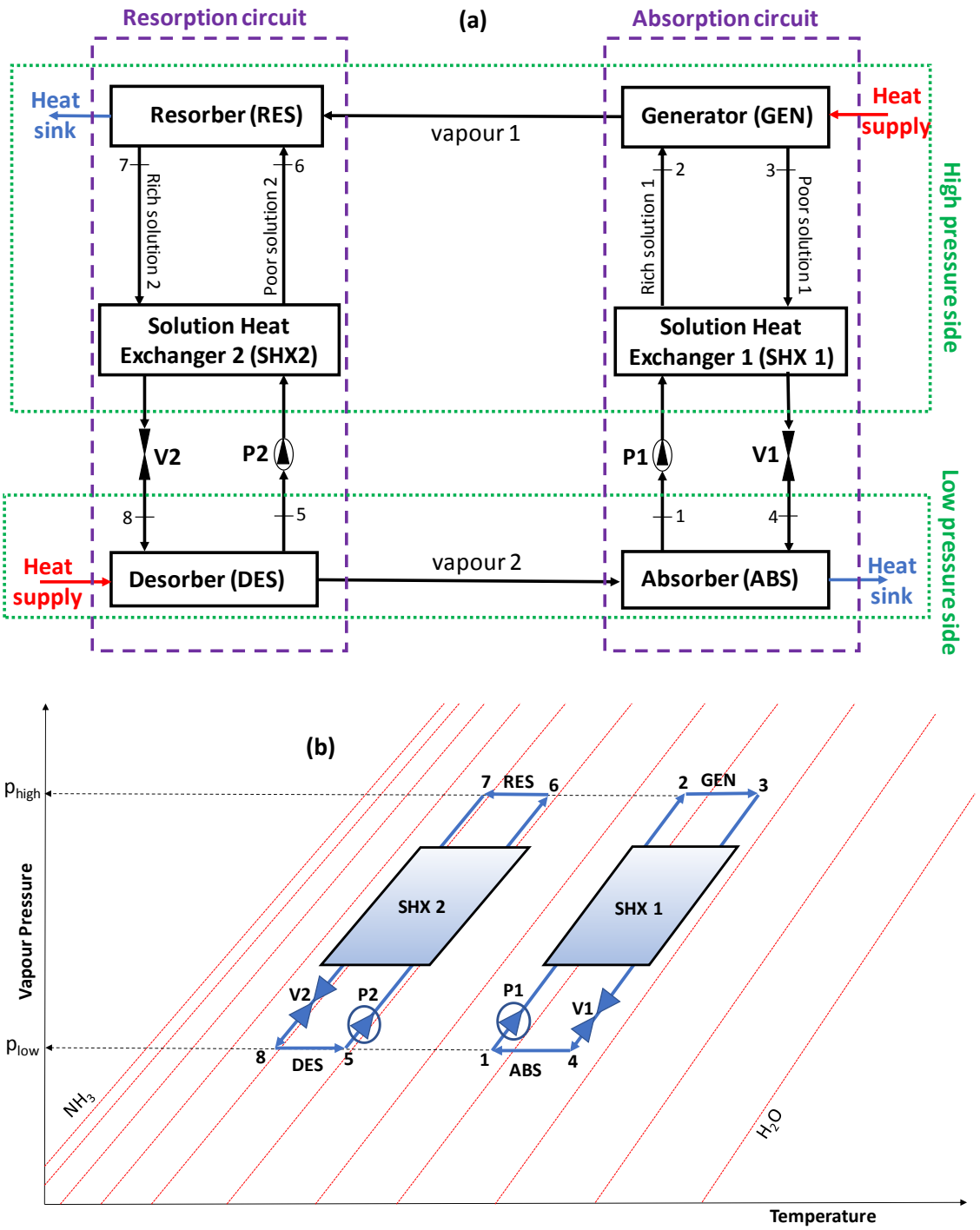

Figure 2.1 ***(a)*** *Scheme of the absorption-resorption cycle.* ***(b)*** *Absorption-resorption cycle on the PTX diagram of the ammonia/water mixture.*

In the conventional ammonia/water absorption cycle is necessary to incorporate a rectification stage after the generator in order to purify the vapour in ammonia, otherwise an excessively high-temperature glide in the evaporator would take place. However, absorption-resorption

cycles do not have this limitation because the vaporization is partial, so the gliding temperature can be chosen. As shown in Figure 2.1a, there are two vapour streams in the absorption-resorption cycle; one leaving the generator (vapour 1) and the other one leaving the desorber (vapour 2). The ammonia concentration and mass flow rate of these vapour streams are different because they are generated under different conditions. At the typical working conditions (pressure, temperature and composition) of the cycle, the concentration of water in vapour 1 is higher than in vapour 2. As a result of this, the water content in the resorption circuit is continuously increasing which leads to a slow depletion of the solution concentration in the resorption circuit. For this reason, it would be necessary to equilibrate the mass balance between both circuits in order to keep the system running under the desired working conditions. Three solutions are possible:

- Use a rectification stage after the generator in order to obtain the same concentration in vapour 1 than in vapour 2. This option implies some limitations that we should take into account. Depending on the working conditions of the cycle, the required temperature in the rectifier could be lower than the temperature provided by the external fluid used for cooling the rectifier. If this happens, another refrigeration system is needed for reducing the temperature of the refrigeration fluid. In these situations, rectification is not a good choice.

- Another option is the use of a “bleeding” or mixing pipe for connecting both solution circuits, thus the excess of water from the resorption circuit can be transferred to the absorption circuit. The bleeding flow is transferred from the high-pressure side of the resorption cycle to the low-pressure side of the absorption cycle. Thus, for the transportation of the solution no additional pump is required. This option is the best from an economical and design point of view because the rectifier is removed. However, an accurate control of the concentrations in the circuits is required in order to regulate the bleeding mass flow rate and avoid the system to drift away from its thermodynamic point of operation.

- The third option is a combination of the previous ones. The rectification stage after the generator is remained in the system but always with the bleeding line as a backup (Figure 1.4b), otherwise the operating range of the cycle would be limited by the temperature of the cooling water in the rectifier. From an economic point of view, this option is the worst because the number of components is increased respect the other options, but the control of the system would be easier.

A deeper study about the influence of the presence/absence of the rectifier on the COP can be found in section 2.2.2.3.

2.2 Thermodynamic model of the absorption-resorption cycle

This section describes the thermodynamic model used for studying the performance of the ammonia/water absorption-resorption system. This model considers only the internal variables of the cycle and it was used for analysing the influence of the effectiveness of the solution heat exchangers, the cycle configuration (presence/absence of the rectifier) and the pressure ratio on the performance of the cycle. According to the results obtained in this section, an adequate operating condition (pressure, ammonia concentration and solution mass flow rates) is suggested for the base case that enables to harness the strengths of the absorption-resorption refrigeration cycle.

A scheme of the configuration of the absorption-resorption cycle considered for the model is shown in Figure 2.2. It can be observed that the configuration selected includes the rectifier and the bleeding line. This configuration was selected in order to study the influence of the rectifier on the performance of the cycle.

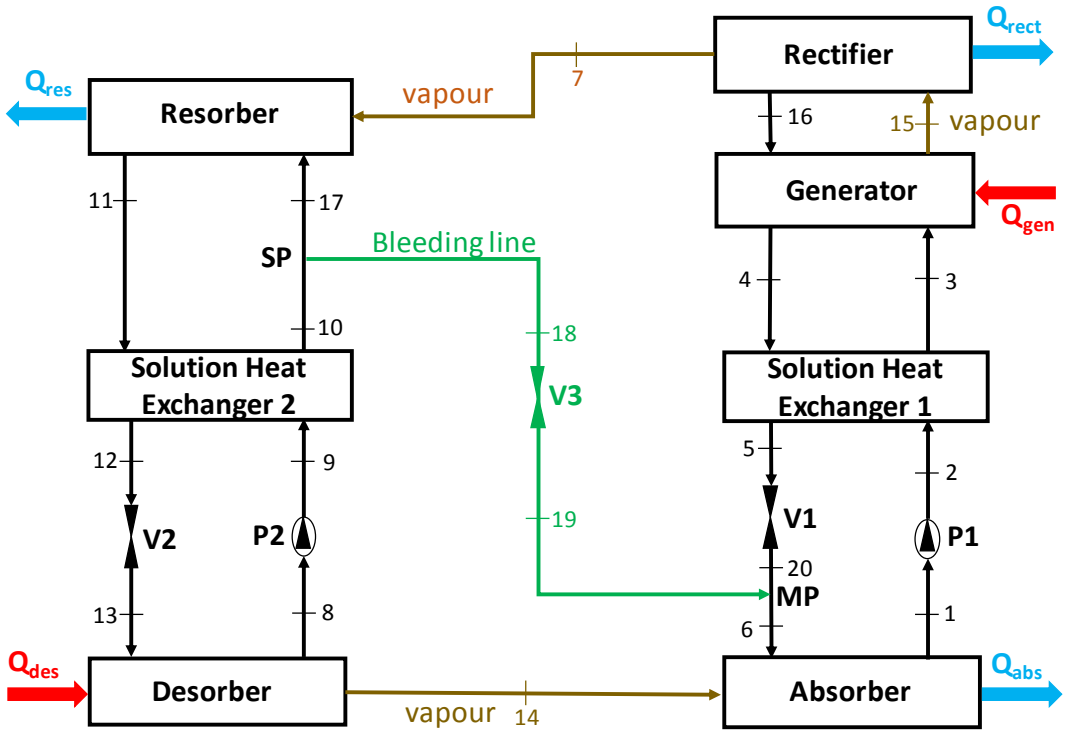

Figure 2.2 Absorption-resorption cycle with rectifier and bleeding line.

The thermodynamic model was developed using Engineering Equation Solver (EES) and is based on the mass and energy balances on each component of the cycle. The thermodynamic properties of the ammonia/water mixture were determined using the EES database [44]. Equations 2.1, 2.2 and 2.3 show the total mass balance, the ammonia mass balance and the energy balance in the desorber, respectively.

$$m_{13} = m_8 + m_{14} \tag{2.1}$$

$$m_{13} \cdot x_{13} = m_8 \cdot x_8 + m_{14} \cdot x_{14} \tag{2.2}$$

$$Q_{des} + m_{13} \cdot h_{13} = m_8 \cdot h_8 + m_{14} \cdot h_{14} \tag{2.3}$$

Equations 2.4 and 2.5 show the total and ammonia mass balances in the combined generator-rectifier unit, while Equations 2.6, 2.7 and 2.8 show the total mass balance, ammonia mass balance and energy balance in the rectifier. Equation 2.9 shows the energy balance in the generator while Equations 2.10 and 2.11 show the energy balance in the absorber and resorber, respectively.

$$m_3 = m_4 + m_7 \tag{2.4}$$

$$m_3 \cdot x_3 = m_4 \cdot x_4 + m_7 \cdot x_7 \tag{2.5}$$

$$m_{15} = m_{16} + m_7 \tag{2.6}$$

$$m_{15} \cdot x_{15} = m_{16} \cdot x_{16} + m_7 \cdot x_7 \tag{2.7}$$

$$m_{15} \cdot h_{15} = Q_{rect} + m_{16} \cdot h_{16} + m_7 \cdot h_7 \tag{2.8}$$

$$Q_{gen} + m_3 \cdot h_3 + m_{16} \cdot h_{16} = m_4 \cdot h_4 + m_{15} \cdot h_{15} \tag{2.9}$$

$$m_6 \cdot h_6 + m_{14} \cdot h_{14} = Q_{abs} + m_1 \cdot h_1 \tag{2.10}$$

$$m_{17} \cdot h_{17} + m_7 \cdot h_7 = Q_{res} + m_{11} \cdot h_{11} \tag{2.11}$$

Power consumption in the solution pumps of the absorption and resorption circuits are shown in Equations 2.12 and 2.13, respectively. Equations 2.14 and 2.15 show the effectiveness and the energy balance in the solution heat exchanger of the absorption circuit, respectively. Equations 2.16 and 2.17 show the effectiveness and the energy balance in the solution heat exchanger of the resorption circuit. The equations for the effectiveness of the solution heat exchangers (Equations 2.14 and 2.16) are written supposing that the streams with lower ammonia concentration (poor solution) are limiting the heat transfer.

$$W_{P1} = m_1 \cdot v_1 \cdot \left(p_{high} - p_{low}\right) \tag{2.12}$$

$$W_{P2} = m_8 \cdot v_8 \cdot \left(p_{high} - p_{low}\right) \tag{2.13}$$

$$Eff_{shx1} = \frac{(T_4 - T_5)}{(T_4 - T_2)} \tag{2.14}$$

$$m_2 \cdot (h_3 - h_2) = m_4 \cdot (h_4 - h_5) \tag{2.15}$$

$$Eff_{shx2} = \frac{(T_{10} - T_9)}{(T_{11} - T_9)} \tag{2.16}$$

$$m_9 \cdot (h_{10} - h_9) = m_{11} \cdot (h_{11} - h_{12}) \tag{2.17}$$

Regarding the bleeding line, the following equations are required. Equation 2.18 corresponds to the mass balance in the split point (SP) of the stream 10. Equations 2.19 and 2.20 show the total and ammonia mass balances between both solution circuits, while Equations 2.21, 2.22 and 2.23 correspond to the total mass, ammonia mass and energy balances in the mixing point (MP) of the absorption circuit.

$$m_{10} = m_{18} + m_{17} \tag{2.18}$$

$$m_7 = m_{14} + m_{18} \tag{2.19}$$

$$m_7 \cdot x_7 = m_{14} \cdot x_{14} + m_{18} \cdot x_{18} \tag{2.20}$$

$$m_{19} + m_{20} = m_6 \tag{2.21}$$

$$m_{19} \cdot x_{19} + m_{20} \cdot x_{20} = m_6 \cdot x_6 \tag{2.22}$$

$$m_{19} \cdot h_{19} + m_{20} \cdot h_{20} = m_6 \cdot h_6 \tag{2.23}$$

Finally, Equation 2.24 shows the coefficient of performance (COP) of the refrigeration cycle expressed as the ratio between the refrigeration load and the energy inputs.

$$COP = \frac{Q_{des}}{Q_{gen} + W_{P1} + W_{P2}} \tag{2.24}$$

The following assumptions were considered [22] for modelling the cycle:

- Heat losses/gains in the components are negligible.
- The cycle operates at steady-state conditions.
- Pressure drops in piping and components are not considered except on the throttling devices.
- The flow arrangement of solution heat exchangers is countercurrent.
- The solution streams leaving the desorber, absorber, generator, rectifier, and resorber are saturated.
- Pumping processes are isentropic and expansion processes in valves are isenthalpic.
- The vapour stream exits the generator at equilibrium conditions with the inlet solution (countercurrent flow arrangement).
- The vapour stream exists the desorber at equilibrium conditions with the outlet solution (parallel flow arrangement).

Finally, the number of independent variables of the cycle must be specified. Applying the method described in Ayou et al. [45], it was determined that 10 independent variables should be chosen as an input data to close the cycle. The variables selected were:

- The outlet temperature of the solution in the generator (T_{gen}), desorber (T_{des}), absorber (T_{abs}), resorber (T_{res}), and rectifier (T_{rect}).
- The high and low-pressure levels in the system (p_{high} and p_{low}).
- The volumetric flow rate of the solution pump (P2) of the resorption circuit.
- The effectiveness of the solution heat exchangers 1 and 2.

2.2.1 Operational high and low-pressure ranges in the ammonia/water absorption-resorption cycle

In the conventional absorption cycle, the low and high-pressures are dependent of the temperature in the evaporator (T_E) and condenser (T_C), respectively. However, in the case of the absorption-resorption cycle there is a range of working pressures that can be chosen for the same temperatures of the heat sources just varying the ammonia concentration of the solution circulating in both solution circuits. This fact can be clearly observed using the PTX diagram of the ammonia/water mixture for representing the operating conditions of the cycle. Figure 2.3a depicts the conventional absorption cycle. Once the temperatures in the condenser and evaporator are set, the high and low-pressure values are thus determined by the cut-off point of the temperature and the line of 100% ammonia mass fraction. In the case of the absorption-resorption cycle, for the same working temperatures, there is a wide variety of cycles working at different pressures and concentrations. Figure 2.3b depicts three of these cycles. The number of all possible cycles are limited within a range that can be determined. The determination of these operational pressure ranges is a very useful tool for the study of the cycle.

Figure 2.4a represents the absorption-resorption cycle on the PTX when T_{abs}, T_{res}, T_{des} and T_{gen} are fixed. T_{abs} is considered to be equal to T_{res} and x_{abs}, x_{res}, x_{des} and x_{gen} are the ammonia mass fractions of the solutions leaving the absorber, resorber, desorber and generator, respectively. The maximum value of the high-pressure ($p_{high,max}$) corresponds to the vapour pressure of the ammonia at T_{res}, which means that pure ammonia is leaving the resorber. The minimum value of the high-pressure ($p_{high,min}$) corresponds to the vapour pressure of the water at T_{gen}, which means that pure water is leaving the generator. When the high-pressure is set to a certain value (p_{high}), the low-pressure (p_{low}) can in turn vary between $p_{low,lower}$ and $p_{low,upper}$ (Figure 2.4a).

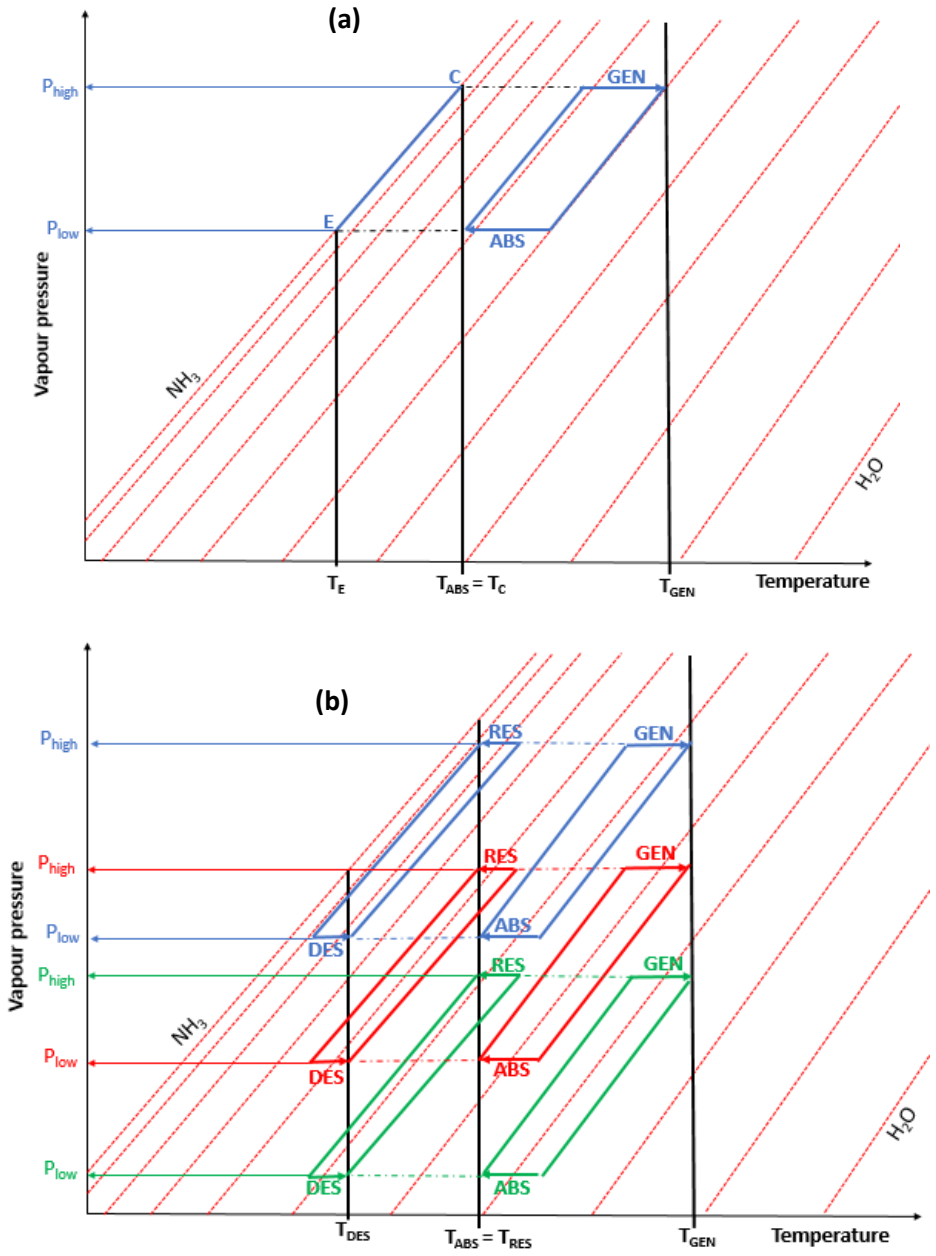

Figure 2.3 PTX diagram of the ammonia/water mixture. Absorber (ABS); Desorber (DES); Generator (GEN); Resorber (RES); Condenser (C) and Evaporator (E). ***(a)*** *Absorption cycle for a fixed temperature levels of the heat sources.* ***(b)*** *Some of the possible absorption-resorption cycles for the same temperature levels.*

$p_{low,lower}$ is obtained when the ammonia concentration in both streams of the absorption circuit are equal ($x_{abs}=x_{gen}\rightarrow\Delta x_{abs}=0$), i.e., there are no absorption/desorption processes in the absorption circuit. $p_{low,upper}$ is obtained when the ammonia concentration in both streams of the resorption circuit are equal ($x_{res}=x_{des}\rightarrow\Delta x_{res}=0$), i.e., there is no absorption/desorption processes in the resorption circuit. Figure 2.4b show the operational high and low-pressure ranges obtained when $p_{low,lower}$ and $p_{low,upper}$ are calculated all over the range of p_{high}. Thus, the yellow-coloured area of Figure 2.4b represents all the possible combinations of p_{high} and p_{low} for a certain value of T_{abs}, T_{res}, T_{des} and T_{gen}.

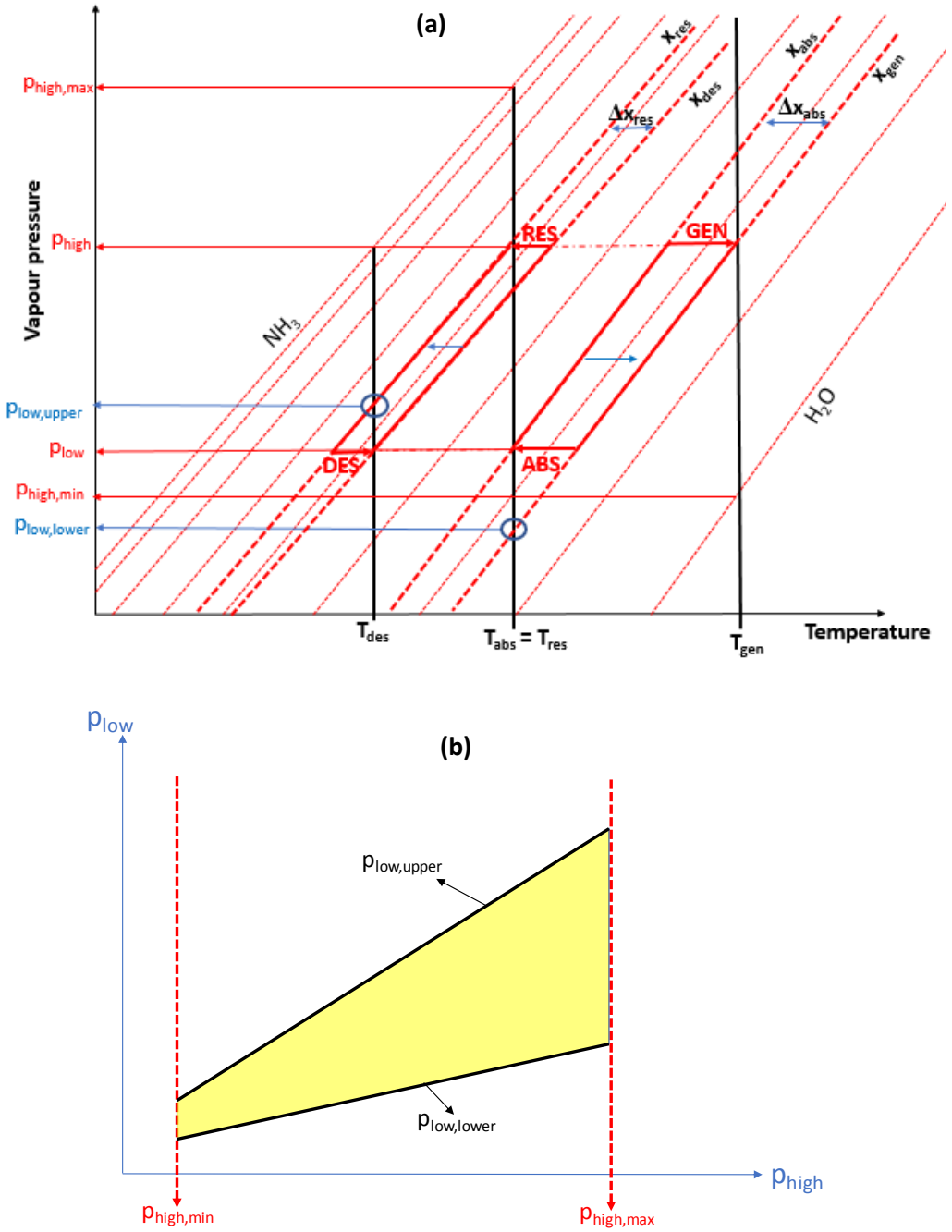

Figure 2.4 ***(a)*** *Determination of* $p_{low,lower}$ *and* $p_{low,upper}$ *on the PTX diagram.* ***(b)*** *Representation of the operational high and low-pressure ranges.*

2.2.2 Sensitivity analysis of the performance of the cycle

A sensitivity analysis of the performance of the cycle was carried out. First, the influence of the temperatures of the heat sources on the operational pressure ranges was evaluated. Secondly, it was studied the effect of the effectiveness of the solution heat exchangers, the pressure ratio and the presence of the rectifier on the COP.

2.2.2.1 Influence of the temperature of the heat sources on the operational pressure ranges

The operational pressure ranges previously shown can be modified when the temperature values of any of the main components of the cycle are changed. The working temperatures

selected as base case were: T_{gen}= 80ºC, T_{des}= -5ºC, T_{abs}=T_{res}= 25ºC. Figure 2.5a shows the influence of T_{des} on the operational pressure ranges. It can be observed that the higher is the value of T_{des} the wider is the range because $p_{low,upper}$ increases. In order to explain this effect, Figure 2.5b depicts the cycle on the PTX diagram. When T_{des} increases to T'_{des}, then $p_{low,upper}$ increases to $p'_{low,upper}$.

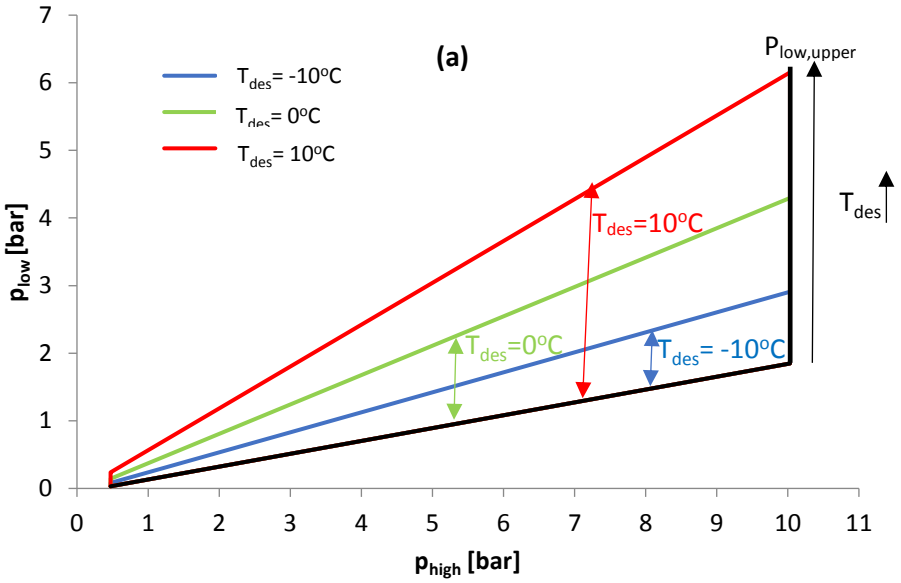

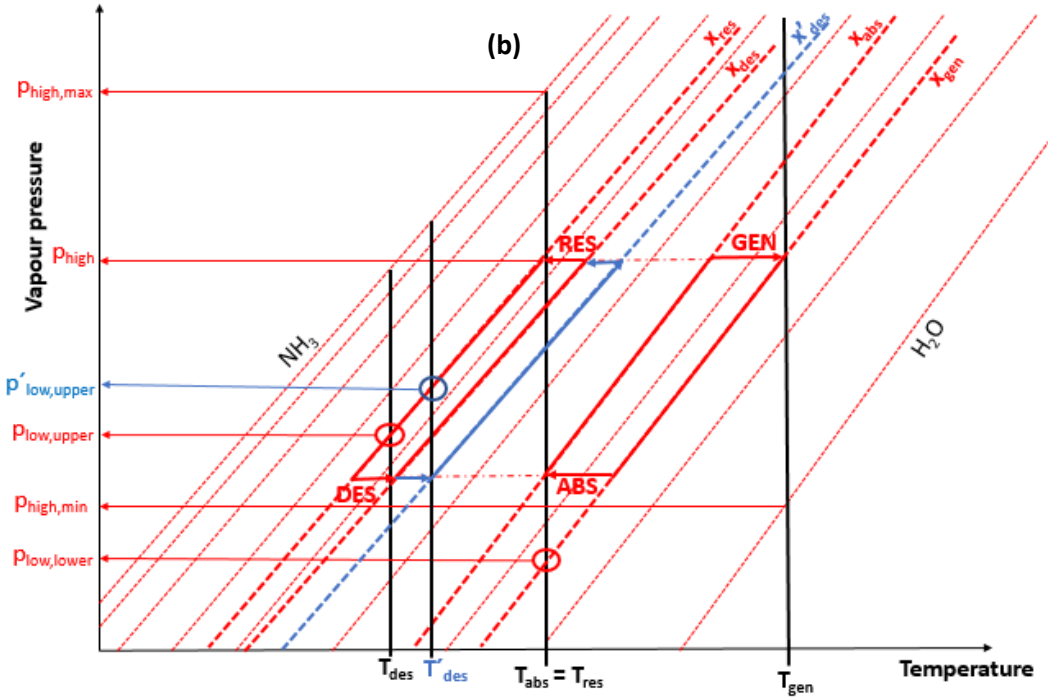

Figure 2.5 ***(a)*** *Influence of T_{des} on the operational pressure ranges (T_{gen}=80ºC; T_{res}=T_{abs}=25ºC).* ***(b)*** *Influence of T_{des} depicted on the PTX diagram.*

Figure 2.6a shows how the operational pressure ranges change with the value of T_{gen}. Increasing T_{gen} means $p_{high,min}$ is higher, but at the same time $p_{low,lower}$ decreases, leading to a bigger

operational pressure range area. Figure 2.6b depicts the cycle on the PTX diagram when T_{gen} increases to T'_{gen}.

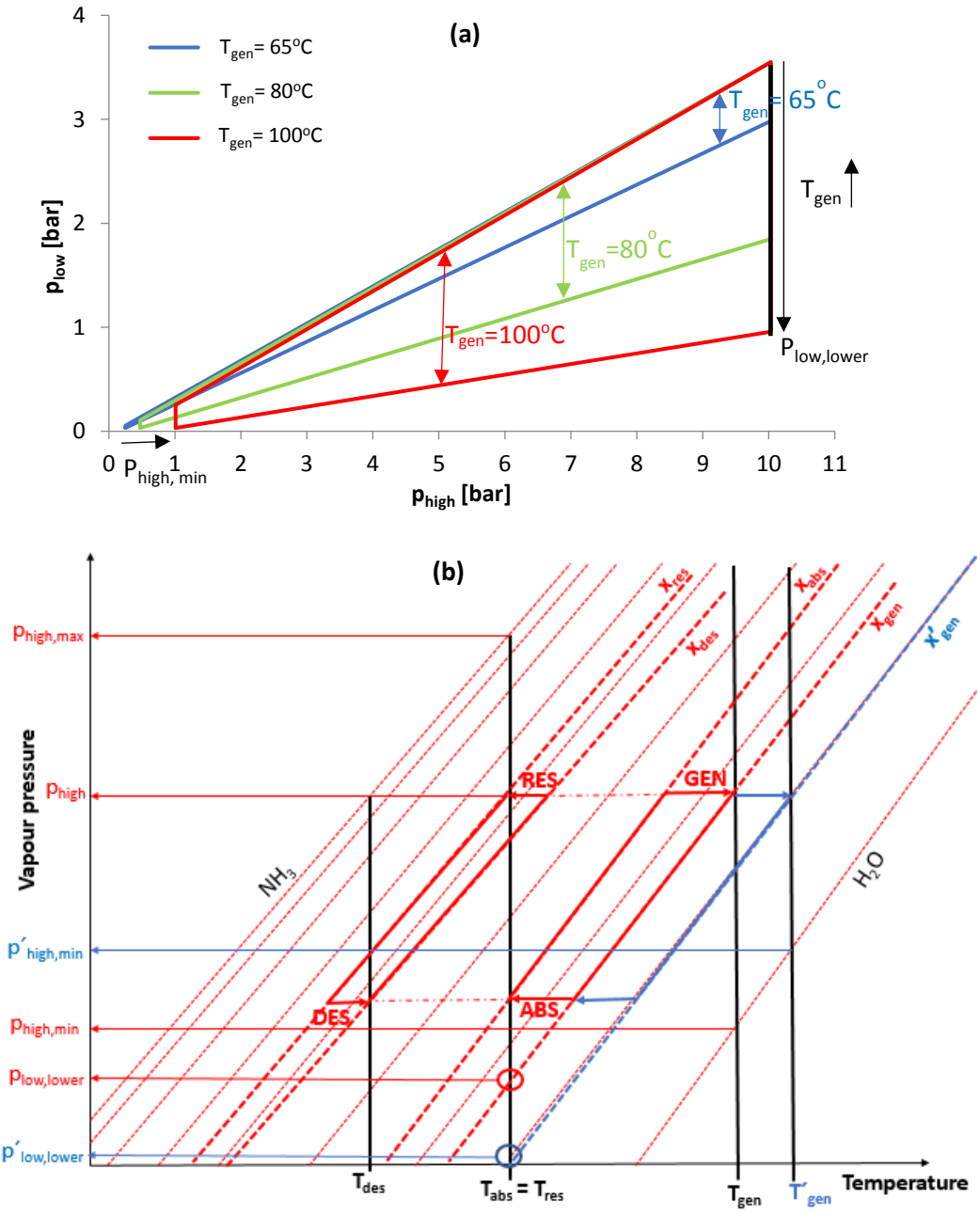

Figure 2.6 ***(a)*** *Influence of T_{gen} on the operational pressure ranges (T_{res}=T_{abs}=25ºC; T_{des}=-5ºC).* ***(b)*** *Influence of T_{gen} depicted on the PTX diagram.*

Finally, the influence of T_{abs} and T_{res} on the operational pressure range is analyzed in Figure 2.7a. It is assumed that the absorber and the resorber operates at the same temperature (T_{abs}=T_{res}). It can be clearly observed that an increase in these temperatures leads to a narrower global operating range but at the same time, higher values of p_{high} are possible because $p_{high,max}$ increases. In order to better understand this effect, Figure 2.7b depicts the cycle on the PTX diagram when T_{abs}= T_{res} decreases to T'_{abs}= T'_{res}.

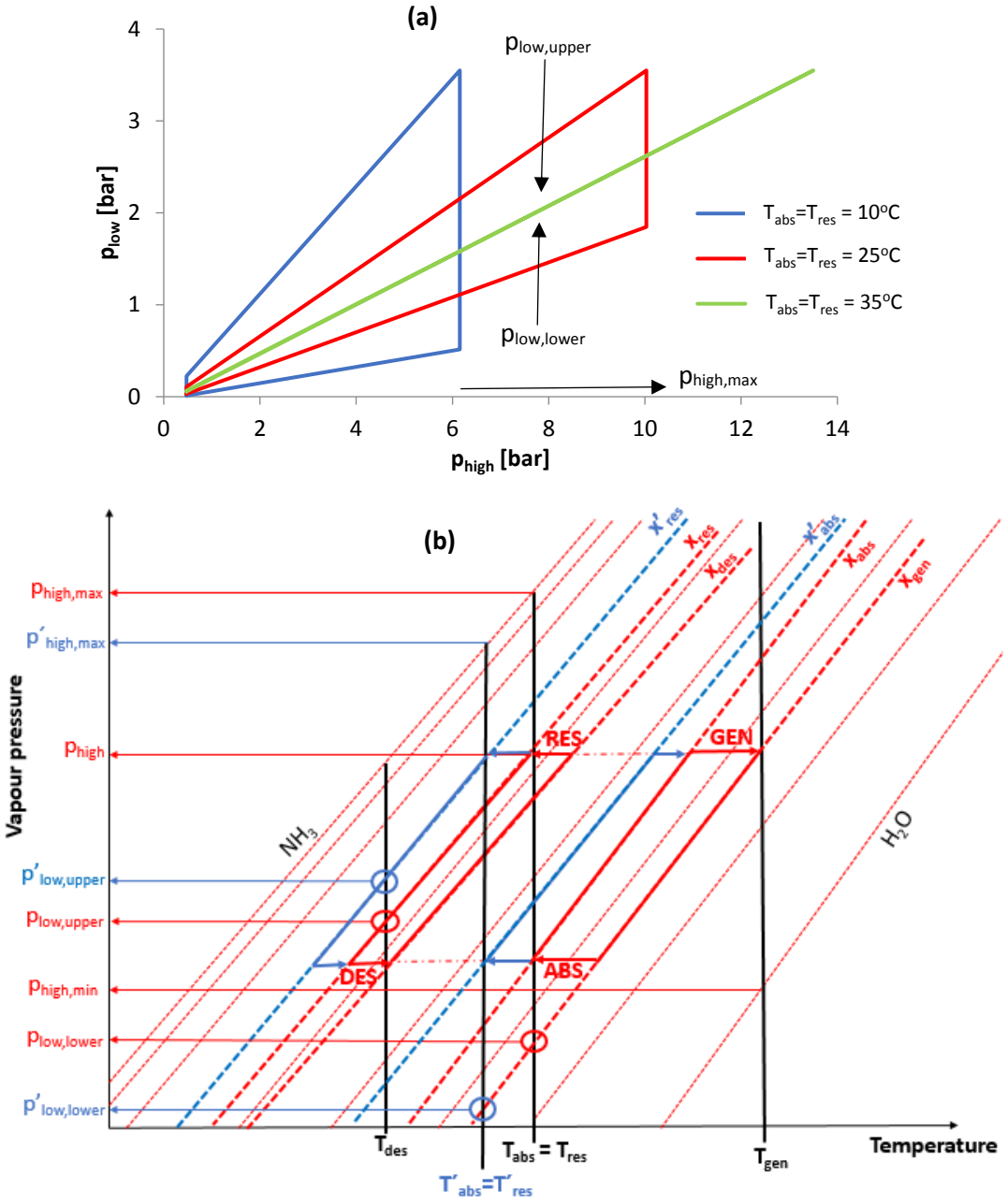

Figure 2.7 ***(a)*** *Influence of T_{abs} and T_{res} on the operational pressure ranges (T_{gen}=80ºC; T_{des}=-5ºC).* ***(b)*** *Influence of T_{abs} and T_{res} depicted on the PTX diagram.*

2.2.2.2 Influence of the effectiveness of the solution heat exchangers on the COP

Table 2.1 lists the input data selected as base case except for the p_{high} and p_{low} values because they will be varied in the sensitivity analysis. The values selected for the base case correspond to the typical operating conditions in the ammonia/water absorption-resorption refrigeration cycle [29][27]. Unless otherwise indicated, these input values will be used in the rest of the sensitivity study.

Table 2.1 Input data for the base case.

T_{gen} [ºC]	T_{des} [ºC]	$T_{abs}=T_{res}=T_{rect}$ [ºC]	$Eff_{SHX1}= Eff_{SHX2}$	q_{vp2} [l/min]
80	-5	25	0.85	9

Once the temperatures of the main components of the cycle are set, the operating pressure ranges can be determined. This range is showed in Figure 2.8 and is necessary for the sensitivity analysis in order to determine the limits of the variables. For example, at p_{high}=5bar, the p_{low} can vary between 0.76 and 1.65 bar.

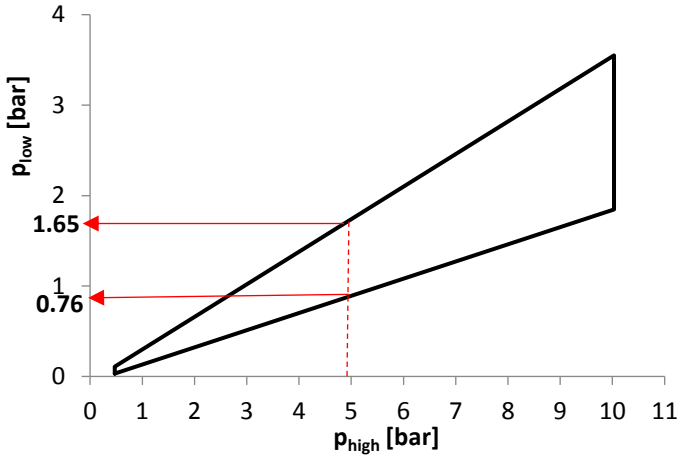

Figure 2.8 Operational pressure ranges for the case study selected.

In a conventional absorption refrigeration cycle, the effectiveness of the solution heat exchanger of the absorption circuit has a strong influence on the COP of the cycle. In an absorption-resorption refrigeration cycle, there are two solution heat exchangers; one placed in the absorption circuit and the other one placed in the resorption circuit (Figure 2.2). Both heat exchangers are very important elements for the study of the performance of the cycle. Figure 2.9 shows the influence of the effectiveness of the solution heat exchangers on the COP at several pressure-ratio values ($\beta=p_{high}/p_{low}$). p_{high} was set at 5bar and p_{low} was varied all over the range (between 0.76 and 1.65 bar). In Figure 2.9a the Eff_{SHX1} was varied from 0 to 1, while the Eff_{SHX2} was kept constant with a value of 1. In Figure 2.9b the Eff_{SHX2} was varied from 0 to 1, while the Eff_{SHX1} was kept constant with a value of 1. Comparing Figure 2.9a and 2.9b, the following conclusions can be deduced:

- Eff_{SHX1} has a stronger effect on the performance of the cycle than the Eff_{SHX2} when the pressure-ratio is higher than 4.

- Eff_{SHX2} becomes critical at lowest pressure-ratio values ($\beta<4$). The cycle cannot work below certain values of Eff_{SHX2}. In the case of $\beta=3.6$ the limit is $Eff_{SHX2}\approx0.15$ and for $\beta=3.3$ the limit is $Eff_{SHX2}\approx0.5$.

Figures 2.9c and 2.9d show the results obtained when p_{high} increases to 8bar. In this case, Eff_{SHX1} has a stronger effect on the performance of the cycle than the Eff_{SHX2} along most of the range. Only at the lowest pressure ratio limit ($\beta<3$) Eff_{SHX2} has a stronger effect on the performance of the cycle than Eff_{SHX1}. Comparing Figures 2.9b and 2.9d, it can be concluded that the higher the p_{high}, the less critical is the value of the Eff_{SHX2} on the performance of the cycle.

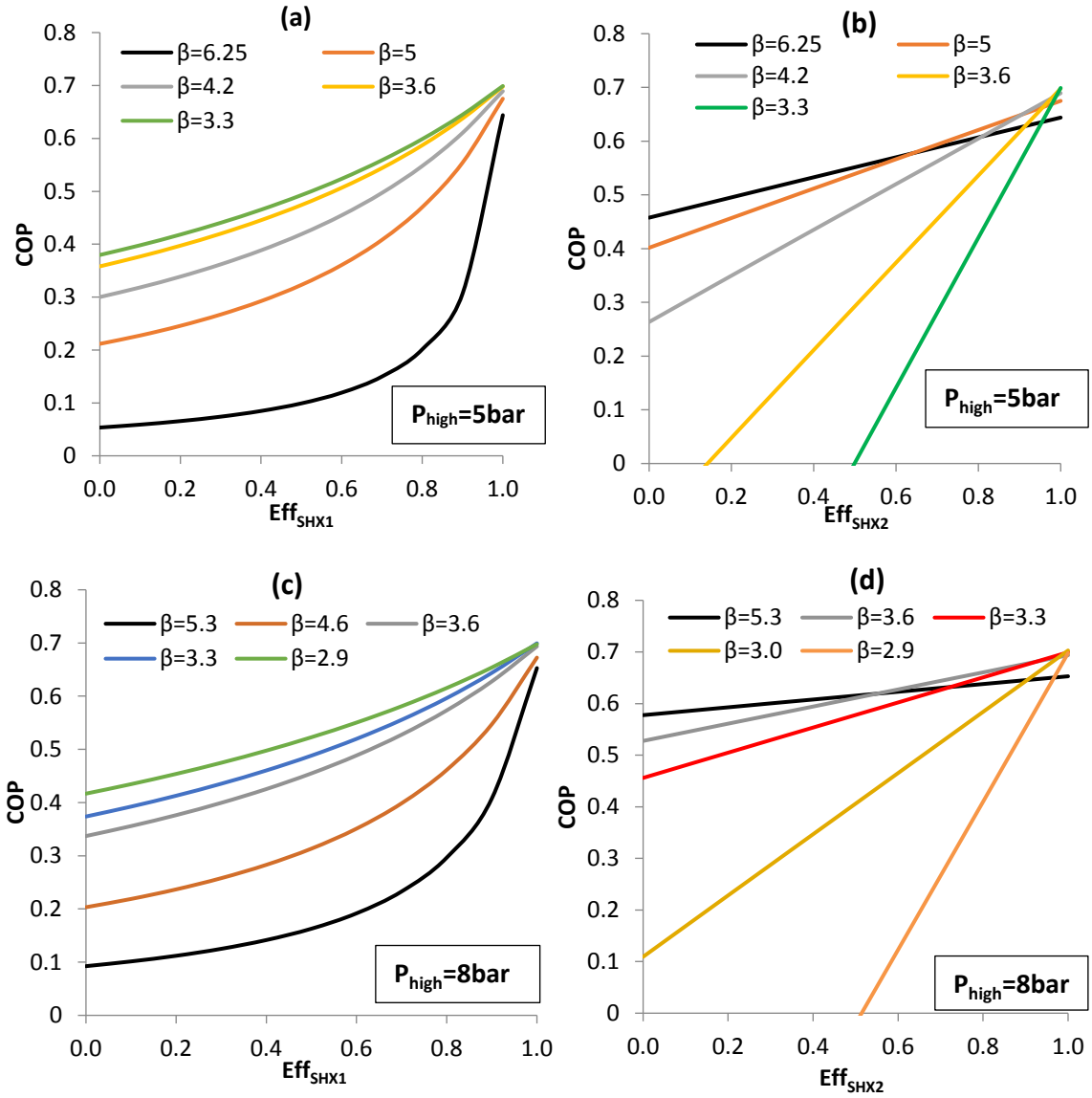

Figure 2.9 ***(a)*** *Effect of Eff_{SHX1} on the COP (p_{high}=5bar).* ***(b)*** *Effect of Eff_{SHX2} on the COP (p_{high}=5bar).* ***(c)*** *Effect of Eff_{SHX1} on the COP (p_{high}=8bar).* ***(d)*** *Effect of Eff_{SHX2} on the COP (p_{high}=8bar).*

Figure 2.10 compares the operational pressure ranges obtained at two different values of Eff_{SHX2} (0.6 and 1). It can be observed that the operational pressure range obtained in the case of Eff_{SHX2}=0.6 (red line) is slightly smaller than in the case of Eff_{SHX2}=1. The yellow-coloured area represents the zone with the lowest pressure ratio values (β<3). As mentioned before, Eff_{SHX2} becomes critical at low pressure-ratio values, even making the cycle cannot work for the temperatures selected. This reduction in the operational pressure range can be explained analysing the scheme of the resorption circuit of the cycle showed in Figure 2.2. The strong and hot solution coming from the resorber is cooled down in the SHX2 by the cold and weak solution leaving the desorber. The lower the Eff_{SHX2}, the higher the inlet temperature of the solution in the desorber is. If the inlet temperature of the solution in the desorber is higher than the desired outlet temperature of the solution in the desorber, the cooling production in the cycle stops.

Therefore, the cycle cannot work under the working temperatures previously fixed. For this reason, a proper design of the solution heat exchanger in the resorption circuit becomes crucial.

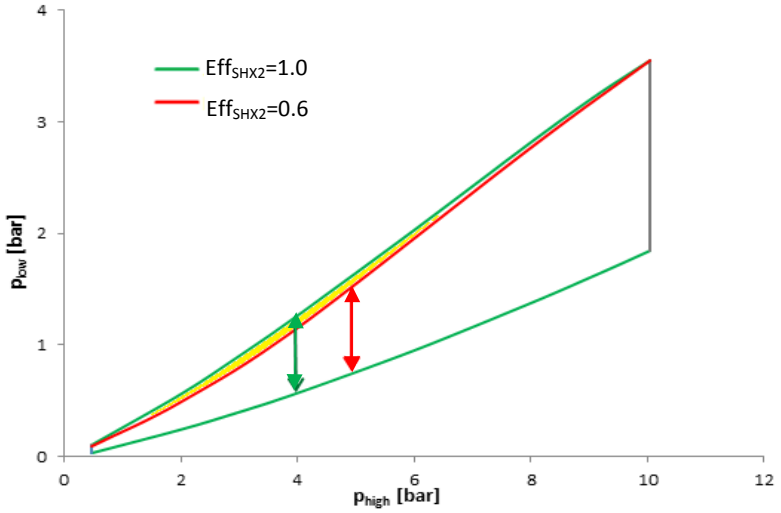

Figure 2.10 Effect of Eff_{SHX2} on the operational pressure ranges.

2.2.2.3 Influence of the cycle pressure ratio on the COP

The influence of the pressure-ratio (β) on the COP is shown in Figure 2.11a. It can be observed that all the curves show a maximum value. The higher the value of p_{high}, the higher the maximum value of COP is. Regarding the p_{low}, it would be interesting to avoid working close to the $p_{low,upper}$ of the range (lowest β) because the COP drops rapidly in that zone. Figure 2.11b shows the influence of the pressure-ratio on the cooling capacity. The higher p_{high} and the higher β, the higher the cooling capacity is. This conclusion is in good agreement with the previous one because the lowest β leads to a cooling capacity and a COP close to zero. Comparing Figure 2.11a and 2.11b it can be concluded that is not possible to reach a maximum COP and a maximum cooling capacity at the same time just varying the pressures. It would be necessary to find a compromise between the cooling capacity and COP depending on the process requirements.

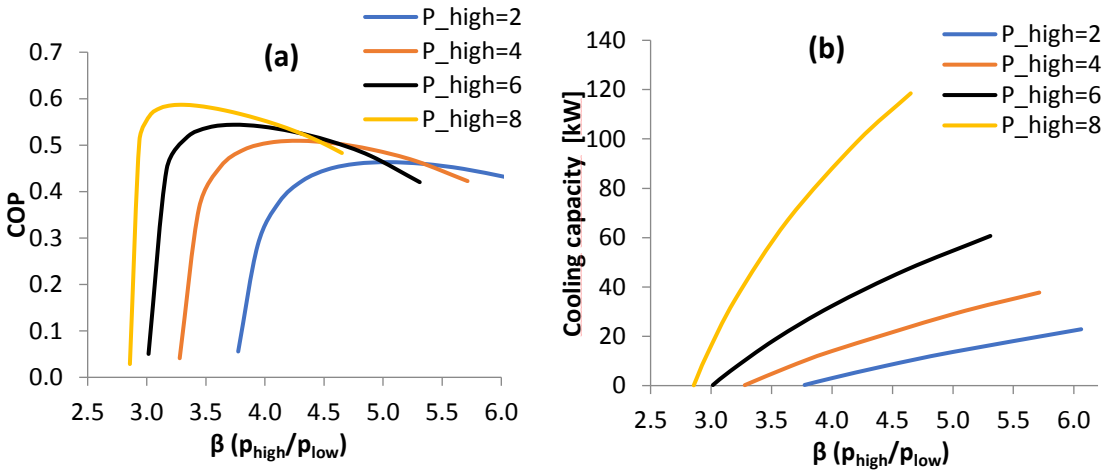

*Figure 2.11 **(a)** Influence of the pressure ratio on the COP at several p_{high}. **(b)** Influence of the pressure ratio on the cooling capacity at several p_{high}.*

2.2.2.4 Cycle configuration: influence of the rectifier on the COP

This section analyses the influence of the rectifier on the performance of the cycle in order to determine if it can be removed from the cycle but keeping a good performance in the system. As mentioned in section 2.1, there are three possible configurations for equilibrating the mass balance between the absorption and the resorption circuits: only bleeding, only rectification or a combination of rectification + bleeding. The possibility of using only rectification is not recommended due to the limitations in the working temperature of the rectifier. These limitations can be observed in Figure 2.12, where the operational pressure range was determined considering only rectification, that is to say, there is not a bleeding line in the system so the mass balance between the solution circuits must be equilibrated by means of changing the temperature in the rectifier in order to obtain the same ammonia concentration in the vapour at the outlet of the rectifier than at the outlet of the desorber. The rest of the temperature values of the base case (T_{gen}, T_{des}, $T_{abs,}$ and T_{res}) were considered constant. In order to make a more realistic study, a constraint in the lowest temperature value at the outlet of the rectifier was considered (T_{rect}≥25ºC). Figure 2.12 shows that the operational pressure range is much smaller compared to the case with the rectifier + bleeding line (Figure 2.8). This fact can be explained by the limitation in the temperature in the rectifier. To obtain the same operational pressure range than in Figure 2.8 it would be necessary to reduce the temperature in the rectifier below 25ºC (which is also the same working temperature considered for the absorber and resorber), and that would mean using a colder cooling water than the one used for cooling the absorber and the resorber. Hence, this cycle configuration is not recommended because in most of cases another refrigeration system would be necessary for cooling down the water.

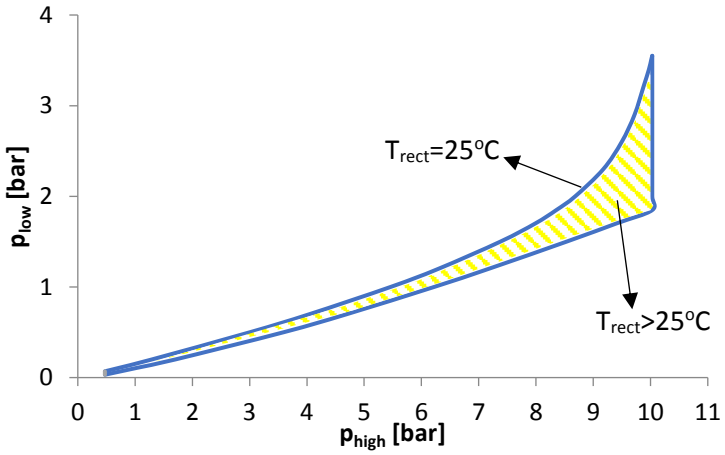

Figure 2.12 Operational pressure ranges when T_{rect}≥25ºC. Cycle configuration: only rectification.

Then, there are only two possible configurations: only bleeding or bleeding + rectifier. The influence of both configurations on the COP is compared in Figure 2.13. The comparison was done at four different values of p_{high} in order to cover most of the operating pressure range (p_{high}=2 bar and p_{high}=9 bar in Figure 2.13a; p_{high}=4 bar and p_{high}=6 bar in Figure 2.13b). In all cases, the combination of bleeding and rectifier provides a slight increase on the COP compared to the configuration without the rectifier. The improvement on the COP observed in the case of p_{high}=2 bar ranges from 3.5 to 8%. In the rest of cases, the improvement remains below 5%. It is important to highlight that the rectifier is usually a quite large and complex component [46], so

removing the rectifier would lead to cheaper and much more compact absorption-resorption systems with an acceptable level of performance loss.

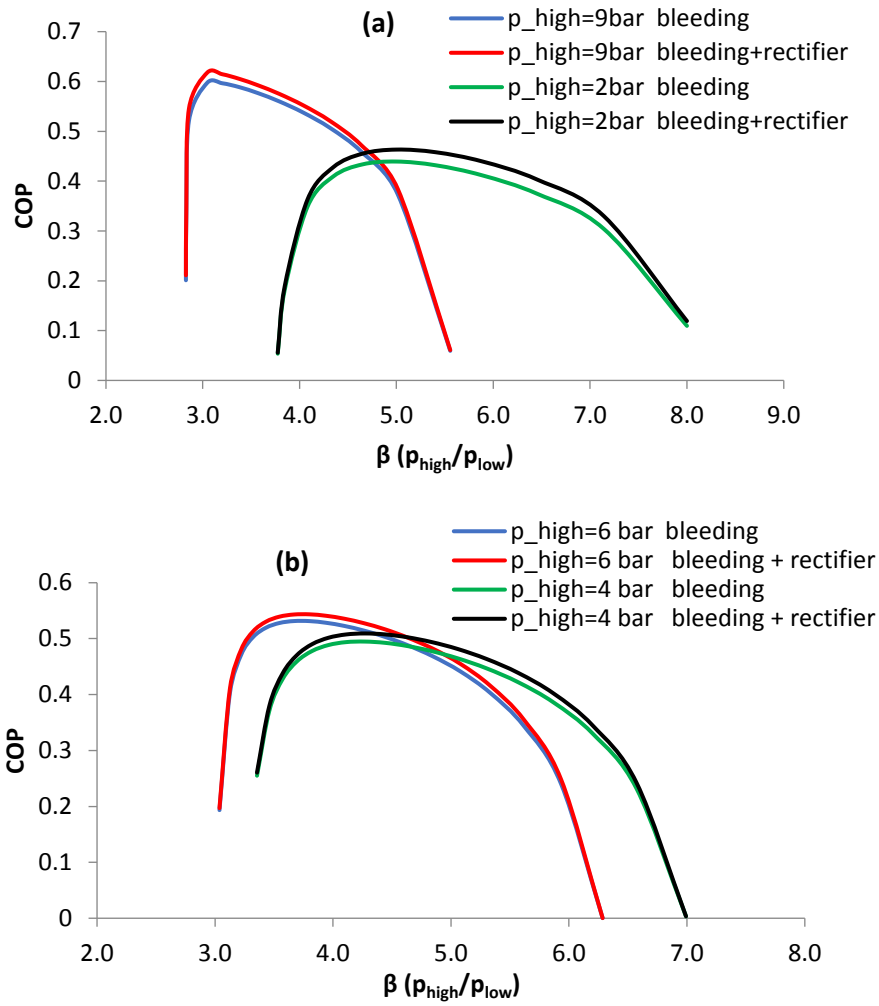

Figure 2.13 Influence of the cycle configuration (bleeding or bleeding+rectifier) on the COP. ***(a)*** *p_{high}=9 bar and p_{high}=2 bar.* ***(b)*** *p_{high}=6 bar and p_{high}=4 bar.*

2.2.2.5 Working conditions for the base case

As mentioned before, one of the main advantages of the absorption-resorption cycles compared to the conventional absorption cycles is the possibility of reducing the operating high-pressure in a very significant way but working at the same temperature levels than in a conventional absorption cycle. However, this reduction of the pressure results in a loss of performance. The conventional absorption cycle is the top limiting case of all possible absorption-resorption cycles when the solution of the resorption circuit is just pure ammonia and the resorber and the desorber are replaced by a condenser and an evaporator respectively. Therefore, there is no point of using the absorption-resorption cycle if the working pressure level is similar to the working pressure of the conventional absorption cycle because the cycle is more complex and difficult to control. It would be recommended to take the advantage that the absorption-resorption technology offers and try to find a compromise between the performance and the

high-pressure level. The following considerations were taken into account for choosing the operating conditions for the base case (Table 2.1):

- Cycle configuration with the bleeding line (removing the rectifier).
- A 50% reduction of the p_{high} value compared to the p_{high} of the conventional absorption cycle. Then, for the base case selected p_{high}=5 bar.
- A p_{low} value above the atmospheric pressure in order to avoid working under vacuum.
- Pressure ratio (β) around 4 in order to obtain a good compromise between the cooling capacity and the COP.

Attending to the previous considerations and the working conditions of the base case, the thermodynamic model was run to determine the mass flow rate and the ammonia concentration in the solution circuits. The working conditions suggested for the base case are shown below:

- p_{high}= 5 bar; p_{low}=1.3 bar
- Mass flow rate in the absorption circuit 1.25 times higher than the mass flow rate in the resorption circuit.
- Ammonia mass fraction of the solution leaving the absorber and the resorber→ x_{abs}=0.36; x_{res}=0.61
- Ammonia mass fraction difference in both circuits → $\Delta x_{abs}\approx 0.07$; $\Delta x_{res}\approx 0.05$
- COP=0.52
- Q_{des}=18kW; Q_{gen}=35kW; Q_{res}=19kW; Q_{abs}=31kW

2.2.3 Thermodynamic model with external heat transfer (UA-type)

The second thermodynamic model developed is a UA-type model that includes also the external streams and it was used for studying the effect of the inlet temperature of the external streams and the size of the heat exchangers (UA values) on the low-pressure, the COP, the cooling capacity (Q_{des}) and the temperature glide in the desorber ($\Delta T_{gliding}$). According to the results obtained in section 2.2.2.3, a cycle configuration with only bleeding was assumed, as shown in Figure 2.14.

The mass and energy balances in the desorber (Equations 2.1-2.3), absorber (Equation 2.10), resorber (Equation 2.11), pumps (Equations 2.12-2.13) and solution heat exchangers (Equations 2.14-2.17) described in the previous model were also used in this one. The mass and energy balances in the generator are shown in Equations 2.25-2.27. Note that these equations are different from the ones used in the previous model due to the absence of the rectifier.

$$m_3 = m_4 + m_7 \tag{2.25}$$

$$m_3 \cdot x_3 = m_4 \cdot x_4 + m_7 \cdot x_7 \tag{2.26}$$

$$Q_{gen} + m_3 \cdot h_3 = m_4 \cdot h_4 + m_7 \cdot h_7 \tag{2.27}$$

Regarding the bleeding line, the following equations are required. Equation 2.28 corresponds to the mass balance in the split point (SP) of the stream 10. Equations 2.29 and 2.30 show the total and ammonia mass balances between both solution circuits, while Equations 2.31, 2.32 and 2.33 correspond to the total mass, ammonia mass and energy balances in the mixing point (MP) of the absorption circuit.

$$m_{10} = m_{15} + m_{17} \tag{2.28}$$

$$m_7 = m_{14} + m_{15} \tag{2.29}$$

$$m_7 \cdot x_7 = m_{14} \cdot x_{14} + m_{15} \cdot x_{15} \tag{2.30}$$

$$m_{18} + m_{16} = m_6 \tag{2.31}$$

$$m_{18} \cdot x_{18} + m_{16} \cdot x_{16} = m_6 \cdot x_6 \tag{2.32}$$

$$m_{18} \cdot h_{18} + m_{16} \cdot h_{16} = m_6 \cdot h_6 \tag{2.33}$$

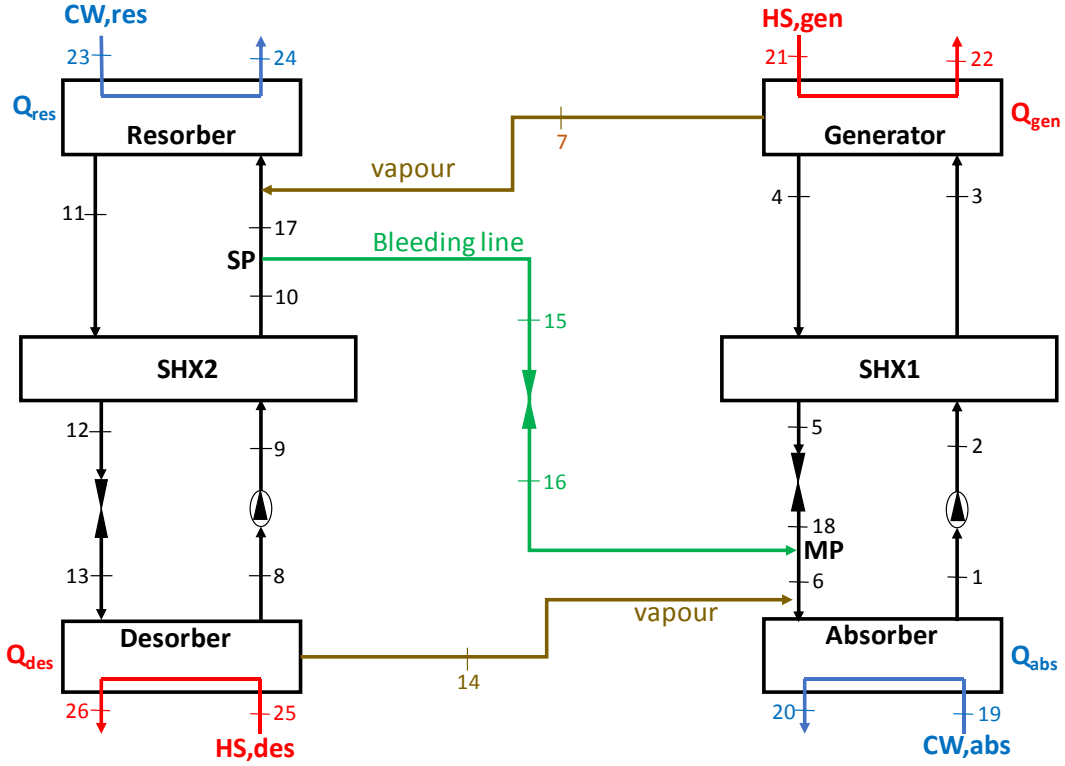

Figure 2.14 Absorption-resorption refrigeration cycle with bleeding and external streams.

Equations 2.34-2.41 are required for determining the heat transferred to the external streams in the generator, absorber, resorber, and desorber, which should be equal to the heat exchanged in the internal streams due to the assumption of negligible heat losses/gains from the components. Water was considered as external fluid for heating the generator and cooling the absorber and the resorber. A mixture of ethylene-glycol/water (30%) was considered for heating the desorber.

$$Q_{gen} = m_{HS,gen} \cdot (h_{21} - h_{22}) \tag{2.34}$$

$$Q_{gen} = UA_{gen} \cdot \Delta T_{lmtd,gen} \tag{2.35}$$

$$Q_{abs} = m_{CW,abs} \cdot (h_{20} - h_{19}) \tag{2.36}$$

$$Q_{abs} = UA_{abs} \cdot \Delta T_{lmtd,abs} \tag{2.37}$$

$$Q_{res} = m_{CW,res} \cdot (h_{24} - h_{23}) \tag{2.38}$$

$$Q_{res} = UA_{res} \cdot \Delta T_{lmtd,res} \tag{2.39}$$

$$Q_{des} = m_{HS,des} \cdot (h_{25} - h_{26}) \quad (2.40)$$

$$Q_{des} = UA_{des} \cdot \Delta T_{lmtd,des} \quad (2.41)$$

where UA is the product of the overall heat transfer coefficient and the heat transfer area and ΔT_{lmtd} is the logarithmic mean temperature difference. In order to improve the numerical performance of the model, Chen's approximation [47] was used to determine the logarithmic mean temperature difference of the heat exchanger. Chen's approximation is given as a function of the hot (h) and cold (c) end temperature differences (ΔT_k^h and ΔT_k^c , respectively) as shown in Equation 2.42:

$$\Delta T_{lmtd}^k \cong \left[\Delta T_k^h \cdot \Delta T_k^c \cdot \frac{\Delta T_k^h + \Delta T_k^c}{2}\right]^{1/3} \quad (2.42)$$

2.2.3.1 Model of the resorber

The resorption circuit is similar to the absorption circuit in an absorption heat transformer, where the absorber is placed at the high-pressure side of the cycle and the desorber at the low-pressure side. As mentioned in section 2.2.2.2, this configuration of the cycle makes the solution heat exchanger of the resorption circuit (SHX2) playing an important role in the performance of the cycle. The weak and cold solution leaving the desorber is preheated in the SHX2 by the rich solution leaving the resorber, therefore, the solution stream entering the resorber is always colder than the solution leaving the resorber. Therefore, for modelling the resorber it is assumed that the vapour leaving the generator is partially absorbed by the cold stream (under adiabatic conditions) before entering the resorber [24,48]. Due to the exothermic absorption process, the solution is heated up until saturation conditions (liquid+vapour) and then enters to the resorber at higher temperature. In the resorber, the two-phase solution is cooled down by the external cooling water, all the vapour is absorbed, and the solution leaves the resorber saturated at T_{res} and p_{high}. The determination of the actual inlet temperature of the solution (after adiabatic absorption process) in the resorber is crucial for determining the heat transferred using Equation 2.39. Figure 2.15 shows the mixing configuration assumed before the resorber in order to determine the inlet temperature of the solution.

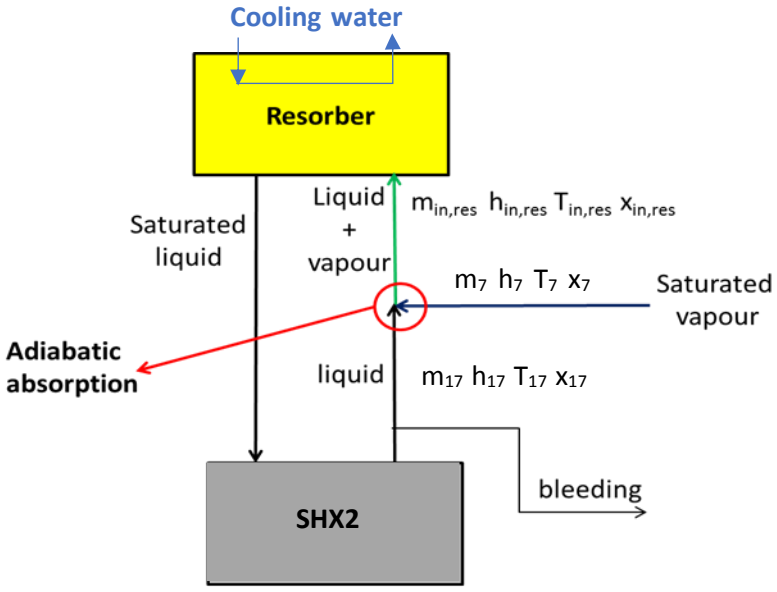

Figure 2.15 Scheme of the adiabatic mixing before the resorber.

The mass and energy balances of the adiabatic absorption process are shown below:

$$m_{17} \cdot x_{17} + m_7 \cdot x_7 = m_{in,res} \cdot x_{in,res} \quad (2.43)$$

$$m_{17} \cdot h_{17} + m_7 \cdot h_7 = m_{in,res} \cdot h_{in,res} \quad (2.44)$$

Once $x_{in,res}$, $h_{in,res}$, and pressure are known, $T_{in,res}$ is determined using the ammonia/water properties [44] and then ΔT_{lmtd} and Q_{res} (Equation 2.39) can be obtained.

The following assumptions were considered for modelling the cycle:

- Heat losses/gains in the components are negligible.
- The cycle operates at steady-state conditions.
- Pressure drops in piping and components are not considered except on the throttling devices.
- The flow arrangement of solution heat exchangers is countercurrent.
- The solution streams leaving the desorber, absorber, generator, and resorber are saturated.
- Pumping processes are isentropic and expansion processes in valves are isenthalpic.
- The vapour streams exist the desorber and the generator at equilibrium conditions with the outlet solution (parallel flow arrangement).
- Equilibrium conditions of the two-phase liquid-vapour mixture after the adiabatic absorption process before entering to the resorber and to the absorber.

2.2.3.2 Input data for the sensitivity analysis

According to the method described by Ayou et al. [45], 17 independent variables should be chosen as an input data for modelling the cycle. The input variables selected were the following:

- The inlet temperatures and flow rates of the four external streams.
- The product of the global heat transfer coefficient and the heat transfer area (UA) of the four heat exchangers (generator, absorber, resorber, and desorber).
- The solution flow rate in the two solution pumps.
- The high-pressure level of the system.
- The effectiveness of the solution heat exchangers.

The input values selected for the base case were taken from the operating conditions of the ammonia/water absorption-resorption refrigeration plant of TU Dresden. Table 2.2 lists the values of all the input variables selected for the sensitivity analysis.

Table 2.2 Input values of the variables selected for the sensitivity analysis.

$qv_{in,CW,abs}$ [m^3/h]	$qv_{in,HS,gen}$ [m^3/h]	$qv_{in,CW,res}$ [m^3/h]	$qv_{in,HS,des}$ [m^3/h]	$T_{in,CW,abs}$ $T_{in,CW,res}$ [°C]	$T_{in,HS,gen}$ [°C]	$T_{in,HS,des}$ [°C]	P_{high} [bar]
3.4	9.5	3.3	7.0	21.2	88.6	0.1	5.0
UA_{abs} [kW/K]	**UA_{gen} [kW/K]**	**UA_{res} [kW/K]**	**UA_{des} [kW/K]**	**Eff_{SHX1}**	**Eff_{SHX2}**	**qv_{P1} [l/min]**	**qv_{P2} [l/min]**
10.4	9.9	6.9	7.7	0.88	0.85	18.9	14.8

UA values of the generator and desorber were experimentally determined by means of the temperature and flow rate measurements obtained in the test bench of TU Dresden and the use of Equations 2.34-2.35 for the UA_{gen} and 2.40-2.41 for the UA_{des}. Figure 2.16 shows the scheme of the absorption-resorption refrigeration system of TU Dresden including the location of the temperature sensors in the cycle. It can be observed that in the generator and in the desorber the inlet and outlet temperatures of the internal and external streams can be measured. However, in the case of the absorber and the resorber there was no temperature sensors just before the inlet of the absorber and the resorber, that is to say, just after the mixing point between the vapour and the solution. Thus, the actual temperature of the solution at the inlet of both components was not measured, and therefore they must be estimated. For this reason, the ΔT_{lmtd} values in the absorber and the resorber were determined following the procedure described in the previous section (2.2.3.1) and then the UA values of these components are estimated. Finally, the effectiveness of the solution heat exchangers were also determined from experimental data using Equations 2.14 and 2.16.

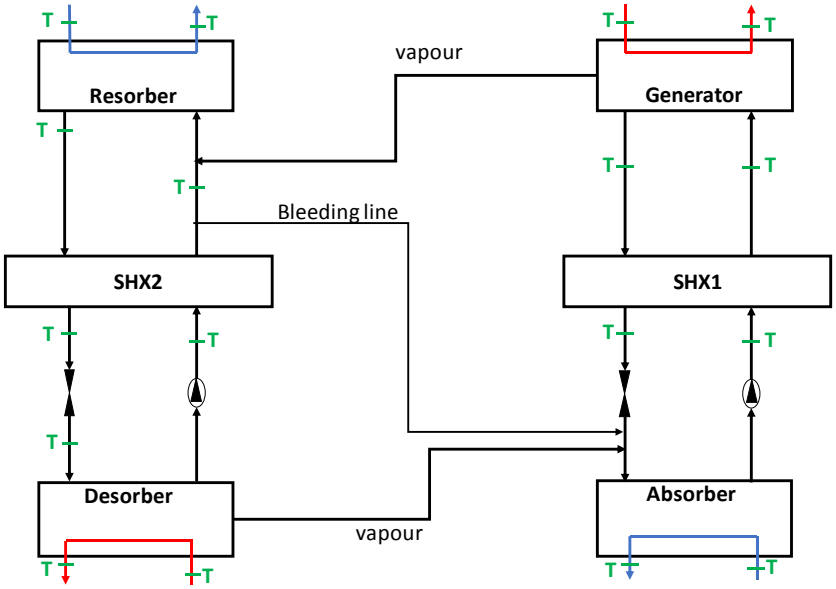

Figure 2.16 Location of the temperature sensors in the absorption-resorption refrigeration system of TU Dresden.

2.2.4 Sensitivity analysis using the thermodynamic model with external heat transfer

In this section, the influence of the inlet temperature of the external streams and the UA values of the heat exchangers on the COP, p_{low}, cooling capacity and temperature glide in the desorber is studied. The variations in the cycle performance as a function of these parameters provide a better understanding of the operating characteristics of this kind of cycles. When one of the input values are varied in the study, the rest of the variables showed in Table 2.2 are kept constant.

2.2.4.1 Effect of the inlet temperature of the external streams on the performance of the cycle

Figure 2.17 shows the effect of the inlet temperature of the external streams on the p_{low} and on the COP. There is a significant influence of $T_{in,HS,des}$ and $T_{in,CW}$ on the COP (Figure 2.17a and 2.17c). As expected, the closer are $T_{in,HS,des}$ and $T_{in,CW}$ to each other, the higher COP is obtained. For the range studied, the sensitivity of COP to $T_{in,HS,des}$ is 2.0% of improvement per ^{o}C. In the case of

$T_{in,CW}$, the COP decreases a rate of approximately 1.9% per °C. On the other hand, increasing $T_{in,HS,gen}$ leads into a decreasing rate on the COP of approximately 1.0% per °C (Figure 2.17b). Regarding the low-pressure level (p_{low}), it is highly influenced by $T_{in,HS,des}$ and to a lesser degree by $T_{in,HS,gen}$ whereas the effect of the $T_{in,CW}$ on the p_{low} value is negligible. The sensitivity of p_{low} to $T_{in,HS,des}$ is 0.024 bar of increment per °C and to $T_{in,HS,gen}$ is 0.017 bar of decreasing per °C.

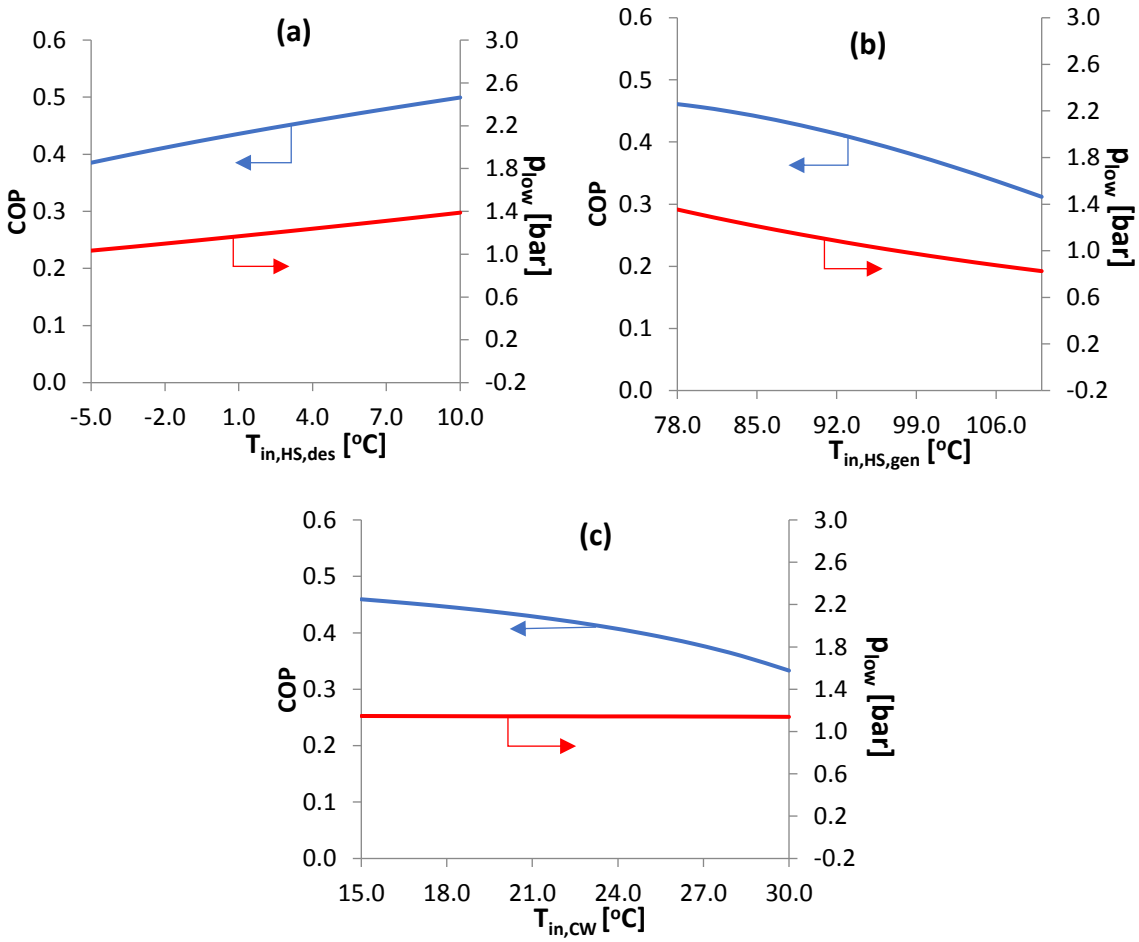

*Figure 2.17 Effect of the inlet temperature of the external streams on the p_{low} and the COP: **(a)** inlet temperature of the ethylene-glycol/water mixture (30%) in the desorber ($T_{in,HS,des}$); **(b)** Inlet temperature of the hot water in the generator ($T_{in,HS,gen}$); **(c)** Inlet temperature of the cooling water in the absorber and resorber ($T_{in,CW}$).*

Figure 2.18 shows the effect of the inlet temperature of the external streams on the cooling capacity of the system (Q_{des}) and on the gliding temperature in the desorber ($\Delta T_{gliding}$), which is defined as the difference between the inlet temperature and the outlet temperature of the external stream in the desorber. Regarding the cooling capacity, there is a positive effect on Q_{des} when $T_{in,HS,des}$ and $T_{in,HS,gen}$ are increased (Figure 2.18a and 2.18b), while there is a negative effect when the inlet temperature of the cooling water ($T_{in,CW}$) is increased (Figure 2.18c). In the case of $T_{in,HS,des}$ and $T_{in,HS,gen}$ the cooling capacity increases in a rate of 1.1 kW/°C and 0.3 kW/°C, respectively. In the case of the $T_{in,CW}$ the Q_{des} decreases in a rate of 1.6 kW/°C. Regarding the gliding temperature it can be observed that the trends are similar to the ones obtained for the cooling capacity. Figure 2.18a and 2.18c show that the higher $T_{in,HS,des}$ and the lower $T_{in,CW}$, the

higher gliding temperature in the desorber is obtained. For the case studied in this section, a maximum gliding temperature of 5.1°C was obtained when $T_{in,HS,des}$=10°C. A similar gliding temperature value (5.0°C) was obtained when $T_{in,CW}$=15°C. On the other hand, the influence of the $T_{in,HS,gen}$ on the $\Delta T_{gliding}$ is not significant.

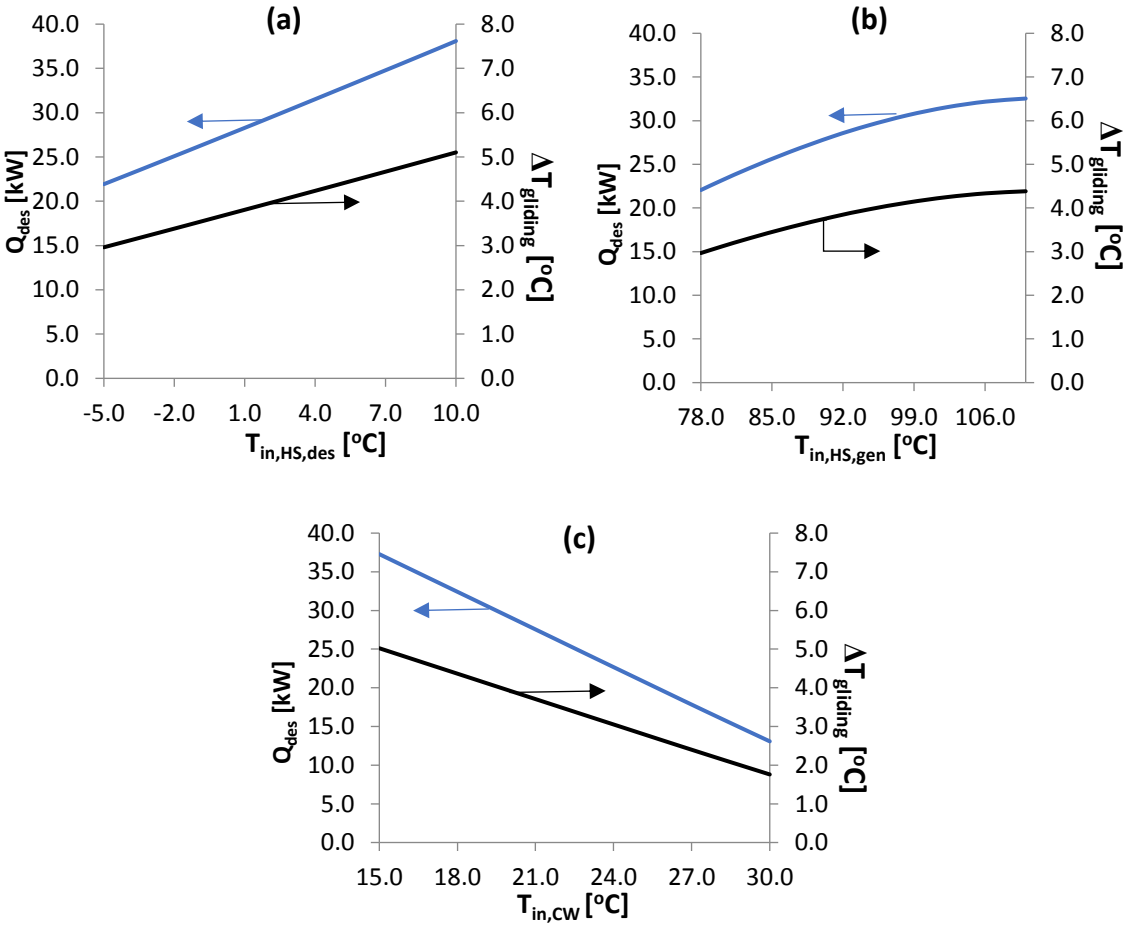

*Figure 2.18 Effect of the inlet temperature of the external streams on the cooling capacity (Q_{des}) and on the gliding temperature ($\Delta T_{gliding}$): **(a)** Inlet temperature of the ethylene-glycol/water mixture (30%) in the desorber ($T_{in,HS,des}$); **(b)** Inlet temperature of the hot water in the generator ($T_{in,HS,gen}$); **(c)** Inlet temperature of the cooling water in the absorber and resorber ($T_{in,CW}$).*

2.2.4.2 Effect of the UA values of the heat exchangers on the performance of the cycle

The heat exchange area multiplied by the overall heat transfer coefficient (UA value) is a very important parameter when designing the heat exchanger because it represents the size of the heat exchanger. Figure 2.19 shows the effect of the UA of the heat exchangers on the COP and on the cooling capacity (Q_{des}). The abscissa of the plots is the relative UA value normalized to the base case UA value of Table 2.2. Regarding the COP, the curves obtained for the resorber, absorber and desorber show a similar trend, which is in good agreement with the behaviour showed in the model developed by Pande and Herold [22]. In their work, Pande and Herold pointed out that, as in the conventional absorption cycles, COP is not particularly sensitive to changes in the heat exchanger size because the increased capacity associated with increased UA causes increased thermodynamic losses, balancing both effects and providing a COP essentially constant over a wide range of UA values. The decrease in COP observed at UA/UA_o values lower than 0.5 can be explained because a heat transfer bottleneck exists in the cycle and the

irreversibilities in that component tend to decrease the overall performance. According to the results showed in Figure 2.19, the sizing considered in the base case for the heat exchangers of the desorber, absorber, and resorber was suitable because no significant improvements on the COP are observed (less than 5% in all cases) when UA is increased. However, in the case of the generator (Figure 2.19b) the curve of the COP shows a maximum for a normalized UA-value of 0.2 and then drops rapidly when $UA/UA_o<0.2$. This can be explained because the reduction of the heat supplied to the generator due to the reduction in the UA-value is higher than the loss of cooling capacity that take place in the range of $0.2<UA/UA_o<1.0$.

Regarding the cooling capacity, a similar behaviour is observed than in the COP study. For UA/UA_o values below 0.5, the cooling capacity drops rapidly in all cases. A 10% increase in the cooling capacity can be reached if the UA of the desorber, absorber or resorber is tripled. In the case of the generator no significant improvement on the cooling capacity is observed when the UA_{gen} value is increased with regard to the value of the base case.

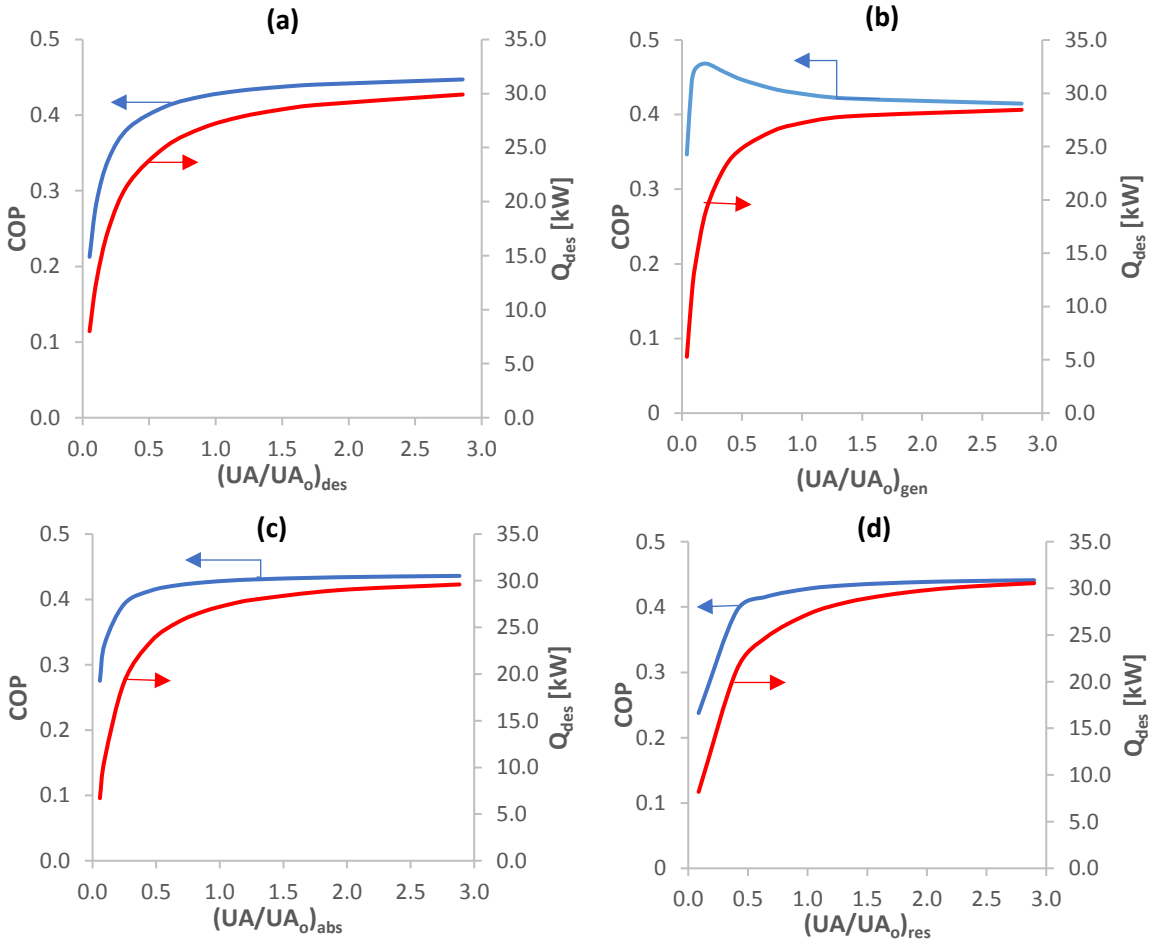

*Figure 2.19 Effect of the UA of the heat exchangers on the COP and p_{low}. **(a)** Desorber; **(b)** Generator; **(c)** Absorber; **(d)** Resorber. UA_o represents the UA value assumed in the base case of Table 2.2.*

Figure 2.20 shows the influence of the UA values of the heat exchangers on the p_{low} and on the gliding temperature ($\Delta T_{gliding}$) in the desorber. Regarding the low-pressure level (p_{low}), it is highly influenced by the UA values of the main components of the absorption circuit (generator and absorber). When the normalized UA-value of the generator or the absorber are lowered below

0.5 the low-pressure value rises rapidly. In the case of the UA-values of the main components of the resorption circuit (resorber and desorber), the effect observed is just the opposite than in the case of the absorption circuit because the low-pressure level of the cycle decreases when the normalized UA-values of the resorber or the desorber are lowered below 0.5. In all cases, there are no significant variation of the low-pressure level when the UA-values are increased over the values set in the base case (Table 2.2). Regarding the gliding temperature, the trend observed is similar to the one obtained in Figure 2.19 for the cooling capacity analysis. In all cases, the maximum $\Delta T_{gliding}$ obtained is approximately 4°C and increasing the size of the heat exchanger over the base case would not provide significant improvements on the gliding temperature.

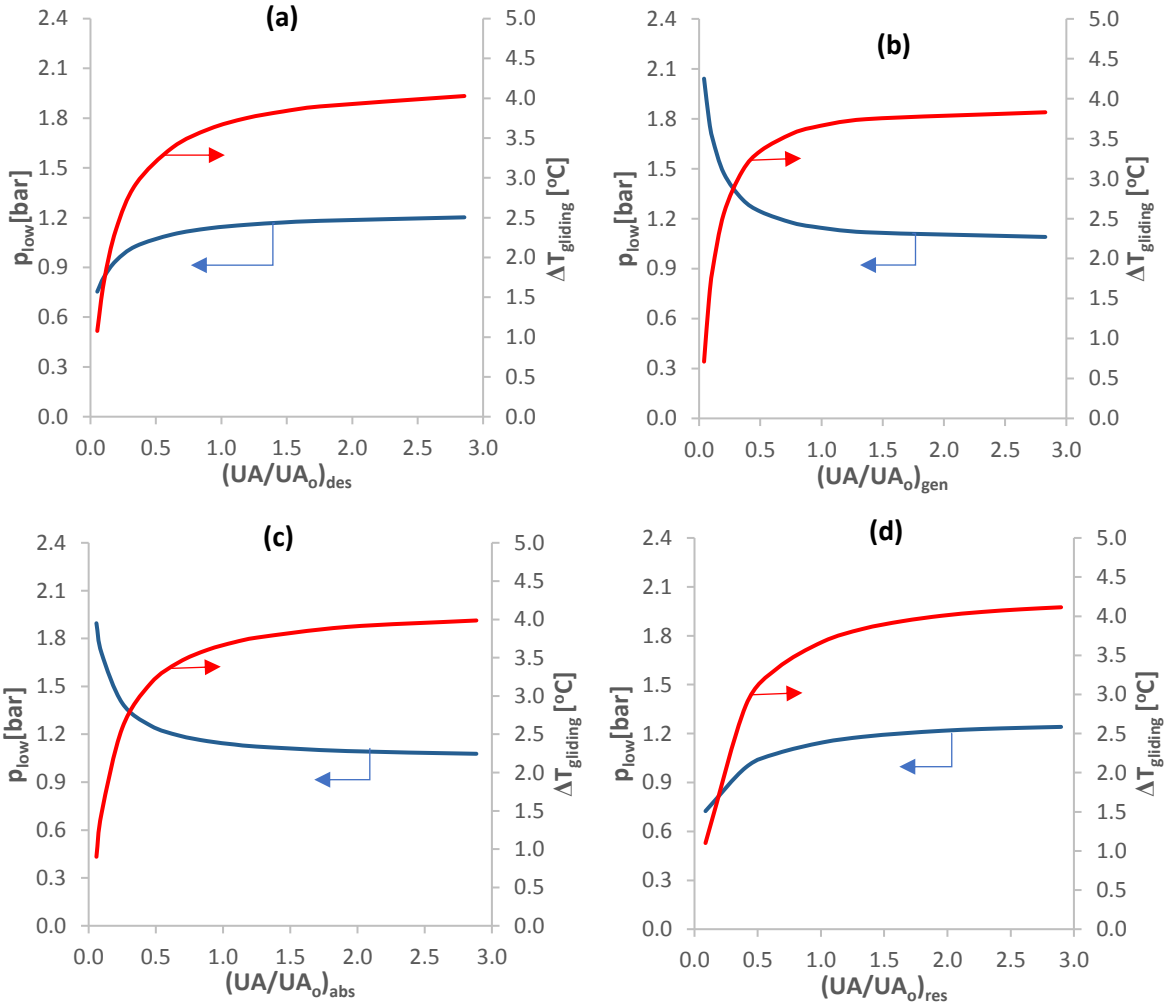

*Figure 2.20 Effect of the UA of the heat exchangers on the $\Delta T_{gliding}$ and p_{low}. **(a)** Desorber; **(b)** Generator; **(c)** Absorber; **(d)** Resorber. UA_o represents the UA value assumed in the base case of Table 2.2.*

2.3 Performance of an absorption-resorption refrigeration plant operating in a test bench

This section describes the 25-kW ammonia/water absorption-resorption refrigeration plant operating in a test bench at Technische Universität Dresden (Germany) and analyses its

experimental performance by means of the thermodynamic model with external heat transfer previously developed.

2.3.1 Description of the plant and the test bench

The plant was designed with the nominal conditions showed in Table 2.3. These conditions were not achieved during the experiments due to several factors that will be explained in detail in this section. Figure 2.21 shows three pictures of the ammonia/water absorption-resorption refrigeration test bench place in the Zentrum für Energietechnik (ZET) of TU Dresden. In these pictures, the main components of the system have been highlighted and labelled. The cycle configuration is similar to the one showed in Figure 2.14; there is no rectifier, so a bleeding pipe is used for equilibrating the mass balances between the absorption and resorption circuits supplying the weak solution at the inlet of the resorber to the inlet of the absorber. As a safety measure, the system is inside of a cabinet with plastic strip shields to protect the workers from any leakage in the test bench. On the top of the cabinet, there is a fan which is automatically switched on when a certain concentration of ammonia is detected.

Table 2.3 Nominal conditions of the 25-kW absorption-resorption refrigeration plant.

Component	Heat duty [kW]	m_{water} [kg/h]	$T_{in,water}$ [ºC]	$T_{out,water}$ [ºC]
Generator	55	6.0	90.0	82.0
Desorber	25	6.0	4.1	0.5
Resorber	40	6.0	26.0	31.7
Absorber	42.5	8.0	26.0	30.6

Every main component of the absorption-resorption refrigeration plant (generator, desorber, absorber, and resorber) consist of a stainless-steel plate heat exchanger (provided by Alfa Laval) and a reservoir installed downstream of the heat exchanger to ensure the phase separation and a continuous supply of fluid to the pumps as well. The solution heat exchangers of both circuits are also plate heat exchangers provided by Alfa Laval. Figure 2.22 shows a scheme of the flow configuration in the plate heat exchangers and Table 2.4 lists their technical data. A special feature of this system is the high number of sight glasses which allow observing what is happening inside the main components of the test bench. The expansion device in both solution circuits is a flow restrictor valve. Finally, a vertical multistage electric pump (EBARA EVM 3 7N5/0.75 M) was selected to be used as solution pump in the absorption and resorption circuits.

Regarding the test bench, the heat is supplied by a district heating network to the generator, where the temperatures of the heating medium can be set in a range of 60-95ºC. The flow rate of the heating water can be set from 4 m^3/h to 12 m^3/h, providing heating rates up to 100 kW. The cooling of the absorber and resorber is realized by a cooling water from a cooling tower. The cooling water flow rate available is 7m^3/h. Here there is the first limitation that impedes to reach the nominal operating conditions of the refrigeration system because the total cooling water flow rate required for reaching the nominal 25-kW of cooling capacity is 14 m^3/h (8 m^3/h for the absorber and 6 m^3/h for the resorber). For the cooling distribution (heat supply to the desorber), a 30% glycol-water-mixture with a freezing point of -14ºC is used. The cold glycol-water mixture was used for ice production in a storage system consisting of 5 ice storage tanks.

Temperature, pressure, and level sensors are located in several key points in the test bench as well as flowmeters for the internal and external streams. Finally, the system is controlled by means of a computer software which provides information about all the measured parameters. Figure 2.23 shows a screenshot of the control panel of the software.

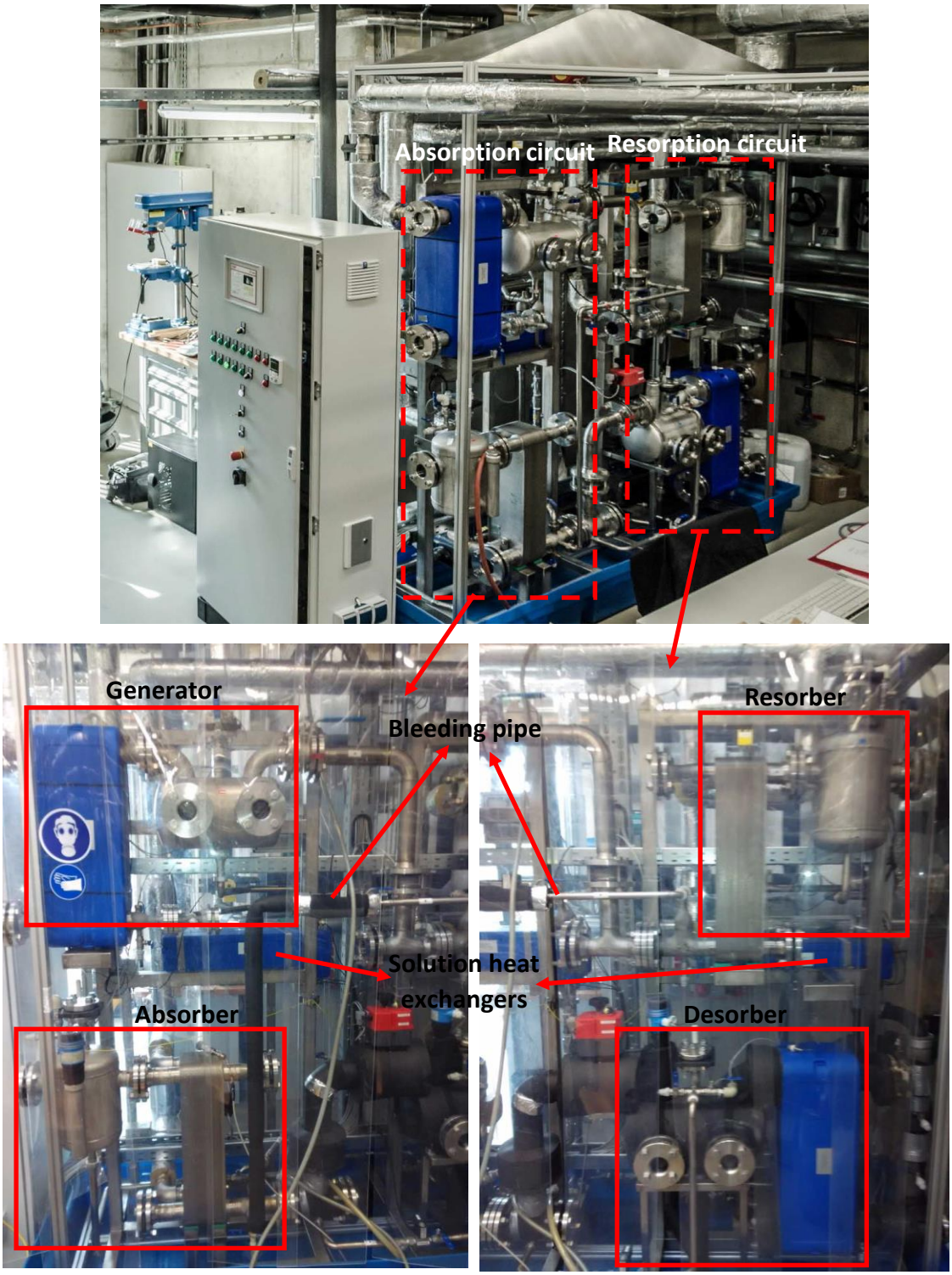

Figure 2.21 Ammonia/water absorption-resorption refrigeration plant in the test bench. Technische Universität Dresden (Germany).

Table 2.4 Datasheet of the heat exchangers used in the experimental plant.

Component	Model	Material	number of plates	Type of plates	Size (mm)
Generator	AlfaNova 76	Stainless steel AISI 316	50	Corrugated	767x192x157
Desorber	AlfaNova 76	Stainless steel AISI 316	50	Corrugated	767x192x157
Resorber	AlfaNova 76	Stainless steel AISI 316	50	Corrugated	767x192x157
Absorber	AlfaNova 76	Stainless steel AISI 316	50	Corrugated	767x192x157
SHX1 (absorption circuit)	AlfaNova 76	Stainless steel AISI 316	40	Corrugated	767x192x128
SHX2 (resorption circuit)	AlfaNova 76	Stainless steel AISI 316	20	Corrugated	767x192x71

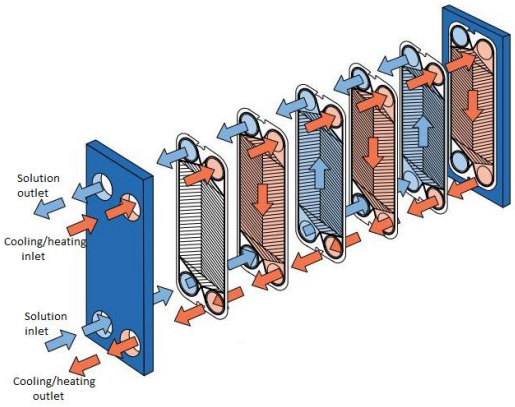

Figure 2.22 Flow configuration in the plate heat exchangers. Scheme provided by Alfa Laval.

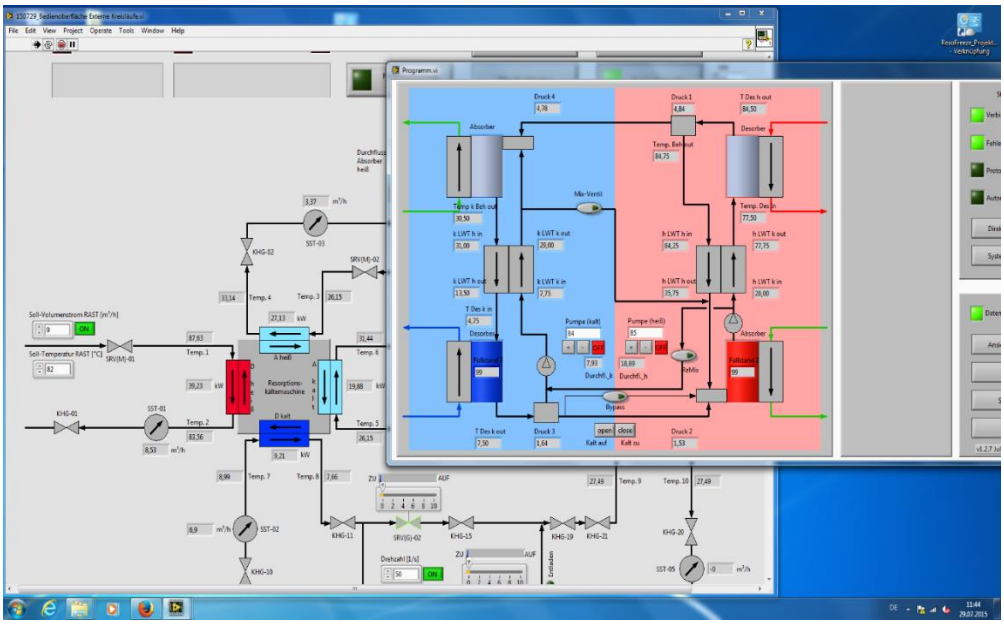

Figure 2.23 Control panel of the absorption-resorption refrigeration plant in the test bench.

2.3.2 Analysis of the experimental performance of the plant

As mentioned in the literature review of Chapter 1, several authors had already pointed out the inherent instability of the resorption cycles due to the additional degree of freedom and this fact make these systems particularly difficult to control. An accurate control of the concentrations in the circuits is required to regulate the bleeding mass flow rate and avoid the system to drift away from its thermodynamical point of operation. Since there is no automatic control of the experimental plant, a solenoid valve placed in the bleeding pipe must be activated manually for the bleeding process. An increment of the water content in the resorption circuit leads to an increase in the temperatures in the desorber due to the lower ammonia concentration in the solution [29]. When this situation takes place, the solenoid valve of the bleeding pipe must be opened for a certain period of time to equilibrate the mass balances between both circuits. This procedure leads to the following issues: first, the system is always working in a discontinuous way. Secondly, the lack of a flowmeter in the bleeding pipe make difficult to know the amount of solution transferred to the absorption circuit. Furthermore, the adjustment of the speed of the solution pumps to reach stable working conditions is also quite difficult. It is necessary to carefully balance the speed of the pumps in order to avoid the reservoirs being flooded and/or emptied. For all these reasons, the possibility of working under steady-state conditions for a long period of time becomes a challenge.

Additionally, pumping problems in the resorption circuit were also found. The solution leaving the desorber is under saturation conditions due to the boiling process in the desorber. For this reason, cavitation problems in the suction line of the pump are quite frequent, impeding the system to work properly even stopping the flow in the resorption circuit because the pump runs completely dry. This problem could be avoided increasing the height between the desorber reservoir and the intake of the pump, but due to the component location in the test bench (Figure 2.21) it was not possible to change the design of the plant. This problem was partially solved when the pump was changed by a new one with lower NPSH (EBARA EVM 3 7N5/0.75 M). With the new pump, the number of shutdowns during the experiments were significantly lower. Cavitation problems do not affect the pump of the absorption circuit, probably because the solution leaving the absorber is not really saturated.

2.3.3 Analysis of the experimental performance using the thermodynamic model

Despite the difficulties found during the experimental work, some good experimental results were obtained. The difficulty of working under steady-state conditions was already pointed out, so it was necessary to select just the experimental data obtained during a short period of time (when the system was working under quasi-stable conditions) to allow direct comparison between the experimental results and the results obtained with the steady-state model described in section 2.2.3. Figure 2.24 shows a scheme of the absorption-resorption cycle with the experimental and theoretical results depicted on it. Black-coloured data represent the results obtained with the model while red-coloured data represent the experimental results. The input data for the simulation (UA values of the heat exchangers, the effectiveness of the solution heat exchangers, the inlet temperature and flow rate of the external streams, the flow rate in the solution circuits and the high-pressure value of the system) were directly taken from the experimental data and are represented by colour green. During the experiment, a pressure drop of 0.2 bar between the absorption and the resorption circuit was registered, so the model was modified in order to take into account this pressure drop. The experimental UA values were determined as shown in section 2.2.3.2. The experimental data selected for this study correspond to the average value for a period of time of 15 minutes.

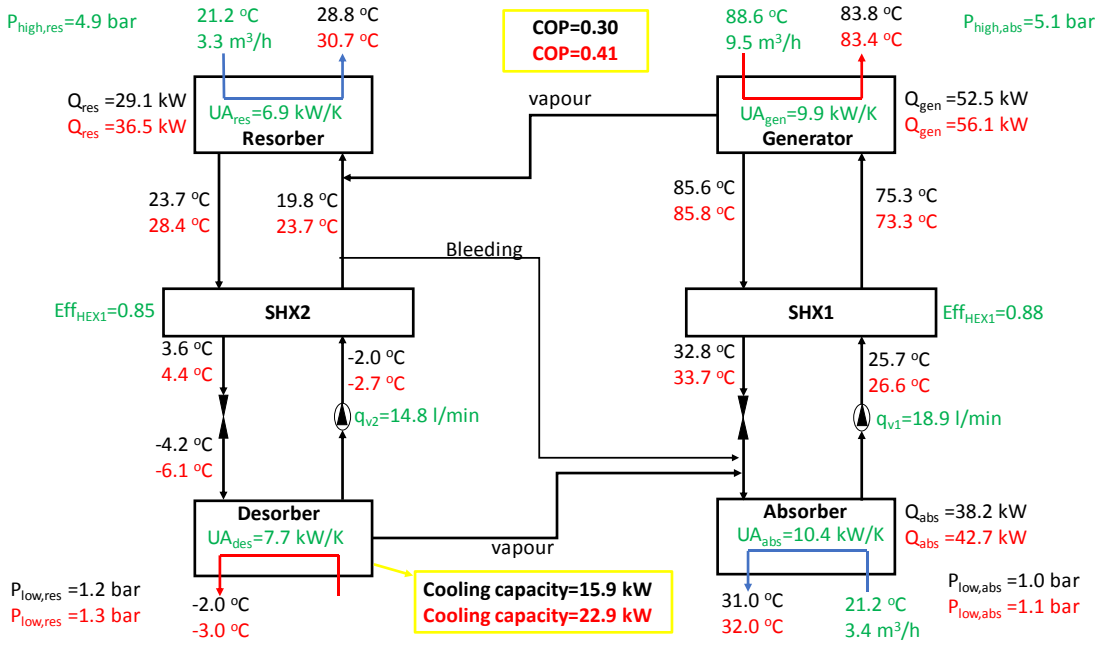

*Figure 2.24 Scheme of the ammonia/water absorption-resorption refrigeration system. Comparison between the experimental and theoretical results. **Green colour** represents input data. **Red colour** represents the results predicted by the model. **Black colour** represents the experimental results.*

The results depicted in Figure 2.24 show a wide deviation in terms of COP and cooling capacity between the experimental measurements and the results predicted by the model. A possible explanation for this disagreement could be that some of the assumptions considered in section 2.2.3 for modeling the cycle were not satisfied in the experiments carried out. The model assumes steady-state conditions but in the experimental test bench this condition was not fully accomplished. There was two flow meters in the solution circuits placed after each solution pump, but there were no flow meters in the rest of the pipes. For this reason, if the level of the liquid in the reservoirs at the outlet of the resorber or the generator are changing (filling or emptying) would mean that the flow rate of the solution leaving the reservoirs is different than the one expected if the system were working under steady state. The absence of flow meters in these parts of the systems make difficult to know precisely the flow rate entering the absorber and the desorber. Furthermore, the absence of flow meter in the bleeding line was also an important source of uncertainty because the control of this stream enables to determine the amount of solution transferred between both solution circuits. Then, the system was working in a discontinuous way all the time, opening and closing the valve of the bleeding line for a certain period of time, but with no assurance that the concentrations in the solution circuits were set at the desired values. Furthermore, the lack of devices to measure the ammonia concentration in the solution circuits make also more difficult the control of the system.

According to the temperatures in the solution circuits showed in Figure 2.24, it can be concluded that the highest deviations were obtained in the resorption circuit, particularly in the resorber. This fact might be an indication of a malfunction of the resorber by means of a poor absorption process of the vapour coming from the generator. As a result, the solution leaving the resorber

would be far from the saturation conditions and then the assumption made in section 2.2.3 concerning to the saturation conditions of the solution leaving the resorber could not be satisfied. Since both the absorber and the resorber have the same design, the subcooling at the outlet of the absorber should be also taken into consideration. However, the subcooling in the absorber is expected to be lower than in the resorber because a better agreement between the experimental results and the ones provided by the model was obtained. Hence, the thermodynamic model of the cycle was modified according to the following assumption: the solutions leaving the resorber and the absorber are not saturated, so there is a certain degree of subcooling. The subcooling of the solutions leaving the resorber ($\Delta T_{sub,res}$) and the absorber ($\Delta T_{sub,abs}$) are defined as follows:

$$\Delta T_{sub,res} = T_{sat,res} - T_{11} \tag{2.48}$$

$$\Delta T_{sub,abs} = T_{sat,abs} - T_{1} \tag{2.49}$$

where $T_{sat,res}$ and $T_{sat,abs}$ are the saturation temperature of the solution at the concentration and pressure conditions at the outlet of the resorber and the absorber, respectively. The subcooling conditions showed in Equations 2.48 and 2.49 are input variables in the new version of the model, replacing the previous assumptions of saturation conditions at the outlet of the absorber and resorber.

A parametric table was created varying the subcooling of the solution at the outlet of the resorber ($\Delta T_{sub,res}$) and the absorber ($\Delta T_{sub,abs}$). The temperature values, COP and heat supplied/released on each component obtained in the parametric study were analyzed to determine if there is a significant improvement in the agreement between the experimental results and the ones obtained with the model. Indeed, a very good agreement was obtained when $\Delta T_{sub,res}$=8.3ºC and $\Delta T_{sub,abs}$=1.5ºC, as shown in Figure 2.25.

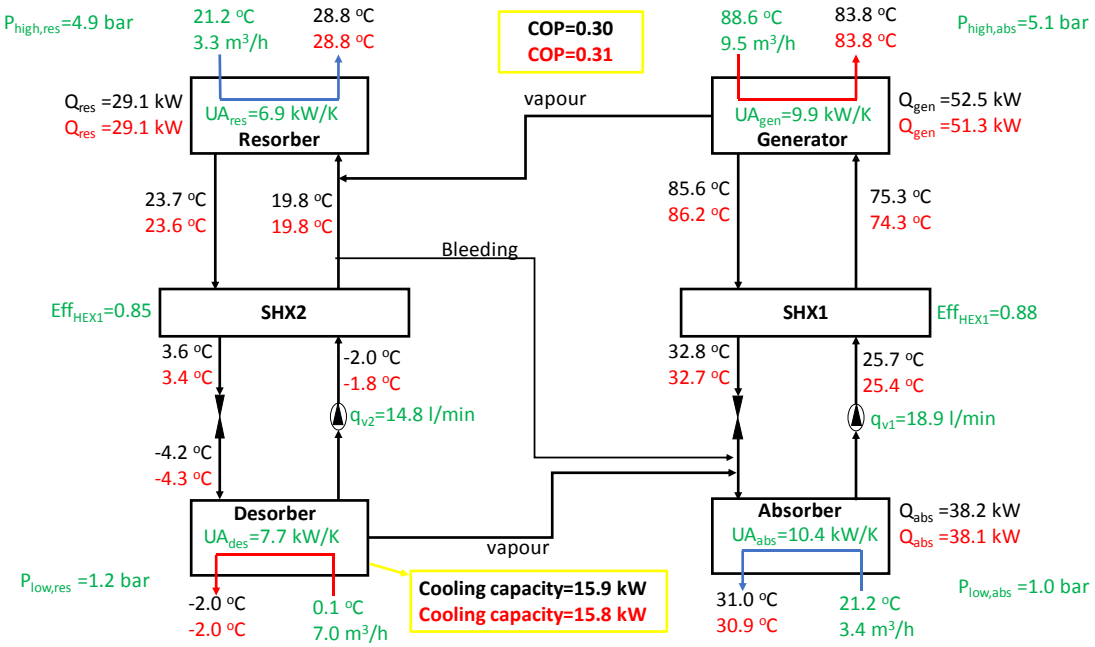

*Figure 2.25 Comparison between the experimental and theoretical results assuming subcooling at the outlet of the resorber and the absorber. **Green colour** represents input data. **Red colour** represents the results predicted by the model. **Black colour** represents the experimental results.*

The deviation between the temperatures predicted by the model and the experimental ones were lower than 1°C in all cases, and the deviation obtained in the COP and cooling capacity was nearly zero. As expected, the subcooling obtained at the outlet of the resorber was much higher than the one obtained in the absorber, so the hypothesis of the poor absorption process in the resorber has been evidenced. A possible reason for this different performance between the resorber and the absorber could be the different temperature of the vapour. In the case of the absorber, the vapour coming from the desorber is much colder than the solution, leading into a cooling effect of the solution that enhance the absorption process. On the contrary, in the case of the resorber, the vapour coming from the generator is much hotter than the solution, leading into a heating effect that runs against the absorption process. If so, the heat transfer area of the resorber must be higher than in the case of the absorber or the vapour distribution into the solution must be improved in order to enhance the mass and heat transfer and then reduce the size of the heat exchanger.

2.4 Measures to improve the performance of absorption-resorption refrigeration plants

In order to enhance the performance of the ammonia/water absorption-resorption refrigeration plant, the research group of Refrigeration, Cryogenics and Compressor Technology of TU Dresden is investigating how to improve the ammonia vapour distribution into the ammonia/water solution using stainless steel lance with drilled holes and membrane lances. The preliminary results obtained show an increase of cooling capacity and the COP [49]. They also studied the optimisation of the bleeding flow rate to maintain continuous operation under stationary conditions. They achieved stable operation for a period of 30 minutes by means of setting the bleeding flow rate at 0.2 l/min.

As mentioned before, the control of the absorption-resorption refrigeration system could be also improved by means of the integration of devices for the in-situ determination of the ammonia concentration in some key points of the cycle. This measurement system of the ammonia concentration should be linked to the control of the flow rate in the bleeding line to ensure the cycle to work under steady-state conditions. For systems based on ammonia/water mixtures, composition is usually measured in real-time from density by means of Coriolis flow and density-meters, but the cost of these devices limits their application when several devices need to be installed. Thus, the challenge for research is to find more economic analytical methods for the in-situ analysis of the working fluid mixture. In the frame of this doctoral thesis, a method based on near-infrared (NIR) spectroscopy for the in-situ determination of the ammonia concentration was studied.

Near-infrared (NIR) spectroscopy is one of the most commonly used techniques for the in-situ analysis of samples due to the low cost of optical fibers that work in this region, to the variety of probes and cells available to work in extreme conditions of pressure and temperature and to the chemometric facilities that are incorporated in the software of the instruments. There are many referenced applications of this technique joint to the multivariate analysis of the spectral data for the analysis of the composition of complex mixtures and for the analysis and control of chemical and physical properties of compounds involved in processes [50–52]. However, this technique has not been fully implemented in absorption heat pumps/refrigeration systems so far. In recent years, our research group have made many efforts to incorporate this technique in experimental test benches to measure the composition of the mixtures typically used in absorption cycles [53–55]. The work carried out in this thesis was mainly focused in the implementation of the NIR spectroscopy to determine the composition of the ammonia/water

mixture circulating in an absorber test bench. The results obtained were published in the International Journal TALANTA [56].

The experimental set up of the NIR measurement system integrated in the absorber test bench consist of a stainless-steel flow cell 15cm high and with an outlet diameter of 5cm equipped with two sapphire windows through which the light passes. The cell was designed and constructed in our research group, however it is possible to find flow cells in the market at a very competitive price. One of the companies that markets these cells is Avantes. Optical fibers were used to direct and record the light from the lamp (HL-2000-CAL tungsten halogen light source) to the detector (Maya 2000 Pro Vis-NIR spectrophotometer). The detector was connected to the computer for spectra acquisition. The data recorded was pretreated using MATLAB subroutines. Pressure and temperature sensors were placed next to the cell. Figure 2.26 shows a picture of the NIR measurement system integrated in the absorber test bench.

The ammonia/water solution flows through the cell whereas the light coming from the source passes across the cell in order to be collected in the spectrophotometer, where the spectra were recorded between 997.6 and 1065 nm. The absorbance values at the maximum of the absorption band (1041 nm) are considered as response in order to determine the relationship between the ammonia mass fraction, pressure, temperature and absorbance. The 1041 absorption band is attributable to the stretching vibration of the -NH functional group present in the NH_3. All the details about the calibration method and the validation of the technique can be found in Barba et al. [56].

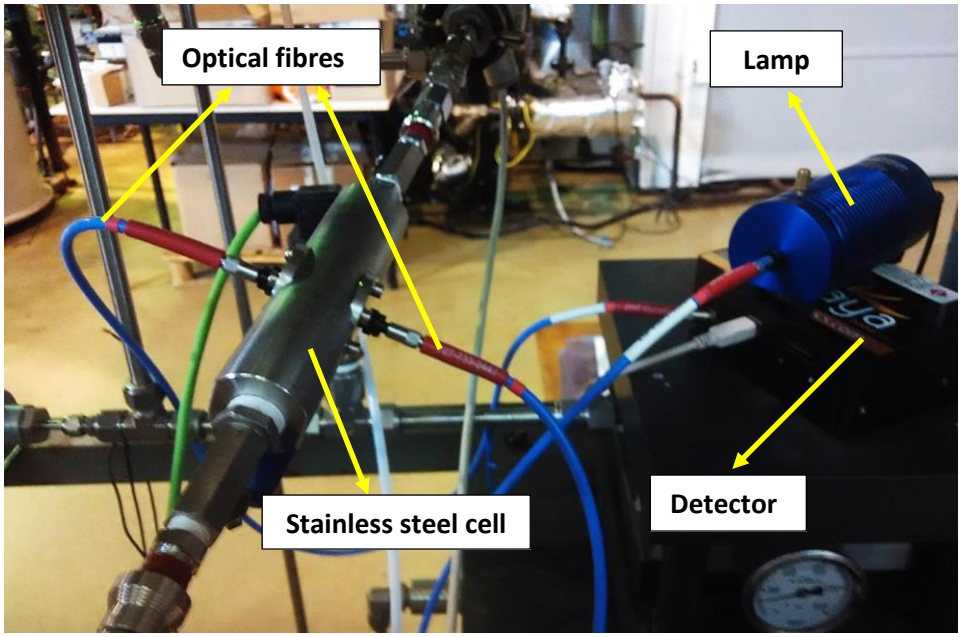

Figure 2.26 Experimental set up for the data acquisition using a NIR measurement system.

The most expensive components of the NIR measurement system are the lamp and the detector. Nevertheless, by means of a multiplexor it would be possible to determine the ammonia concentration at several points in the absorption cycle just using one detector and one lamp. This would lead into an important advantage compared to the conventional Coriolis density meters. As an example, Figure 2.27 shows a scheme of the ammonia/water absorption-

resorption cycle with the NIR measurement system integrated on each stream of the solution circuits. The location of the cells proposed in the scheme was determined to ensure that the solution flowing in such places is highly subcooled in order to avoid two-phase flow that could disturb the measurements of the NIR. As future work, the development of an automated control system of the absorption-resorption cycle based on the NIR measurements could be a very interesting research project because the NIR technique is reliable and cost competitive and might improve the control of the ammonia/water absorption-resorption systems in a very significant way.

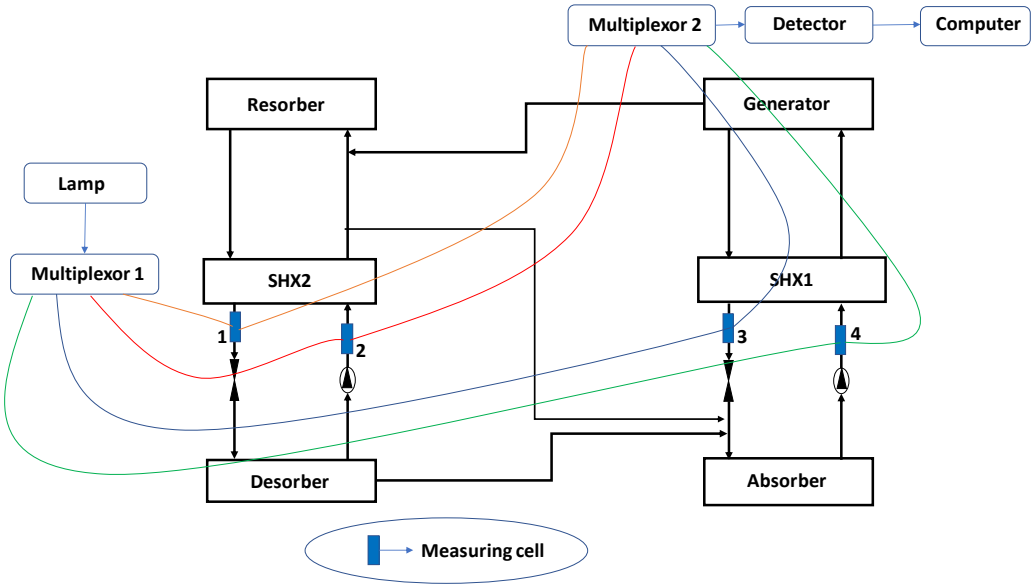

*Figure 2.27 Scheme of the ammonia/water absorption-resorption cycle with the NIR measurement system integrated. **Green**, **blue**, **red** and **orange**-coloured lines represent the optical fibres.*

2.5 Conclusions

In this chapter, the ammonia/water absorption-resorption refrigeration cycle has been studied and its wide operation flexibility was showed. This flexibility can be used for reducing the high-pressure of the system by means of reducing the ammonia concentration in the solution circuits but keeping the same temperature levels of the heat sources. Two thermodynamic models have been developed and used for a sensitivity analysis of the cycle. The main conclusions are listed below:

- The cycle configuration without rectifier is the most favourable because the complexity, size and cost of the system would be lower, and the loss of performance is not significant (below 8%).

- The effectiveness of the solution heat exchanger of the resorption circuit becomes critical below certain values. Then, a proper design of the solution heat exchanger of the resorption circuit is essential not only for the COP but also for the working of the cycle at desired temperatures.

- Reducing the high-pressure leads into lower COP. Furthermore, reaching a maximum value of COP and cooling capacity at the same time is not possible, so it is necessary to find a compromise between the reduction of the high-pressure, the COP and the cooling capacity.

Finally, attending to the results obtained during the study of the cycle, the working conditions suggested for the base case (Table 2.1) were:

- p_{high}= 5 bar; p_{low}=1.3 bar
- Mass flow rate in the absorption circuit 1.25 times higher than the mass flow rate in the resorption circuit.
- Ammonia mass fraction of the solution leaving the absorber and the resorber→ x_{abs}=0.36; x_{res}=0.61
- Ammonia mass fraction difference in both circuits → $\Delta x_{abs}\approx 0.07$; $\Delta x_{res}\approx 0.05$
- COP=0.52
- Q_{des}=18kW; Q_{gen}=35kW; Q_{res}=19kW; Q_{abs}=31kW

A 25-kW ammonia/water absorption-resorption refrigeration plant set up at TU Dresden was described and the difficulty of working under steady-state conditions was pointed out during the experimental work. The implementation of measures for improving the control of the system are required. The thermodynamic model with external heat transfer was used for the analysis of the performance of the plant and it was concluded that the absorption process in the resorber needs to be enhance. A possible explanation to this malfunction could be the higher temperature of the vapour in the resorber (≈85ºC) compared to the absorber (≈0ºC), that leads into a heating effect that runs against the absorption process. Thus, the size of the resorber must be higher than in the case of the absorber or the vapour distribution into the solution must be improved in order to enhance the mass and heat transfer processes.

Finally, a new method based on near-infrared spectroscopy for the in-situ determination of the ammonia concentration was proposed in order to improve the performance of the absorption-resorption plants. By means of a multiplexor, this new method allows to measure the ammonia concentration in several points of the cycle just using one detector and one lamp, leading then in a cheaper alternative than using the conventional Coriolis density-meters.

Nomenclature of chapter 2

COP	[-]	Coefficient of performance
Eff_{SHX1}	[-]	Effectiveness of the solution heat exchanger of the absorption circuit
Eff_{SHX2}	[-]	Effectiveness of the solution heat exchanger of the resorption circuit
h	[J/kg]	Specific enthalpy
m	[kg/s]	Mass flow rate
qv	[l/min]	Volumetric flow rate
Q_{des}	[kW]	Cooling capacity
T	[^oC]	Temperature
UA	[W/K]	Product of the overall heat transfer coefficient and the heat transfer area
W_p	[kW]	Power consumption of the pump
x	[-]	Ammonia mass fraction

Special characters

β	[-]	Pressure ratio (p_{high}/p_{low})
ν	[m^3/kg]	Specific volume

Subscripts

abs	Absorption
CW	Cooling water
ext	External
gen	Generator
HS	Heat supply
in	Inlet
liq	Liquid
lmtd	Logarithmic mean temperature difference
max	Maximum
min	Minimum
out	Outlet
p1	Solution pump of the absorption circuit
p2	Solution pump of the resorption circuit
rect	Rectifier
res	Resorber
sub	Subcooling
sat	Saturation
vap	Vapour

Chapter 3

Theoretical and Experimental Study of the Ammonia/Water Absorption Process Using a Flat Sheet Membrane Module

The main objective of this chapter is the determination of the desired membrane characteristics to be used as contactor for the ammonia absorption process into ammonia/water solutions. As showed in Chapter 1, several authors have already determined the characteristics of the membranes required for the water absorption process into water/lithium bromide mixtures. Regarding the ammonia/water mixture, Schaal [43] highlighted the importance of the pore size and the use of hydrophobic materials in the membrane in order to avoid liquid breakthroughs, but there was no information related to the optimum pore size, thickness or porosity required for the ammonia absorption process.

In this chapter, a hydrophobic microporous flat sheet membrane contactor was proposed and studied as an absorber for the ammonia/water absorption-resorption refrigeration cycle. The heat and mass transfer process in the adiabatic flat sheet membrane module was investigated experimentally and analytically. For the experimental study, a membrane absorber test bench was designed and built. Taking advantage of the availability in our research group of a reverse osmosis flat sheet membrane module, we decided to use it for this first experimental study before buying another commercial hollow fibre membrane module. The information provided by Schaal was used as a basis for the selection of the hydrophobic microporous flat sheet membrane used in this chapter. Moreover, a unidimensional model was developed and validated with the experimental results. The influence of the temperature, concentration, flow rate and membrane characteristics on the absorption process was evaluated. The membrane characteristics suggested at the end of this study were used for the selection of the commercial hollow fibre membrane module used in Chapter 4. The results presented in this chapter were published in Applied Thermal Engineering [57].

3.1 Experimental set-up

An experimental test bench was set up to study the ammonia vapour absorption process in an ammonia/water solution using polymeric porous membranes as contactors. Because there are no commercial membrane modules available on the market for this specific application, a membrane module designed by the manufacturer for reverse osmosis (Sterlitech SEPA CF Module) had to be adapted to meet the requirements of the absorption process. The membrane used (9.5 cm x 14.6 cm) was a hydrophobic polytetrafluoroethylene (PTFE) laminated membrane (Sterlitech) with an average pore size of 0.05 µm. The 60-µm thin active layer (PTFE) is laminated onto a 0.18 mm polypropylene layer. Figure 3.1 shows a scheme of the flat sheet membrane module. The ammonia/water weak solution enters the membrane module and is homogeneously distributed by the feed spacer all over the membrane surface. The ammonia vapour enters the module from the top, crosses the pores of the membrane and is absorbed by the solution in the liquid interface. Then, the ammonia/water solution exits the absorber at higher concentration and higher temperature.

Figures 3.2 and 3.3 show a picture and a detailed diagram of the experimental test bench, respectively. The plant consists of two tanks; one for the weak solution (feed tank) and the other for the strong solution that leaves the membrane absorber (product tank). In turn, it has a solution diaphragm pump (Weimer Hydra-Cell series D03), two filters (90 and 7 microns) for preventing any solid particles from soiling the membrane, a thermostatic bath (HUBER CC 308) for setting the inlet temperature of the solution, a mass flow controller (ALICAT MCS 5slpm) for measuring the ammonia vapour flux, a flat sheet membrane module (Sterlitech SEPA CF Module) and a Coriolis flow and density-meter (EMERSON Micro Motion® Elite® CMF010M) for measuring the flow rate and the density of the solution. The ammonia concentration of the solution was determined from the density, pressure and temperature measurements. The

method described in the previous chapter for the determination of the ammonia concentration using near infrared spectroscopy was not used because this experimental study was conducted prior to the work carried out with the NIR technique. The ammonia used for the experiments was supplied by Carburos Metálicos (purity>99.98%). Finally, several pressure and temperature sensors were located at key points in the plant so that the heat transfer process could be studied. Table 3.1 shows the parameters measured and the accuracy of each instrument.

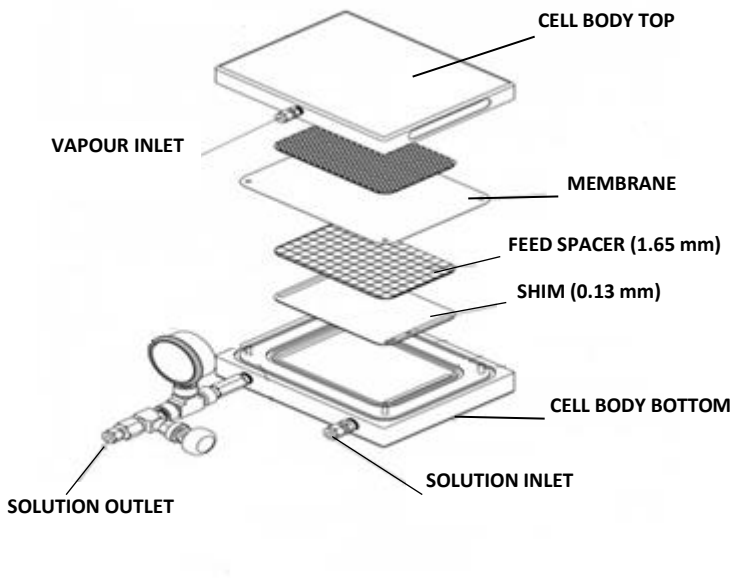

Figure 3.1 SEPA-CF membrane module assembly provided by Sterlitech [58].

Table 3.1 Measured variable and accuracy of the instruments

Instrumentation	Variable measured	Accuracy
Coriolis flow and density meter (CMF010M)	Density and flow rate of the solution.	± 0.5 kg/m^3; $\pm 0.05\%$ of flow rate [kg/h]
Pressure transmitter (WIKA S-10)	Pressure [bar]	$\pm 0.25\%$ (full scale)
PT100	Temperature	± 0.1 K
Mass flow controller (ALICAT MCS 5 slpm)	Mass flow rate of the ammonia vapour	± 0.1 l/min (standard conditions)

The solution inlet conditions (pressure, temperature and flow rate) had to be set before the solution entered the membrane module. During the set-up process the solution was recirculated to the feed tank by using the recirculation circuit and keeping the valve V2 (Figure 3.3) closed. Once the solution inlet conditions had been set to the desired values, V2 was opened and the experiment started. The ammonia vapour flow rate was then increased using the mass flow controller (MFC) until bubbles were observed at the outlet of the membrane module. In order to observe the bubbles, a section of PTFE-tube was installed at the outlet of the membrane

module (Figure 3.2b). The valve V1 remained closed throughout the experiment so it can be assumed that all the ammonia entering the module was absorbed into the solution. The driving force of the absorption process was the difference between the operating gas pressure and the ammonia vapour partial pressure at the membrane-liquid interface. The pressure on both sides of the membrane module had to be controlled to prevent liquid breakthroughs inside the pores when $p_{liq}>p_{gas}$ [43]. For this reason, the pressure difference between the liquid and gas side was kept below 0.1 bar during the experiments by means of V4.

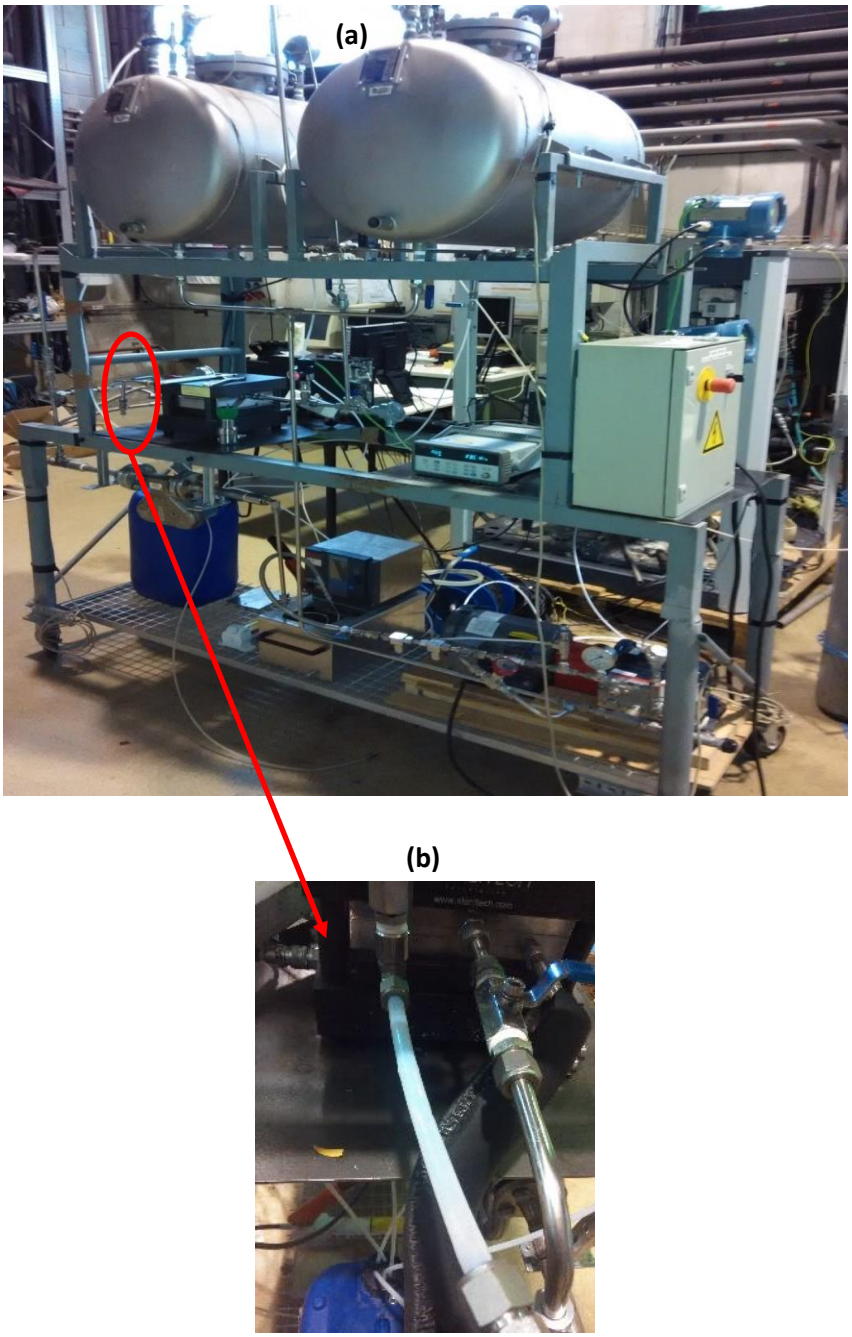

Figure 3.2 ***(a)*** *Picture of the pilot plant experimental test bench.* ***(b)*** *Picture of the outlet of the membrane module with the PTFE tube.*

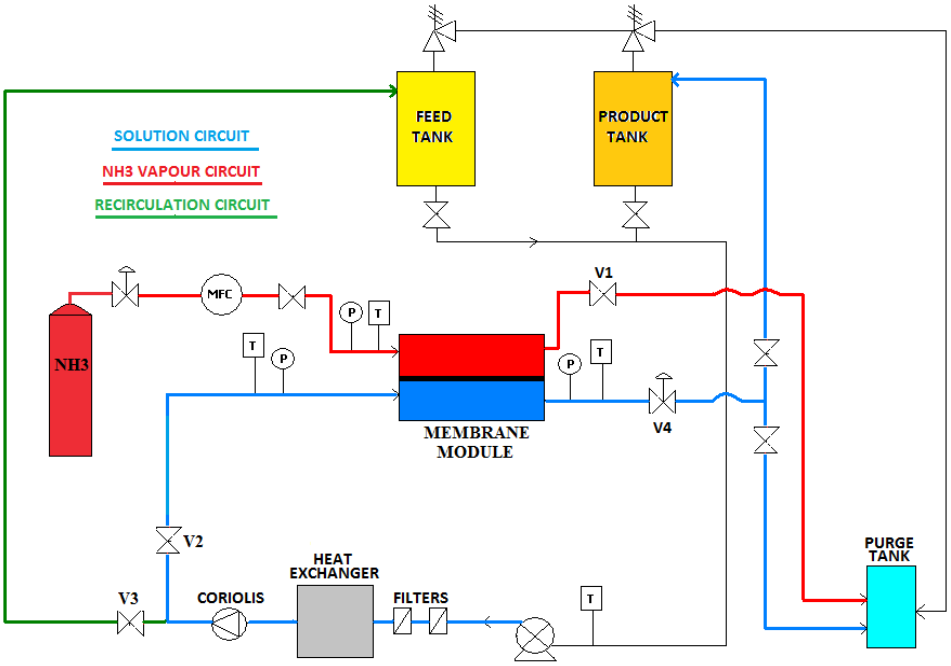

Figure 3.3 Scheme of the pilot plant membrane absorber test bench

3.2 Theoretical model

A unidimensional model was developed using Engineering Equation Solver (EES) to study the adiabatic absorption process when a microporous membrane was used as contactor. Essentially the model determines the amount of ammonia absorbed and the heat generated during the absorption process. The input data are the feed inlet conditions (pressure, temperature, flow rate and ammonia concentration of the solution). The flat sheet membrane module (14.6cm x 9.5cm) was discretized in 146 elements, and the mass and energy balances, transport equations and equilibrium conditions were applied to each one of them.

As far as the thermodynamic and transport properties of the working fluids are concerned, the density and enthalpy were taken from Ibrahim [44], the thermal conductivity was calculated using the Bohne equation from Cuenca et al. [59] and the viscosity, heat capacity and diffusion coefficient of ammonia in water were calculated from Conde [60].

3.2.1 Mass transfer across the pores of the membrane

Two transport resistances were considered to model the ammonia flow across the membrane: the resistance in the liquid boundary layer and the transport resistance across the pores of the membrane. The resistance in the vapour boundary layer was neglected because the ammonia in the gas side is assumed to be pure. Depending on the value of the Knudsen number, Kn (defined as the ratio of the molecule mean free path to pore characteristic diameter), the mechanism by which vapour is transported through the membrane can be any one of the following: (a) Knudsen diffusion (Kn≥10), (b) viscous or Poiseuille flow (Kn<0.01) and (c) transition flow (0.01≤Kn<10). The dusty-gas model [61] assumes that the Knudsen diffusion resistance R_K is in parallel with the Poiseuille flow resistance R_P, obtaining:

$$\frac{1}{R_m} = \frac{1}{R_K} + \frac{1}{R_p} = K_m \tag{3.1}$$

Due to the Knudsen number range obtained in this study (between 1.1 and 1.3), a transition flow has been considered and both resistances have been taken into account. According to the resistance analogy the mass transport coefficient (K_m) can be written as [37]:

$$K_m = \frac{M_{NH3}}{\delta} \cdot \left(\frac{D_k}{R \cdot T_{MM,mean}} + \frac{p_{gas} \cdot B_0}{R \cdot T_{MM,mean} \cdot \mu_{BG}} \right) \tag{3.2}$$

where p_{gas} is the pressure in the gas side, $T_{MM,mean}$ is the mean membrane temperature which is calculated as the average of the vapour and solution interface temperatures and μ_{BG} is the gas viscosity. The tortuosity factor (τ) is calculated by [40]:

$$\tau = \frac{(2-\varepsilon)^2}{\varepsilon} \tag{3.3}$$

The Knudsen diffusion coefficient (D_k) is calculated using equation 3.4 [37]:

$$D_k = K_0 \left(\frac{8 \cdot R \cdot T_{MM,mean}}{\pi \cdot M_{NH3}} \right) \tag{3.4}$$

where K_0 and B_0 are constants defined as follows [33]:

$$K_0 = \frac{\varepsilon \cdot d_p}{3\tau} \tag{3.5}$$

$$B_0 = \frac{\varepsilon \cdot \left(\frac{d_p}{2}\right)^2}{8\tau} \tag{3.6}$$

Finally, the ammonia flux across the membrane (J) is obtained with equation 3.7.

$$J = K_m \cdot (p_{gas} - p_{int}) \tag{3.7}$$

where p_{gas} is the gas pressure and p_{int} is the partial ammonia vapour pressure at the temperature and concentration of the interface. The ammonia flux (J) is calculated for every element of the discretized membrane module because the temperature and the composition change throughout the module.

3.2.2 Mass transfer in the liquid phase

Using the film theory [62], the ammonia concentration at the interface (x_{int}) can be calculated from a mass balance across the solution concentration boundary layer as:

$$x_{int} = x_{BL} \cdot exp\left(\frac{J}{\rho_{NH3} \cdot K_{BL}} \right) \tag{3.8}$$

where ρ_{NH3} is the density of the liquid ammonia, x_{int} is the ammonia concentration at the liquid interface boundary layer and K_{BL} is the mass transfer coefficient between the liquid interface and the bulk solution. K_{BL} is calculated using the formula presented by Gabelman and Hwang [63] for the rectangular membrane module (Eq. 3.9).

$$Sh = \frac{K_{BL} \cdot d_h}{D_{BL}} = 0.18 Re^{0.86} Sc^{0.33} \tag{3.9}$$

where D_{BL} is the diffusion coefficient of ammonia in water. The mass flow rate of the ammonia (vapour) absorbed is determined by:

$$m_{abs} = J \cdot dA \tag{3.10}$$

where dA is the discretized membrane area. Finally, the total and species mass balances are presented in Eq. (3.11-3.13) and Figure 3.4 shows the schematic diagram of the absorption process. A co-current flow between liquid and vapour is assumed.

$$m_{BL}[n+1] = m_{BL}[n] + m_{abs} \tag{3.11}$$

$$m_{BG}[n+1] = m_{BG}[n] - m_{abs} \tag{3.12}$$

$$m_{BL}[n+1] \cdot x_{BL}[n+1] = m_{BL}[n] \cdot x_{BL}[n] + m_{abs} \tag{3.13}$$

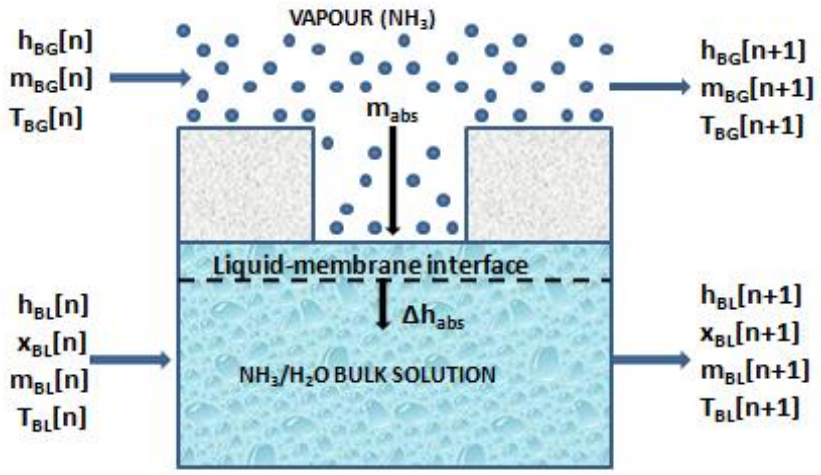

Figure 3.4 Schematic diagram of the absorption process modelled.

3.2.3 Heat transfer

Because the absorber considered is adiabatic, heat is assumed not to be lost to the surroundings [43] and all the heat released during the absorption process is completely transferred to the liquid and vapour phase. The energy balances for the liquid and the vapour sides are shown in equations 3.14 and 3.15, respectively.

$$m_{BL}[n] \cdot h_{BL}[n] + m_{abs}[n] \cdot \Delta h_{abs}[n] = m_{BL}[n+1] \cdot h_{BL}[n+1] + U[n] \cdot dA \cdot (T_{BL}[n] - T_{BG}[n]) \tag{3.14}$$

$$m_{BG}[n] \cdot h_{BG}[n] + U \cdot dA \cdot (T_{BL}[n] - T_{BG}[n]) = m_{BG}[n+1] \cdot h_{BG}[n+1] \tag{3.15}$$

U is the overall heat transfer coefficient (Eq. 3.16) and Δh_{abs} is the heat released in the absorption process.

$$\frac{1}{U} = \frac{1}{\alpha_{BL}} + \frac{\delta}{\lambda_{MM}} + \frac{1}{\alpha_{BG}} \tag{3.16}$$

where α_{BL} is the heat transfer coefficient in the liquid phase and is obtained using the analogy between the heat and mass transfer [32]. α_{BG} is the heat transfer coefficient in the gas phase and is obtained using the correlation shown in Eq. (3.17) developed by Shah and London [64] for rectangular channels.

$$Nu_{BG} = 8.235 \cdot (1 - 2.0421\left(\frac{H}{W}\right) + 3.0853\left(\frac{H}{W}\right)^2 - 2.4765\left(\frac{H}{W}\right)^3 + 1.0578\left(\frac{H}{W}\right)^4 - 0.1861\left(\frac{H}{W}\right)^5) \quad (3.17)$$

where (H/W) is the aspect ratio (height/width) of the rectangular channel.

$$\lambda_{MM} = \varepsilon \cdot \lambda_{BG} + (1 - \varepsilon) \cdot \lambda_{mat} \quad (3.18)$$

λ_{MM} is the membrane thermal conductivity, obtained using Eq. (3.18), where λ_{BG} and λ_{mat} are the thermal conductivity of the bulk gas and the membrane, respectively. The value of λ_{mat} is 0.25 W/(m·K) and it was taken from Khayet et al. [65]. Finally, the interface temperatures are determined with the following energy balance at the liquid-membrane interface (Eq. 3.19) and the energy balance at the vapour-membrane interface (Eq. 3.20).

$$\alpha_{BL}[n] \cdot \left(T_{liq,int}[n] - T_{BL}[n]\right) = J[n] \cdot \Delta h_{abs}[n] - \frac{\lambda_{MM}}{\delta} \cdot \left(T_{liq,int}[n] - T_{vap,int}[n]\right) \quad (3.19)$$

$$\alpha_{BG}[n] \cdot \left(T_{vap,int}[n] - T_{BG}[n]\right) = \frac{\lambda_{MM}}{\delta} \cdot \left(T_{liq,int}[n] - T_{vap,int}[n]\right) \quad (3.20)$$

where $T_{liq,int}$ and $T_{vap,int}$ are the solution-membrane and vapour-membrane interface temperatures, respectively.

3.3 Results

3.3.1 Parametric study

This section discusses how various parameters evolve throughout the membrane module. The base case working conditions in the absorber were set according to the operating conditions proposed in Chapter 2 for the absorber of the ammonia/water absorption-resorption refrigeration cycle. Table 3.2 lists the working conditions and geometrical dimensions of the membrane module used in the study.

Figure 3.5 shows the evolution of the bulk solution concentration and the bulk solution temperature throughout the membrane module at different mass flow rates. Figure 3.6 shows the variation of the ammonia absorption rate (J) throughout the membrane module at different mass flow rates. As expected, the ammonia concentration increases and, because of the adiabatic absorption process, so does the solution temperature. It can also be observed that the higher the flow rate is the lower the increment in the temperature and concentration value (Figure 3.5), but also the higher the ammonia absorption rate is obtained (Figure 3.6). These effects can be explained because the higher amount of ammonia absorbed when the flow rate is increased is not high enough to balance the dilution effect produced when the ammonia vapour is absorbed in a larger amount of solution as a result of the increase in the flow rate. Due to the increment in the temperature and concentration of the ammonia solution, the driving force of the absorption process decreases, so the ammonia flux across the membrane has to decrease throughout the membrane module. This effect can be observed in Figure 3.6.

Table 3.2 Input values for the parametric study.

	Base case	Range
Pressure	1.3 bar	NA
Inlet solution temperature	25 °C	10-31 °C
Inlet gas temperature	25 °C	NA
Inlet solution concentration	32wt%	26-35 wt%
Solution mass flow rate	45 kg/h	10-200 kg/h
Membrane porosity, ε	70%	20-90 %
Membrane thickness, δ_m	60 µm	20-1000 µm
Pore diameter, d_p	0.05 µm	0.01-0.2 µm
Solution/gas channel width	9.5 cm	NA
Solution/gas channel length	14.6 cm	NA
Solution channel height	1.7 mm	NA
Gas channel height	0.17 mm	NA

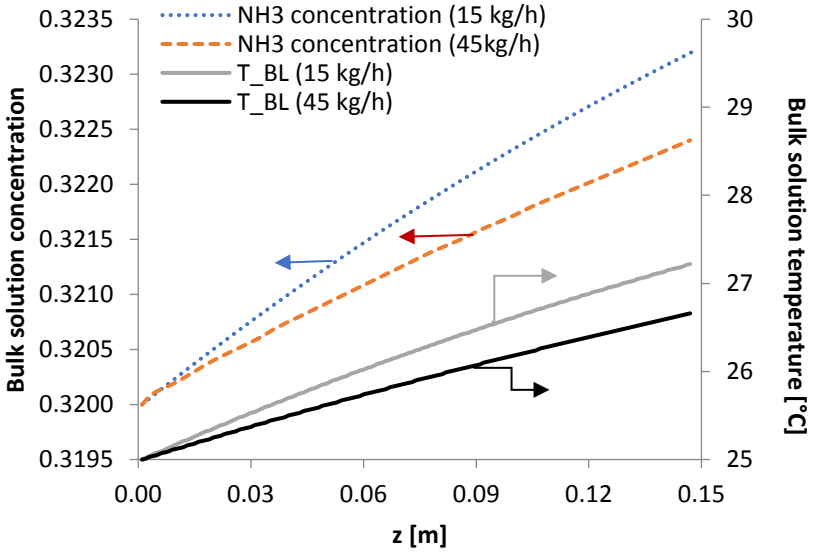

Figure 3.5 Variation of the ammonia concentration and the temperature in the bulk solution throughout the membrane module.

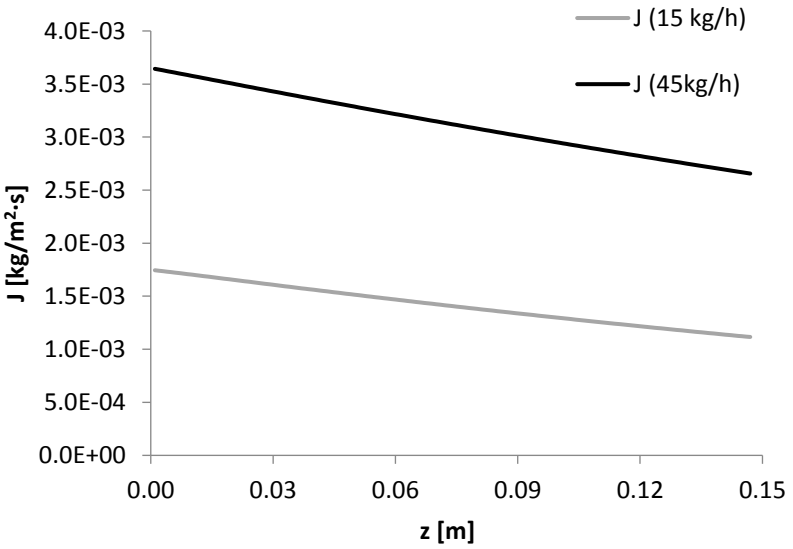

Figure 3.6 Variation of the ammonia absorption rate throughout the membrane module.

The effect of several operating parameters on mass transfer resistances is discussed below. Base case parameters from Table 3.2 were used as default. Resistance to mass transfer inside the membrane was determined using Eq. (3.1) and resistance to mass transfer inside the bulk solution (R_s) was calculated according to Venegas et al [40], where p_{sat} is the saturated ammonia pressure corresponding to the bulk solution temperature and ρ_{NH3} is the liquid ammonia density.

$$R_s = \frac{p_{sat}}{\rho_{NH3} \cdot K_{BL}} \tag{3.21}$$

Figure 3.7 shows the considerable influence of the solution mass flow rate on the mass transfer resistance in the liquid phase.

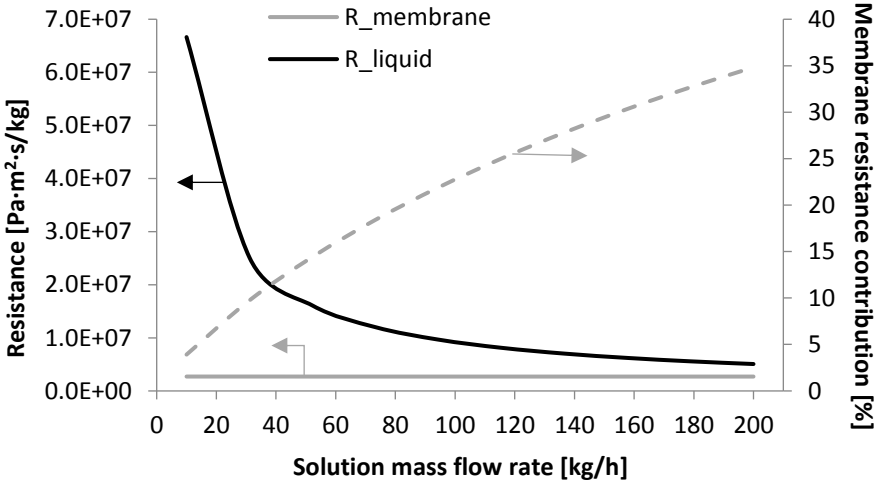

Figure 3.7 Effect of the solution mass flow rate on mass transfer resistances

For the whole range studied, the mass transfer process is mainly governed by the resistance in the liquid phase. This effect is even more marked when the flow rate is lower than 35 kg/h. Increasing the solution mass flow rate decreases the resistance in the liquid phase and the resistance in the membrane becomes significant. Thus, for example, at a solution mass flow rate

of 200 kg/h the membrane resistance represents 35% of the total resistance. Figures 3.8 and 3.9 indicate that for the range studied, the effect of the solution inlet temperature and solution inlet concentration on the mass transfer resistance is almost negligible.

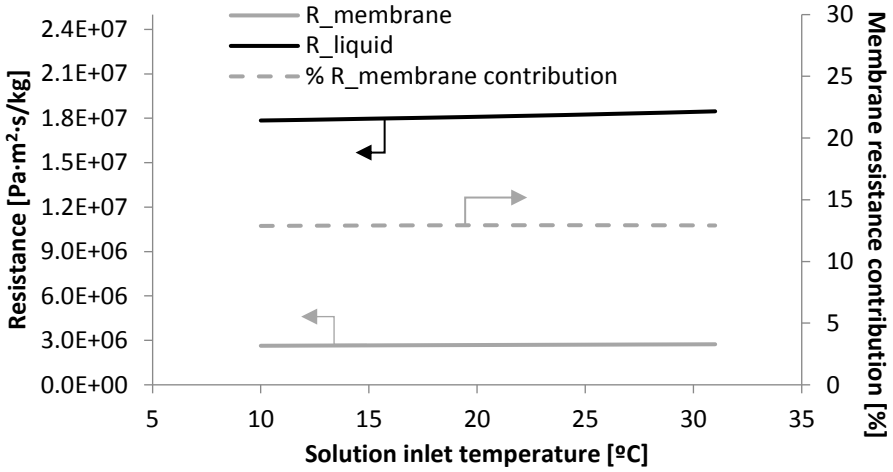

Figure 3.8 Effect of the solution inlet temperature on mass transfer resistances.

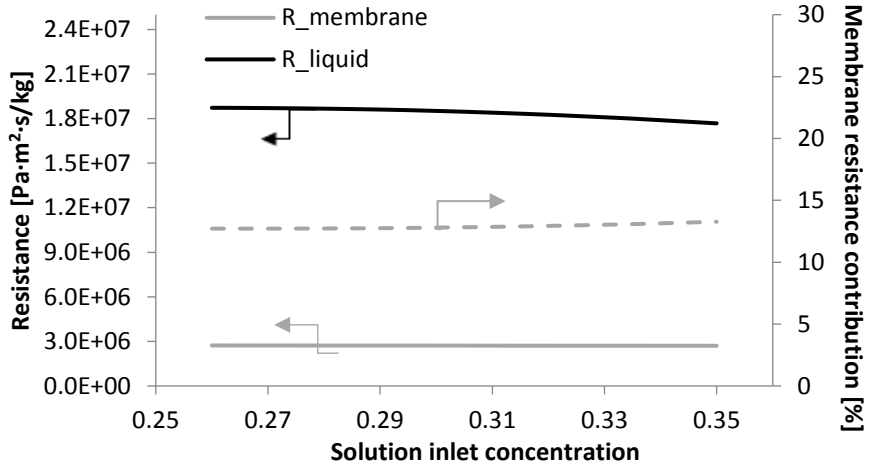

Figure 3.9 Effect of the solution inlet concentration on mass transfer resistances.

The effect of the main membrane characteristics on the mass transfer resistances was also studied. Figure 3.10 shows the effect of the membrane pore diameter on the mass transfer resistances. It can be observed that for pore diameters below 0.03µm the mass transfer resistance across the pores of the membrane is considerable and contributes 44.4% of the total resistance for a pore diameter value of 0.01µm. However, for pore diameters higher than 0.1µm the total resistance is clearly governed by the resistance in the liquid phase. So, it can be deduced that the optimal pore diameter of the membrane is between 0.03µm and 0.1µm. Pore diameters smaller than 0.03µm mean that the resistance of the membrane is too high. On the other hand, pore diameters larger than 0.1µm have no influence on the total resistance (because the liquid resistance is significantly higher) and liquid breakthroughs can take place more easily [43]. Similar behaviour can be observed in Figure 3.11 which shows the effect of the membrane

porosity. As expected, the lower the porosity the higher the membrane resistance. Membrane porosity higher than 40% ensure that the membrane resistance is not dominant.

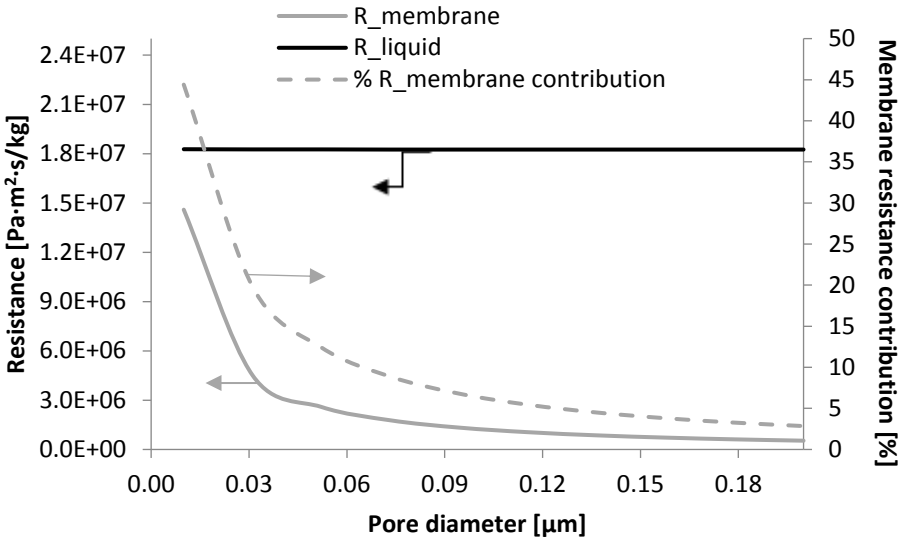

Figure 3.10 Effect of the membrane pore diameter on mass transfer resistances.

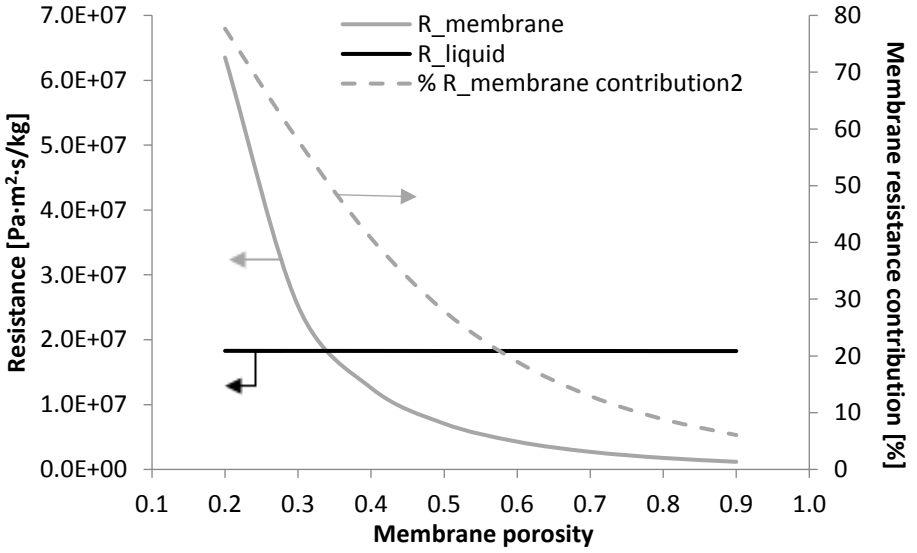

Figure 3.11 Effect of the membrane porosity on mass transfer resistances.

The membrane thickness is also an important parameter that has a considerable influence on the mass transfer resistance. The thicker the membrane is the further the molecules have to travel, and the higher the resistance of the membrane will be. Figure 3.12 shows that the relation between the membrane thickness and the mass transfer resistance in the membrane is directly proportional. According to the results showed in Figure 3.12, a membrane thickness lower than 400µm would be recommended to avoid resistance of the membrane becomes dominant.

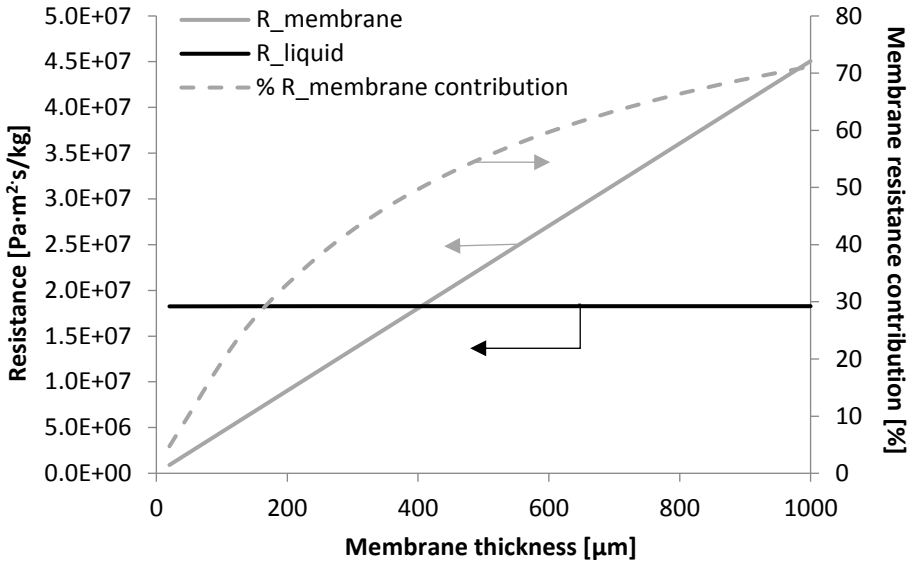

Figure 3.12 Effect of the membrane thickness on mass transfer resistances.

The results obtained in this section are in good agreement with the main conclusions drawn by Ali and Schwerdt [31] and Venegas et al [40] for the water/lithium bromide mixture. The higher the solution mass flow rate is, the lower the resistance in the liquid phase due to the higher value of the mass transfer coefficient (K_{BL}). The porosity of the membrane should be as high as possible and the thickness as low as reasonable in order to maintain the mechanical strength. Regarding the pore diameter, it is important to reduce the mass transfer resistance in the membrane but also to avoid liquid breakthroughs. In order to meet both requirements, an optimal pore size between 0.03µm and 0.1µm is recommended.

3.3.2 Experimental results and validation of the model

Several experiments were carried out in the adiabatic membrane absorber test bench to validate the theoretical results. In all the experimental results presented, the ammonia concentration of the inlet solution was kept within 31.5 and 32.5 wt%. All experiments were done at constant solution mass flow rates. Then, the inlet temperature of the solution was changed within the range selected (subcooling range between 0.6 °C and 11 °C) and the ammonia absorption rate was measured. The same procedure was repeated at different solution mass flow rates. Table 3.3 shows the input values for the experimental study.

Table 3.3 Input values for the experimental study.

	Base case	Range
Inlet solution temperature	--	22-31 °C
Inlet gas temperature	Room temperature	NA
Solution mass flow rate	--	15-45 kg/h
Membrane porosity, ε	70%	NA
Membrane thickness, δ_m	60 µm	NA
Pore diameter, d_p	0.05 µm	NA
Pressure	1.3 bar	NA

Figure 3.13 shows the experimental ammonia absorption flux obtained at different subcooling conditions of the inlet solution. Uncertainty bars have also been included taking into account the accuracy of the instruments shown in Table 3.1 and the uncertainty associated with the experimental procedure.

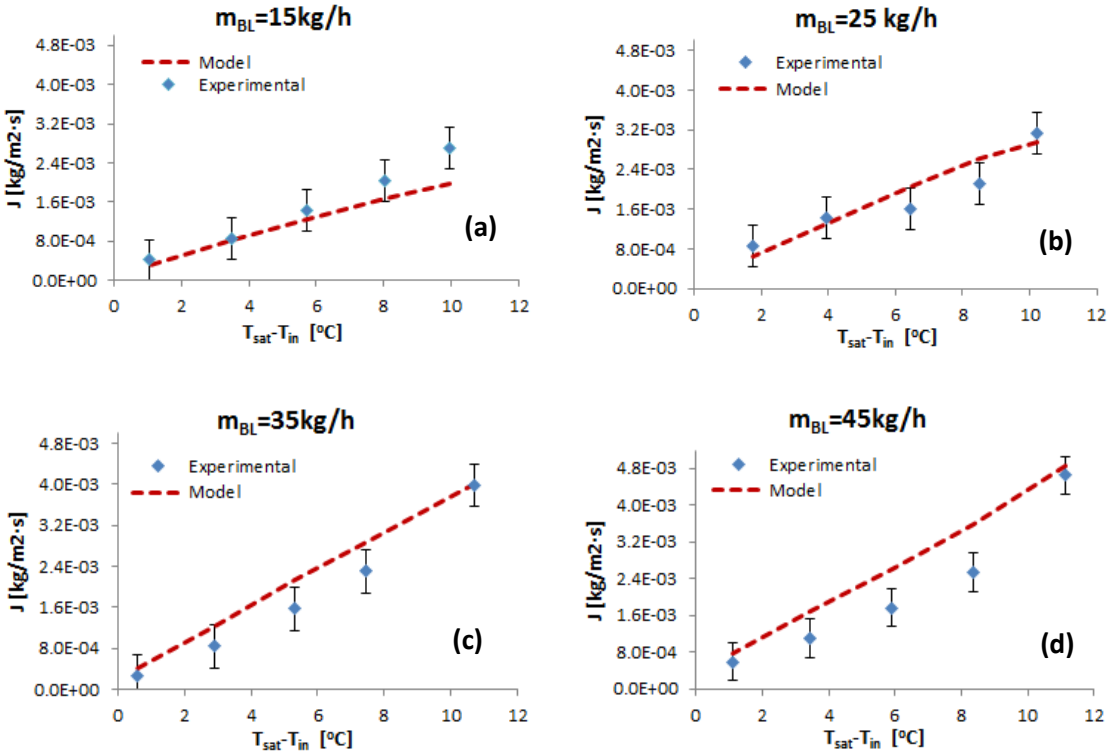

Figure 3.13 Effect of the subcooling of the inlet solution on the ammonia flux at different solution mass flow rates. ***(a)*** *15kg/h;* ***(b)*** *25kg/h;* ***(c)*** *35kg/h;* ***(d)*** *45kg/h.*

As can be observed, there is good agreement between the experimental and the theoretical results, and the Mean Absolute Error of the model predictions with respect to the experimental data is $\pm 3.7 \cdot 10^{-4}$ kg/m^{2}s. As expected, the subcooling conditions of the solution have a considerable influence on the ammonia absorption rate; the higher the subcooling is, the higher the ammonia absorption rate and the increase is almost linear. At the highest solution flow rate of 45 kg/h and the highest subcooling inlet conditions (T_{sat}-T_{in}=11 °C), the absorption rate obtained was 4.7 $\cdot 10^{-3}$kg/(m^{2}s). Figure 3.13 also shows the effect of the solution mass flow rate on the ammonia flux. The higher the solution mass flow rate is, the higher the ammonia absorption rate. However, this increase in the ammonia absorption rate is more pronounced in the range 15-25 kg/h than in the range 35-45 kg/h because the decrease in the liquid mass transfer resistance is lower for the range 35-45 kg/h than for the range 15-25 kg/h (Figure 3.7).

Finally, Table 3.4 shows the outlet temperature of the solution obtained in the experiments (T_{out}) and the one predicted by the model ($T_{out,model}$). The Mean Absolute Error of the model predictions with respect to the experimental data is $\pm$0.6 °C. The largest deviations between the experimental and theoretical values of the outlet temperature of the solution can be explained by the high thermal inertia of the membrane module used (it is a 28-kg-stainless-steel cell) and several experiments were carried out consecutively at different working temperatures.

Table 3.4 Solution outlet temperature obtained. Experimental and model.

m_{BL} [kg/h]	T_{in} [°C]	T_{sat}-T_{in} [°C]	$T_{out,exp}$ [°C]	$T_{out,model}$ [°C]
14.9	22.0	10.0	24.8	25.1
15.2	25.0	8.0	27.8	27.6
15.1	27.0	5.7	28.7	28.9
15.2	29.1	3.5	29.3	30.3
15.1	31.0	1.0	30.6	31.4
25.1	22.0	10.2	24.5	24.8
25.1	25.1	8.5	26.8	27.6
24.9	27.1	6.5	27.9	29.0
25.1	29.2	3.9	29.9	30.4
25.3	31.0	1.8	31.0	31.6
35.1	22.1	10.7	23.6	24.9
35.0	25.1	7.5	26.2	27.0
35.1	27.1	5.3	27.8	28.5
35.0	29.1	2.9	29.4	29.9
35.1	31.0	0.6	31.2	31.2
45.1	22.1	11.1	23.5	24.7
45.1	24.9	8.4	26.1	26.8
45.1	27.0	5.9	27.6	28.3
45.0	29.0	3.4	29.2	29.9
45.2	31.0	1.1	30.9	31.4

3.3.3 Comparison with the experimental results obtained by Schaal

In the study carried out by Schaal [43] three different hollow fibre membrane modules were tested. Table 3.5 lists the main characteristics of each module. Two flow configurations were studied: solution flowing inside the hollow fibres and solution flowing over the outside of the hollow fibres (shell side of the membrane module). The pressure drop was much higher when the solution was flowing inside the hollow fibres so liquid breakthroughs can take place more easily using this configuration.

Table 3.5 Data of the membrane modules used by Schaal [43].

	Membrane Module 1	**Membrane Module 2**	**Membrane Module 3**
$d_{inner,shell}$ (mm)	10	20	22
nº of fibres	1	2100	2100
$d_{inner,fibre}$ (mm)	1.8	0.17	0.17
$d_{outer,fibre}$ (mm)	2.25	0.21	0.21
L_{fibre} (mm)	200	110	170
Average pore size (µm)	0.2	0.04	0.04
A_1 (m^2)*	0.001	0.123	0.190
A_2 (m^2)*	0.0014	0.152	0.236

**A_1 is the membrane surface area calculated using $d_{inner,fibre}$ and A_2 is the membrane surface area calculated using $d_{outer,fibre}$.*

The experimental results presented in this chapter at the highest (45 kg/h) and lowest solution mass flow rate (15 kg/h), and the ones obtained by Schaal are depicted in Figure 3.14. It is important to mention that Figure 3.14 collects only the experimental data from Schaal [43] with a subcooling of the inlet solution lower than 12ºC in order to have the same working range than in the present work. The results obtained in this thesis and the ones obtained by Schaal cannot be directly comparable because the working conditions (p, T, x_{NH3} and Re) and the characteristics of the membrane modules are different. Schaal carried out the experiments at 18ºC, pressure between 2 and 3 bar, ammonia mass fraction of the solution between 0.32 and 0.54 and flow rate of the solution of 60 l/h. Table 3.3 lists the working conditions of the experimental study in the present work. Despite these differences, a roughly comparison between both studies can be done considering the surface area of the membrane modules and the absorption rates obtained. The ammonia absorption rates depicted in Figure 3.14a shows that increasing the surface area of the membrane leads into lower values of J. This effect can be explained because increasing the area of the membrane leads into an increase in the ammonia concentration and temperature of the solution along the membrane module, so the driving force of the absorption process (subcooling) decreases along the module and then the average absorption rate also decreases.

In the experimental work carried out in this chapter, the flat sheet membrane module used had a surface area of 0.01387 m^2, which is one order of magnitude higher than the surface area provided by the membrane module 1 and one order of magnitude lower than the surface area provided by the membrane modules 2 and 3 (Table 3.5). Thus, the absorption rates obtained in the present work should be roughly in the range between the absorption rates provided by the membrane module 1 and the membrane modules 2 and 3. Figure 3.14a shows that this condition is met because the ammonia absorption rate obtained with the flat sheet membrane used in the

present work are lower than the ones obtained by Schaal with the membrane module 1, but higher than the absorption rates provided by Schaal with the membrane modules 2 and 3.

Figure 3.14b shows the effect of the subcooling of the inlet solution on the total amount of ammonia absorbed. As expected, the highest amount of ammonia absorbed is obtained for the membrane module 3 because it provides the highest membrane surface area.

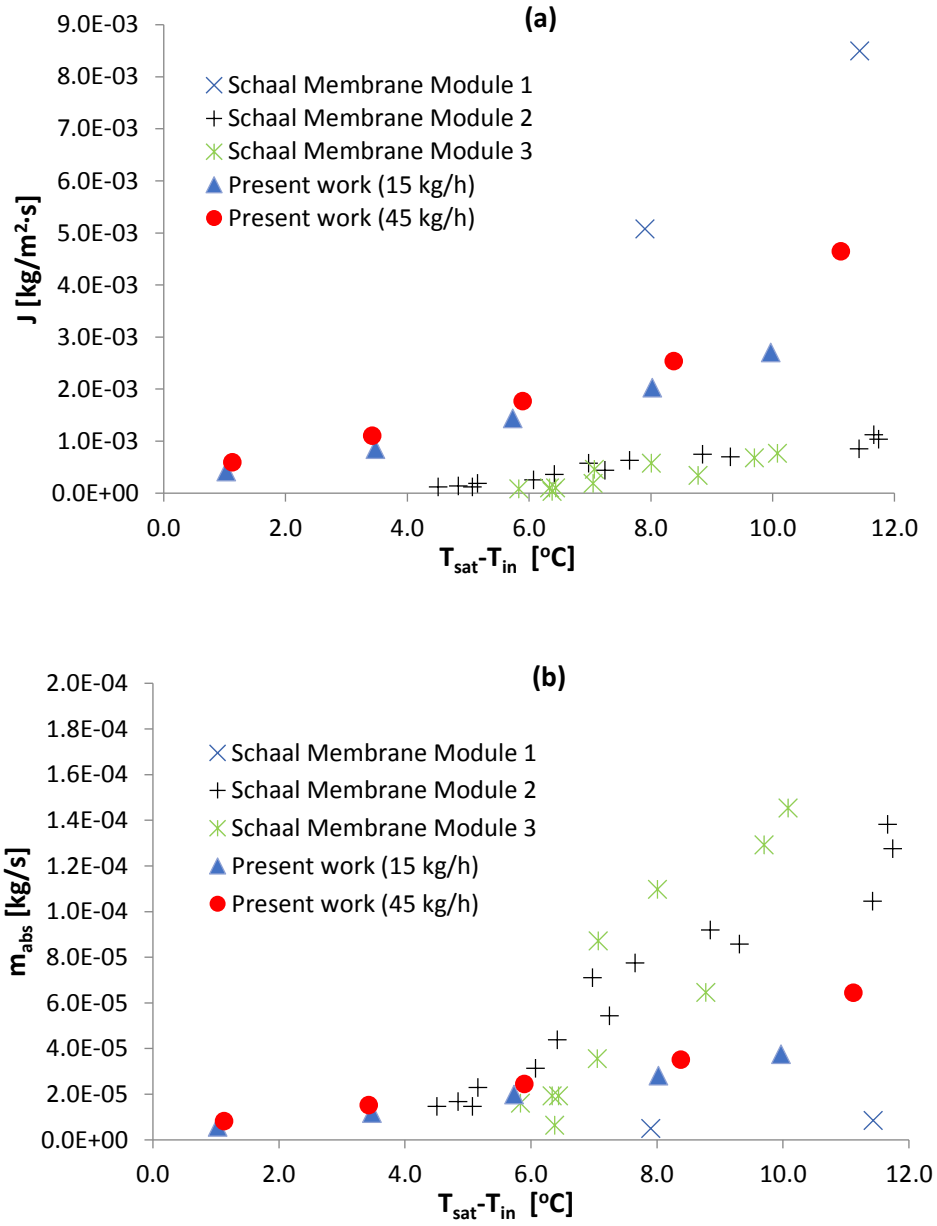

Figure 3.14 Comparison with the experimental results obtained by Schaal. ***(a)*** *Ammonia absorption rate vs subcooling of the inlet solution.* ***(b)*** *Total amount of ammonia absorbed vs subcooling of the inlet solution.*

3.4 Conclusions

This chapter reports a theoretical and experimental study of the ammonia/water absorption process in an adiabatic flat sheet membrane module. For this purpose, an absorber test bench was designed and built and several experiments were carried out in which the flow rate and the

subcooling conditions of the solution were varied. The working conditions in the absorber were determined from the simulation results of the absorption-resorption refrigeration cycle obtained in the previous chapter.

A mathematical model was developed of the heat and mass transfer processes taking place in the membrane module so that the evolution of the concentration, temperature and ammonia flux throughout the membrane module during the absorption process could be studied. The model was validated with the experimental results and the Mean Absolute Error of the model predictions with respect to the experimental data were $\pm 3.7 \cdot 10^{-4}$ kg/m^{2}s for the ammonia absorption rate and ± 0.6 °C for the outlet temperature of the solution.

For the conditions considered in this study, the absorption process is clearly governed by the mass transfer in the liquid phase. At the highest solution flow rate of 45 kg/h and the highest subcooling inlet conditions (T_{sat}-T_{in}=11 °C), the absorption rate was 4.7 $\cdot 10^{-3}$kg/m^{2}s. The experimental results obtained in this work are in accordance with the ones provided by Schaal [43].

The influence of the geometrical parameters of the membrane was studied using a mathematical model. The results showed that the optimal pore diameter of the membrane was between 0.03µm and 0.10µm. Pore diameters smaller than 0.03µm mean that the resistance of the membrane is too high. On the other hand, pore diameters larger than 0.10µm do not improve the mass transfer and can lead more readily to liquid breakthroughs. The porosity of the membrane should be as high as possible (at least higher than 40%) and the thickness lower than 400µm in order to obtain a low transport resistance across the pores of the membrane but at the same time keeping the mechanical robustness. These membrane characteristics will be considered for the selection of the commercial hollow fibre membrane module used in the next chapter.

Nomenclature of chapter 3

A	[m^2]	Area
COP	[-]	Coefficient of performance
D	[m^2/s]	Diffusion coefficient
D_k	[m^2/s]	Knudsen diffusion coefficient
d_h	[m]	Hydraulic diameter
d_p	[m]	Pore diameter
h	[J/kg]	Specific enthalpy
H	[m]	Height of the rectangular channel
J	[$kg/(m^2 \cdot s)$]	Mass flux
K_b	[m/s]	Mass transfer coefficient in the liquid phase
K_m	[$kg/(Pa \cdot s \cdot m^2)$]	Mass transport coefficient in the pores of the membrane
m	[kg/s]	Mass flow rate
M_{NH3}	[g/mol]	Ammonia molecular weight
N_u	[-]	Nusselt number
p	[Pa]	Pressure
R	[$J/(K \cdot mol)$]	Gas constant
R_m	[$Pa \cdot m^2 \cdot s/kg$]	Mass transfer resistance in the membrane
R_k	[$Pa \cdot m^2 \cdot s/kg$]	Knudsen diffusion resistance
R_p	[$Pa \cdot m^2 \cdot s/kg$]	Poiseuille flow resistance
R_s	[$Pa \cdot m^2 \cdot s/kg$]	Mass transfer resistance in the bulk liquid
Re	[-]	Reynolds number
Sc	[-]	Schmidt number
Sh	[-]	Sherwood number
T	[K]	Temperature
U	[$W/m^2 \cdot K$]	Overall heat transfer coefficient
W	[m]	Width of the rectangular channel
x	[-]	Ammonia mass fraction

Special characters

α	[$W/(m^2 \cdot K)$]	Heat transfer coefficient
δ	[m]	Membrane thickness
ε	[-]	Membrane porosity
λ	[$W/(m \cdot K)$]	Thermal conductivity
μ	[Pa·s]	Dynamic Viscosity

ρ	[kg/m^3]	Density
τ	[-]	Tortuosity factor

Subscripts

abs	Absorption
BG	Bulk gas
BL	Bulk liquid
in	Inlet
int	Interface
liq	Liquid
mat	Material
MM	Membrane
out	Outlet
sat	Saturation
vap	Vapour

Chapter 4

Theoretical and Experimental Study of the Ammonia/Water Absorption Process Using a Hollow Fibre Membrane Module

This chapter presents a theoretical and experimental study of the adiabatic absorption process of ammonia into an ammonia/water solution using a polymeric hollow fibre membrane module (Liqui-Cel G501 2.5x8 Extra-Flow) as contactor. The experimental test bench described in Chapter 3 was also used in this study but replacing the flat sheet membrane module by the hollow fibre membrane module. The effect of the subcooling conditions and the mass flow rate of the inlet solution on the ammonia absorption flux was studied. A two-dimensional model was also developed and validated with the experimental results and two case studies were made at different solution mass flow rates to determine the evolution of the ammonia solution concentration, ammonia absorption rate, bulk solution temperature, gas temperature and solution subcooling throughout the hollow fibre membrane module. The two-dimensional model enables to study the evolution of the main operating parameters in the axial and radial direction of the membrane module. The results presented in this chapter were published in Applied Thermal Engineering [66].

4.1 Experimental set up

The test bench described in Chapter 3 was used for the experimental study carried out in this chapter. The membrane characteristics (pore size, porosity, material, and thickness) suggested in the previous chapter were considered for the selection of the commercial hollow fibre membrane module. The membrane module selected was provided by Liqui-Cel® (G501 2.5x8 Extra-Flow) and consisted of a bundle of 10000 hollow fibre membranes. The geometric dimensions of the membrane module are shown in Table 4.1. The ammonia/water solution flows over the outside of the hollow fibres (shell side). The membrane module contains a baffle in the middle of the contactor, which directs the liquid radially across the membrane array [67]. The ammonia vapour stream flows inside the hollow fibres, crosses the pores of the membrane and is absorbed by the solution at the liquid interface. Then, the ammonia/water solution exits the absorber at higher concentration and higher temperature. A scheme of the membrane module can be observed in Figure 4.1. The membrane needs to be hydrophobic and the pressure controlled to prevent liquid breakthroughs inside the pores of the membrane [43]. For this reason, a polypropylene hollow fibre membrane was selected and the pressure difference between the liquid and gas side was kept below 0.3 bar during the experiments.

Table 4.1 Geometric dimensions and characteristics of the hollow fibre membrane module.

Fibres	
Number of fibres	10000
Material	Polypropylene
Inner diameter, d_i (μm)	210
Outer diameter, d_o (μm)	300
Average pore diameter, d_p (μm)	0.03
Effective hollow fibre length, L (m)	0.15
Porosity, ε (%)	45
Effective membrane area (m^2)	1.4
Shell	
Material	Polypropylene
Inside diameter, D_s (cm)	5.55
Central tube diameter, D_t (cm)	2.22

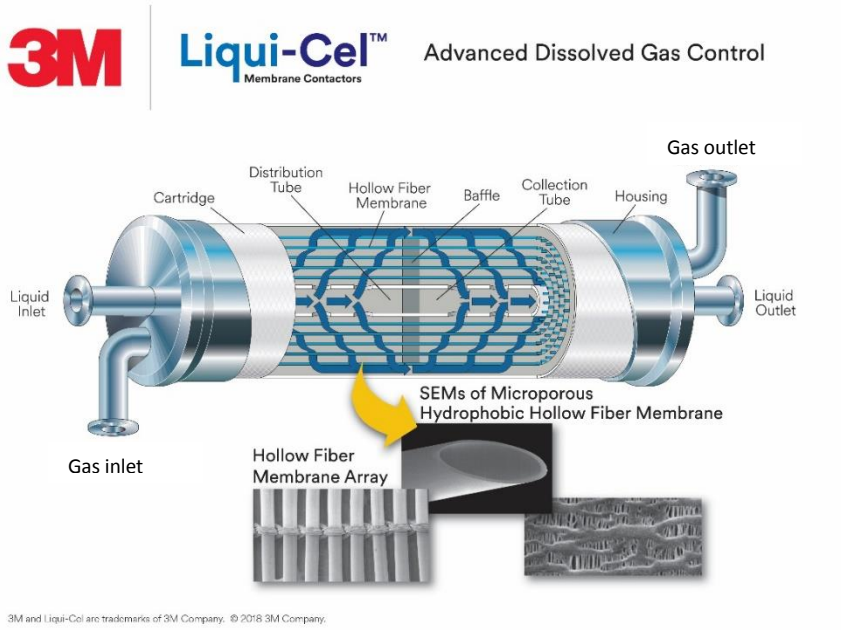

Figure 4.1 Illustration of the Liqui-Cel® Extra-Flow membrane contactor provided by Membrana GmbH [67].

Because the membrane area of the Liqui-Cel® Extra-Flow membrane contactor is 100 times larger than the area of the flat sheet membrane used in Chapter 3, the amount of ammonia absorbed in the experiments carried out in this chapter will be significantly higher. For this reason, the mass flow controller used for measuring the ammonia vapour flux was replaced by another one with wider operating range (Aalborg GFC67). Table 4.2 lists the parameters measured and the accuracy of each instrument.

Table 4.2 Measured variable and accuracy of the instruments.

Instrumentation	Variable measured	Accuracy
Coriolis flowmeter (CMF010M)	Density and flow rate of the solution.	± 0.5 kg/m^3; $\pm 0.05\%$ of flow rate [kg/h]
Pressure transmitter (WIKA S-10)	Pressure [bar]	$\pm 0.25\%$ (full scale)
PT100	Temperature	± 0.1 K
Mass flow controller (Aalborg GFC67)	Mass flow rate of the ammonia vapour	± 1 l/min (standard conditions)

4.2 Theoretical model

A two-dimensional model using Engineering Equation Solver (EES) was developed to study the adiabatic absorption process when a hollow fibre membrane module was used as a contactor. The model predicts the amount of ammonia absorbed (mass transfer process) and the heat exchange rate during the absorption process. Feed inlet conditions (pressure, temperature,

mass flow rate, and ammonia concentration) are input data. As can be observed in Figure 4.1, the membrane module is divided into two parts by an internal baffle, so the model was also divided into two sections. In the first, the feed flows from the central distribution tube to the periphery of the contactor. In the second, the feed flows from the periphery to the centre. Each section was discretized following the scheme shown in Figure 4.2 and a cross-flow configuration between the solution and the gas was assumed.

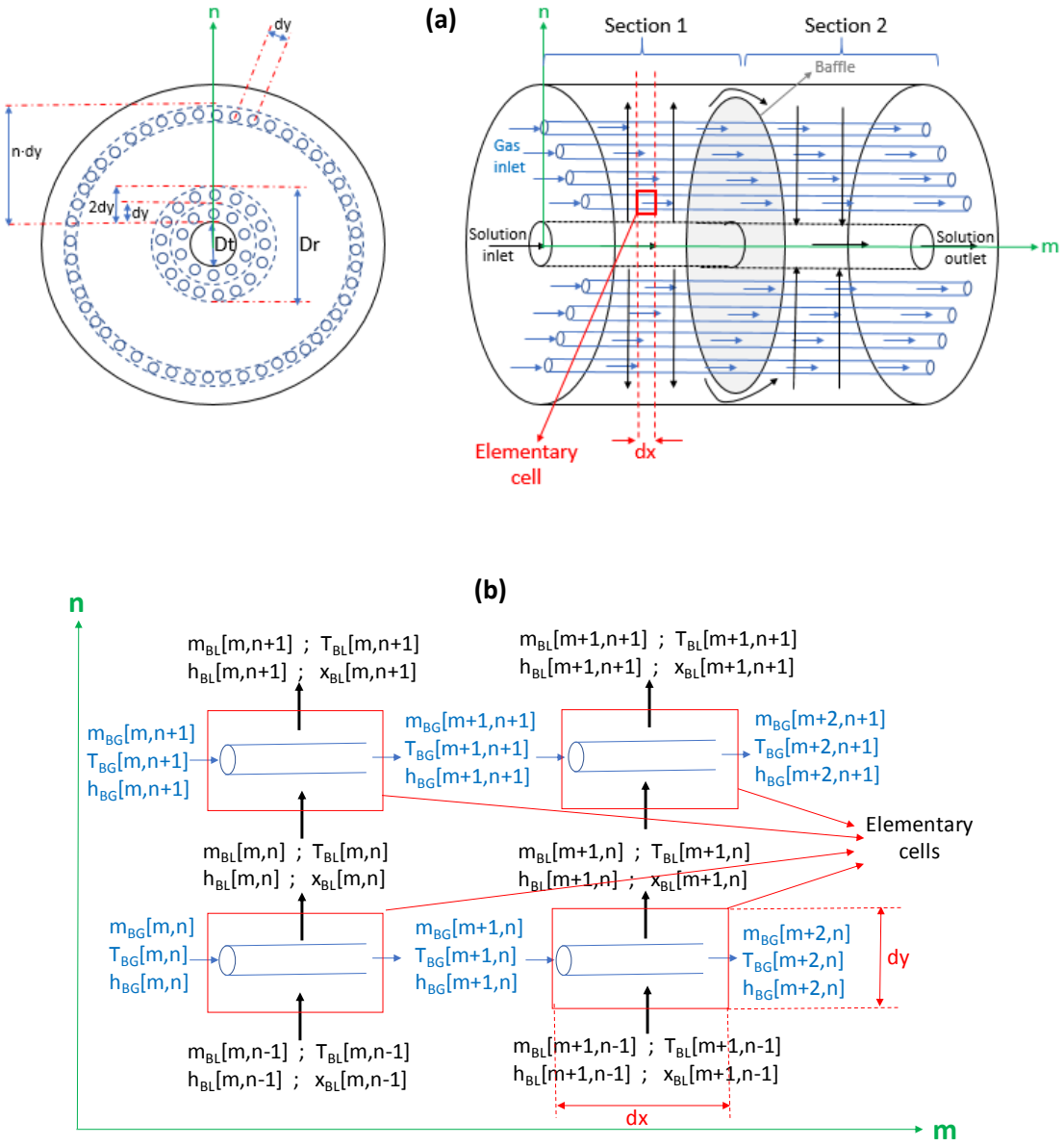

Figure 4.2 Scheme of the discretization of the module. ***(a)*** *Axial and radial sectional view.* ***(b)*** *Cross flow configuration in the elementary cells. The* ***blue arrows*** *represent the gas flow inside the hollow fibres and the* ***black arrows*** *represent solution flow over the outside of the hollow fibres.*

Each section of the module was discretized into 15 elements in the axial direction (m) and 35 rings in the radial direction (n). The stage number (m,n), "m" corresponds to the axial division and "n" to the radial one, as depicted in Figure 4.2. Each ring is considered to be slightly wider

than the fibre diameter (dy > do), where dy is the pitch (gap between the fibres) in the radial and angular direction. The mass and energy balances, transport equations and equilibrium conditions were applied to each of the elements. As far as the thermodynamic and transport properties of the working fluids are concerned, the density, enthalpy, and equilibrium data were taken from Ibrahim and Klein [44], the thermal conductivity was calculated using the Bohne equation from Cuenca at al. [59] and the viscosity, heat capacity and diffusion coefficient of ammonia in water were calculated from Conde [60]. At the end of the first section of the module, the mass and energy balances are applied in order to determine the solution inlet conditions for the second section of the module.

4.2.1 Mass transfer in the membrane

Two transport resistances have been considered for modelling the ammonia flow across the membrane: the resistance of the liquid boundary layer and the transport resistance across the pores of the membrane. Resistance in the vapour boundary layer is neglected because the ammonia in the gas side is assumed to be pure. The ammonia vapour crosses the pores of the membrane and is absorbed by the solution in the liquid-membrane interface. The dusty-gas model was used to model the mass transport inside the pores of the membrane, so the Knudsen diffusion resistance is parallel to the Poiseuille flow resistance [40]. The range of the Knudsen number (Kn) in this study was between 0.05 and 1.9. This range meets the requirements of the transition flow (0.01<Kn<10), so both resistances have been taken into account and the mass transport coefficient (Km) can be written as [37]:

$$K_m = \frac{M_{NH3}}{\delta} \cdot \left(\frac{D_k}{R \cdot T_{MM,mean}} + \frac{p_{gas} \cdot B_0}{R \cdot T_{MM,mean} \cdot \mu_{BG}} \right) \tag{4.1}$$

where p_{gas} is the pressure on the gas side, $T_{MM,mean}$ is the mean membrane temperature which is calculated as the average of the vapour and solution interface temperatures and μ_{BG} is the gas viscosity. According to the information provided by the manufacturer, the tortuosity factor (τ) was 2.5. The membrane thickness (δ) was taken from the data sheet of the membrane (45μm). The Knudsen diffusion coefficient (D_k) is calculated using Eq. (4.2) [37]:

$$D_K = K_0 \cdot \left(\frac{8 \cdot R \cdot T_{MM,mean}}{\pi \cdot M_{NH3}} \right)^{0.5} \tag{4.2}$$

where K_o and B_o are constants defined as follows [33]:

$$K_0 = \frac{\varepsilon \cdot d_p}{3\tau} \tag{4.3}$$

$$B_0 = \frac{\varepsilon \cdot \left(\frac{d_p}{2} \right)^2}{8\tau} \tag{4.4}$$

where ε is the membrane porosity and dp is the mean pore diameter. The ammonia flux across the membrane (J) is obtained with Eq. (4.5):

$$J = K_m \cdot \left(p_{gas} - p_{int} \right) \tag{4.5}$$

where p_{int} is the partial ammonia vapour pressure at the temperature and concentration of the interface (T_{int} and x_{int} respectively). p_{int} is calculated for every element of the discretized membrane module because the temperature and the composition change throughout the module.

4.2.2 Mass transfer in the liquid phase

Figure 4.3 shows a scheme of the mass transfer process in the liquid phase. After crossing the pores of the membrane, the ammonia vapour is absorbed by the solution in the liquid interface. Then, the ammonia absorbed diffuses from the liquid-membrane interface to the bulk solution due to the concentration gradient.

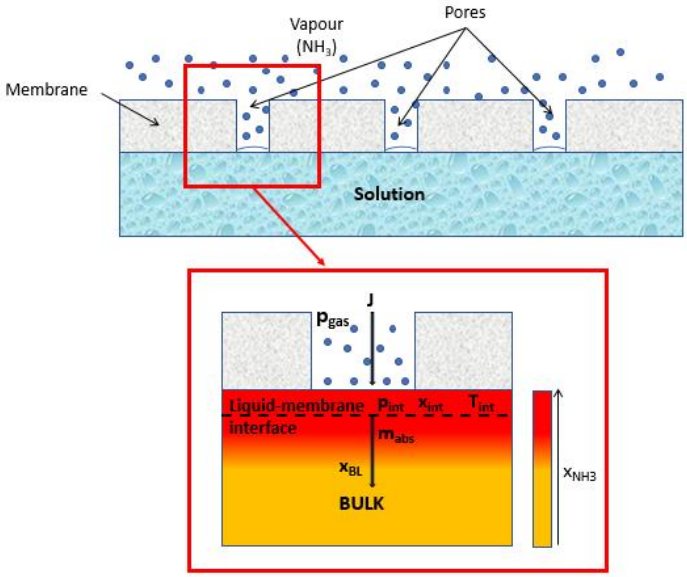

Figure 4.3 Mass transfer process in the liquid phase.

According to the film theory [62], the ammonia concentration at the interface (x_{int}) can be calculated using Eq. (4.6):

$$x_{int} = x_{BL} \cdot exp\left(\frac{J}{\rho_{NH3} \cdot K_{BL}}\right) \tag{4.6}$$

where ρ_{NH3} is the density of the liquid ammonia, x_{int} is the ammonia concentration at the liquid interface boundary layer and K_{BL} is the mass transfer coefficient between the solution boundary layer and the bulk solution. There are many correlations reported in the literature for the determination of K_{BL} in the shell side of cross-flow hollow fibre membrane modules. Table 4.3 lists the most widely used. In a following section (4.3.1.1), a comparison between all of the correlations presented in Table 4.3 was carried out in order to select the one that provides the best agreement between the experimental and the theoretical results. In such correlations, D_{BL} is the diffusion coefficient of ammonia in water, d_o is the outer diameter of the hollow fibre and d_h is the hydraulic diameter, which is defined as follows:

$$d_h = \frac{{D_s}^2 - {D_t}^2 - n_f \cdot {d_o}^2}{n_{f,total} \cdot d_0} \tag{4.7}$$

where D_s is the inner diameter of the housing of the membrane module, D_t is the outer diameter of the distribution/collection tube and $n_{f,total}$ is the total number of fibres. Due to the cross-flow

configuration of the Liqui-Cel® 2.5x8 Extra-Flow membrane module (Figure 4.1), the solution velocity (v) in between the hollow fibres in the module was determined using the equation presented by Mahmud et al. [68].

$$v = \frac{\frac{2 \cdot q_v}{\pi \cdot L \cdot (D_S - D_t)} \cdot \log\left(\frac{D_S}{D_t}\right)}{1-\varphi} \tag{4.8}$$

where q_v is the volume flow rate of the solution. The length of each compartment is half the module length, L, as the module was split in the centre by an internal baffle (Figure 4.1). The packing fraction (φ) is calculated as following [69]:

$$\varphi = \frac{n_{f,total} \cdot d_o^2}{D_S^2 - D_t^2} \tag{4.9}$$

Table 4.3 Empirical correlations for shell-side mass transfer in cross-flow commercial modules.

Authors	Correlation
Wickramasinghe et al. [70]	$Sh = \frac{K_{BL} \cdot d_o}{D_{BL}} = 0.15 \cdot Re^{0.8} Sc^{0.33} \quad when \quad Re > 2.5$ $Sh = \frac{K_{BL} \cdot d_o}{D_{BL}} = 0.12 \cdot Re \cdot Sc^{0.33} \quad when \quad Re \leq 2.5$
Fouad et al. [71]*	$Sh = \frac{K_{BL} \cdot d_h}{D_{BL}} = 0.41 \cdot Re^{0.36} Sc^{0.33}$
Zheng et al. [69]	$Sh = \frac{K_{BL} \cdot d_h}{D_{BL}} = 2.15 \cdot Re^{0.42} Sc^{0.33}$
Baudot et al. [72]	$Sh = \frac{K_{BL} \cdot d_h}{D_{BL}} = 0.56 \cdot Re^{0.62} Sc^{0.33}$
Shen et al. [73]	$Sh = \frac{K_{BL} \cdot d_h}{D_{BL}} = 0.055 \cdot Re^{0.72} Sc^{0.33}$
Schöner et al. [74]*	$Sh = \frac{K_{BL} \cdot d_h}{D_{BL}} = \varepsilon \cdot 1.76 \cdot Re^{0.82} Sc^{0.33}$
Mahmud et al. [75]	$Sh = \frac{K_{BL} \cdot d_o}{D_{BL}} = 0.39 \cdot Re^{0.59} Sc^{0.33}$

**Correlations modified by Shen et al.* [73].

The mass flow rate of the ammonia vapour absorbed (m_{abs}) is determined by:

$$m_{abs}[m,n] = J[m,n] \cdot dA[n] \tag{4.10}$$

where dA is the discretized membrane area that is calculated as follows:

$$dA[n] = N_f[n] \cdot \pi \cdot d_o \cdot d_x \tag{4.11}$$

N_f is the number of fibres on each ring, d_o is the outer diameter of the fibre and d_x is the length of the elementary cell in the axial direction.

$$N_f[n] = \frac{L_{circ}[n]}{dy} \tag{4.12}$$

where $L_{circ}[n]$ is the outer perimeter of each ring and d_y is the width of the ring and also the distance between the fibres in the ring (Figure 4.2a).

$$L_{circ}[n] = \pi \cdot D_r[n] \tag{4.13}$$

$D_r[n]$ is the outer diameter of each ring and is calculated as follows:

$$D_r[n] = D_t + 2 \cdot n \cdot dy \tag{4.14}$$

where "n" is the radial stage number.

Finally, the total and species mass balances are required in order to complete the model.

$$m_{BL}[m,n] = m_{BL}[m,n-1] + m_{abs}\ [m,n] \tag{4.15}$$

$$m_{BG}[m+1,n] = m_{BG}[m,n] - m_{abs}[m,n] \tag{4.16}$$

$$m_{BL}[m,n] \cdot x_{BL}[m,n] = m_{BL}[m,n-1] \cdot x_{BL}[m,n-1] + m_{abs}[m,n] \tag{4.17}$$

4.2.3 Heat transfer

An adiabatic absorber was considered in the model, so all the heat released during the absorption process is completely transferred to liquid and vapour and heat is assumed not to be lost to the surroundings. The energy balances for the liquid and the vapour sides are shown in equations (4.18) and (4.19), respectively.

$$m_{BL}[m,n-1] \cdot h_{BL}[m,n-1] + m_{abs}[m,n] \cdot \Delta h_{abs} = m_{BL}[m,n] \cdot h_{BL}[m,n] + U \cdot dA[n] \cdot (T_{BL}[m,n] - T_{BG}[m,n]) \tag{4.18}$$

$$m_{BG}[m,n] \cdot h_{BG}[m,n] + U \cdot dA[n] \cdot (T_{BL}[m,n] - T_{BG}[m,n]) = m_{BG}[m+1,n] \cdot h_{BG}[m+1,n] \tag{4.19}$$

Δh_{abs} is the heat released in the absorption process. A constant value of Δh_{abs} (2007046.4 J/kg) was taken from Mahmoud [76]. U is the overall heat transfer coefficient and is define as:

$$\frac{1}{U} = \frac{1}{\alpha_{BL}} + \frac{d_0 \cdot \ln\left(\frac{d_0}{d_i}\right)}{2 \cdot \lambda_{MM}} + \frac{d_0}{d_i \cdot \alpha_{BG}} \tag{4.20}$$

where d_i is the inner diameter of the fibre, α_{BL} is the heat transfer coefficient in the liquid phase and is obtained using the analogy between the heat and mass transfer [32] and α_{BG} is the heat transfer coefficient in the gas phase. According to the Hausen correlation [77] for laminar flow in circular tubes, the Nusselt number in the gas can be determined as follows:

$$Nu_{BG} = 3.66 + \frac{\left(0.0668 \cdot \frac{d_i}{L} \cdot Re_{BG} \cdot Pr_{BG}\right)}{\left(1 + 0.04 \cdot \left(\frac{d_i}{L} \cdot Re_{BG} \cdot Pr_{BG}\right)^{2/3}\right)} \quad (4.21)$$

Thermal conductivity of the polypropylene (λ_{MM}) is taken to be equal to 0.17 $W \cdot m^{-1}K^{-1}$ following the literature [78]. Finally, the interface temperatures are determined with the following energy balance at the liquid-membrane interface (Eq. 4.22) and the energy balance at the vapour-membrane interface (Eq. 4.23).

$$\alpha_{BL} \cdot \left(T_{liq,int}[m,n] - T_{BL}[m,n]\right) \cdot d_0 = J[m,n] \cdot \Delta h_{abs}[m,n] \cdot d_0 - \frac{2 \cdot \lambda_{MM}}{ln\left(\frac{d_0}{d_i}\right)} \cdot \left(T_{liq,int}[m,n] - T_{vap,int}[m,n]\right) \quad (4.22)$$

$$\alpha_{BG} \cdot \left(T_{vap,int}[m,n] - T_{BG}[m,n]\right) \cdot d_i = \frac{2 \cdot \lambda_{MM}}{ln\left(\frac{d_0}{d_i}\right)} \cdot \left(T_{liq,int}[m,n] - T_{vap,int}[m,n]\right) \quad (4.23)$$

where $T_{liq,int}$ and $T_{vap,int}$ are the solution-membrane and vapour-membrane interface temperatures, respectively.

4.3 Results

4.3.1 Experimental results and validation of the model

The experiments were carried out assuming the inlet operating conditions of the absorption-resorption refrigeration cycle for the absorber and the resorber. These operating conditions were determined in Chapter 2. It should be pointed out that the experiments were carried out under adiabatic conditions with no cooling water during the absorption process. The effect of the solution mass flow rate and the subcooling conditions of the inlet solution on the ammonia absorption rate was studied. Table 4.4 lists the range of the working conditions during the experiments.

Table 4.4 Range of working conditions during the experiments.

	ABSORBER	**RESORBER**
x_{NH3}	0.29 – 0.32	0.56 – 0.60
p [bar]	1.3 – 1.5	5.0 – 5.5
T_{inlet} [°C]	24 - 35	15 - 28
m_s [kg/h]	50-75-100	50-100-150

Figure 4.4 shows the effect of the subcooling of the inlet solution on the ammonia flux. Figure 4.4a shows the results obtained working under the absorber conditions of the absorption resorption cycle at three solution mass flow rates. Figure 4.4b shows the results obtained working under the resorber conditions.

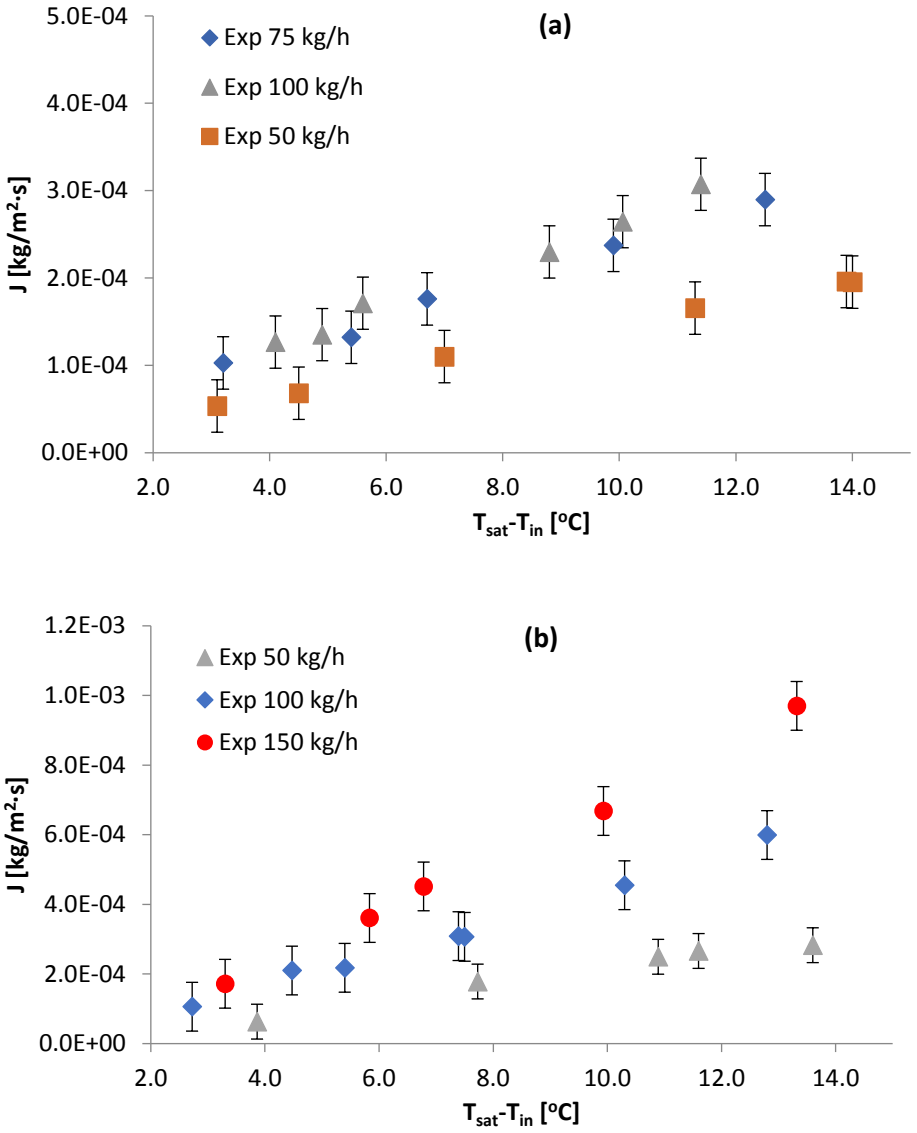

Figure 4.4 Effect of the subcooling of the inlet solution on the ammonia flux at different solution mass flow rates. ***(a)*** *Absorber working conditions.* ***(b)*** *Resorber working conditions.*

As expected, the subcooling conditions of the solution have a strong influence on the ammonia absorption rate; the higher the subcooling the higher the ammonia absorption rate is. The mass flow rate is also an important factor because the higher the mass flow rate, the higher the ammonia flux. This effect is much stronger in the experiments under resorber conditions. Indeed, for the same subcooling conditions and solution mass flow rate, the ammonia flux is always higher when the system is working under resorber conditions. This can be explained by the higher diffusion coefficient of ammonia in water (D_{BL}) and the higher Sherwood number (Sh) obtained that lead to a higher liquid mass transfer coefficient when working under resorber conditions. The maximum J obtained under absorber conditions was $3.1 \cdot 10^{-4}$ kg/(m^2·s) at 100 kg/h and 11.4ºC of subcooling, while the maximum J obtained under resorber conditions was $9.7 \cdot 10^{-4}$ kg/(m^2·s) at 150 kg/h and 13.3ºC of subcooling.

Uncertainties of the ammonia absorption rate (J) measured in the experiments and showed in Figure 4.4 were obtained using the method proposed in Technical Note 1297 of the National

Institute of Standards and Technology Technical (NIST) and implemented in EES software [79]. Regarding the effective hollow fibre length and the number of fibres of the bundle, there are small discrepancies between the values provided by the manufacturer (Table 4.1) and the values measured by Schöner et al. [74]. These discrepancies were quantified in 0.15cm±0.01cm for the effective hollow fibre length and 10000±50 for the number of fibres. Then, these uncertainties and the ones showed in Table 4.2 were used for the uncertainty propagation.

4.3.1.1 Comparison with the experimental results obtained by Schaal

In Chapter 3 (section 3.3.3) a comparison between the experimental results obtained by Schaal [43] and the experimental results obtained with the flat sheet membrane module was done. Due to the differences in the experimental conditions and designs of the membrane modules between both studies, a rough comparison was only possible. However, for the experimental results obtained under resorber conditions in this chapter it would be possible to make a more accurate comparison because in both studies a hollow fibre membrane module was used and the experimental conditions are close to each other (Table 4.5). The data selected from Schaal [43] for this comparison corresponds to the experiments carried out in the Membrane module 2 with the solution flowing to the shell side because this configuration is most similar to the flow configuration of the Liqui-Cel hollow fibre membrane module used in this chapter.

Table 4.5 Range of working conditions selected for the comparison.

	Schaal [43] **(Membrane module 2)**	**Present work (Resorber)**
x_{NH3}	0.50-0.53	0.56 – 0.60
p [bar]	3.0-3.3	5.0 – 5.5
T_{inlet} [°C]	18	15 - 28
m_s [kg/h]	45	50-100-150
$A_{membrane}$ [m^2]	0.152	1.4

Figure 4.5 compares the results obtained by Schaal and the results obtained in the present work in terms of ammonia absorption rate (J) and total amount of ammonia absorbed (m_{abs}) and a good agreement was obtained. The comparison in terms of J (Figure 4.5a) shows that the ammonia absorption rate obtained by Schaal is higher than the one obtained in the present work at similar mass flow rate (50 kg/h), which was to be expected because the membrane surface area of the Membrane module 2 is ten times lower than the membrane surface area of the Liqui-Cel membrane module. In fact, the results obtained by Schaal in terms of J are similar to the results obtained at 150 kg/h in the Liqui-Cel module. However, the total amount of ammonia absorbed is significantly higher in the case of the experiments carried out with the Liqui-Cel hollow fibre membrane module due to the higher flow rate and membrane surface area (Figure 4.5b). Comparing the results obtained at similar mass flow rate (45 kg/h in Schaal and 50kg/h in the present work), the higher amount of ammonia absorbed in the present work leads into a higher increment in the concentration than in the case of Schaal.

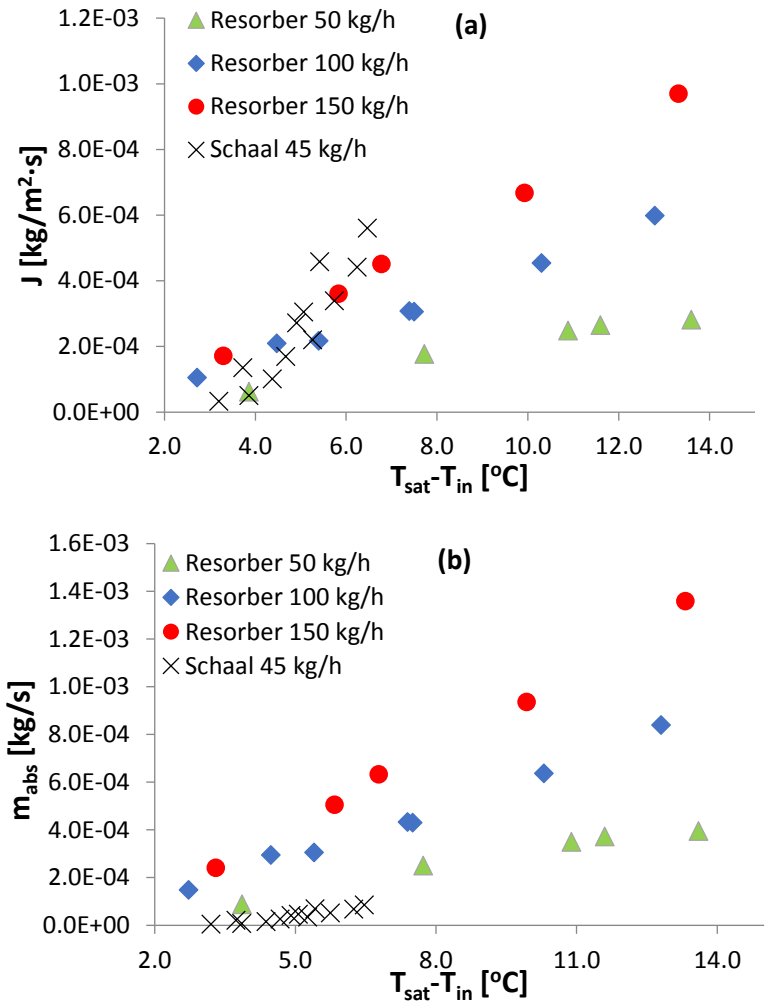

Figure 4.5 Comparison with the experimental results obtained by Schaal with the membrane module 2 and flow to the shell side. ***(a)*** *Ammonia absorption rate vs subcooling of the inlet solution.* ***(b)*** *Total amount of ammonia absorbed vs subcooling of the inlet solution.*

4.3.1.2 Selection of the correlation for determining the mass transfer coefficient in the shell side

In this section, the results obtained with the model using the correlations showed in Table 4.3 are compared with the experimental results obtained in the test bench in order to select the one that provides the best agreement between the theoretical and the experimental results. The experimental data selected for the comparison are shown in Table 4.6. Data from 1 to 3 correspond to the experiments carried out under absorber working conditions and data from 4 to 6 correspond to the experiments carried out under resorber working conditions. Table 4.7 shows the results obtained when the model described in section 4.2 was run using the correlations showed in Table 4.3 for the determination of the solution mass transfer coefficient in the shell side (k_{BL}). The input data for the model are the experimental data showed in Table 4.6 (pressure, inlet temperature, ammonia solution concentration and solution mass flow rate). The values of the ammonia absorption rate (J) and the temperature of the solution at the outlet of the membrane module obtained with the model are compared with the experimental ones in terms of relative error for the J (Eq. 4.24) and temperature deviation for T_{out} (Eq. 4.25). Finally, the selection of the correlation that provides the best agreement between the theoretical and the experimental results was done in terms of the Mean Absolute Error (MAE) for J and T_{out}.

$$Error\ J\ (\%) = \left(\frac{J_{model} - J_{exp}}{J_{exp}}\right) \cdot 100 \quad (4.24)$$

$$Error\ T_{out} = T_{out,model} - T_{out,exp} \quad (4.25)$$

Table 4.6 Experimental data selected for the comparison between the correlations of Table 4.3.

Data	m_s [kg/h]	T_{inlet} [°C]	$x_{NH3,inlet}$	p [bar]	T_{sat}-T_{in} [°C]	J [kg/(m²·s)]	T_{out} [°C]
1	49.0	31.4	0.292	1.4	7.0	**1.1E-04**	**36.9**
2	75.0	31.8	0.294	1.4	6.7	**1.8E-04**	**37.4**
3	100.0	28.2	0.302	1.4	8.8	**2.3E-04**	**33.9**
4	50.0	24.8	0.556	5.2	7.7	**1.8E-04**	**31.0**
5	101.0	22.9	0.578	5.3	7.5	**3.1E-04**	**28.9**
6	152.0	23.1	0.597	5.6	6.8	**4.5E-04**	**28.2**

Table 4.7 Comparison between the correlations and the experimental data.

	Zheng et al. [69]				***Schöner et al.** [74]			
Data	**J [kg/(m²·s)]**	**T_{out} [°C]**	**Error J [%]**	**Error T_{out} [°C]**	**J [kg/(m²·s)]**	**T_{out} [°C]**	**Error J [%]**	**Error T_{out} [°C]**
1	1.8E-04	36.8	59.9	-0.1	1.7E-04	36.8	55.7	-0.1
2	3.0E-04	37.0	67.6	-0.4	2.9E-04	37.0	63.2	-0.4
3	2.8E-04	34.6	23.7	0.7	2.8E-04	34.6	23.1	0.7
4	1.8E-04	31.5	-0.6	0.5	1.7E-04	31.5	-2.1	0.5
5	3.3E-04	29.5	6.3	0.6	3.3E-04	29.5	6.1	0.6
6	4.1E-04	28.7	-9.7	0.5	4.1E-04	28.7	-9.6	0.5
	MAE (J) ±5·10⁻⁵ kg/(m²·s)		**MAE T_{out} ±0.5°C**		**MAE (J) ±5·10⁻⁵ kg/(m²·s)**		**MAE T_{out} ±0.5°C**	

	Wickramasinghe et al. [70]				**Mahmud et al.** [75]			
Data	**J [kg/(m²·s)]**	**T_{out} [°C]**	**Error J [%]**	**Error T_{out} [°C]**	**J [kg/(m²·s)]**	**T_{out} [°C]**	**Error J [%]**	**Error T_{out} [°C]**
1	1.2E-04	36.9	11.9	0.0	1.6E-04	36.8	48.8	-0.1
2	2.0E-04	36.9	11.5	-0.5	2.7E-04	37.0	51.5	-0.4
3	2.5E-04	34.1	7.4	0.2	2.8E-04	34.6	21.0	0.7
4	1.5E-04	31.2	-14.4	0.2	1.7E-04	31.5	-4.7	0.5
5	3.0E-04	29.1	-2.7	0.2	3.2E-04	29.4	4.6	0.5
6	3.8E-04	28.4	-16.5	0.2	4.0E-04	28.7	-10.9	0.5
	MAE (J) ±3·10⁻⁵ kg/(m²·s)		**MAE T_{out} ±0.2°C**		**MAE (J) ±4·10⁻⁵ kg/(m²·s)**		**MAE T_{out} ±0.5°C**	

	Shen et al. [73]				Baudot et al. [72]			
Data	J [kg/(m²·s)]	T_{out} [ºC]	Error J [%]	Error T_{out} [ºC]	J [kg/(m²·s)]	T_{out} [ºC]	Error J [%]	Error T_{out} [ºC]
1	1.2E-04	36.9	8.2	0.0	1.7E-04	36.8	51.0	-0.1
2	1.8E-04	37.0	3.2	-0.4	2.7E-04	37.0	55.1	-0.4
3	2.3E-04	33.6	-1.5	-0.3	2.8E-04	34.6	21.7	0.7
4	1.5E-04	30.9	-18.7	-0.1	1.7E-04	31.5	-4.0	0.5
5	2.7E-04	28.5	-12.9	-0.4	3.2E-04	29.5	5.1	0.6
6	3.3E-04	27.8	-26.9	-0.4	4.0E-04	28.7	-10.5	0.5
	MAE (J) $\pm 4\cdot10^{-5}$ **kg/(m²·s)**		**MAE T_{out}** ± 0.3**ºC**		**MAE (J)** $\pm 5\cdot10^{-5}$ **kg/(m²·s)**		**MAE T_{out}** ± 0.5**ºC**	

*Fouad et al. [71]			
J [kg/(m²·s)]	T_{out} [ºC]	Error J [%]	Error T_{out} [ºC]
1.5E-04	36.8	40.5	-0.1
2.4E-04	36.9	35.4	-0.5
2.7E-04	34.5	17.2	0.6
1.7E-04	31.5	-7.2	0.5
3.1E-04	29.3	0.4	0.4
3.8E-04	28.4	-16.8	0.2
MAE (J) $\pm 4\cdot10^{-5}$ **kg/(m²·s)**		**MAE T_{out}** ± 0.4**ºC**	

The results obtained in Table 4.7 show that the correlations provided by Zheng et al., Schöner et al., Mahmud et al., Baudot et al., and Fouad et al. provide a good agreement with the experimental results under resorber conditions. However, they provide wide deviations when compared with the experimental data obtained under absorber conditions. In the case of the correlation provided by Shen et al. the conclusion is just the opposite; very good agreement under absorber conditions but not so good under resorber conditions. Finally, the correlation of Wickramasinghe et al. provides good results in both working conditions and also provides the lowest Mean Absolute Error in both the outlet temperature and the ammonia absorption rate. For this reason, the correlation provided by Wickramasinghe et al. was selected for the determination of the mass transfer coefficient of the solution flowing in the shell side of the module.

4.3.1.3 Validation of the model

The theoretical model has been validated with the experimental results obtained in the test bench. Figure 4.6 shows a comparison between the ammonia absorption rate (J) measured during the experiments and the results predicted by the model. The comparison shows a good agreement between the predictions and the experimental results, with a relative error lower than 20% in all cases. The Mean Absolute Error of the model predictions with respect to the experimental data is $\pm 3\cdot10^{-5}$ kg/m²s. Deviations were highest for resorber working conditions at

subcooling above 10°C. No significant differences were obtained when the mass flow rate was increased. Regarding the heat transfer process, Table 4.8 shows the outlet temperature of the solution obtained in the experiments ($T_{out,exp}$) and the one predicted by the model ($T_{out,model}$). The Mean Absolute Error of the model predictions with respect to the experimental data is ±0.3°C.

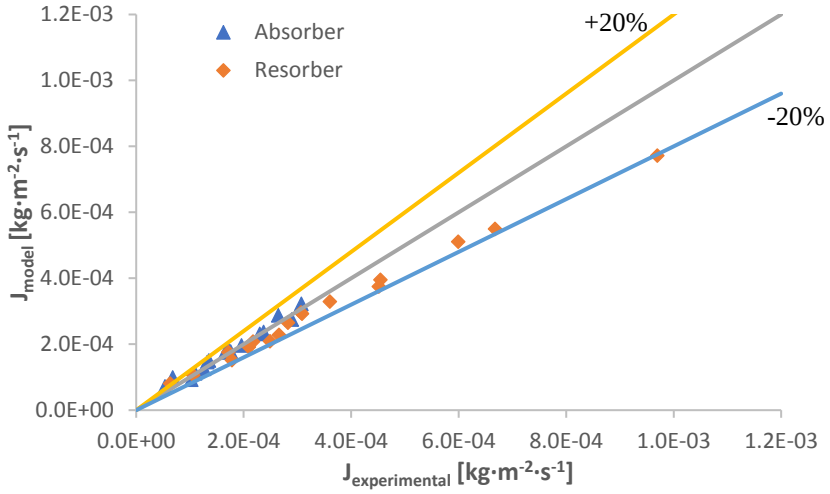

Figure 4.6 Comparison of the J experimental with the J obtained with the theoretical model.

Table 4.8 Outlet temperature of the solution after the absorption process. Comparison between the experimental and the theoretical results.

	ABSORBER				RESORBER			
	T_{sat}-T_{in} [°C]	T_{in} [°C]	$T_{out,exp}$ [°C]	$T_{out,model}$ [°C]	T_{sat}-T_{in} [°C]	T_{in} [°C]	$T_{out,exp}$ [°C]	$T_{out,model}$ [°C]
50 kg/h	3.1	33.6	**35.8**	**35.8**	3.9	28.2	**30.9**	**31.3**
	4.5	33.7	**36.7**	**37.0**	7.7	24.8	**31.0**	**31.1**
	7.0	31.4	**36.9**	**36.5**	10.9	22.3	**30.7**	**30.9**
	11.3	27.9	**36.4**	**36.6**	11.6	21.7	**30.8**	**31.0**
	13.9	24.1	**34.1**	**34.1**	13.6	14.8	**26.1**	**26.4**
75 kg/h	3.2	34.7	**37.7**	**37.0**	NA	NA	NA	NA
	5.4	33.4	**37.3**	**36.9**				
	6.7	31.8	**37.4**	**36.8**				
	9.9	28.7	**36.3**	**35.9**				
	12.5	24.2	**33.6**	**32.9**				
100 kg/h	4.1	31.8	**34.6**	**34.2**	2.7	28.2	**30.1**	**30.2**
	4.9	32.1	**35.2**	**35.2**	4.5	27.5	**30.9**	**30.9**
	5.6	34.8	**38.8**	**38.6**	5.4	25.6	**29.4**	**29.8**
	8.8	28.2	**33.9**	**33.6**	7.4	23.1	**28.8**	**29.0**
	10.1	28.5	**35.1**	**35.4**	10.3	21.0	**28.7**	**29.2**
	11.4	24.7	**32.3**	**32.5**	12.8	16.9	**27.1**	**27.7**
150 kg/h	NA	NA	NA	NA	3.3	25.4	**27.8**	**27.7**
					5.8	24.4	**28.7**	**28.8**
					6.8	23.1	**28.2**	**28.4**
					9.9	21.2	**29.0**	**29.1**
					13.3	19.0	**29.7**	**30.0**

4.3.2 Case study

The theoretical model validated with the experimental results is used in this section to study the evolution of several parameters in the membrane module. The case study selected was taken from the experiments carried out under absorber working conditions. It should be pointed out that at the inlet the solution is subject to considerable subcooling (T_{sat}-T_{in}=11.7ºC) to prevent the liquid from reaching saturation conditions in the membrane module. The inlet conditions of the case study selected are listed in Table 4.9.

Table 4.9 Case study selected for the theoretical study.

T_{in} [ºC]	p [bar]	x_{NH3}	T_{gas} [ºC]	m_{BL} [kg/h]
29	1.6	0.3045	19.8	98.8

Figures 4.7-4.11 show the evolution of the ammonia solution concentration, ammonia absorption rate, bulk solution temperature, gas temperature and solution subcooling in the membrane module, respectively. All the figures are divided into three parts: (a) shows a scheme of the upper part of the hollow fibre membrane module (based on the scheme shown in Figure 4.2a) and the contours of the parameters studied in each figure by means of a colour scale; (b) and (c) show the evolution of each parameter in the radial and axial direction in the first and second section of the module, respectively. The radial direction (n) in the first section is discretized into 35 rings (n from 1 to 35), starting in the central tube and finishing at the top of the module, where the solution is collected before entering the second section. The second section is also discretized into 35 rings (n from 36 to 70), but in this case starting at the top of the module and finishing in the central tube, where the solution is finally collected. The membrane module was also discretized into 30 elements in the axial direction (m) but only elements 1, 3, 5, 15, 16, 18, 20 and 30 were selected for representation in the figures.

In the first section of the module (Figures 4.7b-4.11b), the ammonia solution concentration (x_{NH3}=0.317) is highest in the upper-left side of the section (Figures 4.7a and 4.7b line m=1). This is because the temperature of the gas is much lower than the liquid temperature in this area (line m=1 of Figures 4.9b and 4.10b) so there is a cooling effect in the solution that improves the driving force of the absorption process. For the same reason, Figure 4.8b shows that the ammonia absorption rate (J) is significantly higher at the beginning of the module (m=1) than in the rest of the first section (m=3-15). As expected, there is a downward trend of J in the radial direction due to the increase in the ammonia concentration (Figure 4.7b) and the temperature of the bulk solution (Figure 4.9b). The temperature of the bulk solution increases in the radial direction due to the heat generated during the absorption process. The temperature of the gas shows a trend similar to that of the temperature of the bulk solution, and reaches its maximum value in the upper-right part of the section (Figure 4.10a). It is also important to highlight that the temperature of the gas is nearly the same as the temperature of the bulk solution in the axial half of the first section. To see this effect clearly, Figure 4.12 depicts the evolution of the temperature difference between the solution and the gas (T_{BL}-T_{BG}) in the membrane module. Figure 4.12b shows that the temperature difference remains below 1ºC in most of the first section. The subcooling degree of the solution (Figure 4.11b) is similar to the ammonia flux (J) because both are directly proportional (Eq. 4.5).

In the second section of the module (Figures 4.7c-4.11c), the evolution of the ammonia solution concentration, ammonia absorption rate, bulk solution temperature and solution subcooling

show the same trend as in the first section. However, in the second section there is greater uniformity in the axial direction than in the first section. There are two reasons for this. First, the driving force of the absorption process is much lower in the second section due to the higher concentration and temperature of the solution. And second, the temperature difference between the gas and liquid is smaller in this section (Figure 4.12c). Figure 4.12c (lines m=18, 20, and 30) shows that (T_{BL}-T_{BG}) are close to zero, so the cooling effect of the gas stream generated in the first section (which enhances the mass transfer) is almost negligible in most of the second section of the module. The importance of the cooling effect produced by the gas stream is particularly evident in line m=16 in Figure 4.12c, where the gas stream at the bottom left of the second section (this cold gas comes from the bottom right of the first section of the module) cools the solution and increases the absorption rate (J) in this area instead of decreasing it (Figure 4.8c).

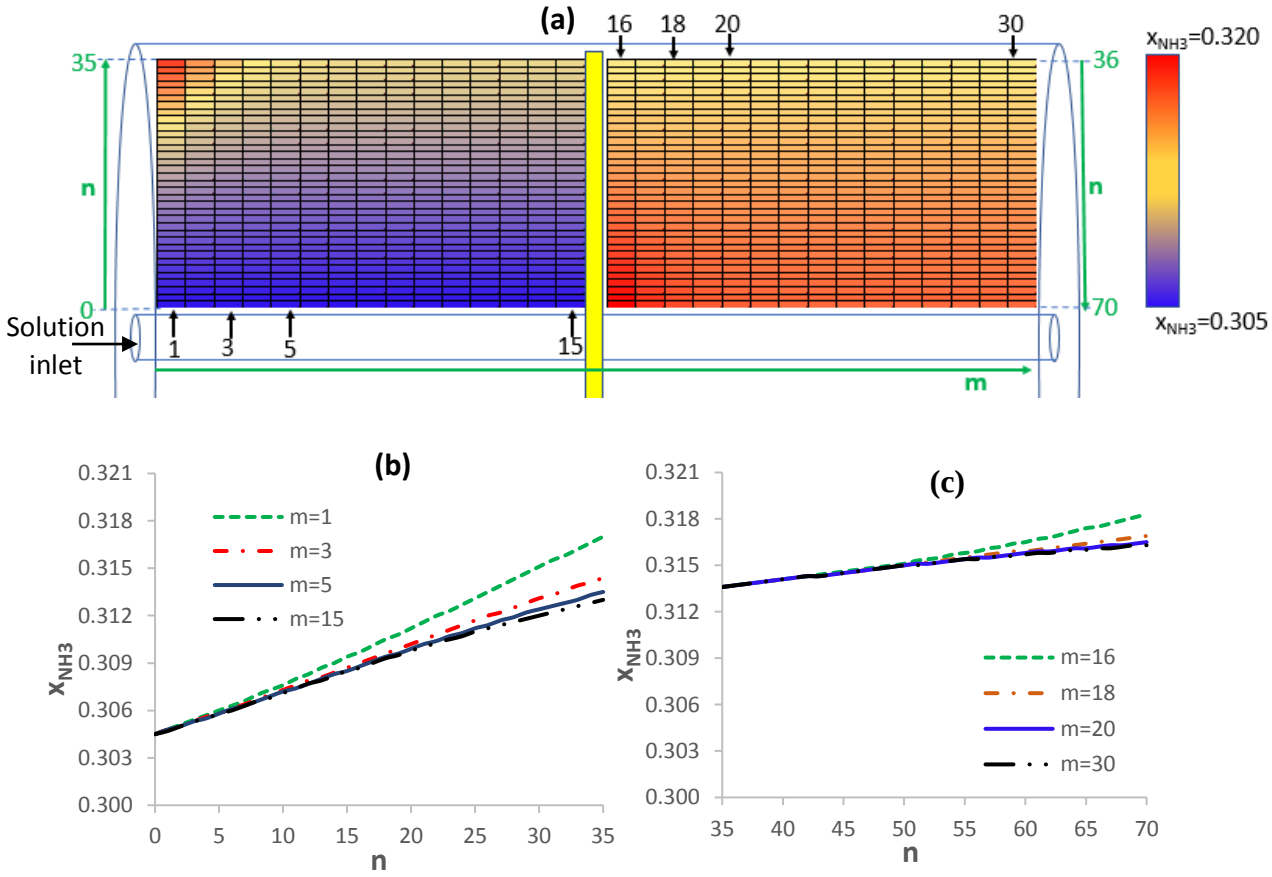

Figure 4.7 ***(a)*** *Contours of the ammonia concentration profile in the hollow fibre membrane module.* ***(b)*** *Evolution of ammonia concentration in the radial direction (n from 0 to 35) in the first section of the module.* ***(c)*** *Evolution of ammonia concentration in the radial direction (n from 36 to 70) in the second section of the module.*

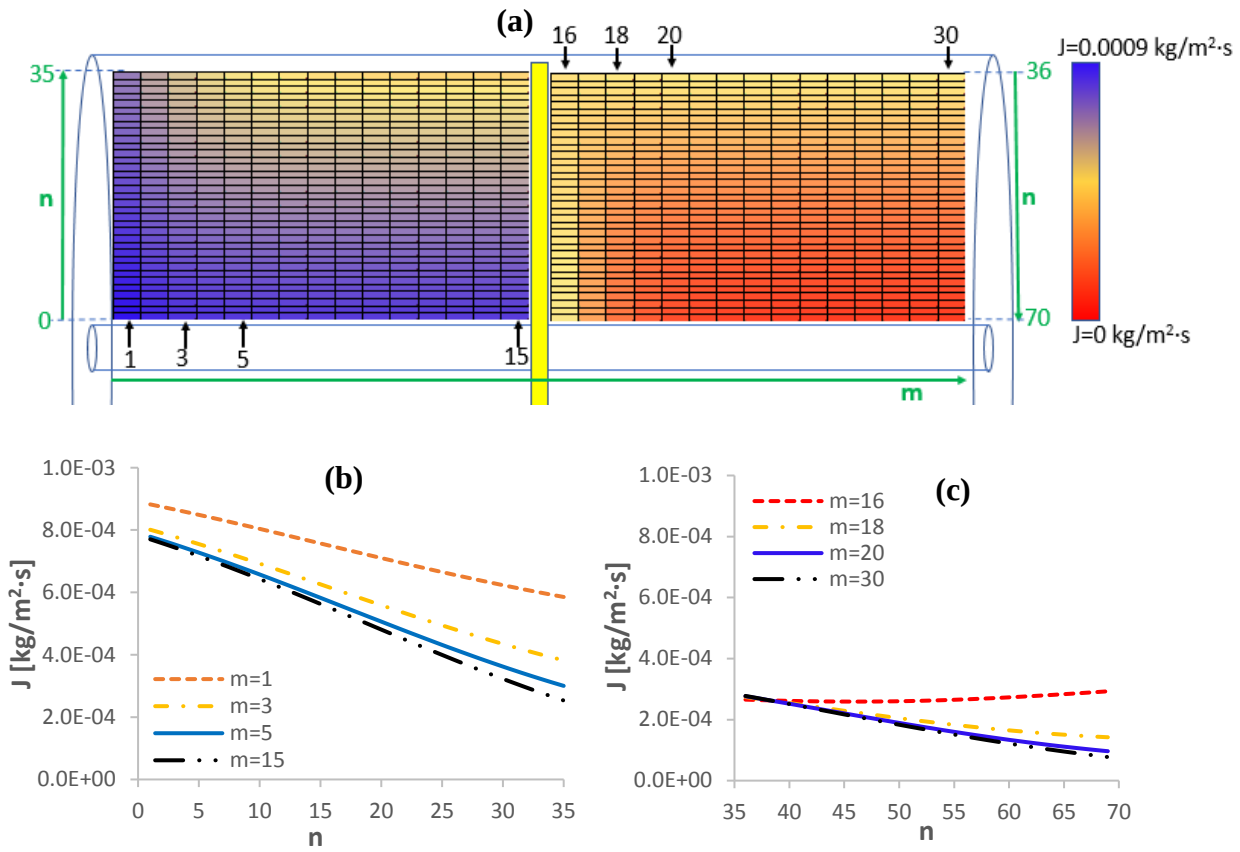

Figure 4.8 ***(a)*** *Contours of the ammonia absorption rate profile in the hollow fibre membrane module.* ***(b)*** *Evolution of ammonia absorption rate in the radial direction (n from 0 to 35) in the first section of the module.* ***(c)*** *Evolution of ammonia absorption rate in the radial direction (n from 36 to 70) in the second section of the module.*

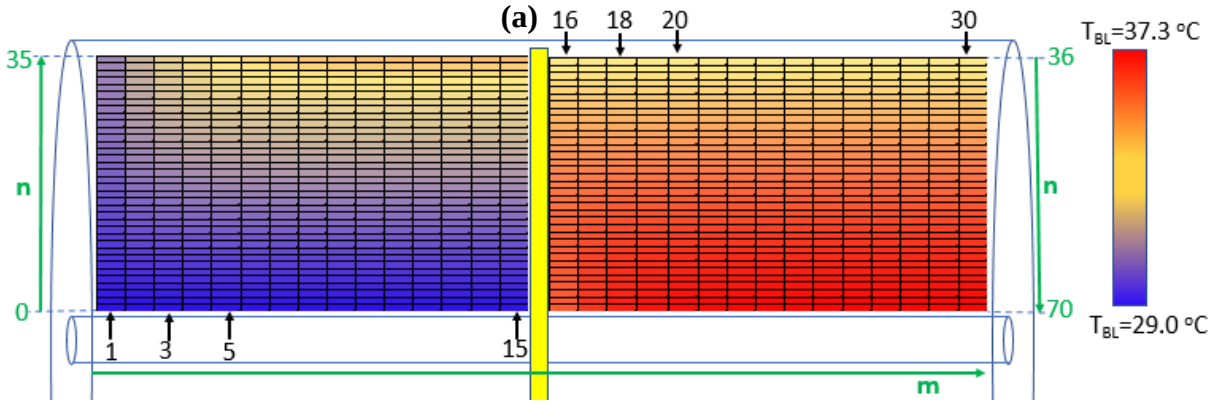

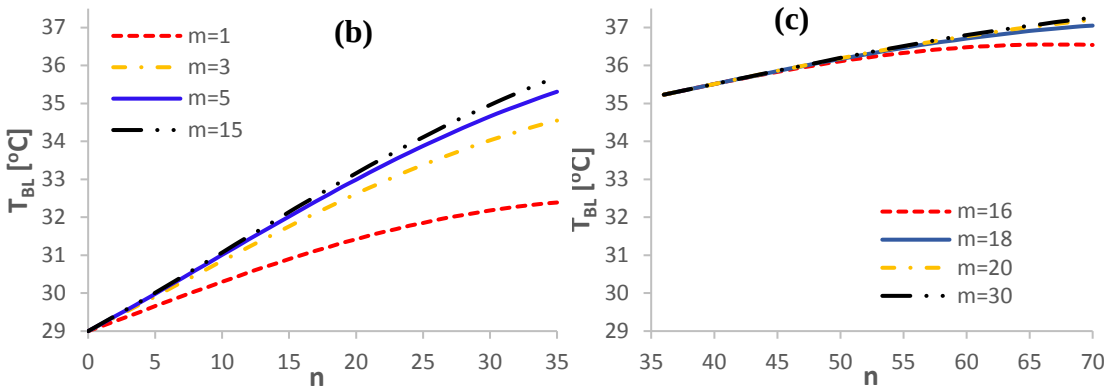

Figure 4.9 ***(a)*** *Contours of the bulk solution temperature profile in the hollow fibre membrane module.* ***(b)*** *Evolution of bulk solution temperature in the radial direction (n from 0 to 35) in the first section of the module.* ***(c)*** *Evolution of bulk solution temperature in the radial direction (n from 36 to 70) in the second section of the module.*

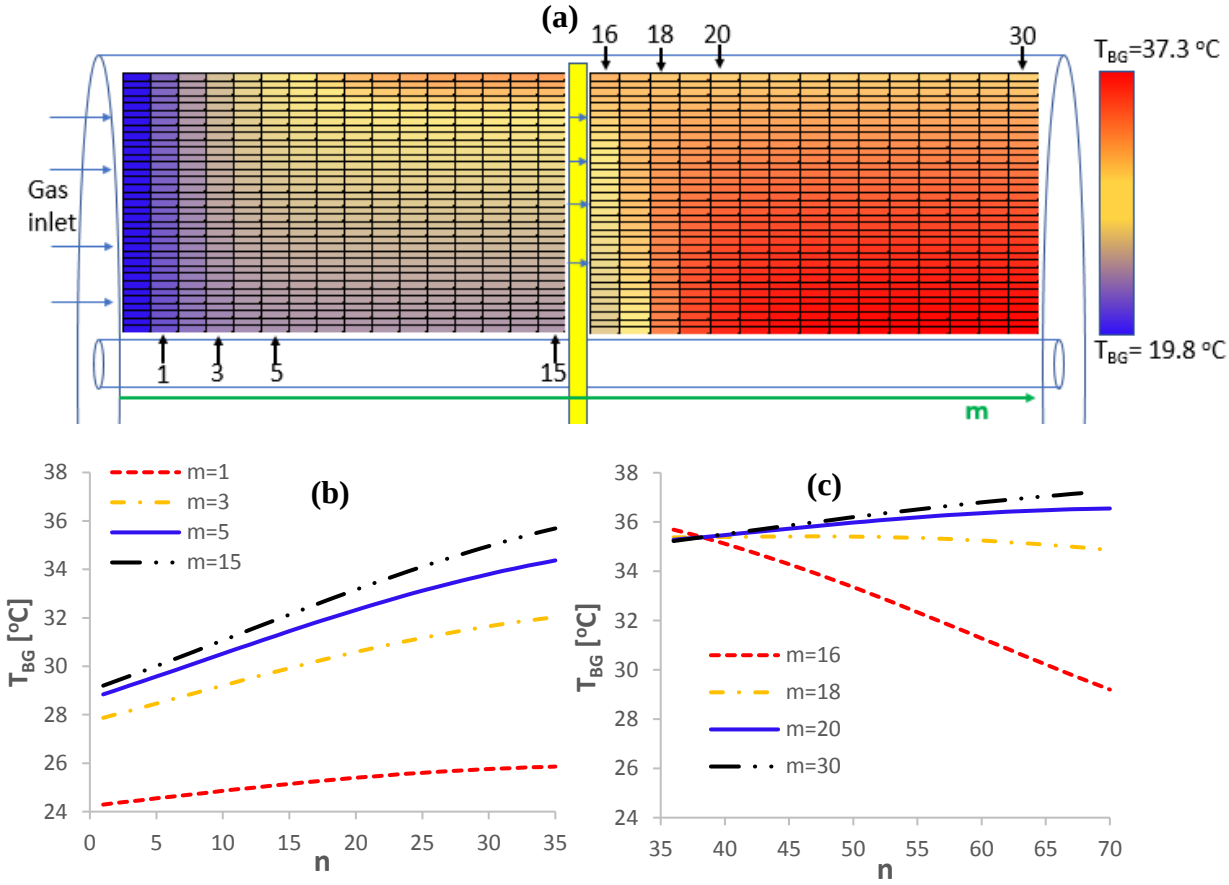

Figure 4.10 ***(a)*** *Contours of the gas temperature profile in the hollow fibre membrane module.* ***(b)*** *Evolution of gas temperature in the radial direction (n from 0 to 35) in the first section of the module.* ***(c)*** *Evolution of gas temperature in the radial direction (n from 36 to 70) in the second section of the module.*

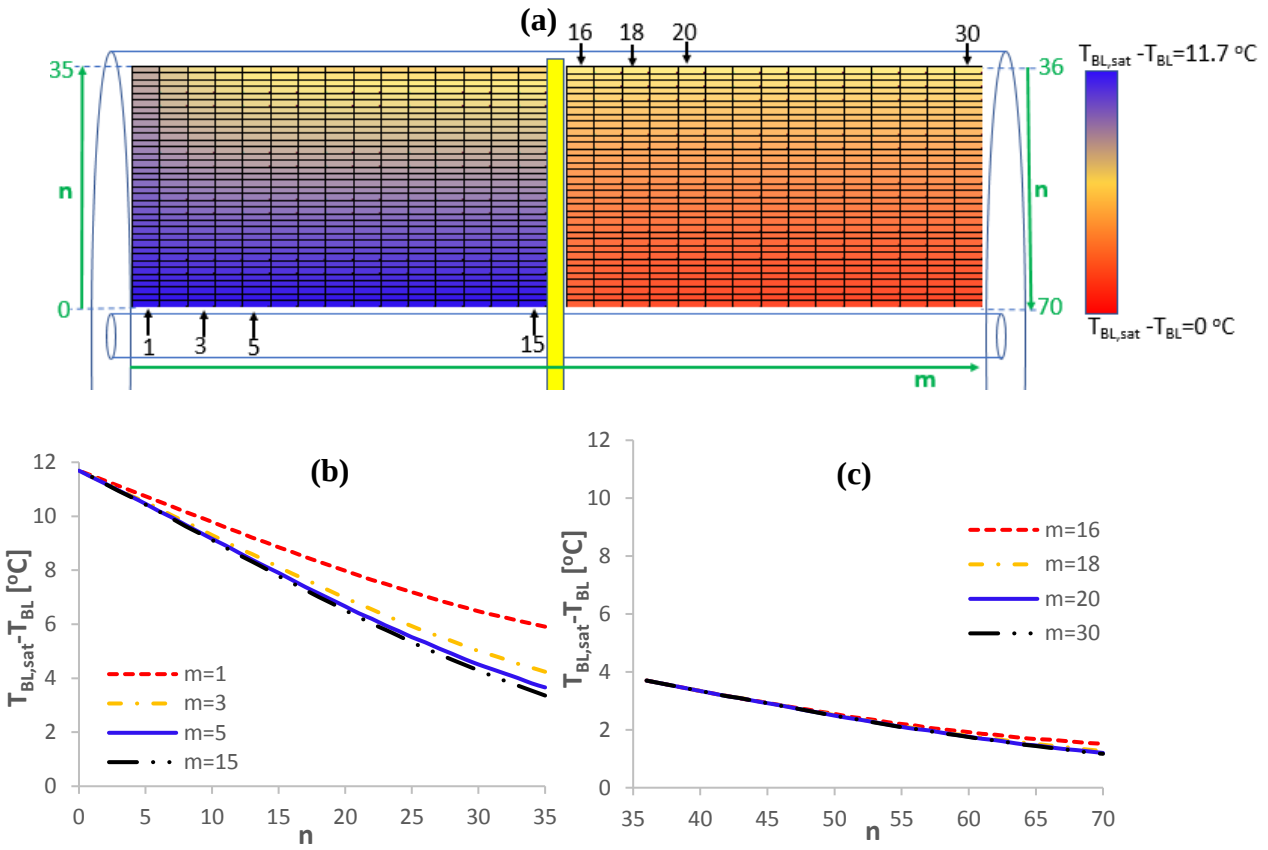

Figure 4.11 ***(a)*** *Contours of the solution subcooling profile in the hollow fibre membrane module.* ***(b)*** *Subcooling evolution in the radial direction (n from 0 to 35) in the first section of the module.* ***(c)*** *Subcooling evolution in the radial direction (n from 36 to 70) in the second section of the module.*

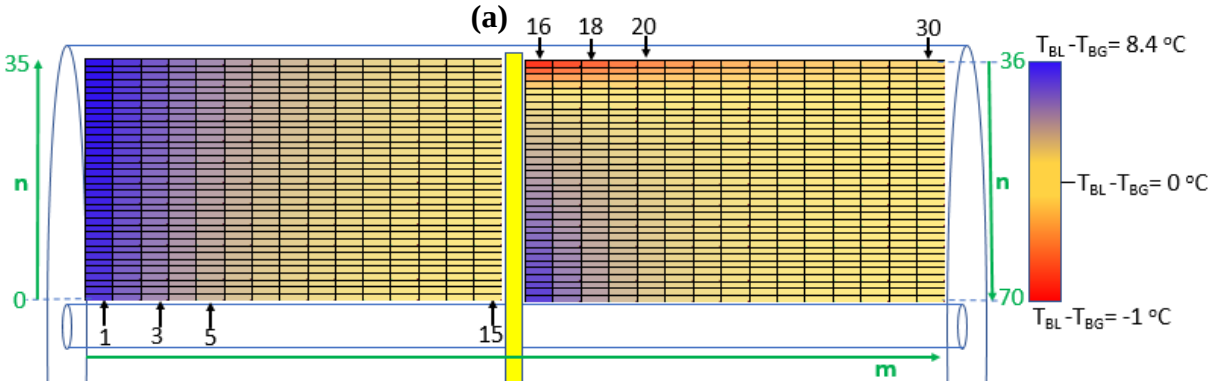

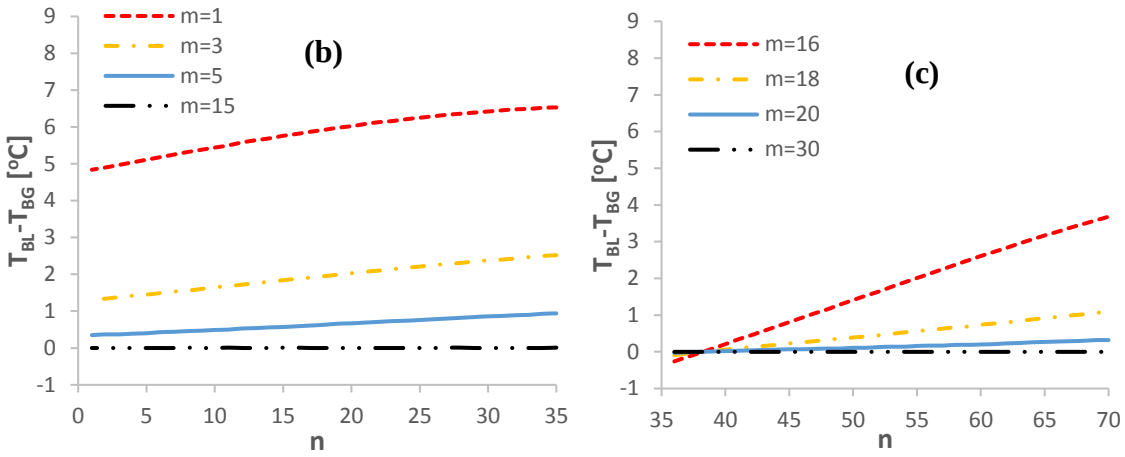

Figure 4.12 ***(a)*** *Contours of the temperature difference between the solution and the gas (T_{BL}-T_{BG}) in the hollow fibre membrane module.* ***(b)*** *T_{BL}-T_{BG} evolution in the radial direction (n from 0 to 35) in the first section of the module.* ***(c)*** *T_{BL}-T_{BG} evolution along the radial direction (n from 36 to 70) in the second section of the module.*

Figures 4.8 and 4.11 clearly show that much of the ammonia is absorbed in the first section of the membrane module. This is explained by the adiabatic working conditions that rapidly decrease the driving force in the membrane module. However, a higher amount of ammonia can be absorbed if the solution mass flow rate is increased. According to the data sheet provided by the manufacturer of the hollow fibre membrane module, the maximum mass flow rate for the solution on the shell side is around 600 kg/h, four times higher than the maximum flow rate tested during the experiments (150 kg/h). Due to limitations in the experimental test bench it was not possible to reach higher mass flow rates. However, the theoretical model previously validated can be used to predict the performance of the membrane module working at maximum flow rate. Figures 4.13 and 4.14 show the ammonia absorption rate and the solution subcooling in the membrane module for the same case study listed in Table 4.9 but in this case the solution mass flow rate (m_{BL}) is increased to 600 kg/h.

A comparison of Figures 4.13b and 4.13c with Figures 4.8b and 4.8c shows that the ammonia absorption rate at 600 kg/h is much higher than in the first case study (98.8 kg/h). In fact, the lowest J obtained at the end of the second section in Figure 4.13c (0.00079 $kg \cdot m^{-2} \cdot s^{-1}$) is close to the maximum J obtained in the first case study at the inlet of the module in Figure 4.8b (0.00093 $kg \cdot m^{-2} \cdot s^{-1}$). This may be because the mass transfer process is clearly governed by the mass transfer resistance in the liquid phase, so the higher the Reynolds number is, the higher the mass transfer coefficient in the liquid phase (Table 4.3). In the membrane module, there are no big differences in the evolution of the subcooling in the axial direction in the case with a mass flow rate of 600 kg/h (Figure 4.14b), there are more uniformity compared to the case study with m_{BL}=98.8 kg/h (Figure 4.11b). The subcooling of the solution at the outlet of the second section (Figure 4.14c) is 3ºC, significantly higher than in the case study shown in Figure 4.11c (below 1.5ºC).

The experimental and theoretical results obtained show that the Liqui-Cel G501 2.5x8 Extra-Flow membrane module is a reliable and useful device for the ammonia absorption process. However, due to the limitations of the adiabatic absorption process, the possibility of integrating some non-porous fibres for the cooling water in the membrane absorber needs to be studied in

order to meet the requirements of the absorption-resorption refrigeration cycle. Chen *et al.* [42] developed a model of a hybrid absorber-heat exchanger for the ammonia-water absorption cycle based on the design of the Liqui-Cel® hollow fibre membrane module. However, their unidimensional model does not reflect the real cross-flow configuration of this membrane module, so the contours of the main parameters could not be obtained in the axial and radial direction in the membrane module. For this reason, the two-dimensional model developed and validated here can be a very good basis for designing a hybrid heat exchanger-membrane absorber because it provides information about the contours of the main parameters in the module in the axial and radial direction, so a detailed and specific design can be made as shown in the next chapter.

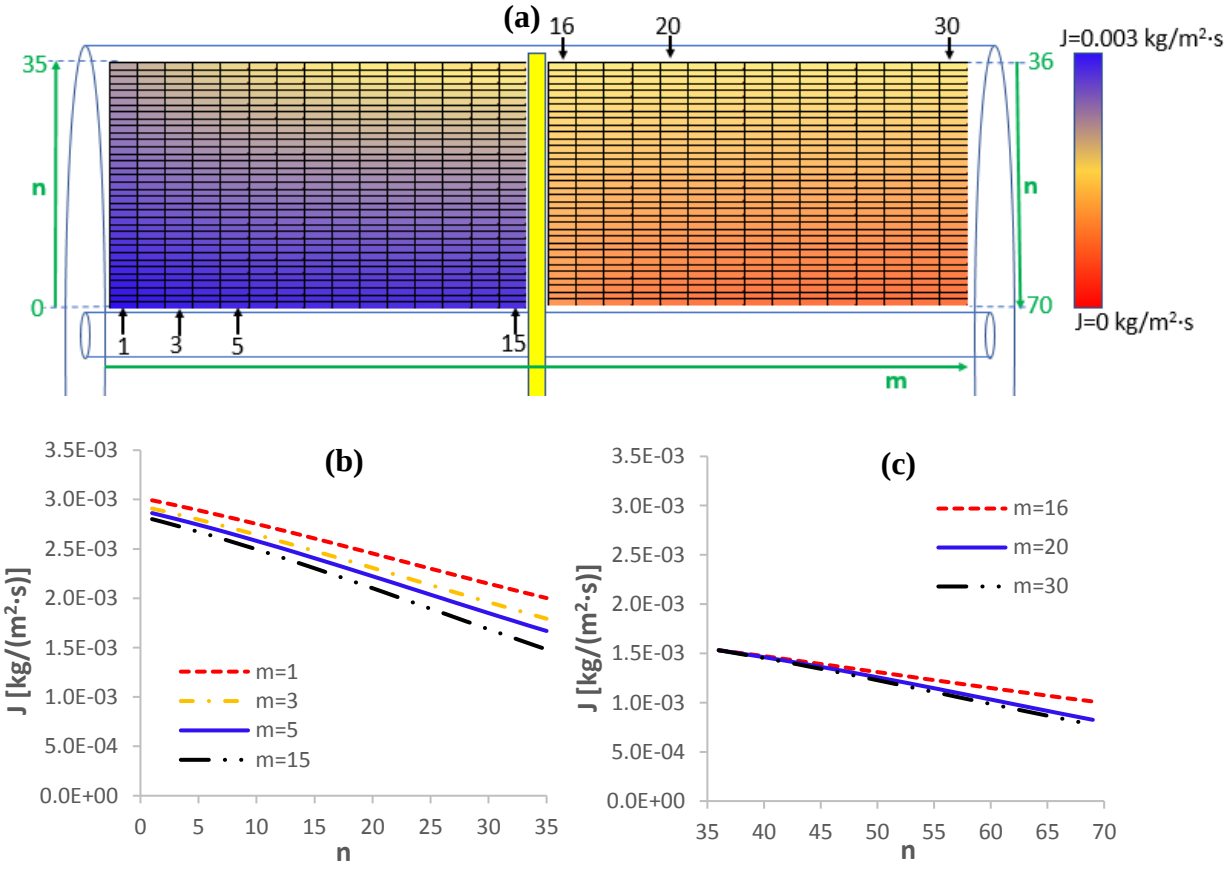

Figure 4.13 ***(a)*** *Contours of the ammonia absorption rate profile in the hollow fibre membrane module. Solution mass flow rate 600 kg/h.* ***(b)*** *Evolution of the ammonia absorption rate in the radial direction (n from 0 to 35) in the first section of the module.* ***(c)*** *Evolution of the ammonia absorption rate in the radial direction (n from 36 to 70) in the second section of the module.*

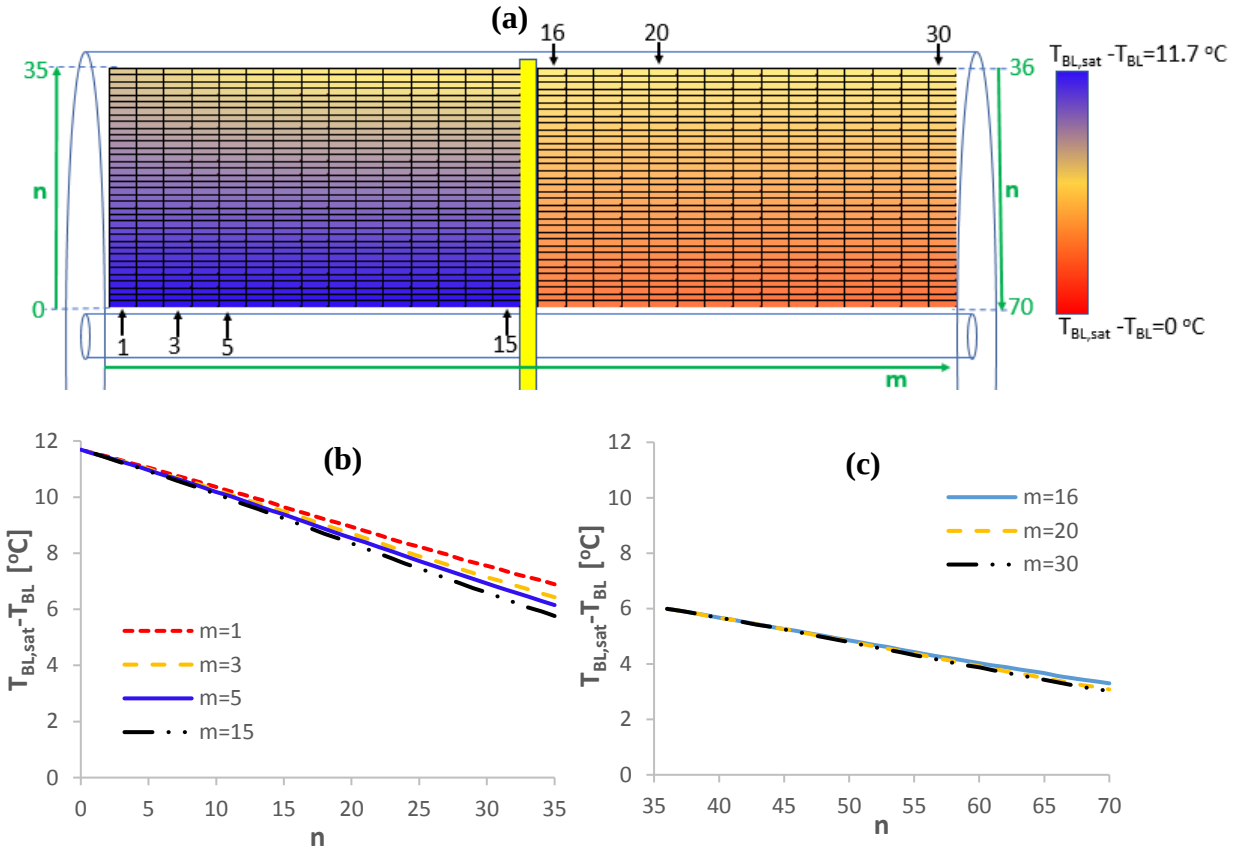

Figure 4.14 ***(a)*** *Contours of the solution subcooling profile in the hollow fibre membrane module. Solution mass flow rate 600 kg/h.* ***(b)*** *Subcooling evolution in the radial direction (n from 0 to 35) in the first section of the module.* ***(c)*** *Subcooling evolution in the radial direction (n from 36 to 70) in the second section of the module.*

4.4 Conclusions

This chapter reports a theoretical and experimental study of the adiabatic ammonia/water absorption process in a commercial hollow fibre membrane module. Several experiments were carried out in which the solution mass flow rate and the inlet subcooling conditions of the solution were varied. The working conditions were determined from the simulation results of the absorption-resorption refrigeration cycle obtained in Chapter 2. The higher the subcooling conditions of the solution, the more ammonia absorption rate was recorded. The same behaviour was observed when the solution mass flow rate was increased. The maximum J obtained under absorber conditions was $3.1 \cdot 10^{-4}$ kg/(m^2·s) at 100 kg/h and 11.4°C of subcooling, while the maximum J obtained under resorber conditions was $9.7 \cdot 10^{-4}$ kg/(m^2·s) at 150 kg/h and 13.3°C of subcooling. It was observed a significant difference between the results obtained under resorber and absorber working conditions; for the same subcooling conditions and mass flow rate, the ammonia flux observed working under resorber conditions is much higher than when working under absorber conditions. This fact can be explained by the higher diffusion coefficient of ammonia in water (D_{BL}) and the higher Sherwood number (Sh) obtained that lead to a higher liquid mass transfer coefficient when working under resorber conditions. A two-dimensional model was also developed and validated with the experimental results and agreement was very good. The Mean Absolute Error of the model predictions of J with respect to the experimental data is $\pm 3 \cdot 10^{-5}$ kg/m^{2}s and ±0.3°C for the predictions of the temperature of the solution at the outlet of the membrane module.

The two-dimensional model was used to study the evolution of the ammonia solution concentration, ammonia absorption rate, bulk solution temperature, gas temperature and solution subcooling in the membrane module. The results obtained in the first case study (m_{BL}=98.8 kg/h) show that the ammonia is mainly absorbed in the first section of the module due to the adiabatic process that leads to a continuous decrease in the subcooling conditions of the solution in the membrane module. As expected, this effect was also observed when the solution mass flow rate was increased to 600 kg/h, but in this case the ammonia absorption rate was an order of magnitude greater due to the higher mass transfer coefficient in the liquid phase obtained. Also, the subcooling of the solution at the outlet of the membrane module was significantly higher when the solution mass flow rate was increased. The model validated in this chapter is used as a basis for a new two-dimensional model of a hybrid heat exchanger-hollow fibre membrane absorber that is shown in the next chapter. The new two-dimensional model with integrated heat exchanger enables to design more compact and enhanced absorbers and resorbers for the ammonia/water absorption-resorption refrigeration cycle.

Nomenclature of chapter 4

dA	[m^2]	Discretized membrane area
D	[m^2/s]	Diffusion coefficient
D_k	[m^2/s]	Knudsen diffusion coefficient
d_0	[m]	Outer diameter of the hollow fiber
d_i	[m]	Inner diameter of the hollow fiber
d_p	[m]	Pore diameter
D_s	[m]	Inner diameter of the shell of the module
D_t	[m]	Outer diameter of the central tube
dx	[m]	Length of the discretization element in the axial direction
dy	[m]	Width of the discretization ring in the radial direction. Also gap between the fibers
h	[J/kg]	Specific enthalpy
J	[$kg/(m^2 \cdot s)$]	Mass flux
K_{BL}	[m/s]	Mass transfer coefficient in the liquid phase
K_m	[$kg/(Pa \cdot s \cdot m^2)$]	Mass transport coefficient in the pores of the membrane
L	[m]	Membrane module length
m	[-]	Segment m
m_{abs}	[kg/s]	Mass flow rate of the ammonia (vapour) absorbed
m_{BL}	[kg/s]	Solution mass flow rate
m_{BG}	[kg/s]	Gas mass flow rate
M_{NH3}	[g/mol]	Ammonia molecular weight
n	[-]	Segment n
N_f	[-]	Number of fibers
N_u	[-]	Nusselt number
p	[Pa]	Pressure
R	[$J/(K \cdot mol)$]	Gas constant
Re	[-]	Reynolds number
Sc	[-]	Schmidt number
Sh	[-]	Sherwood number
T	[K]	Temperature
U	[$W/m^2 \cdot K$]	Overall heat transfer coefficient
x	[-]	Ammonia mass fraction

Special characters

α	[$W/(m^2 \cdot K)$]	Heat transfer coefficient

δ	[m]	Membrane thickness
ε	[-]	Membrane porosity
φ	[-]	Packing fraction
λ	[W/(m·K)]	Thermal conductivity
μ	[Pa·s]	Dynamic Viscosity
ρ	[kg/m^3]	Density
τ	[-]	Tortuosity factor

Subscripts

abs	Absorption
BG	Bulk gas
BL	Bulk liquid
in	Inlet
int	Interface
liq	Liquid
MM	Membrane
out	Outlet
sat	Saturation
vap	Vapour

Chapter 5

Design of a Hybrid Heat Exchanger-Hollow Fibre Membrane Absorber for the Ammonia/Water Absorption-Resorption Refrigeration Cycle

In previous chapters, the adiabatic ammonia absorption process was studied experimentally and theoretically. However, only one adiabatic absorption stage is not enough to reach the desired ammonia concentration at the outlet of the absorber in a real cycle due to the heat released during the absorption process. This heat leads into an increase of the temperature of the solution, and therefore the ammonia absorption rate drops rapidly. To achieve a greater increment in the ammonia solution concentration it would be necessary to transfer the heat released to an external fluid in order to avoid the temperature of the solution increasing during the absorption process. There are two options for studying the integration of membrane modules as contactors in absorption cycles:

- Adiabatic absorption + Cooling in heat exchangers (several stages), as shown in Figure 5.1. This configuration was tested by Schaal [43] in an ammonia/water absorption refrigeration plant. A plate heat exchanger was used for cooling the solution before the adiabatic absorption stage. The operating capability of membrane absorbers was demonstrated but it was not possible to achieve the desired cooling capacity (6.7 kW) because the number of membrane modules required would provide too high pressure drop.

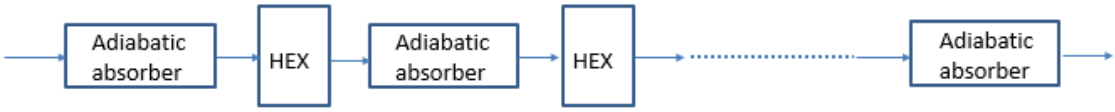

Figure 5.1 In series adiabatic absorber + cooling stage configuration.

- Hybrid heat exchanger-membrane absorber, where the absorption and cooling processes take place in the same device. This configuration provides more compact refrigeration systems, but the design of the module is more complex. As far as the author concern, there are no commercial hybrid heat exchanger-membrane absorbers available in the market. This configuration was proposed by Chen et al. [42] in order to be integrated in an absorption chiller.

This chapter aims to design two hybrid heat exchanger-hollow fibre membrane absorbers in order to be used as an absorber and as a resorber in a 25-kW ammonia/water absorption-resorption refrigeration cycle. To achieve this goal, the hollow fibre membrane module described in Chapter 4 was taken as a basis for the design of the hybrid heat-exchanger-hollow fibre membrane absorber. The same characteristics of the membrane (pore size, porosity, thickness and material) and flow configuration (cross-flow) were considered (Table 4.1 of Chapter 4). Furthermore, the model developed and validated in the previous chapter was modified to include some non-porous hollow fibres inside the membrane module for the cooling water flow, as shown in Figure 5.2. These non-porous hollows fibres are supposed to have the same thickness, diameter and material (polypropylene) than the porous fibres showed in Table 4.1 of Chapter 4.

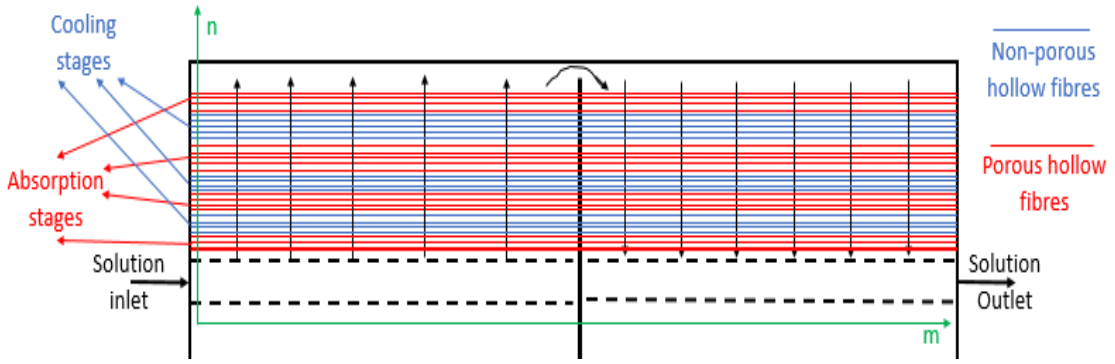

Figure 5.2 Axial sectional view of the hybrid heat exchanger-hollow fibre membrane absorber.

5.1 Theoretical model

A two-dimensional model using Engineering Equation Solver (EES) was developed to study the non-adiabatic ammonia absorption process when a hybrid heat exchanger-hollow fibre membrane module was used as a contactor. The model predicts the amount of ammonia absorbed (mass transfer process) and the heat transferred to the cooling water. Feed inlet conditions (pressure, temperature, mass flow rate, and ammonia concentration) and cooling water inlet conditions (mass flow rate, temperature and pressure) are input data. As shown in Figure 5.2, the membrane module consists of adiabatic absorption stages, where the solution absorbs the ammonia vapour that crosses the porous hollow fibres, and of refrigeration stages, where the solution is cooled down by the cooling water flowing inside the non-porous hollow fibres and no absorption takes place. The number of stages for the absorption and for the cooling were determined in order to meet the requirements of the base case selected for the absorber and for the resorber in a 25-kW ammonia/water absorption-resorption refrigeration cycle. As it was explained in Figure 4.1 of the previous chapter, the membrane module is divided into two parts by an internal baffle, so the model was also divided into two sections. In the first, the feed flows from the central distribution tube to the periphery of the contactor. In the second, the feed flows from the periphery to the centre. Each section was discretized following the scheme shown in Figure 5.3 and a cross-flow configuration between the solution and the gas and between the solution and the cooling water was assumed. Each section of the module was discretized into 15 elements in the axial direction (m). The number of rings in the radial direction (n), and therefore the size of the membrane module, will be varied in order to determine the membrane surface area required to meet the requirements of the base case selected from the study of the absorption-resorption refrigeration cycle. The stage number (m,n), “m” corresponds to the axial division and “n” to the radial one, as depicted in Figure 5.3.

The mass and energy balances, transport equations and equilibrium conditions were applied to each of the elements. As far as the thermodynamic and transport properties of the working fluids are concerned, the density, enthalpy, and equilibrium data of the ammonia/water mixture were taken from Ibrahim and Klein [44], the thermal conductivity was calculated using the Bohne equation from Cuenca et al. [59] and the viscosity, heat capacity and diffusion coefficient of ammonia in water were calculated from Conde [60]. The thermodynamic properties of the water were already implemented in the EES database and they were taken from McBride et al. [80]. At the end of the first section of the module a complete mixing of the solution is considered.

The mass and energy balances are applied in order to determine the solution inlet conditions for the second section of the module.

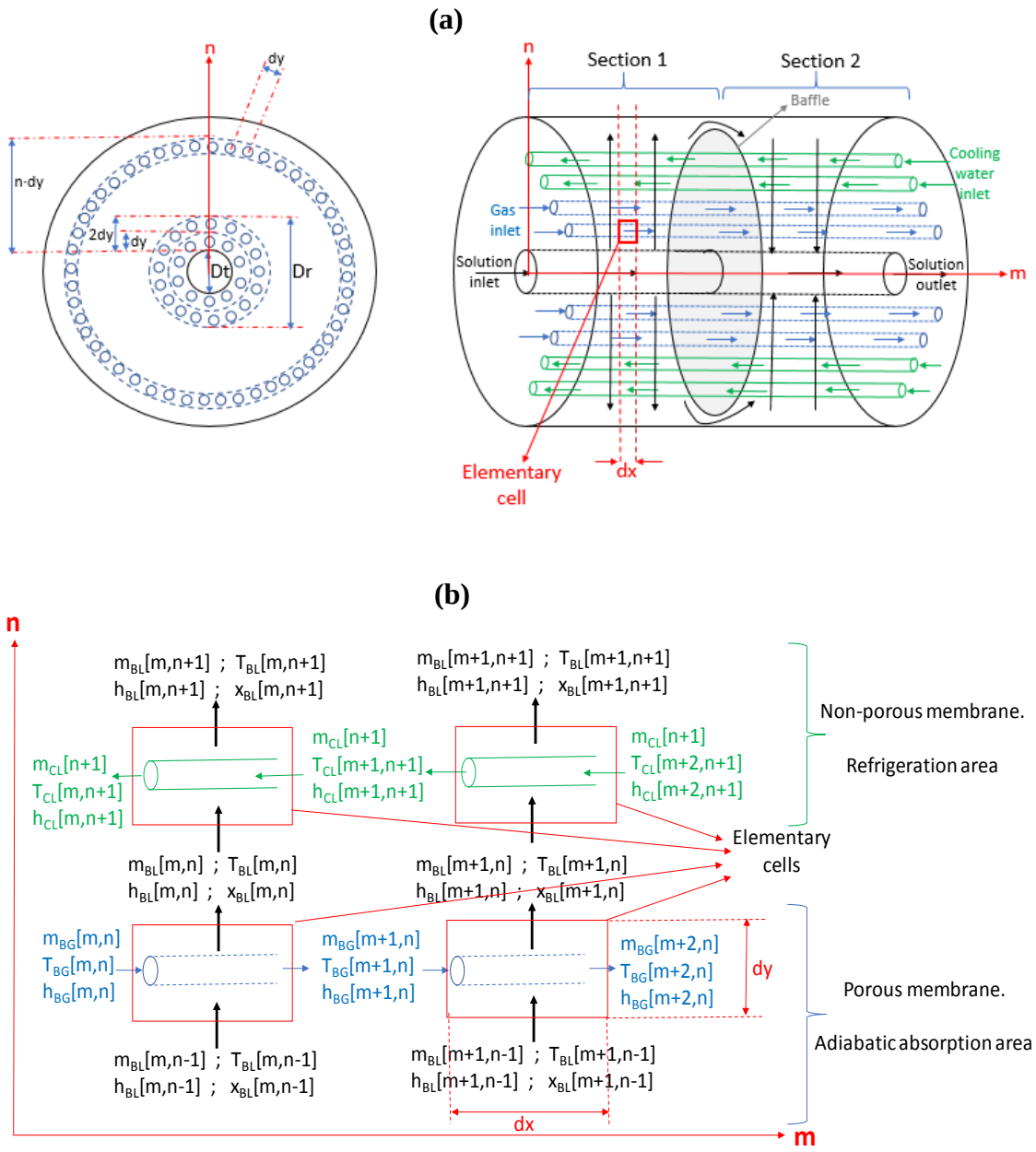

Figure 5.3 Scheme of the discretization of the module. ***(a)*** *Axial and radial sectional view.* ***(b)*** *Cross flow configuration in the elementary cells. The* ***blue arrows*** *represent the gas flow inside the porous hollow fibres, the* ***green arrows*** *represent que cooling water flow inside the non-porous hollow fibres and the* ***black arrows*** *represent solution flow over the outside of the hollow fibres.*

5.1.1 Adiabatic absorption stages

Regarding the adiabatic absorption process that take place in the porous hollow fibre membranes, all the equations showed in Chapter 4 for the mass and heat transfer (from Eq. 4.1 to Eq.4.23) were also used in this model.

5.1.2 Refrigeration stages

In these stages, the heat generated during the adiabatic absorption process is transferred to the cooling water that is flowing inside the non-porous hollow fibres. There is no mass transfer process in these stages. The energy balances for the solution and the cooling water sides are shown in equations (5.1) and (5.2), respectively.

$$m_{BL}[m,n-1]\cdot h_{BL}[m,n-1]+U_{CL}\cdot dA[n]\cdot(T_{CL}[m,n]-T_{BL}[m,n])=m_{BL}[m,n]\cdot h_{BL}[m,n] \quad (5.1)$$

$$m_{CL}[n]\cdot h_{CL}[m-1,n]-U_{CL}\cdot dA[n]\cdot(T_{BL}[m,n]-T_{CL}[m,n])=m_{CL}[n]\cdot\ h_{CL}[m,n] \quad (5.2)$$

Where T_{CL}, m_{CL} and h_{CL} are the temperature, mass flow rate and enthalpy of the cooling water. U_{CL} is the overall heat transfer coefficient and is defined as follows:

$$\frac{1}{U_{CL}}=\frac{1}{\alpha_{BL}}+\frac{d_0\cdot\ln\left(\frac{d_0}{d_i}\right)}{2\cdot\lambda_{MM}}+\frac{d_0}{d_i\cdot\alpha_{CL}} \quad (5.3)$$

where d_i is the inner diameter of the fibre, α_{BL} and α_{CL} are the heat transfer coefficient in the solution and in the cooling water, respectively. α_{BL} is obtained using the correlation of Wickramasinghe et al. [70]. Regarding α_{CL}, the Hausen correlation [77] for laminar flow in circular tubes was used and the Nusselt number in the cooling water was obtained using Eq. (4.21). Thermal conductivity of the polypropylene (λ_{MM}) is taken to be equal to 0.17 $W\cdot m^{-1}K^{-1}$ following the literature [78].

5.2 Operating conditions of the absorption-resorption cycle

In this section, the model of the absorption-resorption cycle described in section 2.2.3 of Chapter 2 was used to determine the ammonia concentration and the solution flow rate in the absorber and the resorber that meet the requirements showed in Figure 5.4. These requirements correspond to the case study selected in Chapter 2 for the sensitivity analysis of the cycle.

Before starting to design the hybrid heat exchanger-hollow fibre membrane absorbers is important to point out that the integration of a membrane contactor in the resorber would require some modifications in the cycle configuration. The reason is because the vapour coming from the generator is a saturated mixture of ammonia/water and has a higher temperature than the solution entering the resorber. Thus, when the vapour and the solution are put in contact by means of a membrane, the vapour would reduce its temperature and then condensation would take place, blocking the pores of the membrane and therefore reducing the mass transfer across the membrane. In order to avoid this issue, before entering the vapour into the membrane module it would be necessary to cool down the vapour to a temperature equal or lower than the temperature of the solution entering the resorber. This can be done by means of an additional external heat exchanger using a cooling water stream or by means of an internal heat transfer between the cold solution leaving the desorber and the vapour obtained in the generator. This last option was selected in our model and the resulting cycle configuration can

be observed in Figure 5.5. The condensed solution obtained in the additional heat exchanger is returned to the generator. In the case of the absorber, this problem does not take place because the vapour generated in the desorber is always colder than the solution entering the absorber. Another important effect of this new configuration on the performance of the cycle is the reduction of the flow rate in the bleeding pipe (nearly zero) due to the water condensation produced in the heat exchanger 3.

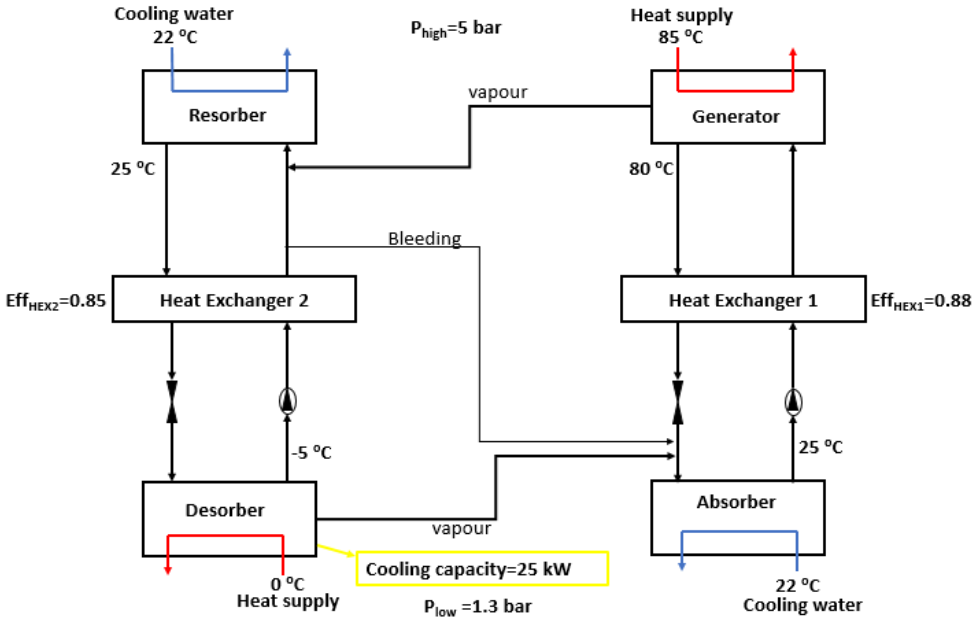

Figure 5.4 Absorption-resorption refrigeration cycle. Input variables for determining the operating conditions of the base case.

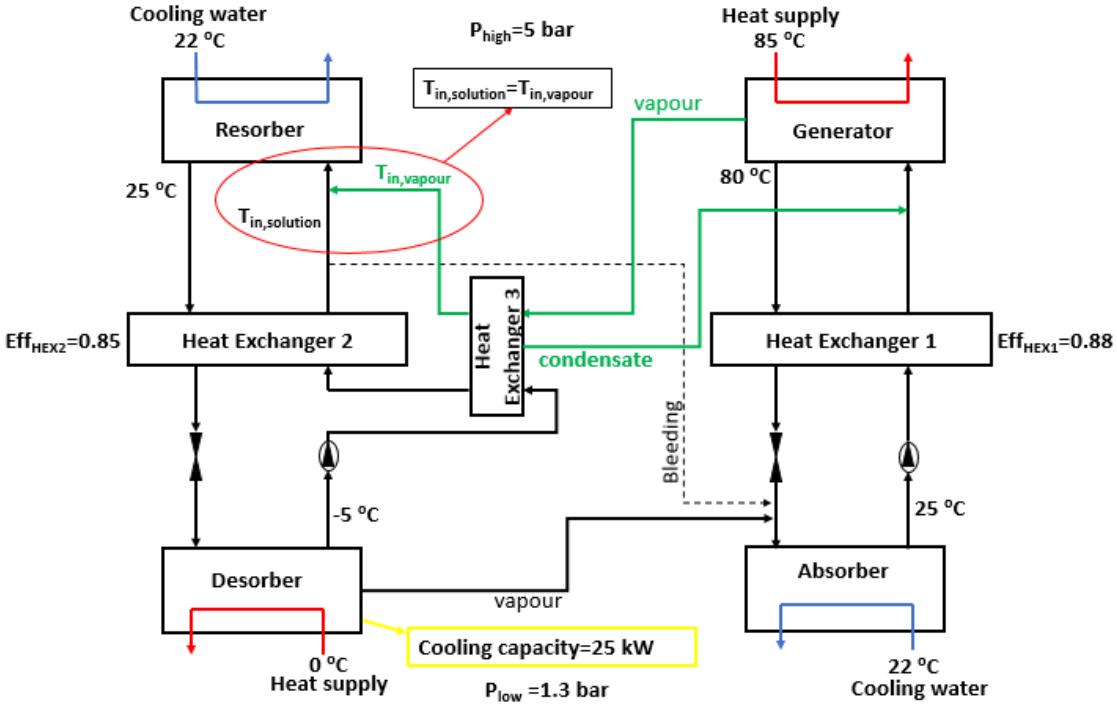

Figure 5.5 Absorption-resorption refrigeration cycle modified: precooling of the vapour before entering the resorber.

The theoretical model of the ammonia/water absorption-resorption refrigeration cycle modified according to Figure 5.5 was run and the operating conditions obtained for the absorber and for the resorber are showed in Figure 5.6. These conditions will be taken as a reference in the following section for the design of the hybrid heat exchanger-hollow fibre membrane absorbers.

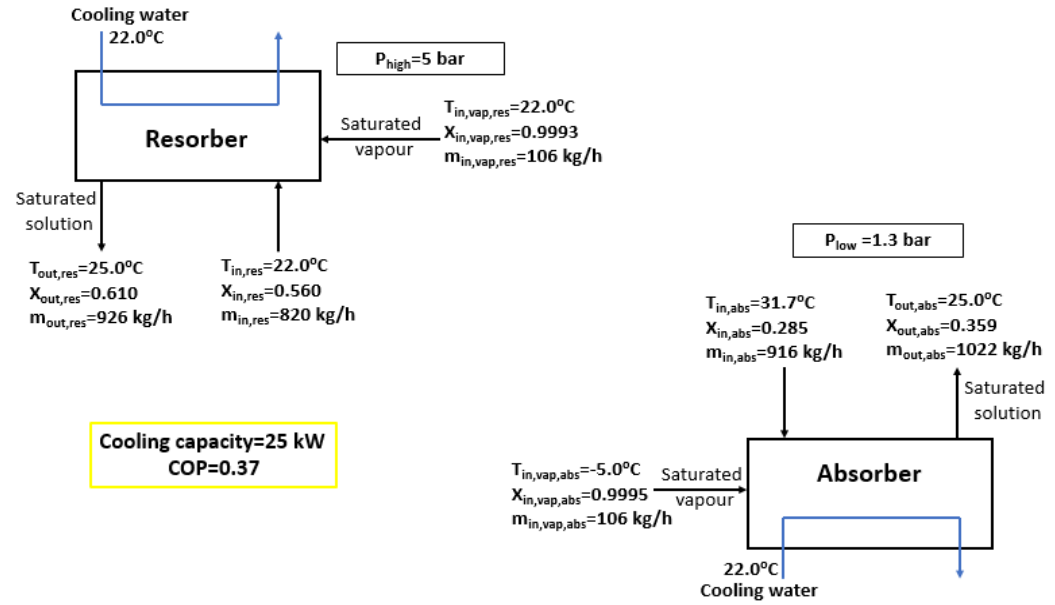

Figure 5.6 Working conditions in the absorber and in the resorber.

5.3 Design of a hybrid heat exchanger-hollow fibre membrane absorber for the 25-kW ammonia/water absorption-resorption refrigeration cycle

The following procedure was carried out to design the hybrid heat exchanger-hollow fibre membrane absorbers (HEXHFMA) that meet the requirements of the cycle of Figure 5.6. In order to better understand the procedure, Figures 5.7-5.10 are also included.

1. The geometric dimensions and membrane characteristics of the Liqui-Cel® hollow fibre membrane module showed in Table 4.1 of Chapter 4 were taken as initial values for the design of the HEXHFMA. However, in order to avoid high pressure drops in the membrane module the manufacturer recommended solution flow rates lower than 0.68 m^3/h, which is lower than the solution flow rates required in the base case of Figure 5.6. Then, for the design of the HEXHFMA of the base case it would be necessary to reduce the velocity of the solution through the shell side of the module in order to minimize the pressure drop. Thus, the initial length of the membrane module is assumed to be double than the length of the membrane module described in Chapter 4 (2x15cm=**30cm**).

2. The two-dimensional adiabatic model described and validated in Chapter 4 is used for the initial step. The model is run using as input values the inlet variables of the absorber showed in Figure 5.6. Then, the results obtained at the outlet of the membrane absorber are compared to the outlet conditions in the absorber showed in Figure 5.6. If the outlet solution of the membrane module is far from the saturation conditions and far from the desired ammonia concentration, the absorption area is then increased by adding new rings of porous hollow fibre membranes. This process is repeated until the outlet conditions of the solution are close to the saturation, that is to say, no significant improvements are observed in the solution concentration at the outlet of the module.

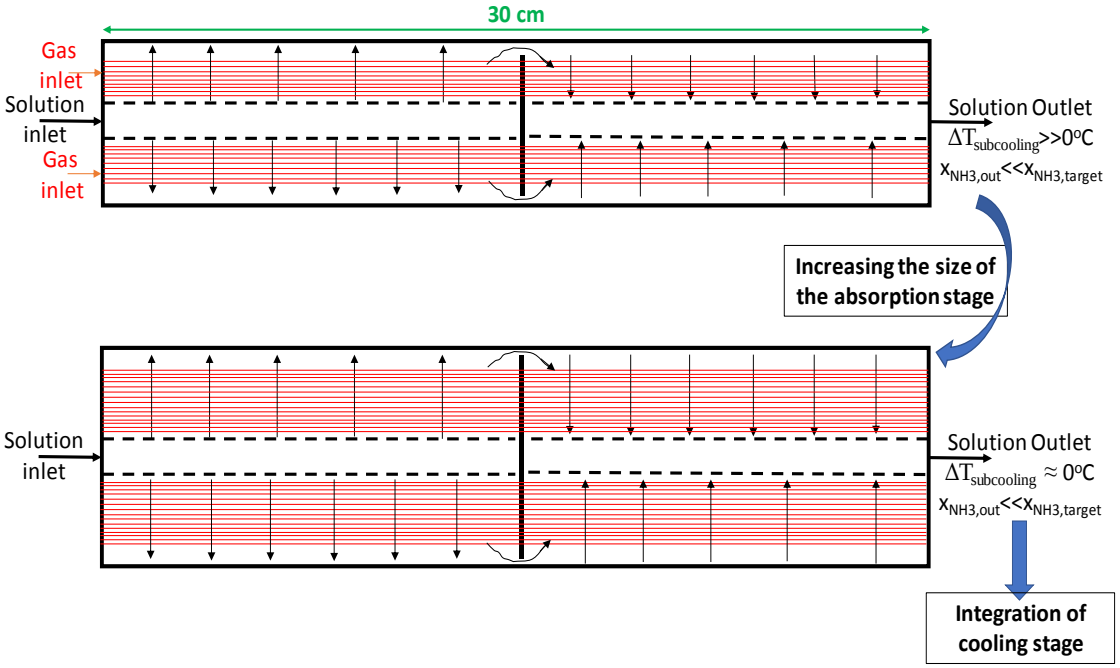

*Figure 5.7 Adiabatic membrane absorber. **Red** lines represent the porous hollow fibre membranes.*

3. The non-porous hollow fibre membranes for cooling are integrated just after the adiabatic absorption stage. As initial assumption, each cooling stage consists of 25 rings. Initially, the velocity of the cooling water flowing inside the non-porous hollow fibres is assumed to be 1 m/s. The model of the membrane absorber with cooling integrated was already described in section 5.1 of this chapter.

4. The model with the cooling stage integrated is run. If the outlet conditions of the solution do not meet the requirements of the base case, additional adiabatic and cooling stages are added. Points 2 to 4 of this procedure are repeated until obtaining the outlet conditions of the solution approach to the outlet conditions required for the base case.

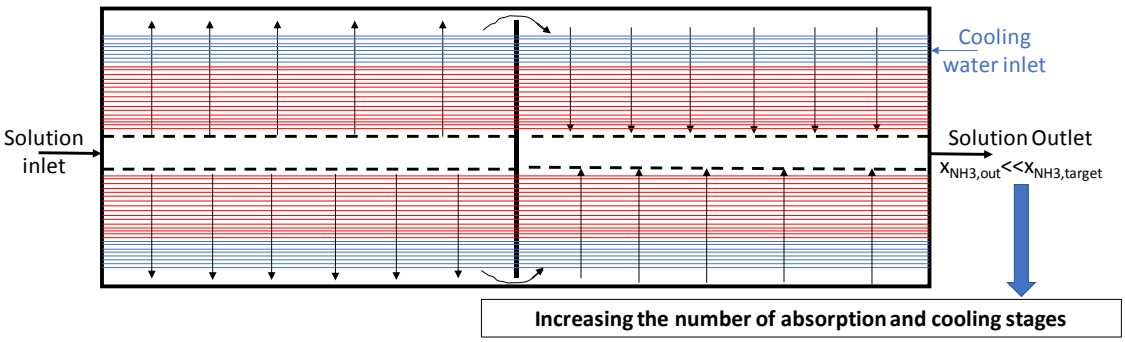

*Figure 5.8 Hybrid heat exchanger-hollow fibre membrane absorber with one cooling stage and one adiabatic absorption stage. **Red** lines represent the porous hollow fibre membranes and **blue** lines represent the non-porous hollow fibre membranes.*

5. The number of rings required on each cooling stage is optimized. The model is run and the temperature difference between the solution and the cooling water on each ring is

analyzed. If this temperature difference approach to zero before the end of the cooling stage mean that the cooling stage is oversized and some non-porous hollow fibres can be removed. If possible, the temperature difference between the cooling water and the solution should be kept over 3ºC.

6. The number of rings required on each absorption stage is also optimized. If possible, the ammonia absorption rate (J) on each ring must be kept above 10^{-4} kg/(m^2·s). This condition was specially referred to the first section of the module, where the high subcooling of the solution (high driving force) allow to keep high absorption rates. In the second section of the module this condition cannot be satisfied because the solution is close to the saturation conditions.

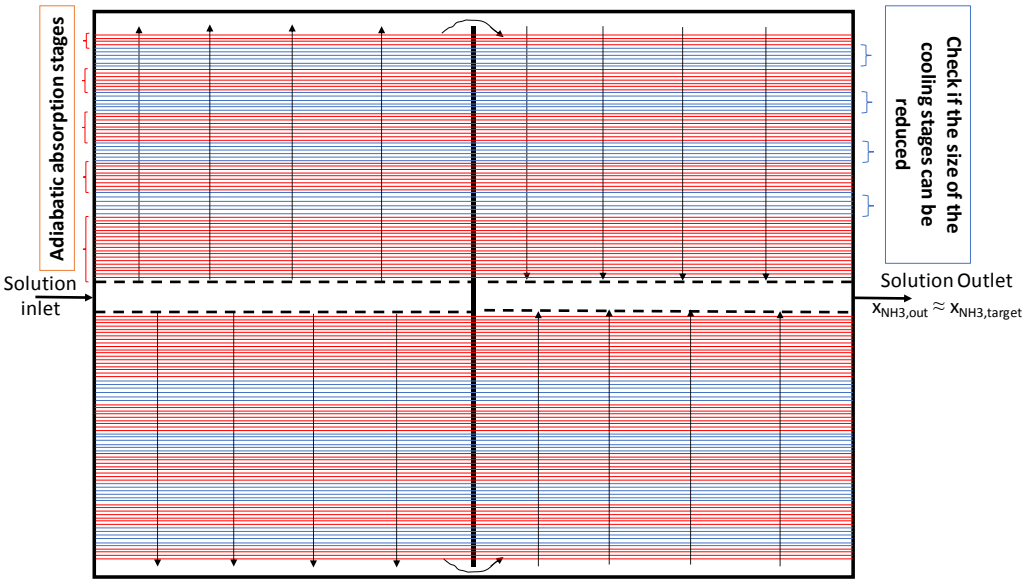

Figure 5.9 *Hybrid heat exchanger-hollow fibre membrane absorber with several adiabatic absorption and cooling stages.*

7. Finally, the cooling water flow rate is optimized in order to reduce water flow rate but keeping the outlet conditions of the solution within the range desired ($\pm$15% of deviation in the total amount of ammonia absorbed).

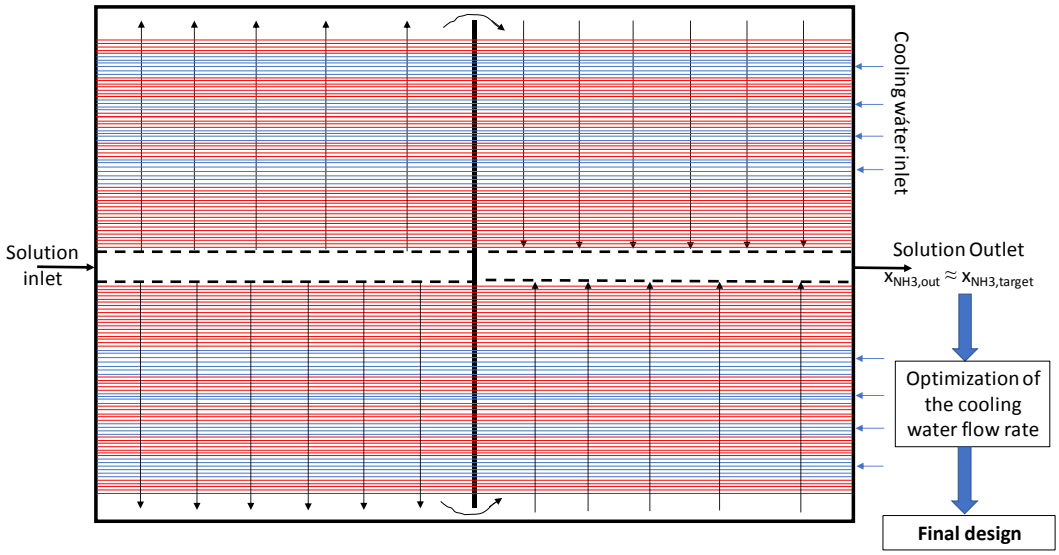

Figure 5.10 Final design of the hybrid heat exchanger-hollow fibre membrane absorber.

5.3.1 Absorber design

The procedure previously explained was used for the design of a HEXHFMA for the absorber of the 25-kW ammonia/water absorption-resorption refrigeration cycle. The geometric dimensions and membrane characteristics of the HEXHFMA are listed in Table 5.1 and a scheme of the membrane module designed can be observed in Figure 5.11. The same gap between the hollow fibre bundle and the housing of the membrane module than in the Liqui-Cel® membrane module was assumed (0.55 cm).

Table 5.1 Geometric dimensions and membrane characteristics of the HEXHFMA designed to be used as an absorber in the 25-kW ammonia/water absorption-resorption refrigeration system.

HEXHFMA (ABSORBER)	
Total number of fibres	446522
Total effective membrane area (m^2)	126
Number of porous fibres	322614
Total effective porous membrane area (m^2)	91.2
Number of non-porous fibres	123908
Number of absorption stages	6
Number of cooling stages	5
Material	Polypropylene
Fibres inner diameter, d_i (µm)	210
Fibres outer diameter, d_o (µm)	300
Average pore diameter, d_p (µm)	0.03
Effective hollow fibre length, L (m)	0.30
Porosity, ε (%)	45
Surface-to-volume ratio (m^2/m^3)	5802
Shell	
Material	Polypropylene
Outer diameter (cm)	32.0
Inside diameter, D_s (cm)	30.9
Central tube diameter, D_t (cm)	2.22

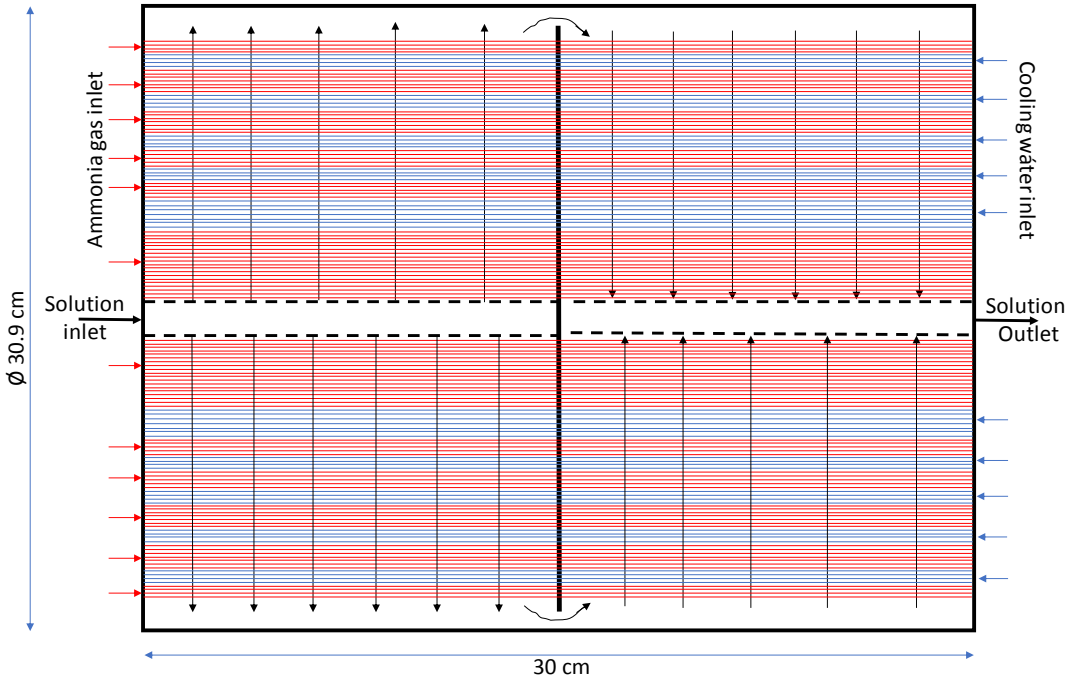

Figure 5.11 Scheme of the final design of the absorber for the 25-kW absorption-resorption refrigeration cycle.

Six adiabatic absorption stages were required to absorb all the ammonia. The first adiabatic section consists of 99 rings, the second one consists of 50 rings, sections three to five consist of 35 rings each one and the last section consists of 15 rings. Moreover, five cooling stages were required for rejecting the heat generated during the absorption process by means of a cooling water supply of 9.7 m^3/h at 22^{o}C. This flow rate provides a water velocity inside the fibres of 0.63 m/s. The first cooling stage consists of 21 rings and the rest of stages comprises 15 rings each one. The overall results obtained with the model and their comparison with the working conditions of the 25-kW absorption-resorption refrigeration cycle are depicted in Figure 5.12.

The results obtained show a very good agreement between the target conditions and the ones obtained. There is a small deviation in the outlet solution concentration that corresponds to a reduction in the total amount of ammonia absorbed of 7.5%. The deviation obtained in the outlet temperature of the solution was 0.7^{o}C. It is important to highlight that the saturation conditions assumed at the outlet of the absorber in the model of the absorption-resorption cycle are not a realistic assumption in practice. In absorption machines there is always a certain subcooling in the solution at the outlet of the absorbers because reaching saturation conditions would require a very large absorber area.

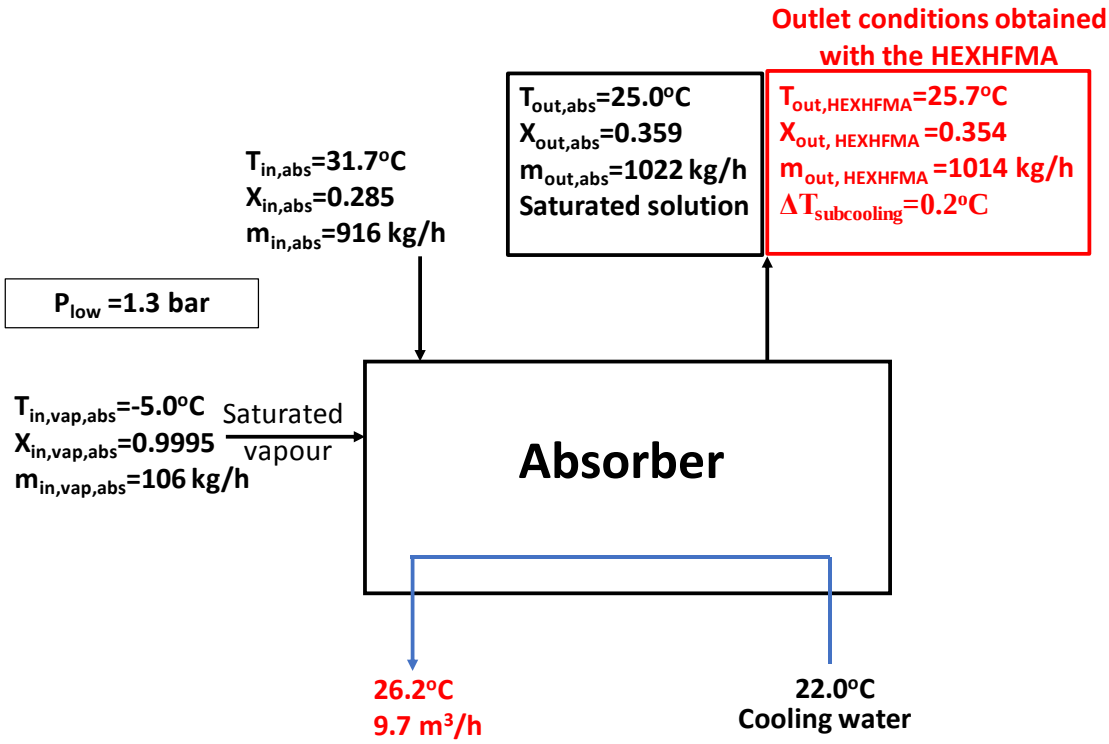

Figure 5.12 Comparison between the working conditions of the 25-kW absorption-resorption refrigeration cycle and the results obtained with the model of the HEXHFMA: absorber.

5.3.1.1 Evolution of the main parameters along the HEXHFMA (Absorber)

Figures 5.13-5.17 show the evolution of the ammonia solution concentration, bulk solution temperature, ammonia absorption rate, subcooling of the solution and the temperature difference between the solution and the fluid inside the fibres (ammonia gas and cooling water) in the HEXHFMA, respectively. All the figures are divided into three parts: (a) shows a scheme of the upper part of the hollow fibre membrane module (based on the scheme shown in Figure 5.3a) and the contours of the parameters studied in each figure by means of a colour scale; (b) and (c) show the evolution of each parameter in the radial direction in the first and second section of the module, respectively. The radial direction (n) in the first section is discretized into 350 rings (n from 1 to 350), starting in the central tube and finishing at the top of the module, where the solution is collected before entering the second section. The second section is also discretized into 350 rings (n from 351 to 700), but in this case starting at the top of the module and finishing in the central tube, where the solution is finally collected. The membrane module was also discretized into 30 elements in the axial direction (m) but only elements 1, 3, 5, 15, 16, 20 and 30 were selected for representation in the figures. The plateaus showed in Figure 5.13, the peaks showed in Figures 5.14, 5.16 and 5.17 and the blank areas of Figure 5.15 are caused by the cooling stages of the HEXHFMA.

In the first section of the module (Figures 5.13b-5.17b), the ammonia solution concentration is highest in the upper-left side of the section (Figures 5.13a and 5.13b line m=1). This is because the temperature of the gas is much lower than the liquid temperature in this area (line m=1 of Figure 5.17b) so there is a cooling effect in the solution that improves the driving force of the absorption process. This effect is particularly evidenced in Figure 5.15b, where the evolution of the ammonia absorption rate (J) is studied. Figure 5.15b shows that the trend of the ammonia

absorption rate is completely different at the beginning of the module (m=1) than in the rest of the first section (m=3-15). For m=3-15, as expected, there is a downward trend of J in the radial direction due to the increase in the ammonia concentration and the temperature of the bulk solution. However, for m=1 the ammonia absorption rate increases in the upper part of the module due to the large temperature difference (≈18ºC) between the gas and the solution (Figure 5.17b) that cool down the solution (Figure 5.14b). The maximum J and x_{NH3} obtained were $1.36 \cdot 10^{-3}$ kg/(m^2·s) and 0.382 respectively, and both were obtained in this area (m=1). Unfortunately, due to the low temperature of the solution in this area, the cooling water causes a heating effect on the solution (m=1, Figure 5.14b) that leads into a reduction of the subcooling (m=1, Figure 5.16b). In any case, this behaviour only takes place in the area close to the gas inlet (m=1) because the temperature of the gas and the temperature of the solution approach to each other rapidly (m=3-15, Figure 5.17b) and the cooling effect of the gas stream becomes almost negligible.

Comparing the results obtained in the first section (Figures 5.13b-5.17b) with the second section (Figures 5.13c-5.17c) it can be clearly observed that in the second section there is greater uniformity in the axial direction in all the parameters studied. This effect can be explained because the temperature difference between the solution and the fluids inside the fibres (ammonia gas and cooling water) is smaller in this section (Figure 5.17c).

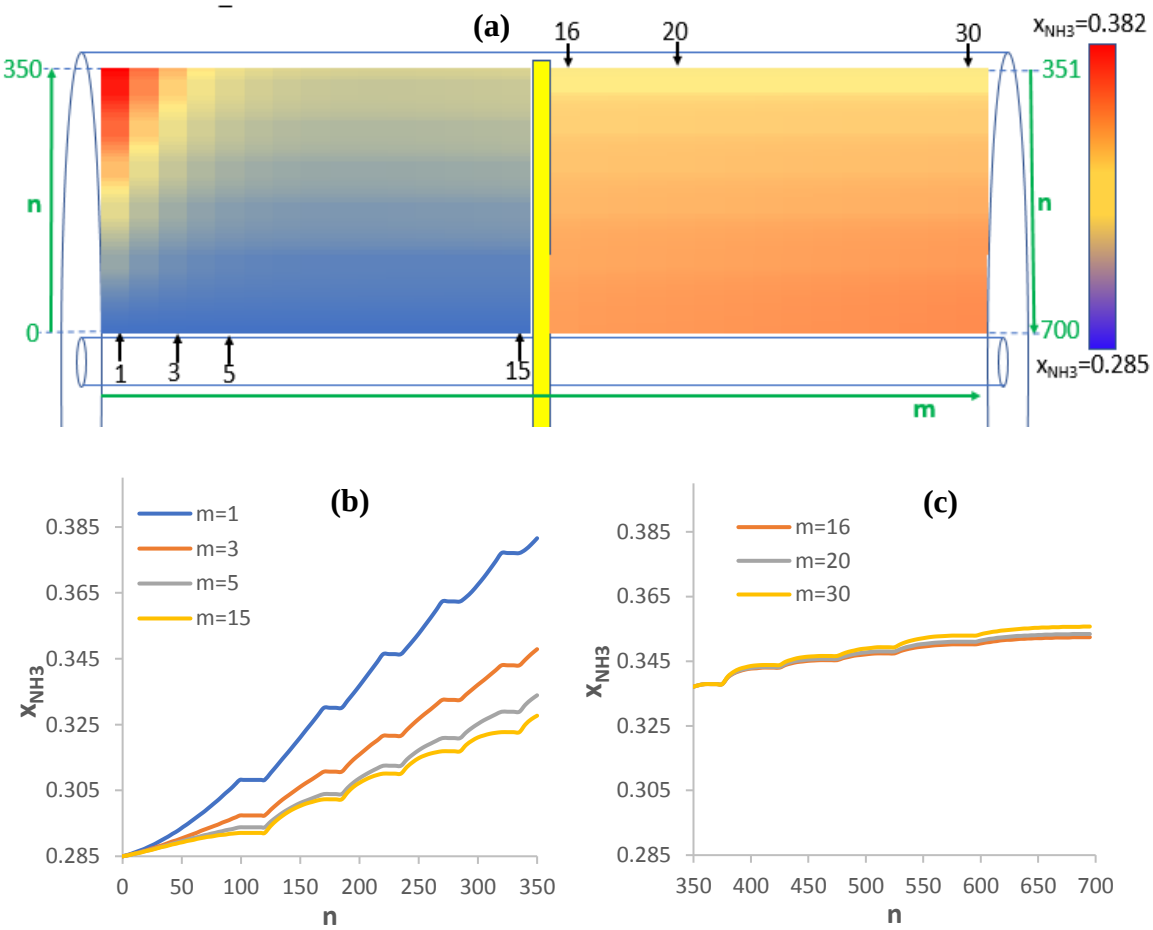

Figure 5.13 ***(a)*** *Contours of the ammonia concentration profile in the HEXMFMA (Absorber).* ***(b)*** *Evolution of ammonia concentration in the radial direction (n from 0 to 350) in the first section of the module.* ***(c)*** *Evolution of ammonia concentration in the radial direction (n from 351 to 700) in the second section of the module.*

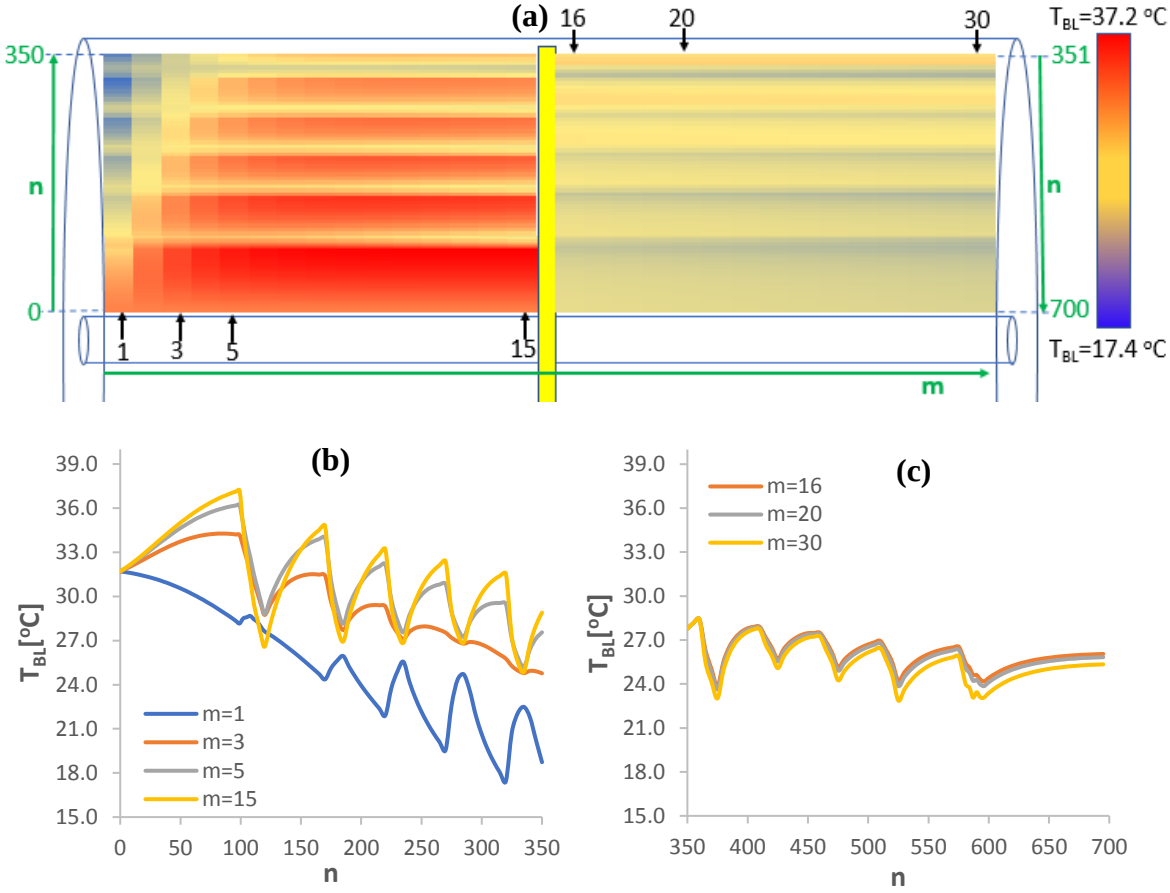

Figure 5.14 ***(a)*** *Contours of the bulk solution temperature profile in the HEXHFMA (Absorber).* ***(b)*** *Evolution of bulk solution temperature in the radial direction (n from 0 to 350) in the first section of the module.* ***(c)*** *Evolution of bulk solution temperature in the radial direction (n from 351 to 700) in the second section of the module.*

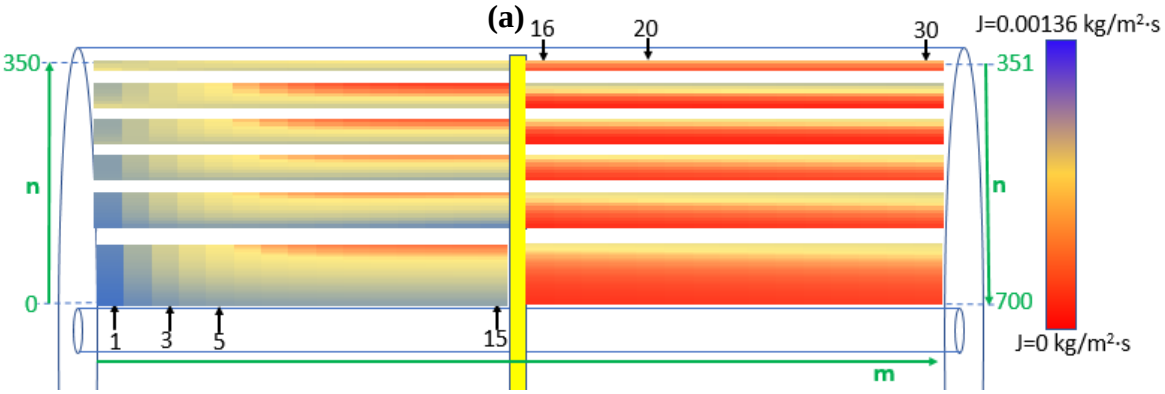

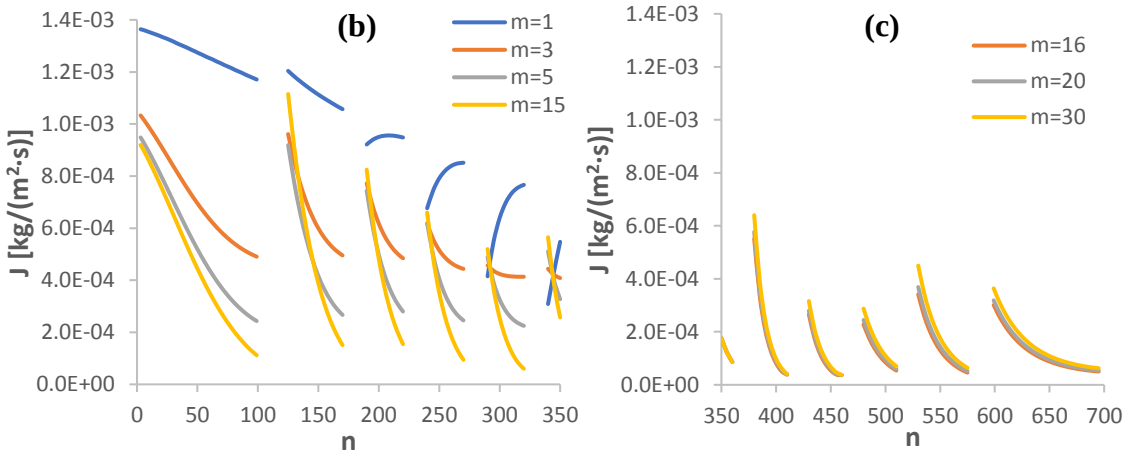

Figure 5.15 ***(a)*** *Contours of the ammonia absorption rate profile in the HEXHFMA (Absorber).* ***(b)*** *Evolution of ammonia absorption rate in the radial direction (n from 0 to 350) in the first section of the module.* ***(c)*** *Evolution of ammonia absorption rate in the radial direction (n from 351 to 700) in the second section of the module.*

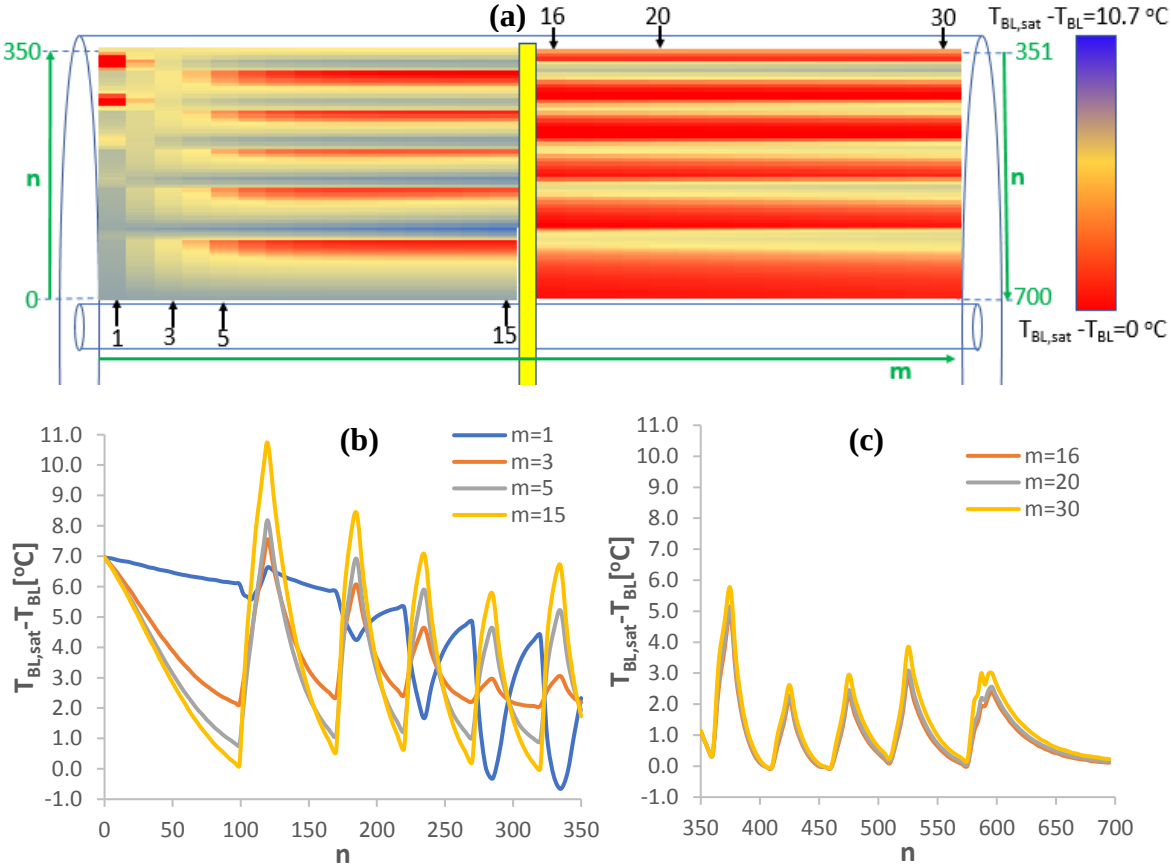

Figure 5.16 ***(a)*** *Contours of the solution subcooling profile in the HEXHFMA (Absorber).* ***(b)*** *Subcooling evolution in the radial direction (n from 0 to 350) in the first section of the module.* ***(c)*** *Subcooling evolution in the radial direction (n from 351 to 700) in the second section of the module.*

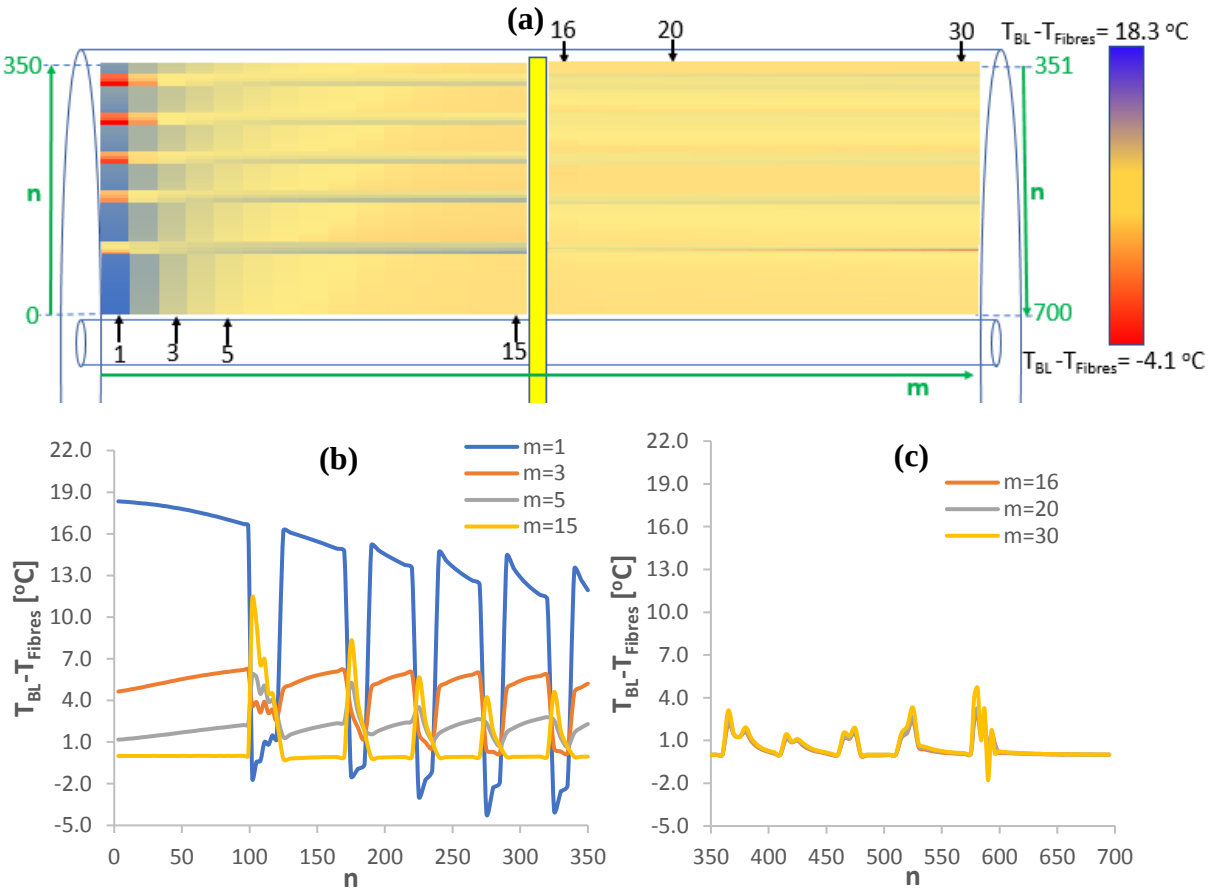

Figure 5.17 ***(a)*** *Contours of the temperature difference between the solution and the fluid inside the fibres (gas and cooling water) in the HEXHFMA (Absorber).* ***(b)*** T_{BL}-T_{Fibres} *evolution in the radial direction (n from 0 to 350) in the first section of the module.* ***(c)*** T_{BL}-T_{Fibres} *evolution along the radial direction (n from 351 to 700) in the second section of the module.*

5.3.2 Resorber design

The same procedure was also used for the design of a HEXHFMA for the resorber of the 25-kW ammonia/water absorption-resorption refrigeration cycle. The geometric dimensions and membrane characteristics are listed in Table 5.2. Seven adiabatic absorption stages were required to absorb all the ammonia. The first adiabatic section consists of 99 rings, the second one consists of 50 rings, sections three to five consist of 35 rings each one, section six has 30 rings and the last section 10 rings. Moreover, six cooling stages were required for rejecting the heat generated during the absorption process by means of a cooling water supply of 15.1 m^3/h at 22°C. This flow rate provides a water velocity inside the fibres of 0.75 m/s. The first cooling stage consists of 21 rings and the rest of stages comprises 15 rings each one. The overall results obtained with the model and their comparison with the working conditions of the 25-kW absorption-resorption refrigeration cycle are depicted in Figure 5.18.

Table 5.2 Geometric dimensions and membrane characteristics of the HEXHFMA designed to be used as a resorber in the 25-kW ammonia/water absorption-resorption refrigeration system.

HEXHFMA (RESORBER)	
Total number of fibres	546554
Total effective membrane area (m^2)	154.5
Number of porous fibres	384899
Total effective porous membrane area (m^2)	108.8
Number of non-porous fibres	161655
Number of absorption stages	7
Number of cooling stages	6
Material	Polypropylene
Fibres inner diameter, d_i (µm)	210
Fibres outer diameter, d_o (µm)	300
Average pore diameter, d_p (µm)	0.03
Effective hollow fibre length, L (m)	0.30
Porosity, ε (%)	45
Surface-to-volume ratio (m^2/m^3)	5815
Shell	
Material	Polypropylene
Outer diameter (cm)	35.2
Inside diameter, D_s (cm)	34.1
Central tube diameter, D_t (cm)	2.22

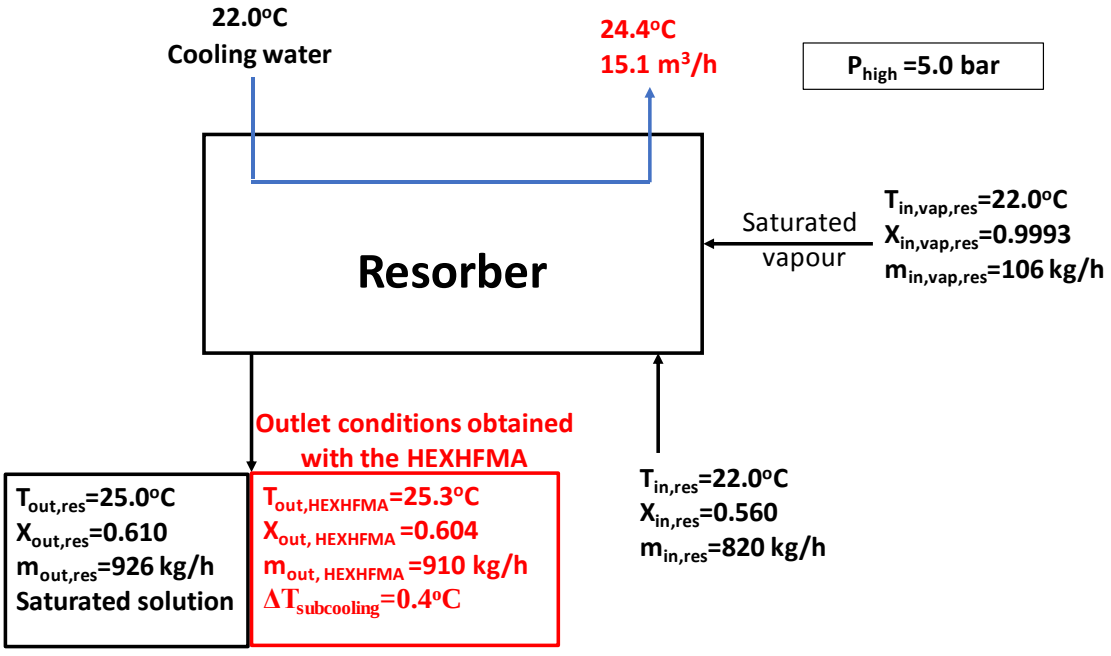

Figure 5.18 Comparison between the working conditions of the 25-kW absorption-resorption refrigeration cycle and the results obtained with the model of the HEXHFMA: resorber.

As expected, the complete saturation of the solution was not achieved and 0.4ºC of subcooling was obtained at the outlet. The small deviation in the outlet solution concentration corresponds

to a reduction in the total amount of ammonia absorbed of 15%. The deviation obtained in the outlet temperature of the solution was 0.3°C.

5.3.2.1 Evolution of the main parameters along the HEXHFMA (Resorber)

Figures 5.19-5.23 show the evolution of the ammonia solution concentration, bulk solution temperature, ammonia absorption rate, subcooling of the solution and the temperature difference between the solution and the fluid inside the fibres (ammonia gas and cooling water) in the HEXHFMA designed for the resorber, respectively. The radial direction (n) in the first section is discretized into 390 rings (n from 1 to 390), starting in the central tube and finishing at the top of the module, where the solution is collected before entering the second section. The second section is also discretized into 390 rings (n from 391 to 780), but in this case starting at the top of the module and finishing in the central tube, where the solution is finally collected. The membrane module was also discretized into 30 elements in the axial direction (m) but only elements 1, 3, 5, 15, 16, 20 and 30 were selected for representation in the figures. The plateaus showed in Figure 5.19, the peaks showed in Figures 5.20, 5.22 and 5.23 and the blank areas of Figure 5.21 are caused by the cooling stages of the HEXHFMA.

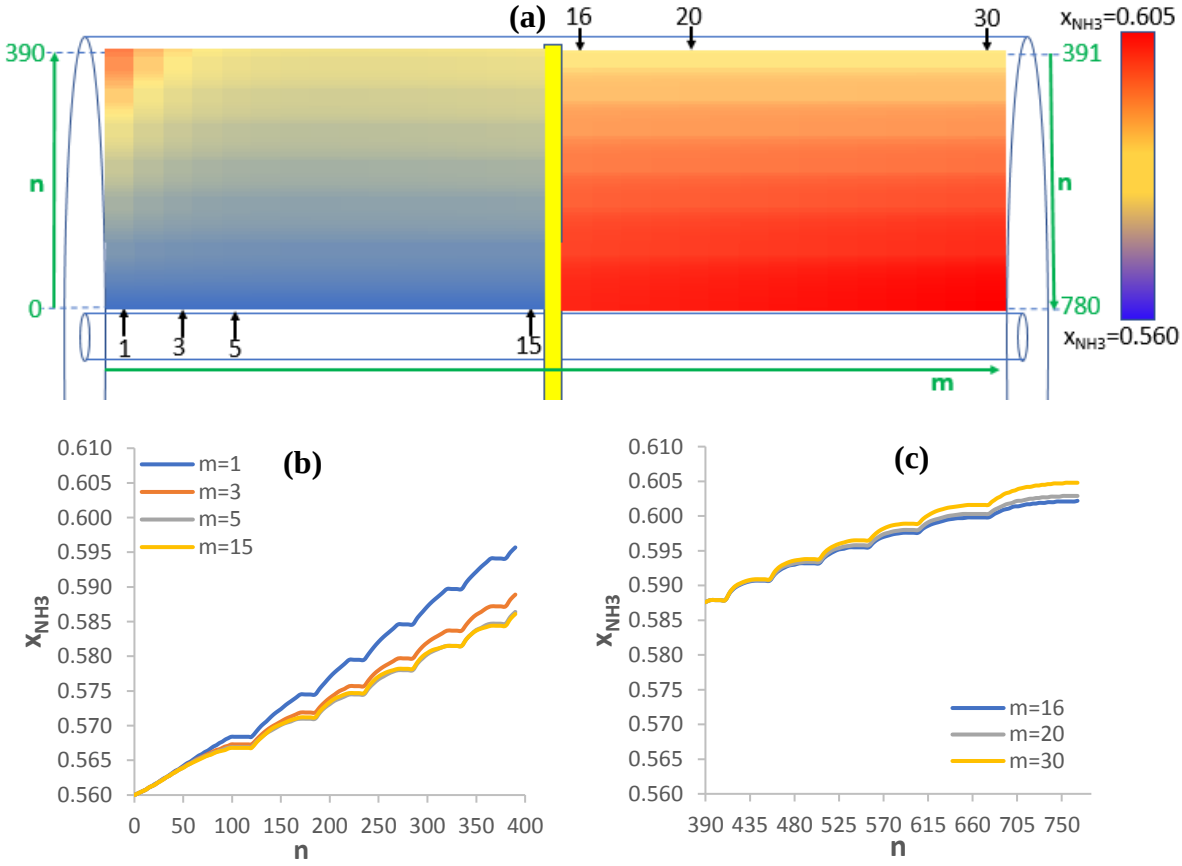

Figure 5.19 ***(a)*** *Contours of the ammonia concentration profile in the HEXMFMA (Resorber).* ***(b)*** *Evolution of ammonia concentration in the radial direction (n from 0 to 390) in the first section of the module.* ***(c)*** *Evolution of ammonia concentration in the radial direction (n from 391 to 780) in the second section of the module.*

In the case of the resorber, the inlet temperature of the ammonia gas is the same than the inlet temperature of the solution, so the cooling effect observed in the previous section (absorber working conditions) do not take place in the resorber. For this reason, the profiles of the

parameters studied show a similar trend all along the membrane module. As expected, the maximum ammonia absorption rate ($1.24 \cdot 10^{-3}$ kg/m^2·s) was obtained at the inlet of the solution (Figure 5.21b), where the subcooling of the solution was also the highest (9.1ºC), as shown in Figure 5.22b. The temperature difference between the solution and the gas remains always below 3ºC for m=1, and it is nearly zero from m=5 to the end of the membrane module (Figure 5.23b and 5.23c).

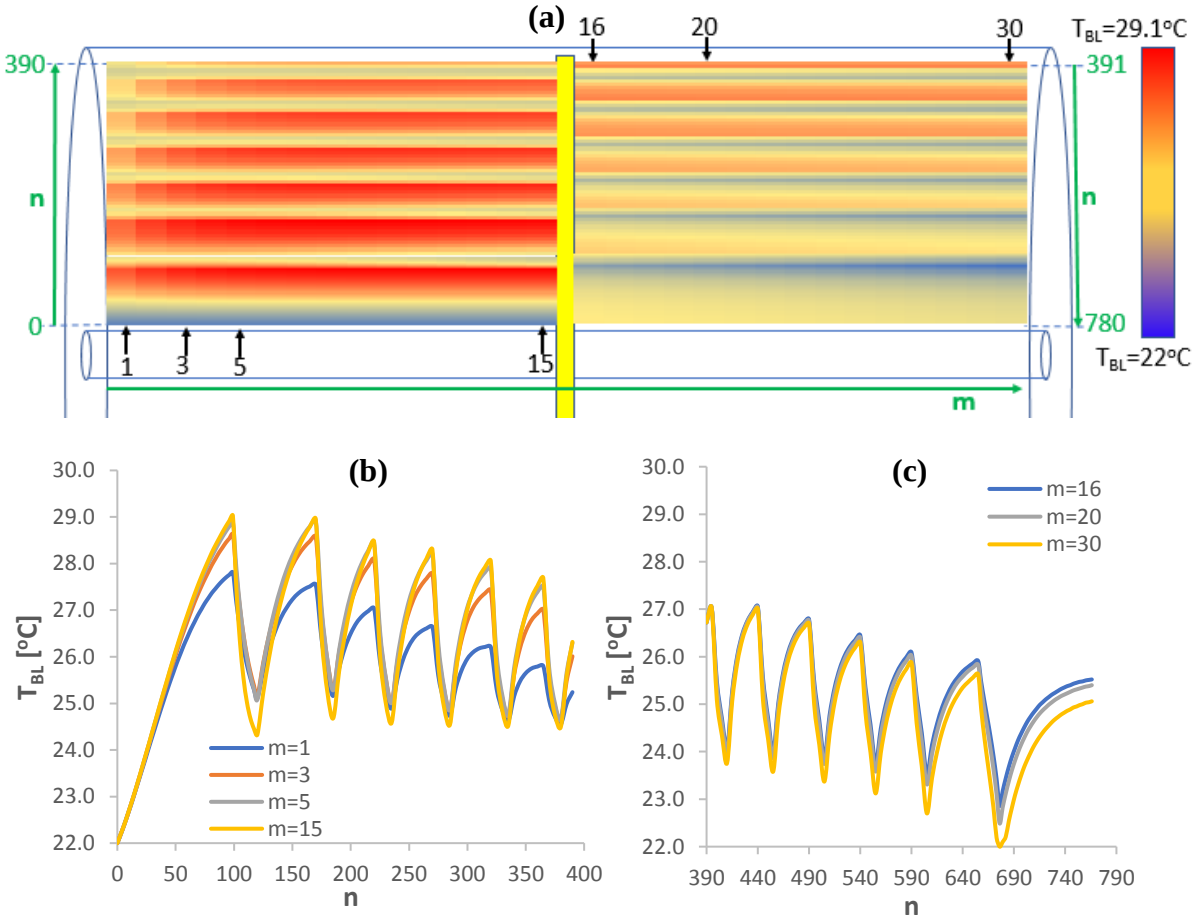

Figure 5.20 ***(a)*** *Contours of the bulk solution temperature profile in the HEXHFMA (Resorber).* ***(b)*** *Evolution of bulk solution temperature in the radial direction (n from 0 to 390) in the first section of the module.* ***(c)*** *Evolution of bulk solution temperature in the radial direction (n from 391 to 780) in the second section of the module.*

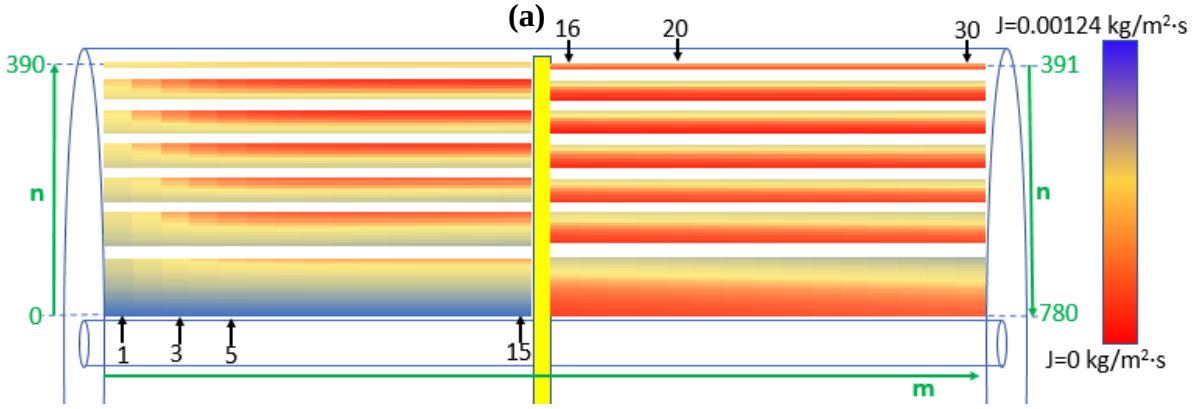

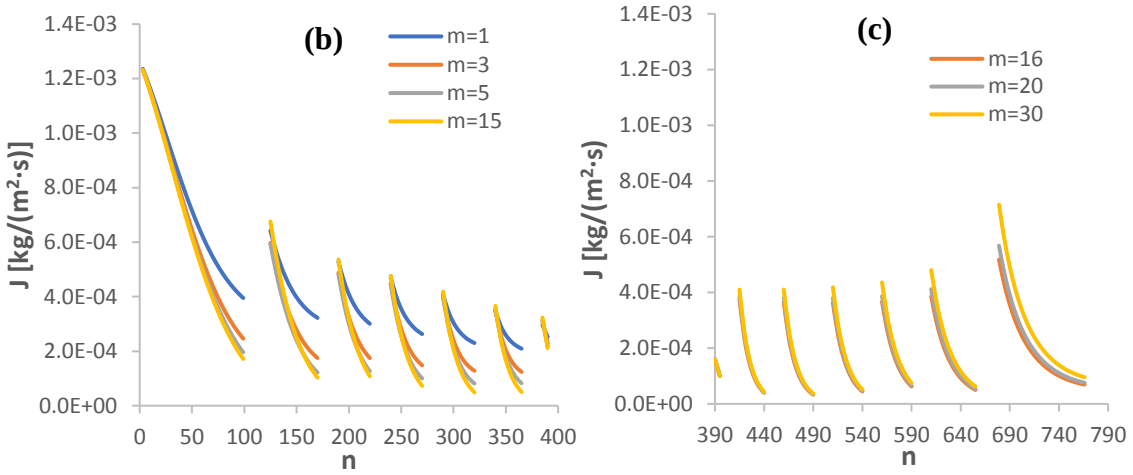

Figure 5.21 ***(a)*** *Contours of the ammonia absorption rate profile in the HEXHFMA (Resorber).* ***(b)*** *Evolution of ammonia absorption rate in the radial direction (n from 0 to 390) in the first section of the module.* ***(c)*** *Evolution of ammonia absorption rate in the radial direction (n from 391 to 780) in the second section of the module.*

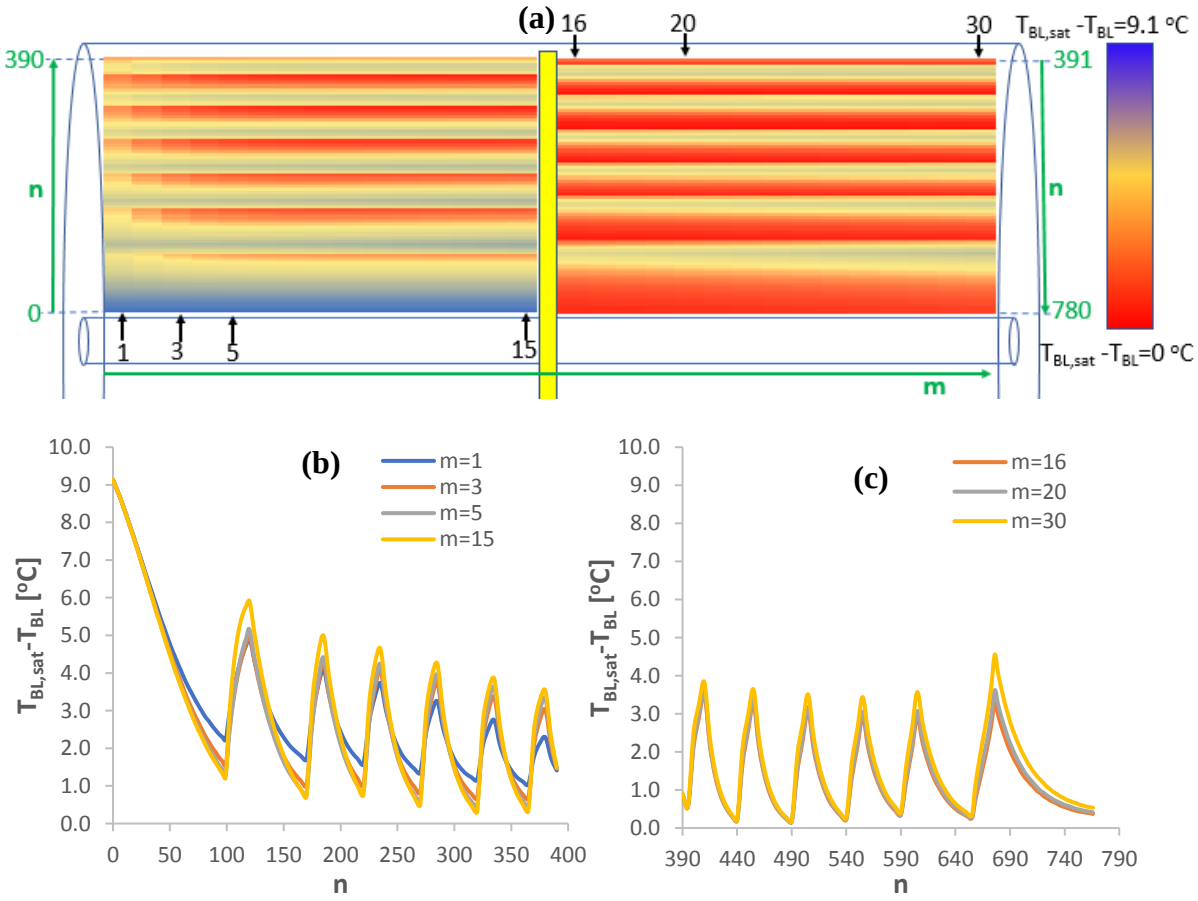

Figure 5.22 ***(a)*** *Contours of the solution subcooling profile in the HEXHFMA (Resorber).* ***(b)*** *Subcooling evolution in the radial direction (n from 0 to 390) in the first section of the module.* ***(c)*** *Subcooling evolution in the radial direction (n from 391 to 780) in the second section of the module.*

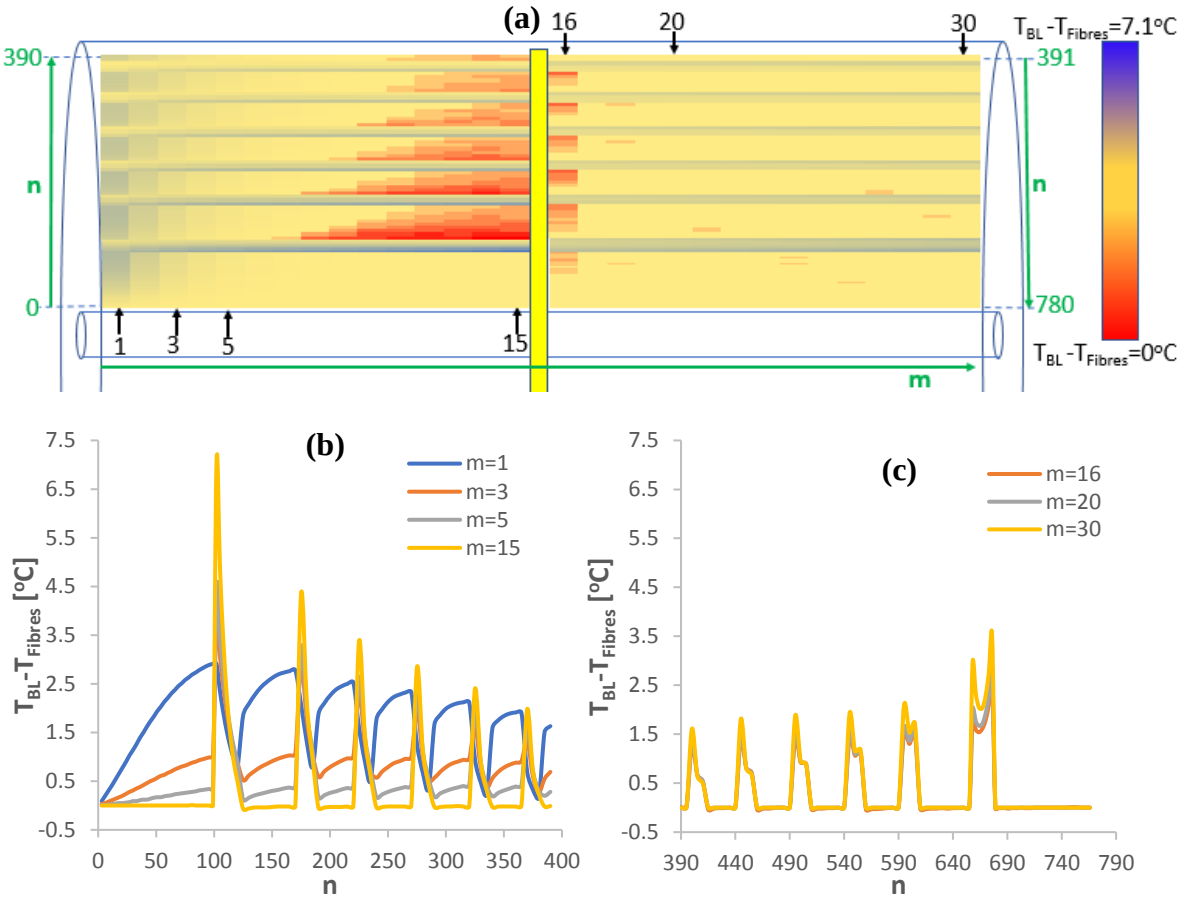

Figure 5.23 ***(a)*** *Contours of the temperature difference between the solution and the fluid inside the fibres (gas and cooling water) in the HEXHFMA (Resorber).* ***(b)*** *T_{BL}-T_{Fibres} evolution in the radial direction (n from 0 to 350) in the first section of the module.* ***(c)*** *T_{BL}-T_{Fibres} evolution along the radial direction (n from 351 to 700) in the second section of the module.*

5.3.3 Comparison between both designs (Absorber and Resorber)

Despite the amount of ammonia vapour entering the absorber and the resorber was the same (106 kg/h), the resorber design required a bigger membrane area than the absorber and much more cooling water flow rate. Specifically, the resorber designed was 22% bigger (in terms of total effective membrane area) than the absorber. According to the experimental results obtained in Chapter 4, the adiabatic working conditions in the resorber leads into higher mass transfer coefficient in the solution side and hence higher ammonia absorption rates (J). However, the results obtained in this section shows just the opposite behaviour. Two main factors can explain this discrepancy: first, the higher temperature difference between the solution and the cooling fluid when the HEXHFMA is working under absorber conditions. This larger temperature difference leads into more efficient heat transfer in the cooling stages and hence into a lower cooling water flow rate. The second factor is the inlet temperature of the vapour. In the experimental results obtained in Chapter 4 the inlet temperature of the gas was not controlled, so the gas entered to the membrane module at room temperature (around 20-25°C). In the absorber of the absorption-resorption refrigeration cycle of the case study the inlet temperature of the gas is -5°C. This cold vapour stream leads into a cooling effect on the ammonia/water solution in the area close to the vapour inlet that increases the absorption rate in a very significant way. In order to confirm this hypothesis, the model of the HEXHFMA for the

absorber was run with the same inlet conditions showed in Figure 5.6 except for the inlet temperature of the vapour, that was increased in order to be equal to the inlet temperature of the solution (31.7°C). With this modification, the cooling effect of the gas stream cannot take place and a much lower amount of ammonia should be absorbed. Figure 5.24 depicts the results obtained.

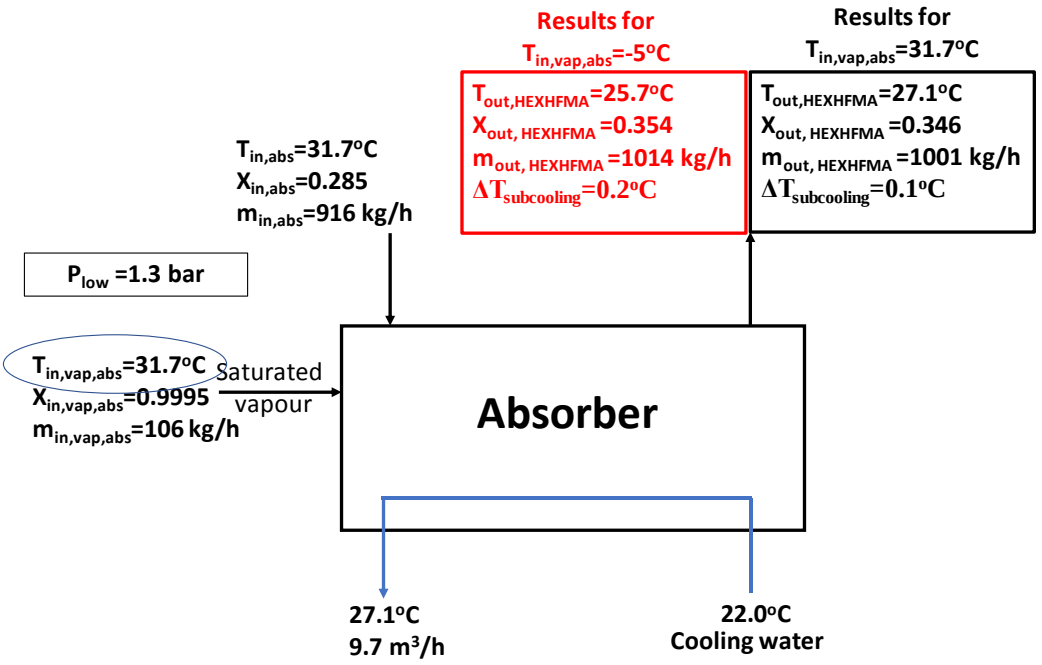

Figure 5.24 Comparison between the results obtained in the absorber at two different inlet temperatures of the vapour.

The results obtained in the comparison shows clearly the influence of the inlet temperature of the vapour. The amount of ammonia absorbed fell in 13 kg/h (12% of the total) when the inlet temperature of the vapour was increased from -5°C to 31.7°C.

According to the results obtained in this chapter it can be concluded that the HEXHFMA performs better if it is placed in the absorber. The low inlet temperature of the vapour coming from the desorber leads into higher ammonia absorption rates and, therefore, into smaller designs of the HEXHFMA. Furthermore, the integration of the HEXHFMA in the resorber would mean that the absorption-resorption cycle must be modified because an additional heat exchanger must be integrated in order to reduce the temperature of the vapour at the inlet of the resorber and then avoid water condensation in the membrane that could block the pores.

5.4 Discussion of the results obtained

In this section, the results previously showed are compared to the ones obtained by Schaal [43] and Chen et al. [42]. Moreover, a comparison was made between the hybrid heat exchanger-hollow fibre membrane absorber designed in this chapter and the typically used absorbers in absorption cycles (plate absorbers and shell and tube absorbers). The comparison was made in terms of absorber heat duty per absorber volume.

5.4.1 Comparison with Schaal and Chen et al.

As mentioned at the beginning of this chapter, Schaal [43] studied the performance of an ammonia/water absorption refrigeration plant when the hollow fibre membrane contactors were integrated in the absorber. The experimental configuration of the membrane absorber was similar to the one showed in Figure 5.1, where the adiabatic absorption stage consisted of several hollow fibre membrane absorbers arranged in parallel. A plate heat exchanger were used for cooling the solution before the adiabatic absorption stage. The operating capability of membrane absorbers was demonstrated but it was not possible to implement a membrane absorber with enough membrane surface to absorb all the ammonia required to meet the nominal cooling capacity (6.7 kW) of plant due to the high pressure drop registered. Therefore, the refrigeration plant was operated at lower cooling capacity and the driving force for the absorption inside the absorber was very high. The subcooling of the solution at the inlet of the absorber varied from 20ºC to 29ºC, leaving the membrane absorber with a subcooling above 10ºC in all cases. The absorber heat duty per absorber volume reported by Schaal varies from 9000 to 15000 kW/m^3, depending on the working conditions and the arrangement of the membrane modules. It is important to note that these values reported by Schaal were obtained as the product of the volumetric ammonia absorption rate (mol·m^{-3}·s^{-1}) in the membrane absorber and the enthalpy of vaporization of the ammonia (kJ/mol), so the volume of the plate-heat exchanger used for cooling down the solution before entering the membrane absorber was not taken into consideration. Therefore, when the additional volume for the cooling will be taken into account, lower values of the volume-specific heat duty are expected.

The results obtained in this chapter show a heat duty per volume of 2400 kW/m^3 for the absorber and 1700 kW/m^3 for the resorber, which are far from most of the values provided by Schaal. This discrepancy can be explained because in our case study the subcooling of the solution was much lower both at the inlet (7ºC) and at the outlet (0.2ºC). When the solution approaches the saturation conditions the driving force of the absorption process approaches zero and then a very large membrane area is required to continue absorbing ammonia.

In the work presented by Chen et al. [42], a simulation study of the integration of a hybrid membrane absorber-heat exchanger in an ammonia-water absorption chiller was carried out. The cycle selected for the study was based in the one presented by Chua et al. [81] which includes heat integrations in the refrigerant heat exchanger, rectifier, solution heat exchanger and solution-cooled heat exchanger. The membrane modules designed by Chen et al. [42] were also based in the cross-flow design provided by the Liqui-Cel® hollow fibre membrane contactor [67], but for the mathematical model a counter-current flow configuration was assumed. Two hybrid membrane absorber-heat exchanger were designed by Chen et al. One for the solution-cooled absorber and the other for the water-cooled absorber. Regarding the solution-cooled absorber, the results obtained by Chen et al. agree very well in terms of heat duty per absorber volume (2300 kW/m^3) with the results obtained in this chapter (2400 kW/m^3). However, in the case of the water-cooled absorber the heat duty per absorber volume was five times higher (11000 kW/m^3). This fact can be explained by two factors: first, the inlet temperature difference between the cooling water (35ºC) and the solution (70ºC) was much higher than in the case study analysed in this chapter (22ºC the cooling water and 31.7ºC the solution). Secondly, the ratio between the cooling water mass flow rate and the solution mass flow rate was much higher in the case study of Chen et al. (Ratio=26) than in the present work (Ratio=10).

As mentioned before, the improvement of the absorber heat duty per absorber volume obtained in the HEXHFMA designed in this chapter is restricted by the low subcooling conditions

of the solution along the membrane module (Figures 5.16 and 5.22), reaching almost complete saturation at the outlet. In real absorption refrigeration systems, there is usually a certain degree of subcooling (3-5^{o}C) at the outlet of the absorbers in order to minimize the surface area of the absorber. Therefore, if the subcooling conditions of the solution and the solution mass flow rate of the case study (Figure 5.12) were higher, then the amount of ammonia absorbed and, therefore, the heat duty per absorber volume, would increase in a very significant way. To confirm this statement, the model of the HEXHFMA for the absorber (Table 5.1) was run but now the inlet conditions were modified in order to increase the subcooling of the inlet solution from 7^{o}C to 25^{o}C. The solution and the cooling water flow rate were also increased from 916 kg/h to 2000 kg/h and from 9.7 m^3/h to 15.3 m^3/h, respectively. The results obtained under these new working conditions show a four-fold increase in the total amount of ammonia absorbed and a heat duty per absorber volume of 10000 kW/m^3 for the same HEXHFMA design showed in Table 5.1. The outlet subcooling of the solution was 1.5^{o}C. These results confirm the potential in terms of compactness of the membrane modules reported by Schaal [43] and Chen et al. [42].

5.4.2 Comparison between the hybrid heat exchanger-hollow fibre membrane absorber and the typically used absorbers

Table 5.3 lists the heat duties per absorber volume of different types of ammonia/water absorbers reported in the literature and in the present work. They correspond to the shell and tube absorbers (falling film type) and to the plate and frame absorbers (both falling film and bubble).

Table 5.3 Absorber heat duties per absorber volume of different types of ammonia/water absorbers reported in the literature.

Reference	Type of absorber	Absorber heat duty per volume [kW/m^3]
Schaal [43]	Shell and tube (Falling film)	300
Lee et al. [82]	Shell and tube (Falling film)	100-300
Kwon and Jeong [83]	Helical coil (Falling film)	20-220
Schaal [43]	Plate heat exchanger (Falling film)	1000
Triché et al. [84]	Plate heat exchanger (Falling film)	500-1600
Cerezo et al. [85]	Plate heat exchanger (bubble)	1000-2300
Present work (TU Dresden)	Plate heat exchanger (bubble)	1600 - 2400

The lowest values were reported by the shell and tubes absorbers (around 300 kW/m^3). On the other hand, the results obtained when the plate heat exchangers were used as an absorber showed heat duties per absorber volume one order of magnitude greater; around 1000 kw/m^3 for the falling-film type and around 2000 kW/m^3 for the bubble absorber type. These values are

in accordance with the one obtained in this chapter (1700-2400 kW/m^3) for the HEXHFMA designed to meet the requirements of the case study, so it could be concluded that there are not significant differences in terms of compactness between the plate heat bubble absorbers and the design of the HEXHFMA proposed in this thesis. However, as mentioned before, the working conditions of the case study selected were not favourable to reach high specific cooling capacities due to the assumption of saturation conditions at the outlet of the absorber. When this limitation was avoided, and a simulation was carried out assuming higher inlet subcooling conditions and higher solution mass flow rate, the heat duty per volume obtained was significantly higher (10000 kW/m^3) than the values provided by the plate bubble absorbers. This improvement in terms of compactness provided by the membrane absorbers compared to the plate absorbers can be explained because the surface-to-volume ratio of the HEXHFMA is much greater (5800 m^2/m^3) than the one provided by the plate absorbers (around 200-300 m^2/m^3). Furthermore, the lower density of the polymeric materials compared to the stainless-steel would lead into much lighter absorbers.

5.4.3 Alternative designs of polymeric membrane absorbers with heat exchanger integrated

There are no membrane modules with the heat exchanger integrated available in the market. Some prototypes were developed by the German company Makatec GmbH. They proposed an alternative design that combines the spiral wound and the hollow fibre membrane contactors, as shown in Figure 5.25 [20]. In this prototype, the ammonia gas flows inside the hollow fibres while the solution and the cooling water are in counter-flow configuration and separated by a non-porous membrane rolled-up around the centre body of the module. The main advantage of this configuration is the continuous cooling provided during the absorption process. Instead of having adiabatic absorption stages in series with cooling stages, both the absorption and the cooling take place continuously all along the membrane module.

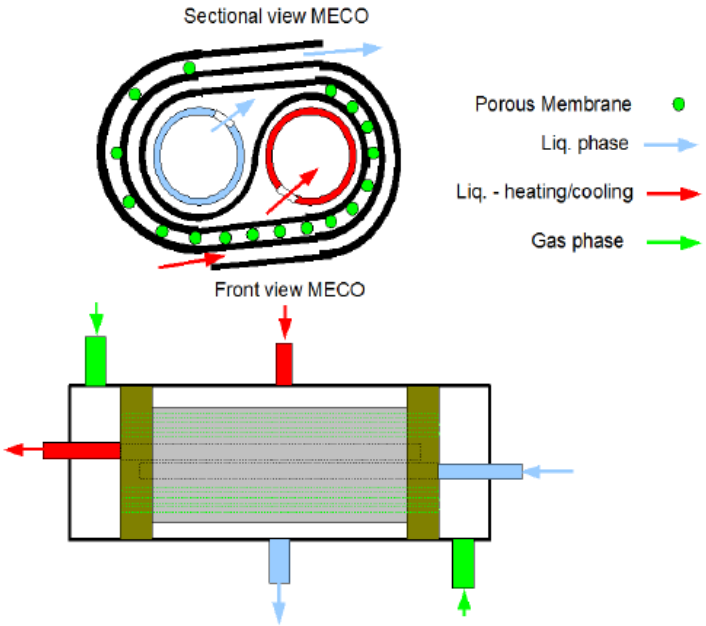

Figure 5.25 Scheme of the membrane absorber with cooling integrated designed by Makatec GmbH. Illustration taken from Weimer [20].

However, all these prototypes had to face the same problem: the potting material required to avoid internal leakages between the cooling water and the solution. This potting material must withstand the working conditions of the absorber (pressure and temperature) and the chemical attack produced by the ammonia. This problem could not be solved in the prototypes developed by Makatec and some internal leakages between the solution side and the cooling water side were detected. This challenge needs to be solved in order to have reliable membrane absorbers.

5.5 Conclusions

In this chapter, the design of two hybrid heat exchanger-hollow fibre membrane absorber (HEXHFMA) was carried out. Each one was designed in order to be used as an absorber and as a resorber in a 25-kW ammonia/water absorption-resorption refrigeration plant, respectively. The theoretical model developed was based on the model validated in Chapter 4 for the study of the adiabatic ammonia absorption process using a hollow fibre membrane module as contactor. In order to integrate the cooling inside the membrane module, some non-porous hollow fibre membranes were used for the flow of the cooling water. The HEXHFMA consist of several interleaved adiabatic absorption stages and cooling stages until obtained the desired conditions of the solution (temperature and ammonia concentration) at the outlet of the module.

Before starting to design the hybrid heat exchanger-hollow fibre membrane absorbers, the configuration of the absorption-resorption cycle had to be modified in order to avoid water condensation in the membrane of the resorber. The modification consists of an additional heat transfer between the cold solution leaving the desorber and the vapour produced in the generator.

A procedure for the design of the HEXHFMA was described and the results obtained showed that the membrane area of the HEXHFMA for the resorber is 22% bigger than for the absorber. Moreover, the resorber requires 35% more cooling water than the absorber. These diferences can be explained by the higher temperature difference between the solution and the cooling water when the HEXHFMA is working under absorber conditions and by the much lower inlet temperature of the vapour entering the absorber compared to inlet temperature of the vapour entering to the resorber (-5^{o}C and 22^{o}C respectively). This cold vapour produces a cooling effect that improves the mass transfer in the absorber.

The compactness of the design of the HEXHFMA was evaluated in terms of absorber heat duty per absorber volume. The values obtained for the HEXHFMA designed in this chapter were far (2400 kW/m^3) from the ones reported by Schaal (between 9000 and 15000 kW/m^3). This discrepancy can be explained by two main reasons: first, the values reported by Schaal did not consider the volume of the plate-heat exchanger used for cooling down the solution before entering the adiabatic membrane absorber; and second, because in our case study the subcooling of the solution was much lower all along the membrane module, reaching almost saturation conditions at the outlet. However, when more favourable working conditions (higher subcooling and solution mass flow rate) are considered, the heat duty per absorber volume increases up to 10000 kW/m^3 for the same HEXHFMA design. These results confirm the potential in terms of compactness of the membrane absorbers, especially when they are compared to the shell and tube absorbers (300 kW/m^3) and the plate bubble absorbers (2000 kW/m^3). Furthermore, due to the much lower density of the polymeric materials compared to the stainless steel it would be expected that the HEXHFMA leads into much lighter absorbers.

Nomenclature of chapter 5

dA	[m^2]	Discretized membrane area
d_0	[m]	Outer diameter of the hollow fiber
d_i	[m]	Inner diameter of the hollow fiber
d_p	[m]	Pore diameter
D_s	[m]	Inner diameter of the shell of the module
D_t	[m]	Outer diameter of the central tube
dx	[m]	Length of the discretization element in the axial direction
dy	[m]	Width of the discretization ring in the radial direction. Also gap between the fibers
Eff_{HEX1}	[-]	Effectiveness of the solution heat exchanger of the absorption circuit
Eff_{HEX2}	[-]	Effectiveness of the solution heat exchanger of the resorption circuit
h	[J/kg]	Specific enthalpy
J	[kg/(m^2·s)]	Mass flux
L	[m]	Membrane module length
m	[-]	Segment m
m_{BL}	[kg/s]	Solution mass flow rate
m_{BG}	[kg/s]	Gas mass flow rate
m_{CL}	[kg/s]	Cooling water mass flow rate
n	[-]	Segment n
p	[Pa]	Pressure
T	[K]	Temperature
U	[W/m^2·K]	Overall heat transfer coefficient
x	[-]	Ammonia mass fraction

Special characters

α	[W/(m^2·K)]	Heat transfer coefficient
ε	[-]	Membrane porosity
λ	[W/(m·K)]	Thermal conductivity

Subscripts

abs	Absorber
BG	Bulk gas
BL	Bulk liquid
CL	Cooling water
in	Inlet
liq	Liquid
MM	Membrane
out	Outlet
res	Resorber
sat	Saturation
vap	Vapour

Chapter 6

General Conclusions and Future Work

6.1 General conclusions

Despite the advantages of using absorption refrigeration systems when low-grade energy sources are available to drive the cycle, these systems have not been fully implemented in the market compared to the vapour-compression technology. The main problem lies in the higher cost and size of the absorption systems, so developing more compact and cheaper equipment is a key factor to make the absorption technology more competitive. Two possible solutions have been proposed in this thesis to face the problems of size and cost of the absorption refrigeration systems: First, the use of polymeric membranes as contactors between the vapour and the solution in the absorbers to reduce their size due to the high surface/volume ratio provided by the membrane modules. Using polymeric materials would also reduce the price of the absorption systems but these materials do not withstand the typically high working pressure of the ammonia/water absorption systems. For this reason, the second solution proposed in this thesis consisted in using the resorption technology to reduce the operating high-pressure of the conventional ammonia/water absorption refrigeration systems.

The initial step was the study of the ammonia/water absorption-resorption refrigeration cycle in order to identify the key factors affecting the performance of the system. Adequate operating conditions were suggested for the base case selected. Next, a theoretical and experimental study was done on the adiabatic ammonia absorption process into ammonia/water solutions using polymeric membranes as contactors. For the experimental work, a test bench was designed and built. The study was divided into two parts: first, a flat sheet membrane module was used for the determination of the desired membrane characteristics for the ammonia absorption process. These characteristics were considered for the selection of a commercial hollow fibre membrane module used in the subsequent step: the study of the adiabatic ammonia absorption process using a hollow fibre membrane module as contactor, where a two-dimensional model was developed and validated with the experimental results. Because there are no commercial hollow fibre membrane modules with heat exchanger integrated available in the market, all the previous studies had to be done under adiabatic conditions. However, the absorption-resorption refrigeration systems require to cool down the solution during the absorption processes in order to keep the absorption potential as high as possible along the absorber. Therefore, the two-dimensional model previously validated was used as a basis for developing a theoretical model of a hybrid heat exchanger-hollow fibre membrane absorber (HEXHFMA). Finally, this model was used for designing two HEXHFMA: One for the absorption circuit and the other one for the resorption circuit of a 25-kW ammonia/water absorption-resorption refrigeration plant.

The following conclusions can be taken from this research work:

- The absorption-resorption systems provide great flexibility in terms of reduction of the high-pressure. However, this reduction in the pressure must be paid for by a reduction of the COP.

- A proper design of the solution heat exchanger of the resorption circuit is essential. If the effectiveness is lower than a certain value, the cycle cannot operate at the desired temperatures.

- The cycle configuration without rectifier is the most favourable because the complexity, size and cost of the system would be lower, and the loss of performance is not significant (below 8%).

- An accurate control of the absorption-resorption systems is a challenge due to the inherent instability of the resorption cycles provided by the additional degree of freedom. The experimental work carried out during the research stay at TU Dresden showed the difficulties for keeping the system working under steady-state conditions.

- A Thermodynamic model of the cycle was developed and used for the analysis of the performance of the 25-kW experimental plant set up at TU Dresden. Such analysis identified a poor absorption process in the resorber. Increasing the size of the plate-heat exchanger or improving the gas/liquid distribution was recommended to enhance the heat and mass transfer.

- A method based on near-infrared (NIR) spectroscopy for the in-situ determination of the ammonia concentration in absorption cycles was developed and the results published in the International Journal TALANTA [56]. Thus, this technique was proposed to improve the performance of the absorption-resorption cycle. By means of a multiplexor, this new method allows to measure the ammonia concentration at several points of the cycle just using one detector and one lamp, leading then in a cheaper alternative than using the conventional Coriolis density-meters.

- The desired membrane characteristics to be used as contactor for the ammonia absorption process are: hydrophobicity, pore size between 0.03μm and 0.10μm, porosity higher than 40% and thickness as low as possible (lower than 400μm) in order to obtain a low transport resistance across the pores of the membrane but at the same time keeping the mechanical robustness. This study constitutes a novelty because it had not been done before for the ammonia/water mixture and the results obtained were published in Applied Thermal Engineering [57].

- According to the desired membrane characteristics previously obtained, a commercial cross-flow hollow fibre membrane module was selected (Liqui-Cel® G501 2.5x8 Extra-Flow) for the experimental study of the adiabatic ammonia absorption process. The results showed an excellent performance of the membrane module working both under absorber and resorber conditions, reaching ammonia absorption rates up to $9.7 \cdot 10^{-4}$ kg/(m^2·s).

- A two-dimensional model was developed and validated with the experimental results obtained with the hollow fibre membrane module. This model constitutes a novelty compared to previous works because it enables to study the evolution of the main operating parameters in the axial and radial direction of the membrane module, so a more realistic information about the profiles inside the cross-flow hollow fibre membrane module can be obtained. The results obtained were published in Applied Thermal Engineering [86]. The Mean Absolute Error of the model predictions with respect to the experimental data was $\pm 3 \cdot 10^{-5}$ kg/m^{2}s for the ammonia absorption rate and ±0.3°C for the prediction of the outlet temperature of the solution.

- In order to use the membrane absorbers in absorption-resorption refrigeration systems it is necessary to integrate the heat transfer because with the adiabatic absorption is not possible to absorb all the ammonia required. Thus, a model of a hybrid heat exchanger-hollow fibre membrane absorber was developed based on the model previously validated of the adiabatic hollow-fibre membrane module. This model was used for designing the absorber and the resorber of a 25-kW ammonia/water absorption-resorption refrigeration plant.

- The ammonia/water absorption-resorption plant must be modified when membrane modules are used as contactors in the resorber. Due to the water content of the vapour produced in the generator, this stream should be cooled down before entering the

membrane module in order to avoid water condensation and pore blocking that could reduce the mass transfer across the membrane.

- The absorber designed consists of six absorption stages and five cooling stages, 126 m^2 of total effective membrane area, 30 cm length and 30.9 cm of diameter. It requires 9.7m^3/h of cooling water at 22^{o}C.

- The resorber designed consists of seven absorption stages and six cooling stages, 154.5 m^2 of total effective membrane area, 30 cm length and 35.2 cm of diameter. It requires 15.1m^3/h of cooling water at 22^{o}C.

- The resorber requires 22% more membrane area and 35% more cooling water than the absorber. These differences can be explained by the higher temperature difference between the solution and the cooling fluid when the HEXHFMA was working under absorber conditions and by the much lower inlet temperature of the vapour entering the absorber compared to inlet temperature of the vapour entering to the resorber (-5^{o}C and 22^{o}C respectively). This cold vapour produces a continue cooling effect that improves the mass transfer in the absorber.

- The results obtained in this thesis confirm the potential in terms of compactness (heat duty per absorber volume up to 10000 kW/m3) and the performance of the membrane absorbers, especially when they are compared to the shell and tube absorbers (300 kW/m3) and the plate bubble absorbers (2000 kW/m3). Furthermore, due to the much lower density of the polymeric materials compared to the stainless steel it would be expected that the HEXHFMA leads into much lighter absorbers.

6.2 Future work

Lastly, suggestions for future research directions are listed below:

- Develop and test an automated control system for the absorption-resorption system based on the NIR measurements.

- Study the integration of membrane contactors in the generator and in the desorber of the ammonia/water absorption-resorption cycles. Particularly challenging is the integration of polymeric membranes in the generator because of the high temperatures.

- Develop a new two-dimensional model of the hybrid heat exchanger-hollow fibre membrane absorber where the presence of water in the vapour was taken into consideration.

- Design and optimization of new configurations of membrane absorber with heat exchanger integrated: spiral wound, plate-and-frame, etc.

- Test new materials that provide chemical resistance, mechanical strength, thermal stability and good thermal conductivity. Low cost and weight of the material are also essential.

- Design, construction and integration of prototypes of hybrid heat exchanger-membrane absorbers in an experimental test bench and study the performance.

REFERENCES

[1] COMMISSION RECOMMENDATION (EU) 2016/1318 of 29 July 2016, (n.d.). http://eur-lex.europa.eu/legal-content/EN/TXT/PDF/?uri=CELEX:32016H1318&from=EN (accessed May 5, 2018).

[2] D. Coulomb, A. Pichard, 29th Informatory Note on Refrigeration Technologies. The Role of Refrigeration in the Global Economy, 2015.

[3] A. Coronas, M. Berdasco, J. Prieto, J.C. Bruno, Current development and perspectives of resorption heat pumps, in: Int. Conf. Mater. Energy, Tianjin (China), 2017.

[4] J. Berghmans, Heat pumps fundamentals, NATO Advanced Study Institutes Series.Series E, Applied Sciences; No 53., in: 1983.

[5] M. Bourouis, M. Vallès, M. Medrano, A. Coronas, Absorption of water vapour in the falling film of water–(LiBr+LiI+LiNO3+LiCl) in a vertical tube at air-cooling thermal conditions, Int. J. Therm. Sci. 44 (2005) 491–498. doi:10.1016/j.ijthermalsci.2004.11.009.

[6] M. Bourouis, M. Vallès, M. Medrano, A. Coronas, Performance of air-cooled absorption air-conditioning systems working with water-(LiBr + LiI + LiNO3 + LiCl), Proc. Inst. Mech. Eng. Part E J. Process Mech. Eng. 219 (2005) 205–213. doi:10.1243/095440805X8601.

[7] J. Mesones, Phase Equilibria of Ammonia Solutions for Absorption Refrigeration Systems. Experimental Determination and Modeling, Universitat Rovira i Virgili, 2014.

[8] H.O. Spauschus, U. Hesse, Reduced pressure carbon dioxide-based refrigeration system, US006073454, 2000.

[9] R. Radermacher, Y. Hwang, Vapor Compression Heat Pumps with Refrigerant Mixtures, CRC, 2005.

[10] Q. Zhou, R. Radermacher, Development of a vapor compression cycle with a solution circuit and desorber/absorber heat exchange, Int. J. Refrig. 20 (1997) 85–95. doi:10.1016/S0140-7007(96)00072-2.

[11] J. Kim, S.R. Park, Y.J. Baik, K.C. Chang, H.S. Ra, M. Kim, Y. Kim, Experimental study of operating characteristics of compression/absorption high-temperature hybrid heat pump using waste heat, Renew. Energy. 54 (2013) 13–19. doi:10.1016/j.renene.2012.09.032.

[12] A. Osenbrück, Verfahren zur Kälteerzeugung bei Absorptionsmaschinen. Deutsches Reichspatent, 1895.

[13] E. Altenkirch, Kompressionskältemachine mit lösungskreislauf, Kältetechnik. 2 (1950).

[14] E. Altenkirch, Der Einfluss endlicher Temperaturdifferenzen auf die Betriebskosten von Kompressionsanlagen mit und ohne Lösungskreislauf, Kältetechnik. 3 (1951).

[15] M. Stokar, C. Trepp, Compression heat pump with solution circuit. Part 1: design and experimental results, Int. J. Refrig. 10 (1987) 87–96.

[16] Institute for Energy Technology, (2018). https://www.ife.no/en/ife/departments/energy_systems/projects/cahp?set_language=en (accessed January 30, 2018).

[17] N.J. Hewitt, J.T. McMullan, B. Mongey, G.A. Molyneaux, Performance Trends in Ammonia-Water Resorption Cycle, in: Proc. 20th Int. Congr. Refrig. IIR/IIF, Sydney,

Australia, 1999.

[18] L.C.M. Itard, Wet compression-resorption heat pump cycles: Thermodynamic analysis and design, Delft University of Technology, 1998. uuid:d51f9478-aa4e-4403-aa8d-11c840f7e7ff.

[19] E. Altenkirch, Reversible Absorptionsmaschinen, Z.f.d. Gesamte Kälte-Industrie 20. (1913) 1–9.

[20] T. Weimer, Resorption cycles for cooling with waste heat using natural refrigerants and compact plate and spiral heat exchangers, in: Int. Work. New Work. Fluids Absorpt. Heat Pumps Refrig. Syst. 22-23 July, Tarragona, Spain, 2013.

[21] H.D. Baehr, The COP of absorption and resorption heat pumps with ammonia-water as working fluid, 1981. doi:10.1016/0140-7007(81)90064-5.

[22] M. Pande, K.E. Herold, The resorption cycle using ammonia and water, in: ASHRAE Trans. Symp., 1996: pp. 1110–1117.

[23] L. Costiuc, I. Costiuc, Solar powered resorption cooling system, in: Bull. Transilv. Univ. Brasov, 2010: p. 2010.

[24] K.E. Herold, R. Radermacher, S.A. Klein, Absorption Chillers and Heat Pumps, Second Edition, CRC Press, 2016. doi:doi:10.1201/b19625-2.

[25] H.M. Sabir, I.W. Eames, Theoretical comparison between lithium bromide/water vapour resorption and absorption cycles, Appl. Therm. Eng. 18 (1998) 683–692. doi:10.1016/S1359-4311(97)00050-1.

[26] Community Research and Development Information Service (CORDIS), (n.d.). http://cordis.europa.eu/project/rcn/16408_en.html (accessed January 25, 2018).

[27] K. Helle, M. Morschel, S. Peil, T. Weimer, S. Haep, Experimental investigation of a new resorption cycle using ammonia as refrigerant, in: 4th IIR Conf. Ammon. Refrig. Technol., Ohrid, Macedonia, 2011.

[28] Institute of Combustion and Power Plant Technology of the University of Stuttgart, (n.d.). http://www.ifk.uni-stuttgart.de/forschung/exp_ein/halbtechnisch/biocool.en.html.

[29] M. Grund, U. Hesse, T. Weimer, K. Rühling, Desing of a novel resorption refrigeration system with an attached ice storage system, in: Proceedings, 6th IIR Conf. Ammon. CO2 Refrig. Technol., Ohrid, Macedonia, 2015.

[30] F. Asfand, M. Bourouis, A review of membrane contactors applied in absorption refrigeration systems, Renew. Sustain. Energy Rev. 45 (2015) 173–191. doi:10.1016/j.rser.2015.01.054.

[31] A.H.H. Ali, P. Schwerdt, Characteristics of the membrane utilized in a compact absorber for lithium bromide–water absorption chillers, Int. J. Refrig. 32 (2009) 1886–1896. doi:10.1016/j.ijrefrig.2009.07.009.

[32] A.H.H. Ali, Design of a compact absorber with a hydrophobic membrane contactor at the liquid – vapor interface for lithium bromide – water absorption chillers, Appl. Energy. 87 (2010) 1112–1121. doi:10.1016/j.apenergy.2009.05.018.

[33] D. Yu, J. Chung, S. Moghaddam, Parametric study of water vapor absorption into a constrained thin film of lithium bromide solution, Int. J. Heat Mass Transf. 55 (2012) 5687–5695. doi:10.1016/j.ijheatmasstransfer.2012.05.064.

[34] Z. Wang, Z. Gu, S. Feng, Y. Li, Application of vacuum membrane distillation to lithium bromide absorption refrigeration system, Int. J. Refrig. 32 (2009) 1587–1596. doi:10.1016/j.ijrefrig.2009.07.002.

[35] R. Nasr Isfahani, K. Sampath, S. Moghaddam, Nanofibrous membrane-based absorption refrigeration system, Int. J. Refrig. 36 (2013) 2297–2307. doi:10.1016/j.ijrefrig.2013.07.019.

[36] F. Asfand, Y. Stiriba, M. Bourouis, CFD simulation to investigate heat and mass transfer processes in a membrane-based absorber for water-LiBr absorption cooling systems, Energy. 91 (2015) 517–530. doi:10.1016/j.energy.2015.08.018.

[37] F. Asfand, Y. Stiriba, M. Bourouis, Impact of the solution channel thickness while investigating the effect of membrane characteristics and operating conditions on the performance of water-LiBr membrane-based absorbers, Appl. Therm. Eng. 108 (2016) 866–877. doi:10.1016/j.applthermaleng.2016.07.139.

[38] F. Asfand, Y. Stiriba, M. Bourouis, Performance evaluation of membrane-based absorbers employing H2O/(LiBr + LiI + LiNO3 + LiCl) and H2O/(LiNO3 + KNO3 + NaNO3) as working pairs in absorption cooling systems, Energy. 115 (2016) 781–790. doi:10.1016/j.energy.2016.08.103.

[39] M. Venegas, M. de Vega, N. García-Hernando, U. Ruiz-Rivas, A simple model to predict the performance of a H2O-LiBr absorber operating with a microporous membrane, Energy. 96 (2016) 383–393. doi:10.1016/j.energy.2015.12.059.

[40] M. Venegas, M. De Vega, N. García-Hernando, Parametric study of operating and design variables on the performance of a membrane-based absorber, Appl. Therm. Eng. 98 (2016) 409–419. doi:10.1016/j.applthermaleng.2015.12.074.

[41] M. Venegas, M. de Vega, N. García-Hernando, U. Ruiz-Rivas, Adiabatic vs non-adiabatic membrane-based rectangular micro-absorbers for H2O-LiBr absorption chillers, Energy. 134 (2017) 757–766. doi:10.1016/j.energy.2017.06.068.

[42] J. Chen, H. Chang, S. Chen, Simulation study of a hybrid absorber–heat exchanger using hollow fiber membrane module for the ammonia–water absorption cycle, Int. J. Refrig. 29 (2006) 1043–1052. doi:10.1016/j.ijrefrig.2006.02.002.

[43] F. Schaal, Membranabsorberfür die Absorptionskältetechnik. Dissertation, Universität Stuttgart, 2008.

[44] O.M. Ibrahim, S.A. Klein, Thermodynamic Properties of Ammonia-Water Mixtures, in: ASHRAE Trans., 1992: pp. 1495–1502.

[45] D.S. Ayou, J.C. Bruno, A. Coronas, Steady-state operational degrees of freedom in absorption chillers and heat pumps: Methodology and case study, Int. J. Refrig. 35 (2012) 1570–1582. doi:10.1016/j.ijrefrig.2012.04.003.

[46] R. Wechsler, P. Wagner, R. Rieberer, Modelling and experimental analysis of the desorber of a gas-fired absorption heat pump, in: I.I. of Refrigeration (Ed.), Proc. 12th IIR-Gustav Lorentzen Nat. Work. Fluids Conf. Edinburgh (United Kingdom), 2016: pp. 744–751.

[47] T.F. Edgar, D.M. Himmelblau, L.S. Lasdon, Optimization of chemical processes, McGraw-Hill, 2001.

[48] J.K. Jensen, W.B. Markussen, L. Reinholdt, B. Elmegaard, On the development of high temperature ammonia-water hybrid absorption-compression heat pumps, Int. J. Refrig.

58 (2015) 79–89.

[49] O. Ziegler, U. Hesse, C. Thomas, Absorption Resorption Refrigeration System - Recirculation of the Solution (Mix Flow) and Fluid Distribution in Plate Heat Exchangers, (n.d.). https://tu-dresden.de/ing/maschinenwesen/iet/kkt/forschung/poster.

[50] M. Blanco, I. Villarroya, NIR spectroscopy: a rapid-response analytical tool, TrAC Trends Anal. Chem. 21 (2002) 240–250. doi:10.1016/S0165-9936(02)00404-1.

[51] S. Macho, M.S. Larrechi, Near-infrared spectroscopy and multivariate calibration for the quantitative determination of certain properties in the petrochemical industry, TrAC Trends Anal. Chem. 21 (2002) 799–806. doi:10.1016/S0165-9936(02)01202-5.

[52] R.M. Balabin, E.I. Lomakina, R.Z. Safieva, Neural network (ANN) approach to biodiesel analysis: Analysis of biodiesel density, kinematic viscosity, methanol and water contents using near infrared (NIR) spectroscopy, Fuel. 90 (2011) 2007–2015. doi:10.1016/j.fuel.2010.11.038.

[53] M.I. Barba, Determinación cuantitativa de la composición de mezclas de trabajo para sistemas de refrigeración mediante espectroscopia de infrarrojo cercano, Universitat Rovira i Virgili, 2016.

[54] M.I. Barba, D. Salavera, M.S. Larrechi, A. Coronas, Determining the composition of ammonia/water mixtures using short-wave near-infrared spectroscopy, Talanta. 147 (2016) 111–116. doi:10.1016/j.talanta.2015.09.037.

[55] M.I. Barba, M.S. Larrechi, A. Coronas, Quantitative analysis of the hydration of lithium salts in water using multivariate curve resolution of near-infrared spectra, Anal. Chim. Acta. 919 (2016) 20–27. doi:10.1016/j.aca.2016.03.022.

[56] M.I. Barba, M. Berdasco, D. Salavera, M.S. Larrechi, A. Coronas, A method based on near-infrared spectroscopy for the in-situ determination of the ammonia concentration in ammonia/water mixtures in an absorber test bench, Talanta. 175 (2017). doi:10.1016/j.talanta.2017.07.083.

[57] M. Berdasco, A. Coronas, M. Vallès, Theoretical and experimental study of the ammonia/water absorption process using a flat sheet membrane module, Appl. Therm. Eng. 124 (2017) 477–485. doi:10.1016/j.applthermaleng.2017.06.027.

[58] Sterlitech Corporation. SEPA CF Cell Manual V1.2., (n.d.).

[59] Y. Cuenca, D. Salavera, A. Vernet, M. Vallès, Thermal conductivity of ammonia + water mixtures over a wide range of concentrations, Int. J. Refrig. 36 (2013) 998–1003. doi:10.1016/j.ijrefrig.2012.10.039.

[60] M. Conde, Thermophysical Properties of {NH3 + H2O} Mixtures for the Industrial Design of Absorption Refrigeration Equipment, Update. (2006).

[61] E.A. Manson, A.P. Malinauskas, Gas transport in porous media: the dusty-gas model., Elsevier, 1983.

[62] L. Martínez, J.M. Rodríguez-Maroto, On transport resistances in direct contact membrane distillation, J. Memb. Sci. 295 (2007) 28–39. doi:10.1016/j.memsci.2007.02.029.

[63] A. Gabelman, S.-T. Hwang, Hollow fiber membrane contactors, J. Memb. Sci. 159 (1999) 61–106. doi:10.1016/S0376-7388(99)00040-X.

[64] R.K. Shah, A.L. London, Laminar Flow Forced Convection in Ducts: A Source Book for Compact Heat Exchanger Analytical Data, Advances in Heat Transfer, Academic Press, Suppl. 1., New York, 1978.

[65] M. Khayet, J.I. Mengual, T. Matsuura, Porous hydrophobic/hydrophilic composite membranes, J. Memb. Sci. 252 (2005) 101–113. doi:10.1016/j.memsci.2004.11.022.

[66] M. Berdasco, A. Coronas, M. Vallès, Study of the adiabatic absorption process in polymeric hollow fiber membranes for ammonia/water absorption refrigeration systems, Appl. Therm. Eng. 137 (2018) 594–607. doi:10.1016/j.applthermaleng.2018.04.004.

[67] Liqui-Cel® (3M Separation and Purification Sciences Division). Product data sheet of the EXTRA-FLOW 2.5x8 X50 hollow fiber membrane module, (n.d.).

[68] H. Mahmud, A. Kumar, R.M. Narbaitz, T. Matsuura, A study of mass transfer in the membrane air-stripping process using microporous polyproplylene hollow fibers, J. Memb. Sci. 179 (2000) 29–41. doi:10.1016/S0376-7388(00)00381-1.

[69] J. Zheng, Z. Dai, F. Wong, Z. Xu, Shell side mass transfer in a transverse flow hollow fiber membrane contactor, J. Memb. Sci. 261 (2005) 114–120. doi:10.1016/j.memsci.2005.02.035.

[70] S.R. Wickramasinghe, M.J. Semmens, E.L. Cussler, Mass transfer in various hollow fiber geometries, J. Memb. Sci. 69 (1992) 235–250. doi:10.1016/0376-7388(92)80042-I.

[71] E.A. Fouad, H.J. Bart, Separation of zinc by a non-dispersion solvent extraction process in a hollow fiber contactor, Solvent Extr. Ion Exch. 25 (2007) 857–877.

[72] A. Baudot, J. Floury, H.E. Smorenburg, Liquid-liquid extraction of aroma compounds with hollow fiber contactor, Am. Intitute Chem. Eng. J. 47 (2001) 1780–1793.

[73] S. Shen, S.E. Kentish, G.W. Stevens, Shell-Side Mass-Transfer Performance in Hollow-Fiber Membrane Contactors, Solvent Extr. Ion Exch. 28 (2010) 817–844.

[74] P. Schöner, P. Plucinski, W. Nitsch, U. Daiminger, Mass transfer in the shell side of cross flow hollow fiber modules, Chem. Eng. Sci. 53 (1998) 2319–2326.

[75] H. Mahmud, A. Kumar, R.M. Narbaitz, T. Matsuura, Mass transport in the membrane air-stripping process using microporous polypropylene hollow fibers: Effect of toluene in aqueous feed, J. Memb. Sci. 209 (2002) 207–219. doi:10.1016/S0376-7388(02)00320-4.

[76] I. Mahmoud, Mass and heat transfer during absorption of ammonia vapor into ammonia-water mixture. Dissertation, Saga University, 2004.

[77] H.Z. Hausen, VDI Beih, Verfahrenstech., 4, 91, 1943.

[78] J.E. Mark, Polymer Data Handbook, Oxford University Press, New York, (1999).

[79] B.N. Taylor, C.E. Kuyatt, Guidelines for evaluating and expressing the uncertainty of NIST measurement results, National Institute of Standards and Technology Technical Note 1297, (1994).

[80] B.J. McBride, M.J. Zehe, S. Gordon, NASA Glenn Coefficients for Calculating Thermodynamic Properties of Individual Species. NASA/TP-2002-211556, (2002).

[81] H.T. Chua, H.K. Toh, K.C. Ng, Thermodynamic modeling of an ammonia–water absorption chiller, Int. J. Refrig. 25 (2002) 896–906. doi:10.1016/S0140-7007(01)00101-3.

[82] S. Lee, L.K. Bohra, S. Garimella, A.K. Nagavarapu, Measurement of absorption rates in horizontal-tube falling-film ammonia-water absorbers, Int. J. Refrig. 35 (2012) 613–632. doi:10.1016/j.ijrefrig.2011.08.011.

[83] K. Kwon, S. Jeong, Effect of vapor flow on the falling-film heat and mass transfer of the ammonia/water absorber, Int. J. Refrig. 27 (2004) 955–964. doi:10.1016/j.ijrefrig.2004.06.009.

[84] D. Triché, S. Bonnot, M. Perier-Muzet, F. Boudéhenn, H. Demasles, N. Caney, Experimental and numerical study of a falling film absorber in an ammonia-water absorption chiller, Int. J. Heat Mass Transf. 111 (2017) 374–385. doi:10.1016/j.ijheatmasstransfer.2017.04.008.

[85] J. Cerezo, M. Bourouis, M. Vallès, A. Coronas, R. Best, Experimental study of an ammonia–water bubble absorber using a plate heat exchanger for absorption refrigeration machines, Appl. Therm. Eng. 29 (2009) 1005–1011. doi:10.1016/j.applthermaleng.2008.05.012.

[86] M. Berdasco, A. Coronas, M. Vallès, Study of the adiabatic absorption process in polymeric hollow fiber membranes for ammonia/water absorption refrigeration systems, Appl. Therm. Eng. 137 (2018). doi:10.1016/j.applthermaleng.2018.04.004.

ANNEX A: Experimental results in the absorber test bench

A.1 Experimental data obtained during the experiments with the flat sheet membrane module

m_s [kg/h]	T_{in} [ºC]	T_{out} [ºC]	$T_{in,gas}$ [ºC]	p_{in} [bar]	$p_{in,gas}$ [bar]	$x_{NH3,in}$	J [kg/m^2·s]	T_{sat} [ºC]	T_{sat}-T_{in} [ºC]
15.2	25.0	27.8	27.2	1.3	1.3	0.318	2.03E-03	33.0	8.0
15.1	27.0	28.7	27.3	1.3	1.3	0.319	1.43E-03	32.7	5.7
15.2	29.1	29.3	27.2	1.3	1.3	0.320	8.44E-04	32.5	3.5
15.1	31.0	30.6	27.7	1.3	1.3	0.322	4.13E-04	32.1	1.0
14.9	22.0	24.8	22.8	1.3	1.3	0.321	2.71E-03	32.0	10.0
25.1	25.1	26.8	25.3	1.3	1.4	0.317	2.11E-03	33.6	8.5
24.9	27.1	27.9	25.2	1.3	1.4	0.317	1.61E-03	33.5	6.5
25.1	29.2	29.9	27.5	1.3	1.4	0.318	1.44E-03	33.1	3.9
25.3	31.0	31.0	27.6	1.3	1.3	0.320	8.51E-04	32.8	1.8
25.1	22.0	24.5	24.9	1.3	1.3	0.321	3.12E-03	32.2	10.2
35.0	25.1	26.2	24.3	1.3	1.3	0.321	2.30E-03	32.5	7.5
35.1	27.1	27.8	24.6	1.3	1.4	0.323	1.57E-03	32.4	5.3
35.0	29.1	29.4	24.8	1.3	1.3	0.324	8.34E-04	32.0	2.9
35.1	31.0	31.2	25.1	1.3	1.3	0.325	2.63E-04	31.6	0.6
35.1	22.1	23.6	24.9	1.3	1.4	0.320	3.98E-03	32.8	10.7
45.1	24.9	26.1	25.4	1.4	1.3	0.320	2.53E-03	33.3	8.4
45.1	27.0	27.6	25.0	1.4	1.3	0.322	1.77E-03	32.9	5.9
45.0	29.0	29.2	25.1	1.4	1.4	0.324	1.10E-03	32.4	3.4
45.2	31.0	30.9	24.9	1.3	1.4	0.324	5.94E-04	32.1	1.1
45.1	22.1	23.5	23.9	1.4	1.4	0.319	4.65E-03	33.2	11.1

A.2 Experimental data obtained during the experiments with the hollow fibre membrane module (Absorber conditions)

m_s [kg/h]	T_{in} [ºC]	T_{out} [ºC]	$T_{in,gas}$ [ºC]	p_{in} [bar]	$p_{in,gas}$ [bar]	$x_{NH3,in}$	J [kg/m²·s]	T_{sat} [ºC]	T_{sat}-T_{in} [ºC]
49.4	24.1	34.1	21.9	1.4	1.4	0.294	1.96E-04	38.0	13.9
48.8	27.9	36.4	23.7	1.4	1.4	0.290	1.66E-04	39.2	11.3
48.9	31.4	36.9	24.7	1.4	1.4	0.292	1.10E-04	38.4	7.0
50.7	33.7	36.7	21.7	1.4	1.4	0.294	6.82E-05	38.2	4.5
50.2	33.6	35.8	22.8	1.4	1.4	0.301	5.36E-05	36.7	3.1
75.2	34.7	37.7	23.9	1.3	1.3	0.291	1.03E-04	37.9	3.2
76.0	33.4	37.3	16.3	1.4	1.4	0.291	1.32E-04	38.8	5.4
75.0	31.8	37.4	18.2	1.4	1.4	0.294	1.76E-04	38.5	6.7
76.0	28.7	36.3	17.3	1.4	1.4	0.297	2.37E-04	38.6	9.9
75.2	24.2	33.6	14.4	1.4	1.4	0.306	2.90E-04	36.7	12.5
100.5	34.8	38.8	19.7	1.4	1.4	0.290	1.71E-04	40.4	5.6
100.0	28.2	33.9	19.5	1.4	1.3	0.302	2.30E-04	37.0	8.8
100.6	32.1	35.2	21.2	1.5	1.5	0.313	1.35E-04	37.0	4.9
98.5	24.7	32.3	13.0	1.4	1.4	0.313	3.07E-04	36.1	11.4
100.0	31.8	34.6	20.0	1.5	1.5	0.321	1.27E-04	35.9	4.1
99.0	28.5	35.1	19.5	1.5	1.5	0.307	2.65E-04	38.6	10.1

A.3 Experimental data obtained during the experiments with the hollow fibre membrane module (Resorber conditions)

m_s [kg/h]	T_{in} [ºC]	T_{out} [ºC]	$T_{in,gas}$ [ºC]	p_{in} [bar]	$p_{in,gas}$ [bar]	$x_{NH3,in}$	J [kg/m²·s]	T_{sat} [ºC]	$T_{sat}-T_{in}$ [ºC]
49.5	21.7	30.8	18.4	5.1	5.1	0.548	2.66E-04	33.3	11.6
50.6	22.3	30.7	22.0	5.2	5.1	0.553	2.49E-04	33.2	10.9
50.0	24.8	31.0	24.6	5.2	5.2	0.556	1.78E-04	32.5	7.7
49.3	28.2	30.9	25.2	5.2	5.1	0.560	6.32E-05	32.1	3.9
50.3	14.8	26.1	21.7	5.4	5.4	0.598	2.83E-04	28.4	13.6
103.7	21.0	28.7	21.1	5.2	5.2	0.568	4.55E-04	31.3	10.3
106.6	23.1	28.8	22.6	5.2	5.1	0.573	3.09E-04	30.5	7.4
99.8	25.6	29.4	21.4	5.1	5.0	0.563	2.18E-04	31.0	5.4
101.9	27.5	30.9	18.8	5.1	5.1	0.560	2.10E-04	32.0	4.5
101.0	28.2	30.1	24.9	5.1	5.1	0.566	1.06E-04	30.9	2.7
100.9	22.9	28.9	21.4	5.3	5.2	0.578	3.07E-04	30.4	7.5
102.1	16.9	27.1	20.1	5.6	5.5	0.597	5.99E-04	29.7	12.8
151.0	19.0	29.7	18.1	5.7	5.7	0.583	9.70E-04	32.3	13.3
148.4	21.2	29.0	20.0	5.7	5.6	0.592	6.68E-04	31.1	9.9
151.9	23.1	28.2	22.6	5.6	5.5	0.597	4.52E-04	29.9	6.8
155.9	24.4	28.7	20.7	5.4	5.3	0.584	3.61E-04	30.2	5.8
155.6	25.4	27.8	23.0	5.6	5.5	0.608	1.72E-04	28.7	3.3

ANNEX B: Flowchart used in the EES simulation of the hollow fibre membrane module